ENHANCING RADIOIODIDE UPTAKE BY MODULATING NIS ENDOCYTOSIS AND DEGRADATION PATHWAYS

By

Ling Zha



UNIVERSITY OF BIRMINGHAM

IMSR

INSTITUTE OF METABOLISM AND SYSTEMS RESEARCH

A thesis submitted to the University of Birmingham for the degree of DOCTOR OF PHILOSOPHY

Institute of Metabolism and Systems Research
College of Medicine and Health
University of Birmingham
September 2024

UNIVERSITY OF
BIRMINGHAM

University of Birmingham Research Archive

e-theses repository

This unpublished thesis/dissertation is copyright of the author and/or third parties. The intellectual property rights of the author or third parties in respect of this work are as defined by The Copyright Designs and Patents Act 1988 or as modified by any successor legislation.

Any use made of information contained in this thesis/dissertation must be in accordance with that legislation and must be properly acknowledged. Further distribution or reproduction in any format is prohibited without the permission of the copyright holder.

Abstract

The effectiveness of radioiodide therapy for differentiated thyroid cancer is often compromised by the mislocalisation of the sodium/iodide symporter (NIS) away from the plasma membrane, as well as its dysregulated expression. While increasing NIS expression has been the focus of previous and on-going studies, mislocalisation remains a significant barrier. This thesis investigates aspects of the post-translational processing of NIS, identifying critical therapeutic opportunities to enhance its function.

Key NIS interactors, including the AP2 adaptor complex, PBF, moesin, and VCP, were explored for their potential roles in NIS endocytosis and trafficking. This revealed that disrupting specific motifs within the NIS C-terminus, particularly the diacidic and dileucine motifs, significantly impacts NIS localisation and function. The efficacy of the specific VCP inhibitors CB-5083 and CB-5339 was appraised in breast cancer cell lines, demonstrating an increase in radioiodide uptake at specific concentrations. However, the effects were not NIS-mediated in all cases. Structural analogues of clotrimazole and NMS-873 were also developed to address bioavailability challenges, demonstrating modest improvements in radioiodide uptake and providing an alternative strategy to modulate NIS degradation. Additionally, the critical impact of NIS dimerisation on its function and trafficking was investigated. Mutations at key residues within the dimerisation interface, particularly K554 and R555, were found to impair NIS dimerisation, reduce iodide uptake, and affect NIS protein expression and localisation.

Thus, new insights into NIS subcellular localisation, processing, function and pharmacological modulation were derived, allowing new strategic approaches to enhancing radioiodide uptake in thyroid cancer to be identified.

Dedication

To my parents for their unwavering belief in my potential and to my husband for his steadfast support and encouragement throughout this journey. Your love and dedication have been my foundation.

Acknowledgements

First and foremost, I wish to express my deepest gratitude to my supervisor, Professor Chris McCabe, for his unwavering support, understanding, and inspiration throughout this journey. His extensive knowledge and guidance have been instrumental in shaping my research, conducting laboratory work, and writing this thesis. His expertise was vital in refining the methodology and research questions, and his insightful feedback challenged me to elevate the quality of my work. His door was always open whenever I faced challenges, and without his steadfast support, this thesis would not have been possible. I am also deeply appreciative of the other members of the McCabe lab: Martin Read, Katie Brookes, and Caitlin E.M. Thornton, whose assistance was essential to the success of my laboratory work. A special mention to Sarinya Wongsanit, whose infectious energy and sense of fun brought light to even the most challenging days in the lab. I would also like to extend my sincere thanks to Professor Vicki Smith and her group, Merve Kocbiyik and Selvambigai Manivannan, for their invaluable support and collaboration throughout this project.

My deepest gratitude extends to my father, who passed away a year ago. His spiritual support throughout my life has been a guiding force, and although he is no longer with me, his influence remains strong. To my Mum, husband, and daughters, who have supported me over the past few years, I cannot thank you enough. Your unwavering belief in me has been a constant source of strength, particularly during the toughest moments of this journey. Finally, to my friends in Birmingham, thank you for the times we spent together and for fostering a friendly, cooperative, and uplifting atmosphere.

Table of Contents

CHAPTER 1 GENERAL INTRODUCTION 1

1.1 The Thyroid Gland and Thyroid Hormones 2
- **1.1.1 An Overview of Thyroid Anatomy 2**
- **1.1.2 Thyroid Hormones: Synthesis and Regulation 4**
- **1.1.3 The Action of Thyroid Hormones 12**
- **1.1.4 Thyroid Dysfunction: Hyperthyroidism and Hypothyroidism 14**

1.2 Thyroid Cancer 16
- **1.2.1 Thyroid Cancer Classification 16**
- **1.2.2 The Epidemiology and Demographics of Thyroid Cancer Worldwide 25**
- **1.2.3 Molecular Pathogenesis and Genetic Alterations in Thyroid Cancer 26**
- **1.2.4. Diagnostic Methods and Treatment of Thyroid Cancer 40**

1.3 The Sodium/Iodide Symporter (NIS) 50
- **1.3.1 Physiological Function of NIS in Thyroid 50**
- **1.3.2 Structural Insights into NIS: Understanding Its Mechanism of Action 52**
- **1.3.3 Regulation of NIS Expression in Thyroid Gland 54**
- **1.3.4 Dysregulation of NIS in Thyroid Cancer 60**
- **1.3.5 NIS Trafficking to the Plasma Membrane 65**
- **1.3.6 NIS Interactome: Its Interaction with PBF, Moesin and VCP 66**

1.4 NIS Importance in Breast Tissue 78
- **1.4.1 NIS Expression in Lactating Mammary Gland 78**
- **1.4.2 NIS in Breast Cancer 80**

1.5 Aims and Hypothesis 84

CHAPTER 2 MATERIALS AND METHODS 87

2.1 Cell Culture 88
- **2.1.1 Source of Cell Lines 88**
- **2.1.2 Providers 89**
- **2.1.3 Growth Conditions and Media 90**
- **2.1.4 Cell Splitting and Seeding 90**

2.2 Primary Thyroid Culture 91

2.3 Plasmid Preparation 92
- **2.3.1 Plasmid AP2σ2 ..... 92**
- **2.3.2 Transformation of DNA into E. coli 93**
- **2.3.3 Plasmid DNA Purification 94**
- **2.3.4 Sequencing 96**

2.4 Site-Directed Mutagenesis of pcDNA3.1-Based Constructs 96

2.5 Transfection 99
- **2.5.1 Plasmids Transfection 99**
- **2.5.2 siRNA Transfection 100**

2.6 Western Blotting 101
- **2.6.1 Protein Harvest 101**
- **2.6.2 Determining Protein Concentration via BCA Assay 102**
- **2.6.3 Western blotting 102**

2.7 Radioiodide Uptake Assay 104

2.7.1 Preparation and Treatment of Cells 104
2.7.2 Radioiodide Uptake Measurement 104

2.8 Bioluminescence Resonance Energy Transfer (BRET) Assay **105**
2.8.1 Introduction of NanoBRET Assay 105
2.8.2 Cell Preparation and Reverse Transfection 107
2.8.3 Luminescence Measurement and NanoBRET Analyses 109
2.8.4 Data Analysis of BRET Assay 109

2.9 Nanoluc Binary Technology (NanoBiT) **110**
2.9.1 Introduction to The NanoBiT Assay 110
2.9.2 Synthesis of Luciferase-Fused Constructs for NanoBiT Assay 111
2.9.3 NanoBiT Assay for Investigating the Interaction between NIS, PBF, AP2σ2 and Moesin 113
2.9.4 Cell Culture and Transfection 114
2.9.5 Cell Harvesting and Assay Preparation 114
2.9.6 NanoBiT Luminescence Measurement 114
2.9.7 Data Transformation and Analysis 115

2.10 Cell Surface Biotinylation Assay **115**

2.11 Statistics **117**

CHAPTER 3 ENHANCING RADIOIODIDE UPTAKE BY ADDRESSING THE MECHANISM OF SODIUM/IODIDE SYMPORTER (NIS) ENDOCYTOSIS ***118***

3.1 Introduction **119**
3.1.1 Introduction to the Mechanisms of Sodium/Iodide Symporter (NIS) Endocytosis 119
3.1.2. The Adaptor Protein 2 (AP2) Complex: Structure, Function, and Involvement in Protein Endocytosis 121

3.2 Materials and Methods **124**
3.2.1 Cell Culture 124
3.2.2 siRNA Transfection 125
3.2.3 Plasmid Preparation and Transfection 125
3.2.4 Western blotting, CSBA and RAI uptake 126
3.2.5 NanoBiT 126
3.2.6 NanoBRET Live Cell Assay 129
3.2.7 Statistical Analysis 130

3.3 Results **130**
3.3.1 NanoBiT Assay for Detecting NIS-AP2S1 Interactions 130
3.3.2 Exploring the Interaction Dynamics of NIS with AP2σ2 135
3.3.3 The Effect of AP2 on Radioiodide Uptake 141
3.3.4 AP2 Alters NIS Subcellular Localisation 142
3.3.5 Real-Time Validation of NIS-PBF Interaction 152
3.3.6 Validation of AP2 Subunit Knockdown 157

3.4 Discussion **159**
3.4.1 Interaction Dynamics of NIS and AP2 159
3.4.2 Functional Impact of AP2 on NIS Localisation and Functionality 162
3.4.3 AP2 and PBF Mediate NIS Endocytosis through the Clathrin-Mediated Pathway 164

CHAPTER 4 MOESIN MODULATES CLATHRIN-MEDIATED NIS INTERNALISATION ***167***

4.1 Introduction **168**

4.2 Materials and Methods **169**

4.2.1 Transient Transfection and siRNA Knockdown 169
4.2.2 Plasmid Preparation 169
4.2.3 NanoBiT Analyses 169
4.2.4 Statistical Analysis 169

4.3 Results **170**
4.3.1 The Effect of AP2 on NIS-Moesin Interaction 170
4.3.2 PBF Knockdown Decrease NIS-Moesin Interaction 172
4.3.3 Moesin Knockdown Increases NIS-PBF Interaction 174
4.3.4 Effect of Moesin Phosphorylation on Interaction with NIS 175

4.4 Discussion **176**
4.4.1 Key Findings 176
4.4.2 Mechanistic Insights 177
4.4.3 Therapeutic Implications 179

CHAPTER 5 THE IMPACT OF VCP INHIBITION ON RAI-UPTAKE IN CANCER CELLS VIA 3 ALTERNATIVE STRATEGIES: (I) CB-5083 AND 5339, (II) CLOTRIMAZOLE ANALOGUES, AND (III) NMS-873 DERIVATIVES 182

5.1 The Effect of CB-5083 and CB-5339 on Radioiodide Uptake in Breast Cancer Cells **183**
5.1.1 Introduction 183
5.1.2 Materials and Methods 187
5.1.3 Results 189
5.1.4 Discussion 196

5.2 Inhibiting VCP Function by Modifying the Structure of Clotrimazole to Improve its Solubility and Effectiveness **197**
5.2.1 Introduction 197
5.2.2 Materials and Methods 204
5.2.3 Results 206
5.2.4 Discussion 217

CHAPTER 6 FURTHER INVESTIGATION INTO NIS DIMERISATION 220

6.1 Introduction **221**

6.2 Materials and Methods **222**
6.2.1 Plasmid Preparation 222
6.2.2 NanoBRET and NanoBiT Assays 223
6.2.3 Western Blot 223
6.2.4 Radioiodide Uptake 223
6.2.5 Statistical Analysis 224

6.3 Results **224**
6.3.1 Impact of K554A and R555A Mutations on NIS Dimerisation Assessed by NanoBiT Assay 224
6.3.2 Mutating Residues of Putative Dimerisation Interface Impairs NIS Function 226
6.3.3 Impact of K554A and R555A Mutations on NIS Protein Expression. 228
6.3.4 Mutating Residues of Putative Dimerisation Interface Affects NIS Plasma Membrane Localisation 229
6.3.5 Impact of K554A and R555A Mutations on NIS Trafficking and Subcellular Localisation 232

6.4 Discussion **237**
6.4.1 Two Mutations Within the Dimerisation Interface Potentially Affect NIS Dimerisation 237

6.4.2 Mutating Residues in the Putative Dimerisation Interface Significantly Impairs NIS Function 238
6.4.3 Impaired Dimerisation Affects NIS Subcellular Localisation 239

CHAPTER 7 CONCLUDING THOUGHTS AND FUTURE DIRECTIONS 241

7.1 Mechanisms of NIS Endocytosis 243
7.1.1 Investigating the Interaction Between NIS and AP2 243
7.1.2 Role of Moesin in NIS Endocytosis 244
7.1.3 Future Directions 244

7.2 Assessing the Impact of VCP Inhibitors CB-5083 and CB-5339 on Radioiodide Uptake in Breast Cancer 246
7.2.1 Future Directions 247

7.3 Optimising Clotrimazole Derivatives and NMS-873 Compounds to Enhance NIS Function and Radioiodide Uptake in Cancer Cells 248
7.3.1 Future Directions 249

7.4 Investigating the Role of NIS Dimerisation 251
7.4.1 Future Directions 252

7.5 Concluding Remarks 253

CHAPTER 8 REFERENCES 255

List of Figures

Figure 1. 1 Thyroid gland anatomy and histology. *3*
Figure 1. 2 The hypothalamic-pituitary-thyroid hormone axis. *6*
Figure 1. 3 Structure of thyroid hormones. *8*
Figure 1. 4 Illustrative representation of thyroid hormone synthesis. *11*
Figure 1. 5 Mechanism of Thyroid Hormone Action. *13*
Figure 1. 6 The derivation of various types and subtypes of thyroid cancer. *17*
Figure 1. 7 Trends in Thyroid Cancer Incidence and Mortality Rates (1992-2022). *26*
Figure 1. 8 The MAPK and related pathways. *37*
Figure 1. 9 The PI3K-AKT signalling pathway and related pathways. *40*
Figure 1. 10 Surgical treatment guidelines for differentiated thyroid cancer. *44*
Figure 1. 11 Secondary structure of the sodium iodide symporter protein. *54*
Figure 1. 12 Regulation of the NUE in Thyroid Cells. *56*
Figure 1. 13 Structure of the PBF protein. *68*
Figure 1. 14 2-D and 3-D structural of Valosin-containing protein (VCP). *72*
Figure 1. 15 Structure of Moesin. *77*
Figure 2. 1 Schematic representation of the NanoBRET assay. *106*
Figure 2. 2 A simplified schematic representation of the NanoBRET assay illustrating subcellular marker localisation and receptor trafficking. *107*
Figure 2. 3 The NanoBiT assay evaluated the interaction between LgBiT and SmBiT tags on two proteins. *111*
Figure 3. 1 Schematic illustrating AP2 subunits and interaction with clathrin and the kinase AAK1. ..... *122*
Figure 3. 2 The structure of AP2. ..... *123*
Figure 3. 3 NanoBiT assay control analysis and validation. *127*
Figure 3. 4 Iodide uptake assessment in HeLa cells with NIS constructs. *131*
Figure 3. 5 Western blot analysis of NIS expression with various tags in HeLa (A) and HEK293 (B) cell lines. *132*
Figure 3. 6 Evaluation of NIS and AP2σ2 interaction using NanoBiT Assays in HEK293 cells. *133*
Figure 3. 7 NanoBiT Assay Analysis of NIS and AP2σ2 interaction in HeLa cells. *134*
Figure 3. 8 Functional implications of putative C-terminal motifs in NIS. *136*
Figure 3. 9 Impact of NIS dileucine and diacidic mutations on AP2σ2 binding. *138*
Figure 3. 10 Influence of AP2σ2 Mutations on NIS Interaction. *140*
Figure 3. 11 Overexpression of WT AP2σ2, AP2σ2 mutant V88D, and AP2σ2 mutant L103S by exogenous transfection affects radioiodide uptake in 8505C-NIS (A) and TPC1-NIS (B) cells *140*
Figure 3. 12 The effect of siRNA transfection on RAI uptake in human primary thyrocytes was assessed for the specified AP2 genes. *141*
Figure 3. 13 Effect of AP2α1 ablation on the cell surface and total NIS protein levels in TPC1-NIS (A) and 8505C-NIS (B) thyroid cancer cell lines. *144*
Figure 3. 14 Total NIS protein (top) and cell surface NIS protein (bottom) in HeLa cells after AP2α1 knockdown and transfection with VO, NIS WT, NIS(E578A/E579A) and NIS (L562A/L563A). *146*
Figure 3. 15 Differential effects of AP2 subunit knockdown on NIS plasma membrane localisation in HEK293 cells. *148*
Figure 3. 16 NanoBRET analysis of the NIS-Kras interaction in HeLa cells following AP2 subunit knockdown. *149*
Figure 3. 17 Differential Impact of AP2α1 knockdown on NIS trafficking across subcellular compartments in HEK293 cells. *151*
Figure 3. 18 Assessment of NIS-PBF interaction in HEK293 cells using NanoBiT assay. *153*
Figure 3. 19 Examination of NIS-PBF interaction in HeLa cells using NanoBiT assay. *154*
Figure 3. 20 Impact of AP2 subunit ablation on NIS-PBF interaction in live HEK293 cells. *155*
Figure 3. 21 NanoBiT assays in HeLa cells transfected with AP2α1, AP2μ2 and AP2σ2 siRNA. *157*
Figure 3. 22 Validation of AP2 subunit knockdown in HEK293 and HeLa cells. *158*
Figure 3.23 Proposed Model of NIS Endocytosis Regulated by PBF and AP2 Complex. *166*
Figure 4. 1 Impact of AP2 subunit knockdown on NIS-moesin interaction in HeLa cells. *171*
Figure 4. 2 PBF knockdown reduces NIS-moesin interaction in HeLa cells. *173*
Figure 4. 3 Moesin knockdown increases NIS-PBF interaction. *174*

Figure 4. 4 Interaction of NIS with wild-type and phosphorylation site mutant moesin (T558A and T558D) in HeLa and HEK293 cells. *176*
Figure 4. 5 siRNA-mediated silencing of moesin resulted in significant increases in radioiodide uptake in TPC1-NIS and 8505C-NIS cell lines. *177*
Figure 4. 6 Putative model of the endocytotic processing of NIS. *180*
Figure 5. 1 The VCP inhibitors CB-5083 and CB-5339 increase radioiodide uptake in TPC1-NIS thyroid cells and L87-NIS cells. *186*
Figure 5. 2 Effect of the VCP inhibitor CB-5083 on radioiodide uptake and protein levels of NIS in breast cancer lines. *190*
Figure 5. 3 Effect of the VCP inhibitor CB-5083 on radioiodide uptake and NIS and VCP protein levels in SUM-52 (left), ZR-75-1 (right) cells after 24 hours of treatment. *192*
Figure 5. 4 Effect of the VCP inhibitor CB-5339 on radioiodide uptake in breast cancer lines after treatment for 24 hours. *194*
Figure 5. 5 Figure 5.5 Effect of the second-generation VCP inhibitor CB-5339 on radioiodide uptake in SUM-52 and ZR-75-1 breast cancer cell lines after 24 hours of treatment. *195*
Figure 5. 6 Modification of clotrimazole and impact on RAI uptake. *200*
Figure 5. 7 Redesign of compound-17 into GB002 using an overlapping model with the VCP inhibitor UPCDC30425. ..... *201*
Figure 5. 8 Predicted logP values of various VCP inhibitors. *203*
Figure 5. 9 CryoEM of NMS873 docking to VCP. *204*
Figure 5. 10 Effects of GB002 on radioiodide uptake in NIS-expressing cell lines. *207*
Figure 5. 11 Modification to the structure of NMS-873 resulted in new compounds. *209*
Figure 5. 12 Effect of compounds 22–25 and SAHA on radioiodide uptake in TPC1-NIS cells after 24 hours of treatment. *212*
Figure 5. 13 Effect of NMS-873 analogues on iodide uptake in 8505C-NIS cells after 24 hours of treatment. ... *214*
Figure 5. 14 Effect of compounds 22–25 on radioiodide uptake in MDA-NIS cells after 24 hours of treatment. *214*
Figure 5. 15 Effects of compounds 22–25 on radioiodide uptake in NIS-expressing cell lines in combination with SAHA (2.5 µM) or SAHA alone after 24 hours of treatment. *216*
Figure 5. 16 Effects of compounds 22-25 on NIS-VCP interaction. *217*
Figure 6. 1 Using the refined NIS homology model, eight novel residues were identified as potentially involved in NIS dimerisation. *222*
Figure 6. 2 The influence of putative dimerisation motifs on NIS dimerisation was assessed via NanoBiT assays. *225*
Figure 6. 3 Radioiodide uptake assay for NIS mutations. *227*
Figure 6. 4 Mutating residues within the putative dimerisation interface alters NIS expression. *228*
Figure 6. 5 Live cell kinetic measurement of NIS-Kras interaction in HEK293 cells. *230*
Figure 6. 6 Live cell kinetic measurement of NIS-Kras interaction in HeLa cells. *231*
Figure 6. 7 NanoBRET analysis of NIS-Rab1 interaction in HEK293 cells (A for K554A, B for R555A, C for K554A/R555A). *233*
Figure 6. 8 NanoBRET analysis of NIS-Rab1 interaction in HeLa cells. *235*
Figure 6. 9 Impact of NIS mutations on interaction with Rab9 in HEK293 cells. *236*

List of Tables

Table 2- 1 Seeding densities for each cell line used in experiments with 6-well and 24-well plates.....91
Table 2- 2 Oligonucleotides used for plasmid sequencing in this study, provided by Source Bioscience UK. 96
Table 2- 3 Primer sequences employed for mutagenesis in this study. 97
Table 2- 4 PCR thermocycler conditions for gene mutagenesis.....98
Table 2- 5 Commercially sourced siRNA products utilised in this study.....101
Table 2- 6 Antibodies utilised in this study for Western blot analysis.....103
Table 2- 7 Catalog and origin of all genes of interest utilised in the NanoBRET assay.....108
Table 2- 8 PCR primers for amplifying genes of interest before insertion into pcDNA3.1 (+) with LgBiT tags were designed as follows:.....112
Table 2- 9 PCR primers for amplifying SmBiT tag onto gene interest.....113
Table 3- 1 Transfection combinations for the NanoBiT assay.....128
Table 3- 2 Transfection combinations for the reverse NanoBiT assay. 129

List of Abbreviations

AAK1	AP2-associated kinase 1
AKT	Protein kinase B
ANOVA	Analysis of variance
AP2	Adaptor protein complex 2
ATC	Anaplastic thyroid carcinoma
cAMP	Cyclic adenosine monophosphate
CCPs	Clathrin-coated pits
CCSs	Clathrin-coated structures
CCVs	Clathrin-coated vesicles
cDNA	Complementary deoxyribonucleic acid
$ClO4^-$	Perchlorate
CNS^-	Thiocyanate
CME	Clathrin-mediated endocytosis
CO-IP	Co-immunoprecipitation
COOH	Carboxylic Acid
CREB	cAMP-responsive element binding protein
CT	Computed tomography
D1	Deiodinase type I
D2	Deiodinase type II
DCIS	Ductal carcinoma in situ
DIT	Di-iodotyrosine
DMSO	Dimethyl sulfoxide
DNA	Deoxyribonucleic acid
DTC	Differentiated thyroid cancer
DUOX	Dual oxidases
EAF	Endocytic accessory factor
EBRT	External beam radiation therapy
ER	Endoplasmic reticulum
ERAD	Endoplasmic reticulum-associated degradation
FBS	Foetal bovine serum
FDA	Food and Drug Administration
FNAB	Fine needle aspiration cytology
FOXE1	Forkhead box protein E1
FTA	Follicular thyroid adenomas
FTC	Follicular thyroid carcinoma
GTP	Guanosine triphosphate
HDACi	Histone deacetylase inhibitors
H_2O_2	Hydrogen peroxide
HBSS	Hank’s balanced salt solution

HCC	Hürthle cell carcinoma
HER2	human epidermal growth factor receptor 2
hNIS	Human sodium iodide symporter
IDC	Infiltrating ductal carcinoma
ILC	Infiltrating lobular carcinoma
IGF-1	Insulin-like growth factor 1
LB	Lysogeny broth
LCIS	Lobular carcinoma in situ
logP	Partition coefficients
MAPK	Mitogen Activated Protein Kinase
MCT	Medullary Thyroid Carcinoma
MCT8	Monocarboxylate transporter 8
MIT	Mono-iodotyrosine
MMPs	Matrix metalloproteinases
MRI	Magnetic resonance imaging
mTOR	Mammalian target of rapamycin
NaCl	Sodium chloride
NIS	Sodium/iodide symporter
NKX2-1	Homeobox-containing transcription factor
NPL4	Nuclear protein localisation protein 4
NTF-2	TSH-responsive factor-1
NUE	NIS upstream enhancer
ORF	Open reading frame
OTC	Oncocytic thyroid carcinoma
PAX8	Paired-Box 8
PBF	Pituitary tumor-transforming gene-binding factor
PBS	Phosphate buffered saline
PDK1	3-phosphoinositide-dependent protein kinase 1
PDTC	Poorly differentiated thyroid cancer
PET	positron emission tomography
PI3K	Phosphoinositide 3-kinase
PIP2	phosphatidylinositol 4,5-bisphosphate
PIP3	phosphatidylinositol 3,4,5-trisphosphate
PKA	Protein kinase A
PM	Basolateral plasma membrane
PPARγ	Peroxisome proliferator-activated receptor gamma
PPFP	PAX8/PPARγ fusion protein
PR	Progesterone
PRRT	Peptide Receptor Radionuclide Therapy
PTC	Papillary thyroid cancer
PTEN	Phosphatase and tensin homolog

PTTG1	pituitary tumor-transforming gene-1 product
PVDF	Polyvinylidene difluoride
RET	Rearranged during transfection
rhTSH	Recombinant human TSH
RIPA	Radioimmunoprecipitation assay
RPMI	Roswell Park memorial institute
RR-DTC	Radioiodine-refractory differentiated thyroid cancer
RT-PCR	Reverse transcriptase polymerase chain reaction
rT3.	3,3',5'-triiodothyrone
RXR	Retinoid X receptor
SAHA	Suberoylanilide hydroxamic acid
SDS	Sodium dodedecyl sulphate
SDS-PAGE	SDS- polyacrylamide gel electrophoresis
SEER	The Surveillance, Epidemiology, and End Results
siRNA	Short interfering ribonucleic acid
T2	3,3'-diiodothyronine
T3	Triiodothyronine
T4	Thyroxine
TBST	Tris-buffered saline with Tween
TCGA	The Cancer Genome Atlas
TERT	Telomerase reverse transcriptase
TG	Thyroglobulin
TGFβ	Transforming growth factor β
TH	Thyroid hormones
TKIs	Tyrosine kinase inhibitors
TKR	Tyrosine-kinase receptor
TNBC	Triple-negative breast cancers
TPO	Thyroid peroxidase
TR	Thyroid hormone receptor
TREs	Thyroid hormone response elements
TRH	Thyrotropin releasing hormone
TSH	Thyroid-stimulating hormone, thyrotrophin
TSHR	Thyroid stimulation hormone receptor
TTF-1	Thyroid transcription factor 1
UBXD1	UBX domain-containing protein 1
UPS	Ubiquitin-proteasome system
VCP	Valosin-containing protein
VEGF	Vascular endothelial growth factor
VEGFR	Vascular endothelial growth factor receptor
VO	Vector only
WDTC	Well-differentiated thyroid cancers

WT	Wildtype
µg	Microgram
µl	Microlitre
µM	Micromolar

CHAPTER 1 GENERAL INTRODUCTION

CHAPTER 1 GENERAL INTRODUCTION

1.1 The Thyroid Gland and Thyroid Hormones

1.1.1 An Overview of Thyroid Anatomy

The thyroid gland, which plays a critical role in the human endocrine system, originates from the pharyngeal pouch and migrates from the foramen cecum at the base of the tongue to its pre-tracheal position during embryonic development (Rosen et al., 2024). This migration is a complex, highly orchestrated process involving an array of genetic and molecular cues. Anomalies in this process can result in ectopic thyroid tissue, potentially leading to thyroid dysfunction (Felice et al., 2004; Zimmermann et al., 2015).

As the thyroid descends, it passes anterior to the hyoid bone and the laryngeal cartilages, ultimately forming a bilobed structure connected by an isthmus, typically inferior to the thyroid cartilage. Occasionally, a pyramidal lobe extends upward from the isthmus, a remnant of the thyroglossal duct, the original path of thyroid descent, which in most cases atrophies and disappears (Nilsson et al., 2017). By around the 10th week of gestation, the thyroid gland has usually reached its definitive location and begins the synthesis of thyroid hormones, marking the functional onset of the gland (Patel et al., 2011; Szinnai et al., 2007). The “normal” thyroid sits posteriorly to the neck muscles and is anchored to the trachea via Berry’s ligament within the pre-tracheal fascia-encased visceral neck compartment (Figure 1.1A). Despite its typical symmetry and central isthmus, the thyroid exhibits significant anatomical variations, including differences in arterial origins, venous drainage patterns and structural anomalies such as pyramidal lobe, ectopic thyroid tissue, or the absence of the

isthmus, all of which have critical surgical and clinical implications (Al-Azzawi et al., 2021).

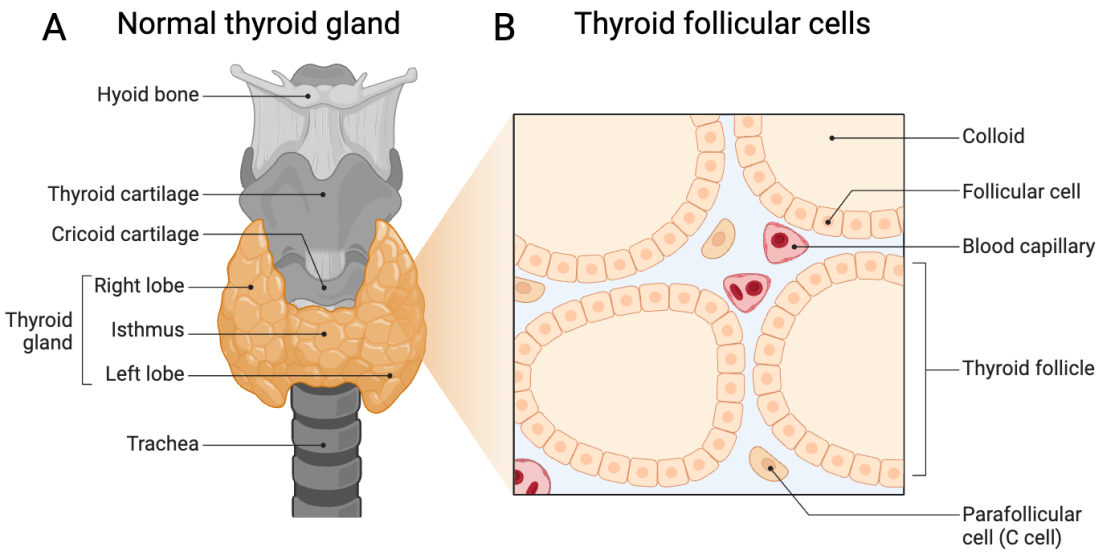


Figure 1. 1 Thyroid gland anatomy and histology. *(A) The thyroid gland in the anterior neck consists of two lobes and an isthmus. (B) Thyroid follicles with a colloid-filled lumen surrounded by follicular epithelial cells. Also shown are parafollicular cells and capillaries between the follicles. (Created with BioRender.com)*

The histological organisation of thyroid tissue determines thyroid hormone biosynthesis. The adult thyroid gland comprises follicles, considered the thyroid gland's functional units, consisting of a polarised single layer of follicular epithelial cells called thyrocytes and follicular lumen surrounded by follicular epithelial cells (Figure 1.1 B). The interior of the follicle is filled with colloids, mainly composed of thyroglobulin. This glycoprotein provides the skeleton for synthesising thyroid hormones and is close to the apical plasma membrane of thyrocytes. The outside of the follicle contacts the blood capillaries between the basolateral plasma membrane of thyrocytes. The parafollicular or C cells are between the follicular cells. They are responsible for calcitonin secretion, a hormone that modulates the concentration of calcium ions in

the blood and plays an essential regulatory role in bones and kidneys (McLaughlin et al., 2023).

Collectively, the primary of the thyroid gland is to utilise iodine to synthesise and release the hormones triiodothyronine (T3) and thyroxine (3,5,3',5'—tetraiodothyronine, T4), which are essential for differentiation, development and metabolic regulation (Boelaert et al., 2005). It also produces calcitonin through parafollicular cells to maintain calcium homeostasis (Carvalho et al., 2017).

1.1.2 Thyroid Hormones: Synthesis and Regulation

As noted, thyroid hormone plays a vital role in development, growth, heart rate, thermogenesis and metabolism, and is regulated by complex positive and negative regulation mechanisms. The primary surveillance regulation mechanism is the hypothalamic-pituitary-thyroid (HPT) hormone axis (Figure 1.2). Hypothalamic thyrotropin-releasing hormone (TRH) is secreted from the hypothalamus and stimulates thyroid-stimulating hormone (TSH) synthesis and release from the anterior pituitary. Hypothalamic TRH plays a critical role in the biosynthesis of thyrotropin by affecting TSH transcription levels and posttranscriptional oligosaccharide chain glycosylation, which is crucial for TSH's normal physiological functions (Persani, 1998). Additionally, TRH binds to G protein-coupled TRH receptors on anterior pituitary cells, triggering intracellular cAMP signalling to stimulate TSH release (Gershengorn, 1993; Hershman, 1974). Subsequently, TSH regulates the expression of thyroid genes by binding to TSH receptors on the thyroid gland and stimulates the synthesis and release of T3 and T4, primarily T4, from the gland (Vassart et al., 1992). At the same time,

expression of the TSH and TRH genes located in the medial and periventricular subdivisions neurons of the hypothalamic paraventricular nucleus (PVN), are negatively controlled by the concentration of thyroid hormones in the bloodstream (Koller et al., 1987; Lechan et al., 1994).

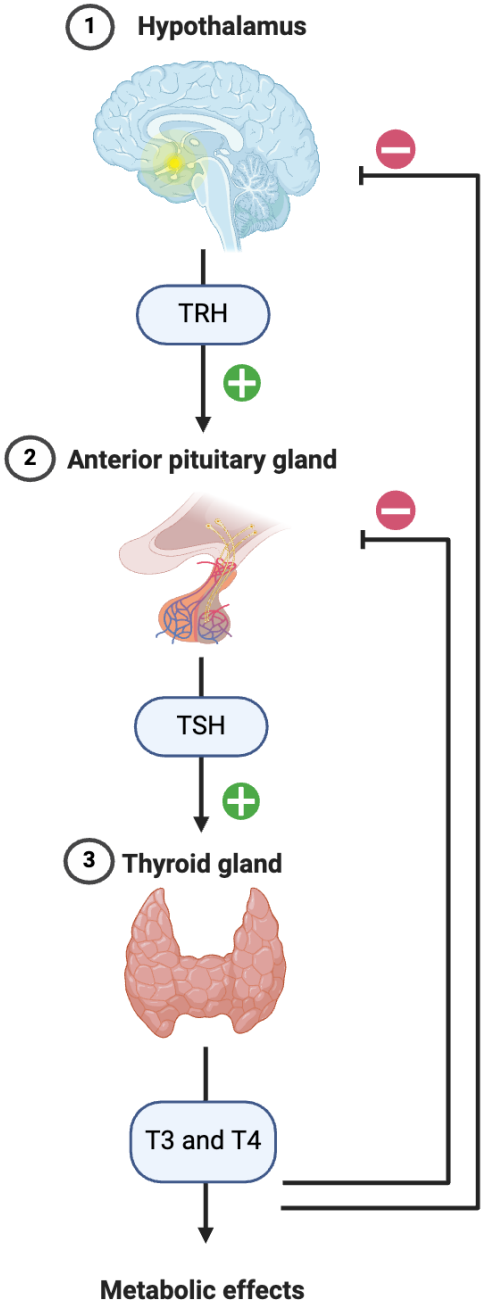


Figure 1. 2 The hypothalamic-pituitary-thyroid hormone axis. *This axis controls the production of thyroid hormones through negative feedback loops. The hypothalamus secretes thyrotropin-releasing hormone (TRH), which stimulates the anterior pituitary gland to release thyroid-stimulating hormone (TSH). TSH acts on the thyroid gland to promote the synthesis and secretion of triiodothyronine (T3) and thyroxine (T4), hormones essential for regulating metabolism. Elevated levels of T3 and T4 inhibit TRH and TSH secretion at the hypothalamic and pituitary levels, forming a classical negative feedback loop to maintain hormonal balance.*

When the concentration of T3 or T4 is high in the bloodstream, then the level of T3, which is converted from peripheral T4 by tanycytes in the third ventricle through deiodinase type II (D2) and can enter TRH neurons in the PVN with the help of the monocarboxylate transporter 8 (MCT8), also increases, thereby inhibiting hypophysiotropic TRH and TSH gene expression and production (Fonseca et al., 2013; Segerson et al., 1987; Visser, 2007).

On the contrary, a low level of TH can, in turn, stimulate the synthesis and release of hypophysiotropic TRH and TSH. In summary, these three types of hormones form a classical endocrine negative feedback loop. This regulation is mostly through thyroid hormone receptor (TR) isoform TRβ2, which can interact with the promoters of TRH and thyrotropic genes and then modulate these genes' expression (Chiamolera et al., 2009; Wondisford et al., 1989).

As above, the thyroid gland synthesises and secretes two hormones, T4 and T3. Both hormones contain iodine atoms as part of their molecular structure (Figure 1.3); therefore, iodine ions play an essential role in hormone synthesis.

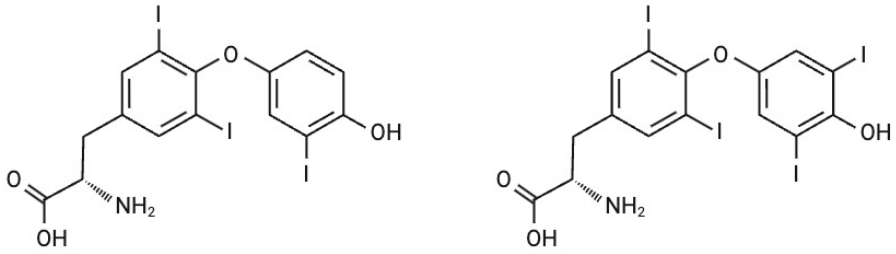


Figure 1. 3 Structure of thyroid hormones. *Thyroid hormones T3 (triiodothyronine) and T4 (thyroxine) are iodine-containing hormones produced by the thyroid gland. The chemical structure of T3 includes three iodine atoms, while T4 contains four. Both hormones are derived from the amino acid tyrosine and are crucial for regulating metabolism in the body.*

The ability of thyroid follicle cells to uptake iodine from the bloodstream, primarily dietary intake absorbed from the small intestine and stomach, is the first step for TH production. This critical step is mediated by the sodium/iodide symporter (NIS, encoded by SLC5A5), a transmembrane protein located in the basolateral plasma membrane of thyroid follicular cells (Mauchamp et al., 1998; Rohner et al., 2014; Smanik et al., 1996). The concentration of iodine ions in thyroid follicles is 20 to 40 times higher than in plasma (Kaminsky et al., 1994). The function of NIS is to transport iodine ions from the bloodstream through the basolateral plasma membrane inward to the cytosol of thyrocytes, and this process requires a differential Na^+ gradient (high concentration in the bloodstream and low concentration intracellularly), which is maintained by the Na^+/K^+ ATPase pump at the plasma membrane. Then, NIS mediates two Na^+ ions along the gradient and one I^- ion against the electrochemical gradient

inward to the thyroid follicular cells (Carrasco, 1993). A similar iodide transport is also found in extrathyroidal tissues, such as the salivary glands, stomach, choroid plexus, lacrimal gland, ciliary body and lactating mammary gland, but TSH regulation of NIS expression and iodide uptake only occurs in the thyroid (Cavalieri, 1997; Wolff, 1964). In the thyroid, TSH stimulates NIS gene expression and activity, thereby increasing iodide uptake into the thyrocytes through Gs α Protein activated adenylate cyclase (Kaminsky et al., 1994).

Conversely, iodide uptake is directly inhibited by competitive inhibitors like thiocyanate and perchlorate (Serrano-Nascimento et al., 2022). The uptake of iodide is diminished when thyrocytes are exposed to a high dose of iodine; this is called the Wolff-Chaikoff effect, first reported in 1948 (Wolff et al., 1948). The Wolff-Chaikoff effect is self-limited, however, with thyrocytes escaping this mechanism after several days of exposure (Braverman et al., 1963; Eng et al., 1999).

After iodide is internalised into the follicles mediated by NIS, it is moved across the apical plasma membrane into the colloid, a process termed “iodide efflux”. Studies show that this process depends on specific transporters located at the apical plasma membrane, such as pendrin, chloride channel 5 (CLC5) and anoctamin-1 (Iosco et al., 2014; Scott et al., 1999; van den Hove et al., 2006).

Once I^- translocates into the colloid, in the presence of adequate hydrogen peroxide (H_2O_2) on the apical membrane, thyroid peroxidase (TPO) catalyse iodide oxidation and incorporation into thyroglobulin (TG) tyrosine residues to produce di-iodotyrosine (DIT) and mono-iodotyrosine (MIT) (Citterio et al., 2019). This process is named

“iodide organification ” due to oxidising iodide and adding it to TG protein. Thyroidal H_2O_2, the essential reducing agent in this step, is produced by a member of the NADPH oxidase family isoform known as dual oxidase 2 (DUOX2) (Szanto et al., 2019). TG is a 660 kDa thyroid-specific glycoprotein synthesised in the rough endoplasmic reticulum and secreted into the follicular lumen via the exocytosis pathway as a pivotal scaffold to provide tyrosine residues for iodination during iodide organification. Its expression is regulated by transcription factors such as Paired-Box 8 (PAX8), homeobox-containing transcription factor (NKX2-1), the forkhead box protein E1 (FOXE1) and their coactivator p300 (Grasberger et al., 2005; Ma et al., 2017). Subsequently, TPO catalyses the coupling of one MIT with one DIT to form T3 or two DIT molecules to form T4, which remain bound to the TG molecule and also formate a few 3,3’,5’-triiodothyrone (reverse T3, rT3), 3,3’-diiodothyronine (T2) and monoiodothyronine moeties (Carvalho et al., 2017). Two molecules of DIT coupling produce T4, which has lower biological activity than T3, but accounts for approximately 80 % of thyroid hormone production (Sapin et al., 2003).

Post coupling, the incorporated TG undergoes endocytosis via macro- and micro-pinocytosis and is re-internalised into the thyrocytes, where proteolytic enzymes cleave and release three different isomers of thyroid hormones: T3, rT3 and T4 from the polypeptide backbone, leading to thyroid hormones effluxing through the basolateral plasma membrane into the bloodstream via MCT8. Other thyroglobulin lysis products, such as iodine tyrosine compounds, are de-iodinated by iodotyrosine dehalogenase (DEHAL1) for iodide recycling. TSH stimulates the complex thyroglobulin trafficking and degradation processes (Brix et al., 1996). However, for the more bioactive hormone T3, only ~20 % of daily produce is originally from the

thyroidal secretion. Importantly, T4 is converted to T3 through by type 1 deiodinase (D1) and type 2 deiodinase (D2) in peripheral tissues, such as the kidney, liver, and skeletal muscles, and D2 is a well-known primary deiodinase enzyme responsible for producing intracellular T3 from the prohormone T4 in specific tissues (Maia et al., 2005). Moreover, the type 3 de-iodinating enzyme (D3) catalyses the inactivation of thyroid hormones rT3 and T2 through the inner ring deiodination of T4 and T3 as inert metabolites (Hulbert, 2000) (Figure 1.4).

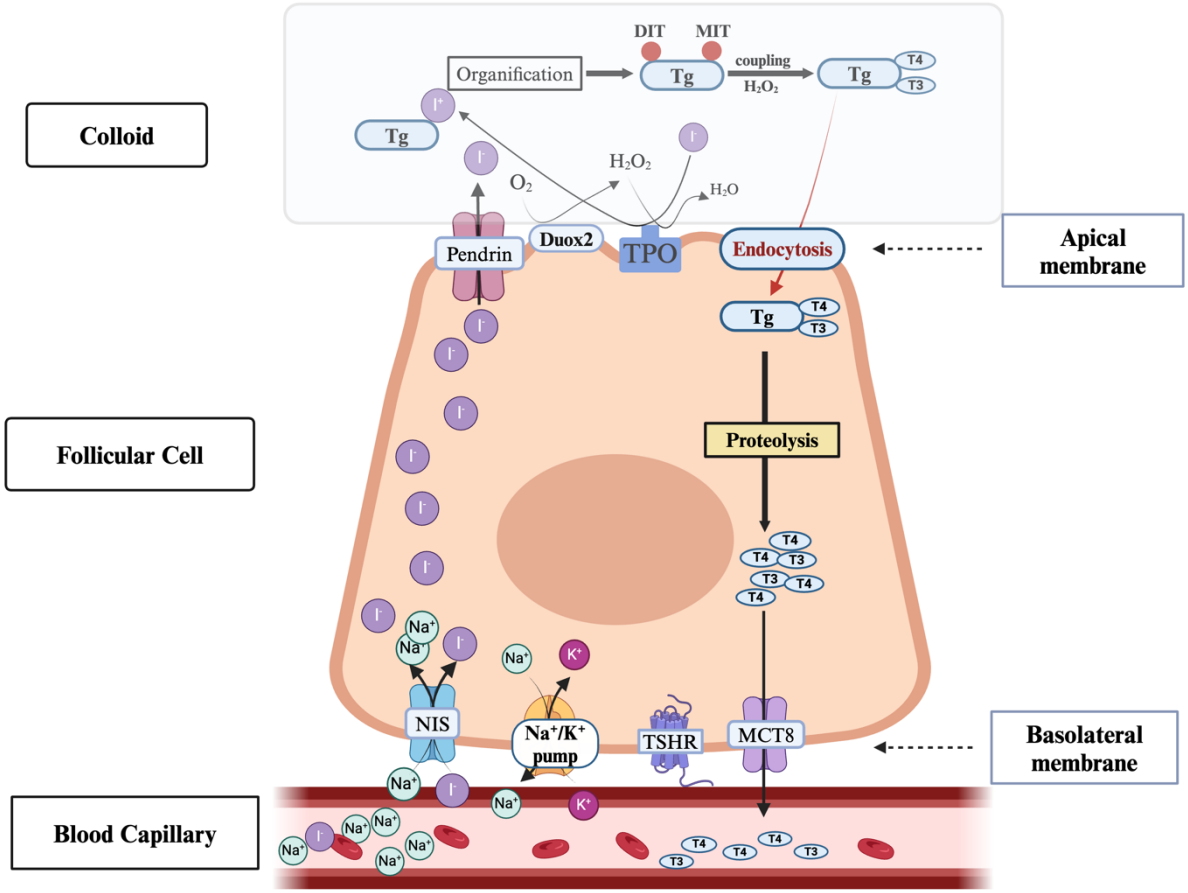


Figure 1. 4 Illustrative representation of thyroid hormone synthesis. *The process begins with NIS facilitating the entry of iodide (I-) from the circulatory system into the thyroid follicular cell. I- is then transported into the follicular lumen via the pendrin channel. Once in the lumen, iodide is oxidised to iodine by TPO, with H2O2 being produced by the enzyme DUOX2. Subsequently, Tg undergoes iodination to form MIT and DIT. Combining these iodinated tyrosines forms T3- and T4-tagged thyroglobulin complexes. These complexes are reabsorbed into the follicular cells, merging with lysosomes, leading to Tg breakdown and the release of T3 and T4. These thyroid hormones are then exported into the bloodstream through MCT8.*

1.1.3 The Action of Thyroid Hormones

It is recognised that T3 exhibits a significantly higher affinity for thyroid hormone receptors (TRs) than T4, and is known as a biologically active hormone (Wejaphikul et al., 2019). Therefore, intracellular thyroid hormone action is mediated by the local T3 available for interacting with the target cells' nuclear-specific TRs. TRs function as transcriptional modulators by binding to thyroid hormone response elements (TREs). TRs can form heterodimers with the retinoid X receptor (RXR), enhancing their binding to the TREs. Unliganded TR can repress target gene transcription by recruiting nuclear protein corepressor complexes, while T3 binding to the ligand binding domain of TRs induces a conformational change in TR, disrupting TR interaction with corepressor and leading to another nuclear protein coactivator recruitment, thereby chromatin remodelling, and activated thyroid hormone-responsive genes transcription. This process is critical for normal development, growth, and metabolic regulation (Brent, 2012; Zhang et al., 2000) (Figure 1.5).

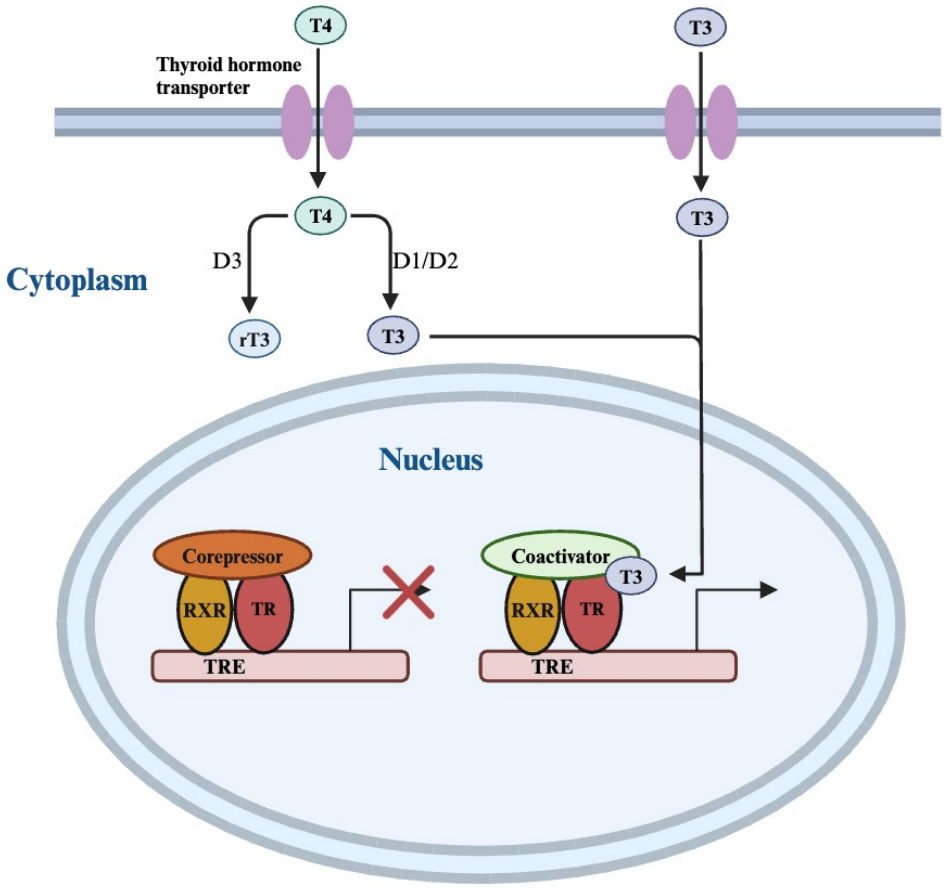


Figure 1. 5 Mechanism of Thyroid Hormone Action. *Specific transport proteins, such as MCT8, facilitate the cellular uptake of thyroid hormones T4 and T3 in select organs like the brain. Without a ligand, TR forms heterodimers with RXR and attaches to TREs on DNA, associating with corepressors such as NCoR or SMRT to inhibit gene transcription. When T3 binds to its receptor's ligand-binding domain, it triggers a conformational shift in helix 12, detaching the corepressor and enabling coactivator attachment. This interaction subsequently attracts polymerase III, initiating the transcription of target genes. Figure adapted from (Brent, 2012).*

However, recent data show that TH actions also involve many rapid non-genomic mechanisms of action. These are independent of intracellular T3 and T3-TR-TREs complexes forming and occurring outside of the nucleus, and hence defined as “non-genomic actions”, distinct from the classic modulation of target gene transcription pathways (Cheng et al., 2010). Thyroid hormone exerts non-genomic actions through several pathways. It requires the receptors located on integrin αvβ3 close to the Arg-

Gly-Asp recognition site, which comprises two binding domains: a T3 binding domain site (S1) and a T3/T4 binding domain site (S2), both unrelated to TRs according to crystallographic and mathematical modelling (Lin et al., 2011). However, it has been recognised that S2 exhibits a higher affinity for T4 than T3 (Hercbergs, 2019). The S1 domain triggers the phosphoinositide 3-kinase (PI3K) /PKB (AKT) pathway, regulating cell proliferation and intracellular-specific protein trafficking to enter the nucleus. The S2 domain facilitates the nuclear translocation of TRβ1 and stimulates the proliferation of tumour cells by activating mitogen-activated protein kinases (MAPK1 and MAPK2).

1.1.4 Thyroid Dysfunction: Hyperthyroidism and Hypothyroidism

As mentioned above, THs act on almost all nucleated cells and tissues through genomic or non-genomic pathways and play a critical role in regulating normal growth, metabolism, and development. Dysfunction of the thyroid gland, whether overactive thyroid (hyperthyroidism) or underactive thyroid (hypothyroidism), is a common occurrence. While thyroid dysfunction is typically identifiable and amenable to treatment, a lack of proper management can result in significant adverse outcomes.

Overt hyperthyroidism is characterised by suppressed serum thyrotropin (TSH) levels and elevated serum concentrations of T3, T4, or both. Globally, the incidence of overt hyperthyroidism ranges from approximately 0.2 % to 1.4 % (Lee et al., 2023). Meanwhile, subclinical hyperthyroidism is defined by low serum TSH levels with normal serum T3 and T4 levels, although determining its precise prevalence in the world population is challenging due to variations in diagnosis thresholds utilised across epidemiological studies. Hyperthyroidism has various causes, with Graves' disease,

an autoimmune disorder where antibodies stimulate TSH receptors on thyroid follicular cells, being the most common. Other causes include toxic multinodular goitre, autonomously functioning thyroid adenomas, thyroiditis, pituitary TSH-secreting adenoma and drug-induced hyperthyroidism (Taylor et al., 2018). Additionally, proptosis is a key symptom often associated with hyperthyroidism, particularly in cases involving Graves' disease (Lindholm et al., 2010). Untreated hyperthyroidism typically presents with symptoms such as weight loss, cardiac problems, nervousness, anxiety, increasing sweating, and diarrhoea (Johnson et al., 1992). Treatment modalities for hyperthyroidism include antithyroid medications, beta-blockers, radioiodine therapy, and surgery.

Overt hypothyroidism is characterised as TSH levels above the reference range and free thyroxine levels below the reference range. The prevalence in the general population varies by region, with estimates ranging from 0-3 % to as high as 3-7 % in the USA and 0-2 % to 3-5 % in Europe, depending on the criteria for diagnosis. Additionally, the distribution of hypothyroidism is higher in areas with either excessive or severe insufficient dietary iodine and predominantly affects women and older people (>65 years) (Chaker et al., 2017). Subclinical hypothyroidism is defined by TSH levels above the reference range with regular free thyroxine levels, and the incidence is more common in iodine-sufficient areas. The prevalence of subclinical hypothyroidism ranges from 4 to 20 % in adult populations; this relatively broad range is determined by age, sex, body mass index, race, dietary iodine intake, and the TSH reference range (Cooper et al., 2012).

The causes of hypothyroidism can be divided into primary (thyroid hormone deficiency), central (thyrotrophin-secreting deficiency or TRH deficiency), and peripheral (extra-thyroidal). Primary accounts for the majority of cases, frequently stemming from chronic autoimmune thyroiditis (Hashimoto's disease), characterised by elevated thyroid peroxidase antibody levels. Clinically, overt hypothyroidism manifests in a variety of ways and is often non-specific, such as fatigue, cold intolerance, weight gain, skin dryness, constipation and increased risk of cardiovascular disease. However, many patients with subclinical hypothyroidism usually have no obvious clinical symptoms. Regarding treatment, levothyroxine monotherapy is standard, intending to normalise TSH concentration and resolve clinical symptoms without over or under-treatment (Jansen et al., 2023; Peeters, 2017).

1.2 Thyroid Cancer

1.2.1 Thyroid Cancer Classification

Thyroid cancer is a malignant neoplasm originating from thyroid follicular cells or thyroid para-follicular C cells (Pryma et al., 2014). It is broadly categorised into four main histological types: well-differentiated thyroid cancer, medullary thyroid carcinoma, anaplastic thyroid carcinoma and poorly differentiated thyroid cancer (Cabanillas et al., 2016). Well-differentiated thyroid cancer (WDTC), stemming from thyroid follicular epithelial cells, includes papillary thyroid cancer, follicular thyroid cancer and oncocytic thyroid cancer and comprises the majority (more than 95%) of all thyroid malignancies (Figure1.6).

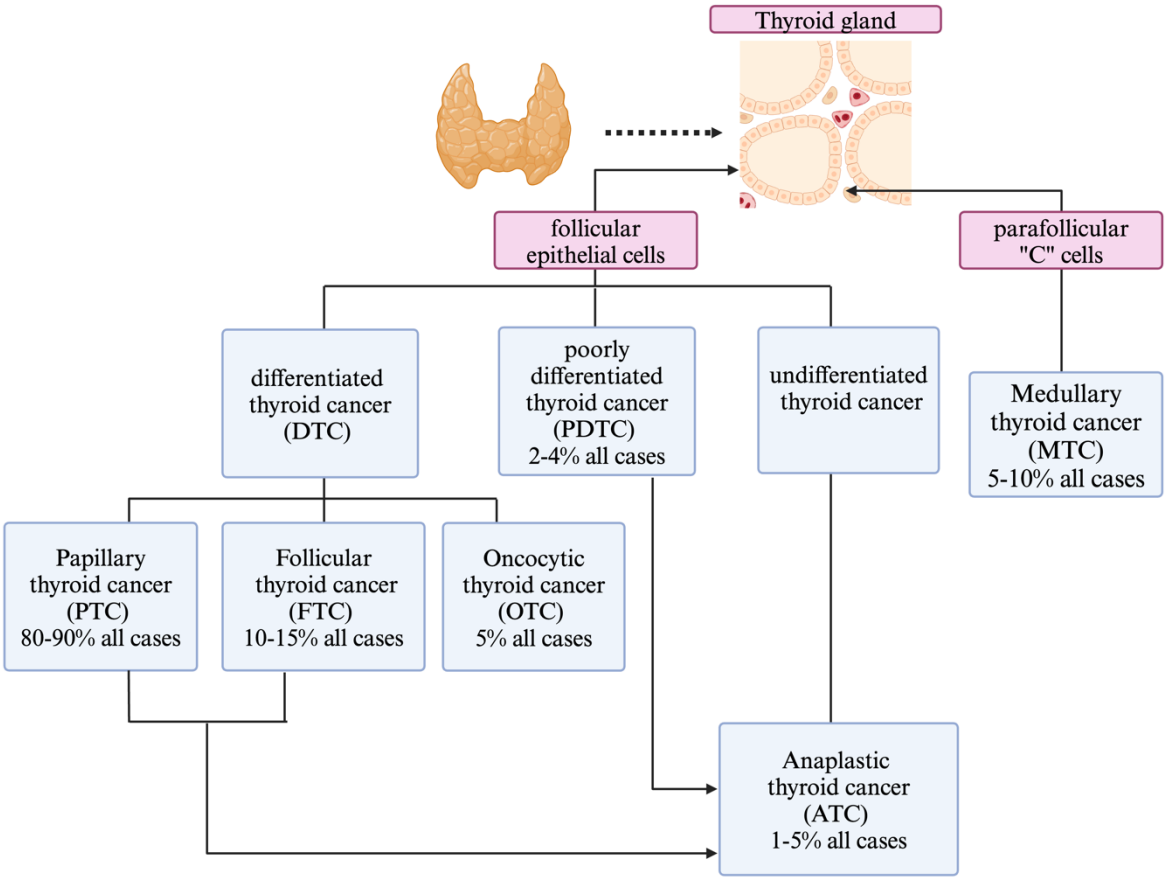


Figure 1. 6 The derivation of various types and subtypes of thyroid cancer. *Thyroid cancer arises from two primary cellular lineages within the thyroid gland: follicular epithelial cells and parafollicular "C" cells. Differentiated thyroid cancer (DTC), encompassing papillary thyroid cancer (PTC), follicular thyroid cancer (FTC), and oncocytic thyroid cancer (OTC), represents the majority of thyroid cancer cases. Poorly differentiated thyroid cancer (PDTC) can occur de novo or develop as a result of progression from DTC subtypes such as PTC and FTC, serving as a transitional state between differentiated and undifferentiated cancers. Anaplastic thyroid cancer (ATC), the most aggressive form, may arise directly from follicular epithelial cells or evolve from PTC, FTC, or PDTC. Medullary thyroid cancer (MTC), arising from parafollicular "C" cells, accounts for 5–10% of cases and is distinct in its origin and biology. Figure and data adapted from (Hofmann et al., 2022; Ibrahimpasic et al., 2019; Pstrąg et al., 2018; Rosai et al., 2017).*

1.2.1.1 Papillary Thyroid Cancer

Papillary thyroid cancer (PTC) is the most frequent subtype of WDTC, comprising 80-90 % of all thyroid carcinomas. Furthermore, PTC tends to be biologically indolent and

generally carries the best overall prognosis despite lymph node metastasis, and the 5-year survival rate of patients can be over 90 % (Ito et al., 2018). However, approximately 10 % of PTC patients will develop distant metastasis, such as cervical lymph node, lung and bone (Hoie et al., 1988; Katoh et al., 2015). Approximately two-thirds of these patients respond well to radioiodine treatment and exhibit a 10-year survival rate of ~60 %. In comparison, the remaining one-third are resistant to radioiodine therapy and face a markedly poor prognosis with a 10-year survival rate of 10-63 % (Shen et al., 2024). PTC has multiple risk factors, and radiation exposure is a crucial factor, especially during childhood exposure or medical high-dose radiation therapy (Mao et al., 2017). Genetic factors, dietary iodine intake, pre-existing benign thyroid disease and being overweight or obese are associated with PTC (Limaiem et al., 2024). Notably, PTC is more common in women than men, being approximately three times higher. Women typically develop the disease at a younger age, and the peak is in their forties, while men tend to peak in their sixties years. However, the incidence rates become equalised by the age of 85 years. Despite women having an earlier onset, male patients often face more aggressive disease at diagnosis, and this is linked to lower disease-free survival and high mortality rates. The causes of PTC gender disparity are poorly understood (Rahbari et al., 2010).

PTC displays diverse gross appearances, ranging from firm, white lesions with calcification to scar-like features, often subcapsular. Cyst formation may be observed, occasionally leading to diagnostic challenges. The cells of PTC have a papillary (‘finger-like’) configuration, and nuclear features in PTC are usually characterised as transparent, enlarged, ground glass, oval shape, and hypodense chromatin, and they frequently overlap each other (Xing, 2013). Roughly 50 % of PTCs belong to the

classical subtype (cPTC), while the remaining 50 % comprise less common histological variants. These variants include the tall cell variant, diffuse sclerosis variant, solid variant, and follicular variant of papillary cancer subtypes (LiVolsi, 2011; Park et al., 2022).

1.2.1.2 Follicular Thyroid Cancer

Following PTC, follicular thyroid carcinoma (FTC) is the second most common carcinoma of DTC. FTC arises from follicular thyroid cells and accounts for approximately 10-15 % of all thyroid carcinoma cases and predominantly affects women, being more commonly diagnosed in the fifth and sixth decades of life (Parameswaran et al., 2017). Unlike PTC, which is known for its excellent prognosis and indolent biological features, FTC is characterised by its tendency to invade blood vessels and metastasise to the bones and lungs (McHenry et al., 2011). Factors that negatively affect survival include elderly age at presentation, having a large-sized tumour, vascular invasion, male gender, and distant metastases (Yamazaki et al., 2024; Zidan et al., 2000). Overall, metastatic FTC leads to poorer clinical outcomes than non-metastatic cases (Parameswaran et al., 2017; Su et al., 2019).

The 2017 WHO classification divided FTC into three subtypes: minimally invasive (MI-FTC), encapsulated angioinvasive (EA-FTC), and widely invasive (WI-FTC), reflecting the extent of tumour capsule and vascular invasion. This stratification, which emphasises the relationship between invasive features and patient survival, is retained in the 2022 WHO classification. Minimally invasive FTC is defined by limited capsular invasion, encapsulated angioinvasive FTC by vascular invasion without significant

capsular disruption, and widely invasive FTC by extensive invasion into the capsule and surrounding tissues (Christofer Juhlin et al., 2023; Yamazaki et al., 2024). FTC is typically detected via ultrasound imaging, fine needle aspiration biopsy (FNAB), and blood biochemistry tests to assess thyroid function. However, a definitive diagnosis requires a histological evaluation following surgical removal of the nodule or the thyroid gland tissue to observe for capsule and vascular invasion to distinguish FTC from benign conditions (Lin et al., 2006). Similar to PTC, patients with FTC generally have an excellent prognosis with a 5-year survival rate of approximately 91 %. However, this prognosis can be significantly worse if the disease metastasises and becomes resistant to radioiodine therapy (Capdevila et al., 2022).

1.2.1.3 Oncocytic Thyroid Carcinoma

The final subtype of DTC is oncocytic thyroid carcinoma (OTC), also known as Hürthle cell carcinoma (HCC). In 2022, WHO reclassified OTC as a distinct entity separate from FTC based on enhanced insights into its unique molecular profile and clinical behaviour. The term “Hürthle cell” is now discouraged, as Hürthle originally described parafollicular C cells (Baloch et al., 2022). OTC is the rarest malignant form of the thyroid gland and represents approximately 5 % of thyroid cancer cases (Bischoff et al., 2024). OTC frequently occurs in the fifth to seventh decades of life and is more common in females. Multiple studies indicated that older age and large tumour size predicted poor survival rates (Kure et al., 2020). Some studies report that OTC is regarded as a more aggressive clinical behaviour and presents the highest incidence rate of distant metastases compared with PTC or FTC. However, owing to its rarity and the contradictory findings from prior studies, the pathological features and

biological behaviour of OTC are yet to be fully understood (Sugino et al., 2012; Yutan et al., 2001). Histologically, OTCs are characterised by encapsulated tumours with capsular and/or vascular invasion, consisting of at least 75 % oncocytic cells. Similar to other DTCs, the diagnosis of OTC requires histologic evidence of capsule or vascular invasion (Bischoff et al., 2024). Clinically, OTC is associated with a higher rate of nodal metastases and metastatic OTC typically exhibits poor response to radioiodine ablation therapy (Canberk et al., 2019). The treatment of OTC can be divided into surgical and non-surgical approaches, with surgical being the primary treatment method (Syed et al., 2022). For OTC larger than 1 cm but smaller than 4 cm without extrathyroidal extension or lymph node metastasis, near-total or total thyroidectomy or unilateral thyroidectomy is initially recommended, while total thyroidectomy is advised for tumours larger than 4 cm (Haugen et al., 2016). However, the role of radioactive iodine (RAI) therapy in OTC treatment remains debated, with some guidelines suggesting its use for tumours larger than 2 cm and those with metastatic disease, despite OTC's decreased iodine uptake and lower responsiveness to RAI therapy (Kure et al., 2020). The prognosis of OTC varies and is primarily influenced by histopathologic features, particularly the extent of capsular and vascular invasion. Notably, due to its low iodine avidity, recurrent OTC can be more challenging to treat, which may lead to poorer clinical outcomes (Baloch et al., 2022).

1.2.1.4 Anaplastic Thyroid Carcinoma

Anaplastic thyroid carcinoma (ATC), also known as undifferentiated thyroid cancer, is extremely aggressive but accounts for a minority (less than 5 %) of thyroid cancer (Chintakuntlawar et al., 2019). The prognosis for ATC is extremely poor, with the 5-

year survival rate for ATC patients with all the Surveillance, Epidemiology, and End Results (SEER) stages combined being 7 %, accounting for approximately 40 % of all thyroid cancer-related mortalities (Lu et al., 2023). ATC is universally classified as stage IV (A, B or C) by the American Joint Committee on Cancer (AJCC) TNM system due to its historically poor prognosis (Bible et al., 2021; Tuttle et al., 2016). The disease typically manifests in the later stages of life, with the median age of onset between 50 and 70 years and fewer than 10 % of cases diagnosed before age 50. Women are more frequently affected than men, with a sex ratio of approximately 2 to 1.5 (Jannin et al., 2022). The primary clinical presentation of ATC is a rapidly enlarging neck mass, often accompanied by compressive symptoms such as pain, hoarseness, dysphagia and a high propensity for metastasis either at diagnosis or during disease (Alhejaily et al., 2023; Are et al., 2006). The primary treatment for ATC involves multidisciplinary and multimodal strategies like surgery, radiotherapy, chemotherapy, external beam radiation therapy (EBRT) and systemic treatment (Jannin et al., 2022). Historically, systemic treatments, including targeted therapies and immunotherapies, were limited for ATC, but in the past decade, these therapeutic options have significantly advanced. A study by Subbiah et al. (2018) demonstrated notable responses in a cohort of 16 ATC patients with $BRAF^{V600E}$ mutations treated with the BRAF inhibitor dabrafenib and the MEK inhibitor trametinib. Based on this study and previous approvals of the combination in melanoma, the FDA has approved this combination for treating ATC patients with the $BRAF^{V600E}$ mutation (Chintakuntlawar et al., 2019; Subbiah et al., 2022). Additionally, emerging evidence suggests that surgical resection following a favourable response to neoadjuvant BRAF inhibitor therapy can lead to prolonged survival, with a reported 1-year overall survival rate of

94 % in a study of 20 patients (Maniakas et al., 2020). Unfortunately, for patients without the BRAF mutation, systematic treatment options remain limited.

1.2.1.5 Medullary Thyroid Carcinoma

Medullary thyroid carcinoma (MTC) is a neuroendocrine thyroid cancer which arises from parafollicular or C cells producing mainly calcitonin (Hamdy et al., 2020). MTC is the third most common thyroid cancer after PTC and FTC and accounts for approximately 5-10 % of all thyroid malignancies (Gogna et al., 2020). Although the incidence of thyroid cancer has shown a marked increase in the last two decades year around the world, there has been no comparable growth in the incidence of MTC (Raue et al., 2015). According to direct analysis of the RET proto-oncogene, MTC primarily manifests in two forms: sporadic and hereditary. Sporadic MTC is the majority and accounts for 75 % of cases, which may be associated with somatic RET mutations. In comparison, the hereditary form comprises about 25 % of cases and is associated with germline RET mutations (Larouche et al., 2019). Moreover, the sporadic form affects females more commonly than males and has a peak incidence at 40-50 years of age range, while hereditary MTC affects both women and men equally (Pacini et al., 2010). The usual clinical presentation of MTC includes a thyroid nodule, typically without additional specific symptoms. However, in some instances, more severe manifestations such as hoarseness, persistent diarrhoea or skin flushing may appear (Maghsoomi et al., 2021). Surgery is the primary and initial treatment for patients with MTC. Since the tumour frequently presents as multifocal and bilateral, commonly metastasising to cervical lymph nodes at the time of diagnosis, studies indicate outcomes are generally improved through total thyroidectomy along with bilateral

cervical lymphadenectomy, which constitutes the essential surgical treatments for affected individuals (Sippel et al., 2008). External radiotherapy is now typically reserved for symptomatic bone or brain metastases, and classic cytotoxic chemotherapy is no longer commonly used due to its low response rates (Wells et al., 2015). Other treatments for advanced MTC include first-line use of multitarget kinase inhibitors like vandetanib and cabozantinib, with ongoing studies on potent selective RET inhibitors such as selpercatinib and pralsetinib showing promising results in cancers that harbour RET mutations.

Additionally, investigational therapies like immunotherapy and Peptide Receptor Radionuclide Therapy (PRRT) offer potential new avenues for treating advanced MTC (Baek et al., 2023; Kim et al., 2021; Maghsoomi et al., 2021; Priya et al., 2017). The National Comprehensive Cancer Network Guidelines indicate that individuals diagnosed with MTC at 40 years or younger have a five-year survival rate of 95 % and a ten-year survival rate of 75 %. In contrast, those diagnosed after age 40 have lower survival rates of 65 % at five years and 50 % at ten years. The prognosis is significantly better when the tumour is confined to the thyroid (Ricci et al., 2023).

1.2.1.6 Poorly Differentiated Thyroid Cancer

Finally, poorly differentiated thyroid cancer (PDTC) is classified as a follicular-cell-derived neoplasm that presents as morphologically and behaviourally intermediate to those of WDTC, such as papillary and follicular carcinomas, and ATC. The WHO guidelines classify poorly differentiated thyroid carcinoma as a type of thyroid cancer with distinct solid or irregular growth, lacking the nuclear features seen in papillary

carcinoma, and showing signs of aggressive disease like rapid cell division and tissue necrosis (Rosai et al., 2017). PDTCs are uncommon, comprising approximately 2 % to 4 % of all malignant thyroid neoplasms, and show increased prevalence in iodine-deficient areas (Volante et al., 2008). The prognosis for PDTC is between that of DTC and ATC, generally with common metastases to the lungs and bones and 5- and 10-year survival rates of patients standing at 70 % and 50 %, respectively (Asioli et al., 2010).

1.2.2 The Epidemiology and Demographics of Thyroid Cancer Worldwide

Thyroid cancer is the most prevalent endocrine system malignancy. There has been a marked increase in diagnosis rates across different countries in recent decades. For instance, between 1975 and 2009, the incidence of thyroid cancer in the United States saw a significant rise, climbing from 2.4 % to 6.6 % of all new cancer diagnoses (Olson et al., 2019). Comparable trends have been documented in Canada, Australia and Western Europe (Morris et al., 2013). At the same time, mortality has not seen a corresponding increase, which is still low or has consistently decreased (Li et al., 2020; Vaccarella et al., 2016) (Figure 1.7). This situation is predominantly thought to result from overdiagnosing the disease, such as with the increased utilisation of ultrasonography and FNAB, alongside the detection of numerous radiographic “incidentalomas” on nonthyroid imaging or other diagnosis techniques (Dal Maso et al., 2018). Risk factors like radiation exposure, especially during childhood, or being overweight or high or deficient iodine intake, may have played a role in the rise of thyroid cancer cases (Dal Maso et al., 2009; Pellegriti et al., 2013). Nevertheless, most

studies indicate that overdiagnosis seems to be the main driver of increasing the incidence rate (Li et al., 2020; Li et al., 2021; Pizzato et al., 2022).

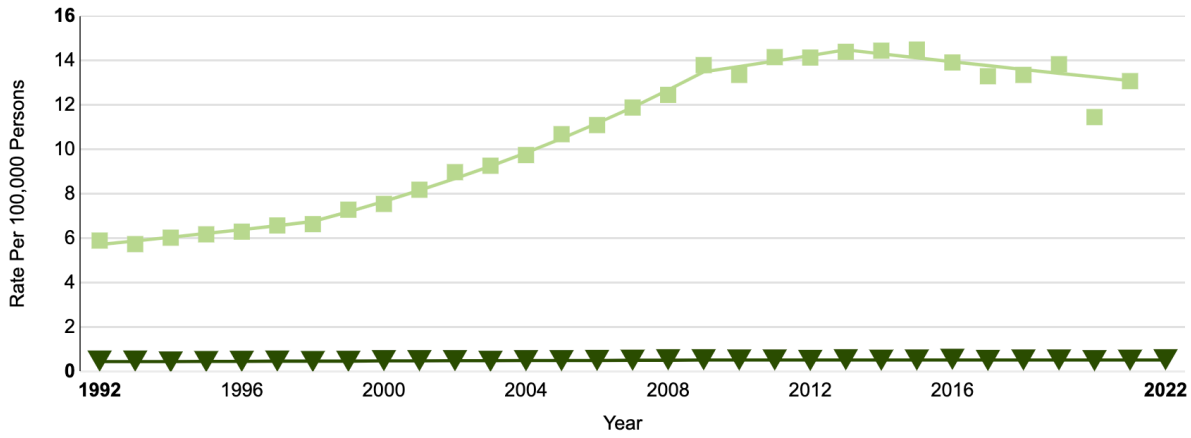


Figure 1. 7 Trends in Thyroid Cancer Incidence and Mortality Rates (1992-2022). *Data downloaded from Surveillance, Epidemiology and End Results (SEER) (https://seer.cancer.gov/statfacts/html/thyro.html). The chart displays trends in thyroid cancer incidence and mortality rates per 100,000 persons in the U.S. population from 1992 to 2022, with data sourced from SEER 12 for new cases and U.S. Mortality for deaths. Incidence rates, represented by green squares, demonstrate a rising trend until 2016, followed by a slight decline, while mortality rates, shown as green triangles, remain consistently low. Modelled trend lines were generated using Joinpoint Trend Analysis Software, excluding the 2020 incidence rate due to potential data inconsistencies caused by the COVID-19 pandemic's impact on SEER cancer reporting.*

1.2.3 Molecular Pathogenesis and Genetic Alterations in Thyroid Cancer

The molecular aetiology of thyroid cancer is characterised by complex genetic alterations that dysregulate crucial signalling pathways essential for cellular growth, apoptosis, proliferation and tumourigenesis. Two essential pathways involved in disease development are the mitogen-activated protein kinase (MAPK) pathway and the phosphatidylinositol 3-kinase protein/AKT (PI3K-AKT) pathway. Mutations in the BRAF or N/H/K-RAS genes generally initiate the activation of the MAPK pathway. The

activation of the PI3K-AKT pathway predominantly occurs through either activating mutations within key signalling molecules or through the inactivation of PTEN, a potent pathway inhibitor.

Additionally, genetic modifications in essential tumour suppressors and proto-oncogenes, such as the RET proto-oncogene, the telomerase reverse transcriptase (TERT) and the tumour protein p53 (TP53), emphasise the multifaceted progression of thyroid cancer. These mutations not only facilitate the malignant transformation but also highlight the heterogeneous genetic landscape foundational to thyroid cancer.

1.2.3.1 Frequent Genetic Alterations in Thyroid Carcinoma

1.2.3.1.1 BRAF Mutations

Genetic mutations are pivotal in the initiation and progression of thyroid cancer but also lay the foundation for innovative therapeutic strategies. The BRAF mutation is the most common genetic change in thyroid cancer, present in approximately 60 % of sporadic papillary thyroid cancers (PTCs), especially within the more aggressive variants like tall-cell PTC (Leandro-García et al., 2023; Xing, 2005). BRAF genetic alterations encompass the classical V600E mutations alongside other non-V600E variants, RAF gene fusions and RAF deletions (Podolski et al., 2019). Among these mutations, the most common is the T1799A nucleotide transversion mutation. This mutation leads to a change in codon 600 of the BRAF protein to the $BRAF^{V600E}$ protein, which is responsible for serine/threonine kinase activation, subsequently constitutively activating the MAPK signalling pathway and suppressing the pro-apoptotic signalling

of the FOXO3 pathway. Studies have proven the $BRAF^{V600E}$ mutation is associated with aggressive clinicopathological behaviours of PTC and poor clinical outcomes, including lymph node metastases, distant invasion, and silencing of thyroid-specific gene expression, hence radioiodine therapy failure and high incidence of disease recurrence (Kim et al., 2012). Another recent study by Enumah et al. (2020) demonstrated that $BRAF^{V600E}$ independently predicted PTC recurrence. However, research by Ito et al. (2009) and Couveia et al. (2013) found no significant correlation between $BRAF^{V600E}$ and tumour aggressiveness in different cohorts. Chen et al. (2021) showed that the combination of $BRAF^{V600E}$ and TERT promoter mutations significantly worsened prognosis, but the predictive value of the $BRAF^{V600E}$ mutation remains uncertain. Overall, while the $BRAF^{V600E}$ mutation remains a significant molecular driver in PTC, its prognostic value varies, and comprehensive molecular testing, including TERT mutation analysis, is crucial for accurate risk stratification and tailored treatment strategies.

In addition, most ATCs arise from well-differentiated thyroid carcinomas and often harbour $BRAF^{V600E}$ or RAS mutations, known drivers of differentiated thyroid carcinoma (Wang et al., 2022). The $BRAF^{V600E}$ mutation rate is approximately 40 % in ATC, though it varies between studies (Duan et al., 2019; Jeon et al., 2016; Pozdeyev et al., 2018). This mutation's significance is underscored by its treatment implications, as selective BRAF inhibitors, alone or combined with MEK inhibitors, have demonstrated promising clinical outcomes in BRAF-mutant ATC patients. For example, studies have reported improved response rates, progression-free survival, and overall survival in patients treated with these targeted therapies (Chintakuntlawar et al., 2019; Subbiah et al., 2018; Subbiah et al., 2022).

1.2.3.1.2 RAS Mutations

RAS mutations play a critical role in the oncogenesis of the thyroid and are the second most common genetic occurrence in thyroid neoplasms (Bikas et al., 2023). Within the human genome, the RAS gene family has three isoforms, NRAS, HRAS and KRAS, and encode proteins of around 21 kDa, which are essential to cellular differentiation, proliferation, migration and apoptosis (Boguski et al., 1993). RAS is associated with guanosine triphosphate (GTP) when activated. Typically, the activity of RAS proteins is stringently regulated through its internal GTP hydrolysis. GTPase hydrolyses GTP and then converts RAS to a deactivated state linked with GDP, halting RAS signalling. However, mutations of RAS disrupt its GTPase function and perpetually maintain RAS in an active state bound to GTP, causing a consequent disruption of RAS-dependent cellular signalling and promoting oncogenesis (Pylayeva-Gupta et al., 2011). Although RAS can aberrantly activate both MAPK and PI3K-AKT pathways, there is a notable bias towards PI3K-AKT pathway activation in thyroid malignancies, potentially elucidated by the observed correlation between RAS mutations and enhanced AKT phosphorylation (Rasheed et al., 2019; Xing, 2013).

The prevalence of RAS mutations varies across the spectrum of thyroid diseases, ranging from benign follicular thyroid adenomas (FTA) to an array of thyroid cancers (Bikas et al., 2023; Marotta et al., 2021). On average, RAS mutations are detected in 30-45 % of cases involving FTC and the follicular variant of papillary thyroid cancer (FCPTC), 20-40 % of PDTC, and 10-20 % of ATC, and are seldom found in classical PTC. Furthermore, these mutations appear in 20-50 % of benign FTA. Identifying RAS mutations in FTA, considered a potential precursor to malignancy, implies a significant

role for activated RAS in the initial stage of FTC development (Xing, 2016). However, the transition from benign to malignant lesions typically requires genetic events beyond RAS mutations, as demonstrated by *in vitro* and transgenic mouse studies, which suggest that RAS mutations alone do not transform thyroid cells unless other alterations like PTEN deletion exist (Bond et al., 1994; Gire et al., 2000; Miller et al., 2009). Clinically, thyroid nodules bearing only RAS mutations are usually non-aggressive, and differentiated thyroid cancers with isolated RAS mutations generally do not display aggressive behaviour (Liu et al., 2016; Marotta et al., 2021).

1.2.3.1.3 RET Mutations and RET/PTC Rearrangement

The RET proto-oncogene encodes for a tyrosine-kinase receptor (TKR) on the cell membrane. It is located on the long arm of chromosome 10 (10q11.2) and was initially discovered in 1985 (Ishizaka et al., 1989; Takahashi et al., 1985). The RET protein is structured into three distinct domains: an N-terminal extracellular domain with a ligand-binding region, a cysteine-rich region with a transmembrane domain, and a cytoplasmic domain that contains an area with protein tyrosine kinase activity (Knowles et al., 2006). Neurotropic factors from the glial cell-line derived neurotrophic factor (GDNF) family, such as GDNF, neurturin, artemin and persephin, serve as ligands for the RET receptor (Salvatore et al., 2021). The interaction with these ligands triggers dimerisation of the receptor, which in turn promotes the autophosphorylation of tyrosine residues, thereby activating downstream signalling pathways, which include MAPK and PI3K-AKT pathways that are involved in cell growth, proliferation and differentiation (Arighi et al., 2005).

The normal RET gene is highly expressed in parafollicular cells (or C-cells), which aligns with its significance in the growth and function of cells derived from the neural crest. In contrast, normal thyroid follicular cells do not typically express the RET gene (Salehian et al., 2013; Takaya et al., 1996; Yue et al., 2021). Point mutations in RET within these C-cells lead to sporadic and hereditary forms of MTC and the genetic conditions of multiple endocrine neoplasia (MEN) types: MEN2A and MEN2B (Santoro et al., 1990). Meanwhile, in thyroid follicular cells, the activation of RET occurs through gene rearrangement, resulting in a chimeric oncogene known as RET/PTC. More than 10 distinct types of RET-PTC translocations have been identified and categorised via their partner genes in PTC (Khan et al., 2020). The most prevalent forms include RET-PTC1, which results from the fusion of the RET tyrosine kinase domain with the 5' region of the gene known as CCD6, and RET-PTC3, characterised by fusion with the nuclear receptor co-activator 4 (NCOA4); these constitute more than 90 % of all arrangements found in papillary carcinomas (Grieco et al., 1990; Nikiforov, 2002). Rearrangements typically lead to ligand-independent dimerisation and persistent activation of the tyrosine kinase function of RET, leading to tumourigenesis (Groot et al., 2006). The presence of RET/PTC rearrangement is a strong indicator of PTC and can assist in the molecular diagnosis via FNAB. If a RET/PTC rearrangement is identified, a total thyroidectomy is advised (Paschke et al., 2017).

1.2.3.1.4 PAX8-PPARγ Fusion

PAX8, a transcription factor crucial for thyroid gland development and cell differentiation, regulates thyroid-specific genes like TG, TPO and NIS (Magliano et al., 2000). The peroxisome proliferator-activated receptor gamma (PPARγ) is a ligand-

activated nuclear hormone receptor family transcription factor rarely expressed in the thyroid (Karger et al., 2005). PPARγ regulates adipocyte differentiation, lipid metabolism and insulin sensitivity (Zhang et al., 2017).

The PAX8/PPARγ rearrangement results from the translocation between chromosomal region 2q13 and 3p25, leading to the synthesis of a fusion transcript that produces the PAX8/PPARγ fusion protein (PPFP) (Sakaguchi et al., 2021). This rearrangement is found in about 60 % of FTCs, a few follicular variant PTCs and 2-10 % of follicular thyroid adenomas (Hlozek et al., 2022; Marques et al., 2002; Raman et al., 2014). Studies suggest that PPFP is an oncoprotein that enhances cell growth and reduces apoptosis (Placzkowski et al., 2008). The detection of PPFP in thyroid nodules of indeterminate pathology is a strong indicator of potential malignancy, often necessitating surgical removal (Nikiforov et al., 2011). Pioglitazone shows promise in treating advanced PPFP-driven thyroid cancers (Dobson et al., 2011; Giordano et al., 2018).

1.2.3.1.5 TERT Promoter Mutations

Telomerase reverse transcriptase (TERT) is the enzymatic core of telomerase, which elongates telomeres at chromosome ends, preserving genomic stability and cellular longevity (Blasco, 2005; Greider et al., 2004; Moyzis et al., 1988). The TERT gene on chromosome 5 includes 16 exons and a promoter region, with promoter mutations being common in various cancers and acting as oncogenes (Aubert et al., 2008; Liu et al., 2016). Two of the most common TERT promoter mutations, C228T and C250T, enhance transcriptional activity and are more prevalent in aggressive thyroid cancers

(Liu et al., 2016). Cancer cells with these mutations express telomerase at elevated levels, maintaining the length of chromosomal telomeres and enabling almost limitless proliferation (McKelvey et al., 2020). TERT mutations are linked to an increased incidence of local or distant metastasis and greater tumour aggressiveness. Additionally, these mutations are rare in benign thyroid conditions but prevalent in thyroid cancers, particularly in aggressive forms like PDTC and ATC. However, well-differentiated variants like PTC and FTC show lower rates. In contrast, MTC rarely shows these mutations (Liu et al., 2016). Thyroid cancers with both TERT promoter and $BRAF^{V600E}$ mutations show higher recurrence rates and greater aggressiveness, suggesting a synergistic effect (Chen et al., 2021; Mady et al., 2020; Shi et al., 2015). Meanwhile, a significant correlation exists between TERT promoter and RAS mutations in thyroid cancers, indicating a potential cooperative effect in cancer progression and aggression (Liu et al., 2016; Vinagre et al., 2013).

1.2.3.1.6 PTEN Mutations or Methylation

Phosphatase and tensin homolog (PTEN) is a dual-specificity phosphatase that targets the 3’ position phosphate on PIP3, catalysing its hydrolysis and consequent degradation and deactivation of PIP3 (Maehama et al., 1998). PTEN is recognised as a crucial tumour suppressor by restraining the PI3K/AKT pathway, which regulates various cellular processes such as proliferation, survival, and motility (Bandargal et al., 2023; Chen et al., 2018). Mutations that lead to a dysfunctional or missing PTEN protein are quite prevalent in ATC, less frequent in PDTC, and relatively rare in FTC (Colombo et al., 2022). Additionally, mutations or deletions of the PTEN gene are the classical genetic alterations that activate the PI3K/AKT pathway and are the genetic

basis for follicular thyroid cell tumourigenesis in Cowden's syndrome (Gustafson et al., 2007). Interestingly, research shows thyroid cancers in patients with Cowden's syndrome predominantly presented as variants of PTC, contrasting with literature that suggests a higher incidence of follicular cancer. This discrepancy likely arises from differences in data sources and the referral nature of the studied institution (Yamashita et al., 2020). Moreover, alteration in the methylation of the PTEN promoter serves as an epigenetic mechanism to deactivate the PTEN gene within thyroid tumours and potentially leads to the stimulation of the PI3K/AKT signalling pathway (Alvarez-Nuñez et al., 2006; Xing, 2007).

1.2.3.1.7 Other Gene Mutations

Aggressive thyroid cancer, particularly ATC and PDTC, may additionally involve genetic mutations beyond the commonly described BRAF, RAS, RET, PAX8/PPARγ fusion, RET/PTC rearrangement, RET mutation, TERT promoter mutation and PTEN inactivation (Acuña-Ruiz et al., 2023). Additional genetic alterations in these aggressive cancers include TP53 mutations, leading to loss of cell cycle regulation, and PIK3CA mutations, activating the PI3K/AKT pathways (Zeng et al., 2024). Other notable mutations are in AKT1, contributing to aberrant PI3K/AKT signalling pathway; NF1, increasing RAS activity; CTNNB (β-catenin), activating the Wnt/β-catenin pathway; EIF1AX, often co-occurring with RAS or TERT mutations, and IDH1, linked to poor prognosis and components of the SWI/SNF complex like ARID1A and SMARCA4. Additionally, NTRK fusions and ALK rearrangements are implicated in various thyroid cancers (Landa et al., 2016; Prete et al., 2021).

Overall, thyroid cancers exhibit distinct genomic mutations associated with their histological subtype, providing essential insights into their molecular pathology. Predominantly, PTCs show mutations in the MAPK pathway genes, such as BRAF and RAS, contributing to around 75 % of cases, with $BRAF^{V600E}$ being the most frequent. Other advanced thyroid cancers may feature PIK3CA and PTEN mutations. Additionally, gene fusions involving RET, BRAF and others, while less common, still play an essential role in about 15 % of PTCs. FTCs often harbour PAX8/PPARγ fusions or RAS mutations, while aggressive ATCs may additionally exhibit TP53 and TERT promoter mutations. MTCs stand apart with predominant RET proto-oncogene mutations, reflecting the unique origin of C-cells (Agrawal et al., 2014; Xing, 2013).

1.2.3.2 Key Signalling Pathways Alterations in Thyroid Cancer

1.2.3.2.1 The MAPK Signalling Pathway

The MAPK signalling pathway is an integral cellular signalling cascade that utilises signals from external stimuli to the nucleus, influencing various critical cellular activities like growth, proliferation, differentiation, movement and apoptosis (Krishna et al., 2008; Schubert et al., 2023). There are four key MAPK pathways which have been delineated in mammalian cells: extracellular-signal-regulated kinase (ERK), c-Jun N-terminal kinases (JNK/SAPK), p38 MAPK and ERK5/BMK1, each playing distinct roles in the cell's response to external stimuli (Yue et al., 2020). The MAPK signalling pathway is triggered by various external factors, including receptor tyrosine kinases, G protein-coupled receptors and cytokines, leading to cellular responses such as proliferation, differentiation and apoptosis. This pathway's hyperactivation may

increase the expression of several pro-tumour proteins like chemokines, vascular endothelial growth factor A (VEGFA), matrix metalloproteinases (MMPs) and others to influence cancer progression and metastases (Jin et al., 2016). It is well recognised that the MAPK pathway is pivotal for cell proliferation and tumourigenesis in thyroid cancers, particularly in PTC.

As outlined above, activating this pathway in thyroid cancer can stem from mutations or rearrangements of crucial genes such as BRAF, RAS, and RET, which appear mutually exclusive (Zaballos et al., 2017). The activation sequence begins with RAS, which becomes activated upon stimulation by extracellular signals through receptor tyrosine kinases (RTKs), then leading to a series of further activations through BRAF and MEK and then ERK phosphorylation. Following its activation, ERK, a pivotal element of the MAPK pathway, translocates into the nucleus and initiates widespread changes in gene expression that govern many cellular functions (Xing, 2013). This transcriptional alteration process significantly elevates the expression levels of several key transcription factors, such as c-FOS, c-JUN, c-MYC, and ELK1. These factors facilitate cellular responses, including growth, differentiation and survival (Xing, 2013). Meanwhile, activation of $BRAF^{V600E}$ mediated MAPK pathway has also been observed to influence the downregulation of several tumour suppressor genes, including the tissue inhibitor of metalloproteinases 3 (TIMP3), death-associated protein kinase 1 (DAPK1) and retinoic acid receptor-β (RARB) (Hu et al., 2006). Additionally, genes crucial for iodide processing in thyroid cells, such as NIS, TSHR and TPO, are downregulated, highlighting their role in altering both tumour-suppressive mechanisms and thyroid-specific metabolic processes (Xing, 2013).

In recent years, selective BRAF inhibition and the targeted suppression of the MAPK pathway have demonstrated efficacy in treating thyroid cancers, particularly those resistant to traditional therapies. Approving tyrosine kinase inhibitors for clinical use marks a significant advancement in the targeted treatment landscape for thyroid cancer (Schubert et al., 2023).

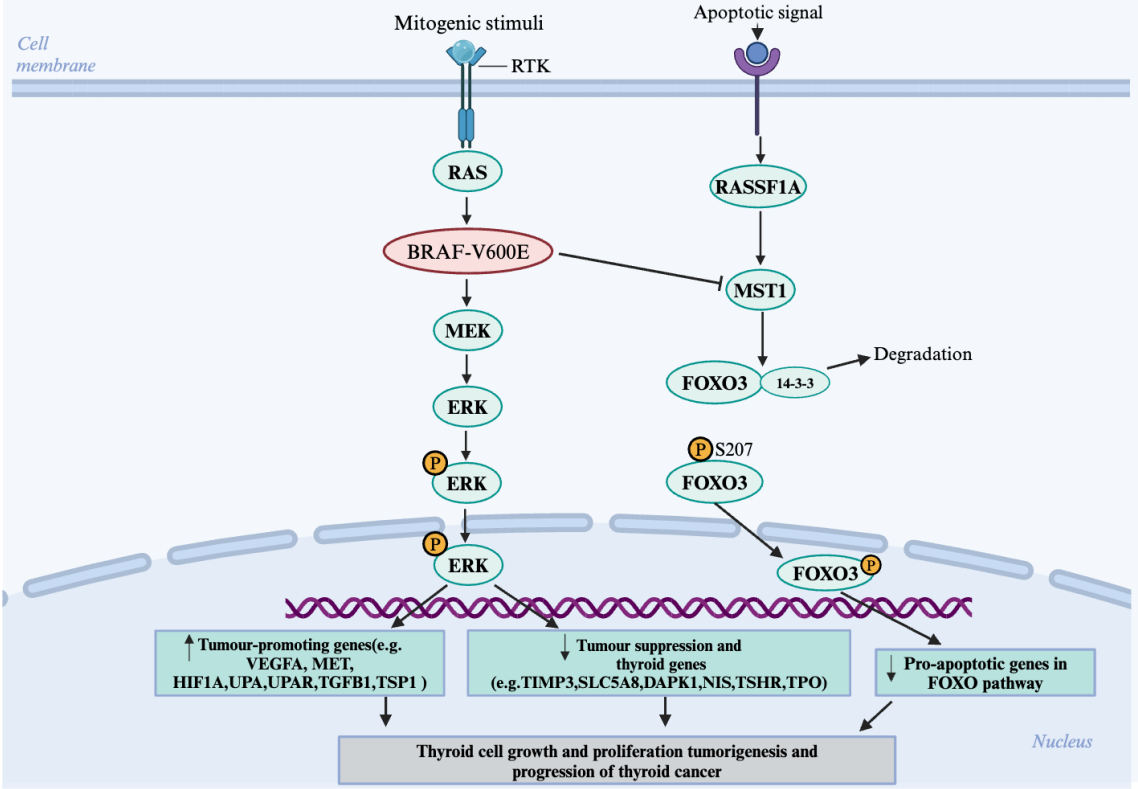


Figure 1. 8 The MAPK and related pathways. *Left - the MAPK pathway: Starting from an external growth signal, it progresses through an activated cell surface receptor to intracellular signalling molecules, including RAS, RAF (specifically BRAF-V600E), MEK and ERK. Once ERK is phosphorylated, it moves into the cell nucleus to influence genes that can promote tumour growth and suppress tumour-suppressing and thyroid-specific genes. Right - the RASSF1–MST1–FOXO3 pathway, normally triggered by signals promoting cell death. RASSF1A activates MST1, which then phosphorylates FOXO3. This leads to the release and activation of FOXO3, allowing it to enter the nucleus and stimulate genes that lead to cell death. However, the BRAF-V600E mutation can inhibit MST1, blocking this pathway and preventing the activation of cell death genes. This shows how BRAF-V600E can powerfully drive thyroid cancer by manipulating multiple pathways to promote tumour growth and suppress cell death. DAPK1, death-associated protein kinase 1; HIF1A, hypoxia-inducible factor 1α; TGFB1, transforming growth factor β1; TSP1, thrombospondin 1; UPA, urokinase*

plasminogen activator; UPAR, urokinase plasminogen activator receptor; Figure adapted from (Xing, 2013).

1.2.3.2.2 The PI3K/AKT Signalling Pathway

The phosphoinositide 3-kinases (PI3Ks) family phosphorylates phosphatidylinositols on the plasma membrane, initiating signalling cascades that regulate cellular processes such as proliferation, survival and angiogenesis (Martini et al., 2014). Protein kinase B (AKT) is a key downstream effector of PI3K, modulating various cellular activities (Fayard et al., 2005). The PI3K/AKT pathway is recognised for its fundamental role in cellular and molecular regulation, such as glucose uptake and cell motility (Figure 1.9). Dysfunction in this pathway has been implicated in the tumourigenesis of multiple cancers through phosphorylation and activation of AKT, especially in head and neck cancers. Genomic studies reveal its frequent mutation and activation in thyroid cancers, indicating its critical role in thyroid carcinogenesis, cell dedifferentiation, invasion and metastasis (Xing, 2010).

In the absence of stimuli, the regulatory subunit of PI3K keeps the catalytic component inactive. Upon activating cell surface receptor tyrosine kinases by external signals, which then activate PI3K through RAS, PI3K transforms phosphatidylinositol 4,5-bisphosphate (PIP2) into phosphatidylinositol 3,4,5-trisphosphate (PIP3), a messenger that activates 3-phosphoinositide-dependent protein kinase 1 (PDK1). PDK1 then activates AKT, leading to its phosphorylation. Once activated, AKT moves into the nucleus to promote genes that drive tumour growth. At the same time, activated phospho-AKT can phosphorylate and deactivate glycogen synthase kinase 3β (GSK3β). Typically, GSK3β acts as an inhibitor of β-catenin; hence, phospho-AKT-

mediated inactivation of GSK3β alleviates the inhibitory effect on β-catenin. As a result, liberated β-catenin translocates into the nucleus, enhancing gene transcription that facilitates tumour progression. Furthermore, phosphorylated AKT in the cytoplasm can activate the mTOR pathway, contributing to tumourigenesis. Phosphorylated AKT also inactivates FOXO3, a pro-apoptotic gene regulator, thereby supporting tumour survival. PTEN serves as a crucial off-switch for this pathway by converting PIP3 back to PIP2, halting the signalling (Xing, 2013). However, genetic alterations such as mutations, deletion or methylation of the PTEN gene lead to PTEN being silenced, keeping the PI3K-AKT pathway constitutively activated and contributing significantly to the progression of thyroid cancer (Zaballos et al., 2017). Furthermore, alterations such as mutations or amplifications in genes such as PIK3CA, AKT1, RAS or RTKs are frequent catalysts for disturbances in the PI3K/AKT signalling cascade (Tanaka et al., 2015). Specifically, in thyroid cancer, while alteration in PI3K pathway components is infrequent in WDTC, they are more common in PDTC and ATC, suggesting the pathway plays a significant role in advancing more aggressive tumour types (Zaballos et al., 2017).

Overall, investigations into the PI3K/AKT/mTOR pathway as a therapeutic target have been at the forefront of oncological research. Compounds inhibiting this pathway have exhibited encouraging results in laboratory and animal studies (Laha et al., 2020).

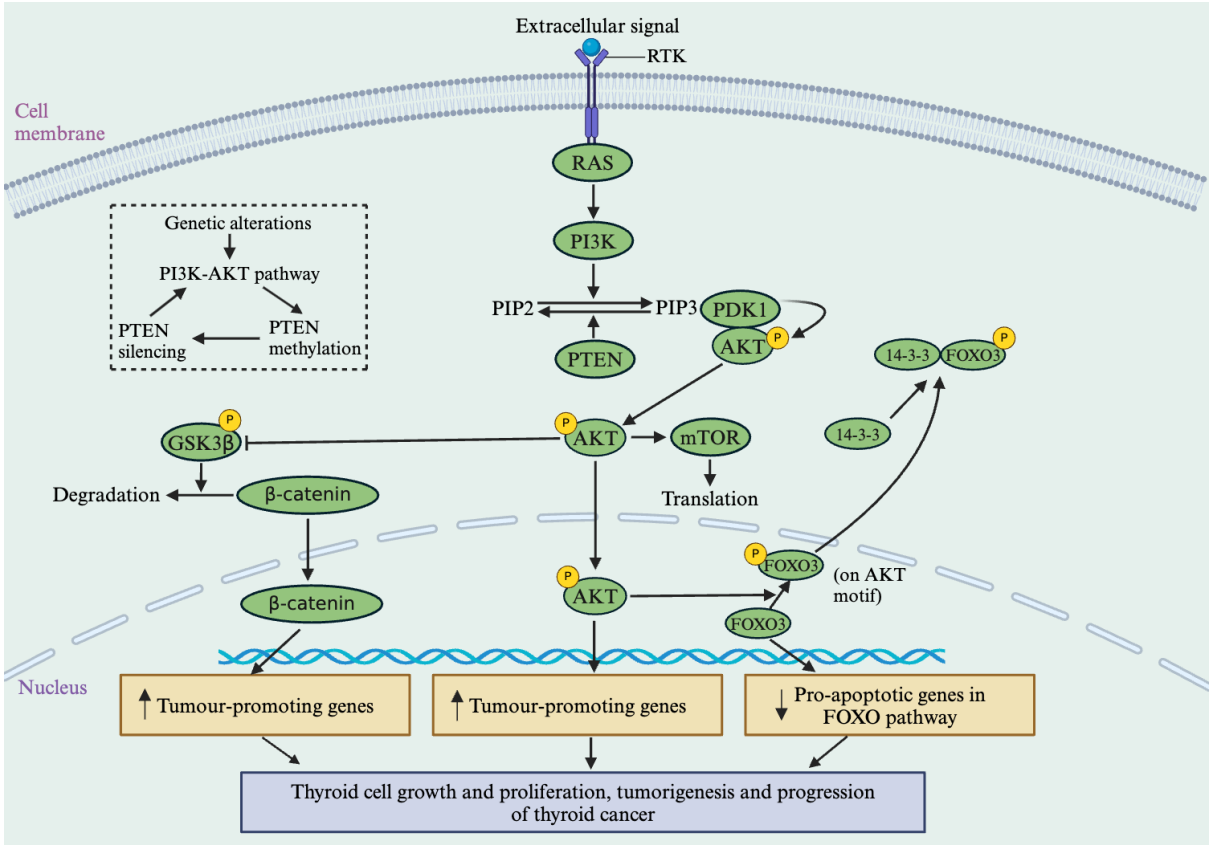


Figure 1. 9 The PI3K-AKT signalling pathway and related pathways. *Extracellular messengers activate cell surface RTKs, stimulating RAS and PI3K. PI3K then converts PIP2 into PIP3, which activates PDK1. PDK1 activates AKT, leading to its phosphorylation. Phosphorylated AKT enhances tumour-related genes in the nucleus and stimulates pathways like mTOR in the cytoplasm, promoting tumourigenesis. It also deactivates GSK3β, limiting the inhibition of β-catenin, which stimulates additional tumour-promoting genes. In the nucleus, phosphorylated AKT moves FOXO3 out of the nucleus, inhibiting its cell death-promoting functions. PTEN normally deactivates this pathway by turning PIP3 back into PIP2, but mutations can silence PTEN, keeping the pathway persistently active, a critical factor in the progression of thyroid cancer. This mechanism underlines the PI3K-AKT pathway's potent role in developing thyroid cancer. Figure adapted (Xing, 2013).*

1.2.4. Diagnostic Methods and Treatment of Thyroid Cancer

The diagnostic approach to thyroid cancer starts with clinical evaluation, including an assessment of symptoms and a thorough neck examination. High-resolution ultrasonography is pivotal for evaluating thyroid nodule characteristics to determine

malignancy risk. When nodules are deemed suspicious, FNAB, guided by ultrasonography, is the definitive step for cytological analysis to confirm the presence of cancer cells. Further imaging such as computed tomography (CT), magnetic resonance imaging (MRI) and positron emission tomography (PET), along with molecular testing for genetic alterations, may be employed to determine cancer spread and subtype, guiding the treatment planning (Cooper et al., 2009; Nikiforov et al., 2013). Therefore, comprehensive diagnostics combine clinical symptoms with various testing methods to confirm the presence and extent of thyroid cancer.

1.2.4.1 Active Surveillance of Thyroid Cancer

Autopsy studies have revealed a significant incidence of subclinical thyroid cancer, particularly small PTCs, which frequently remain clinically dormant (Furuya-Kanamori et al., 2016). The advent of thyroid ultrasound has facilitated the detection and diagnosis of subcentimeter PTCs, leading to the development of active surveillance as a long-term monitoring strategy for these tumours. Long-term studies of small (<1-1.5 cm) PTCs have shown that active surveillance for specific patients is a safe alternative to immediate resection, with minimal rates of tumour growth and new nodal metastases (Ito et al., 2018; Sugitani et al., 2021; Tuttle et al., 2017). Active surveillance, which necessitates expert ultrasound imaging, lifelong monitoring, and robust patient-physician communication, offers the advantage of avoiding the significant surgical risks associated with older patients and those with localised disease; it is particularly suited for individuals who have well-defined, solitary intrathyroidal PTCs measuring ≤1 to 1.5 cm, no suspicious lymph nodes, and are of an older age (Araque et al., 2020). Contraindications for active surveillance

encompass clinical lymph node or distant metastasis at diagnosis, invasion of the trachea or recurrent laryngeal nerve, and high-grade malignancy on cytology, including tall cell variant and poorly differentiated carcinoma (Miyauchi et al., 2019), and patient preference, as some individuals may find it challenging to cope with a surveillance strategy for a known cancer (Hermus et al., 2023).

1.2.4.2 Surgical Approach

Surgical approaches for DTC involve a thyroidectomy, which may be performed as a lobectomy or a total/near-total thyroidectomy with or without lymph node dissection, depending on individual patient factors and tumour characteristics (Figure 1.10). The American Thyroid Association (ATA) risk stratification system estimates the likelihood of persistent or recurrent thyroid cancer. Based on clinical, pathological and molecular features, thyroid cancer is categorised into low, intermediate or high risk for recurrence (Haugen et al., 2016). This classification helps tailor surveillance and treatment for each patient. Most low-risk thyroid cancers can be effectively treated with surgery alone, often opting for thyroid lobectomy for tumours smaller than 4 cm due to its favourable survival outcomes and reduced complication rates compared to total thyroidectomy (Stevens et al., 2023). For WDTC tumours equal to or larger than 4 cm or for cancer affecting both lobes of the thyroid and without evidence of gross extrathyroid extension, neck lymph node or distant metastases, a total thyroidectomy is generally recommended to ensure complete removal of the malignant tissue (Boucai et al., 2024).

Additionally, for preoperative findings of more aggressive tumours, such as lymph node metastases or PTC with gross extrathyroid extension or distant metastases, total thyroidectomy along with lymph node dissection may be performed to manage potential metastases or recurrence (Nguyen et al., 2015). Surgical removal is the primary and often the only curative strategy for MTC, focusing on preoperative evaluations to guide surgical extent and addressing associations of MEN syndromes like phaeochromocytoma or hyperparathyroidism (Wells et al., 2015).

ATC is a rare and highly aggressive type of thyroid cancer and is responsible for the majority of the fatalities related to thyroid carcinoma (Lu et al., 2023). Immediate intervention is crucial. The treatment of ATC typically integrates surgery (if applicable), which aims to obliterate the tumour. However, in reality, surgery is very rarely possible for ATC due to its aggressive and advanced presentation at diagnosis. After surgery, therapeutic strategies may include external beam radiation therapy, conventional chemotherapy, or combined BRAF inhibitor (dabrafenib) and MEK inhibitor (trametinib) for patients with the $BRAF^{V600E}$ mutation (Jannin et al., 2022; Subbiah et al., 2018; Subbiah et al., 2022). ATC Management is best coordinated by a multidisciplinary team for a comprehensive approach to care, emphasising complete lesion resection when possible (Leo et al., 2020).

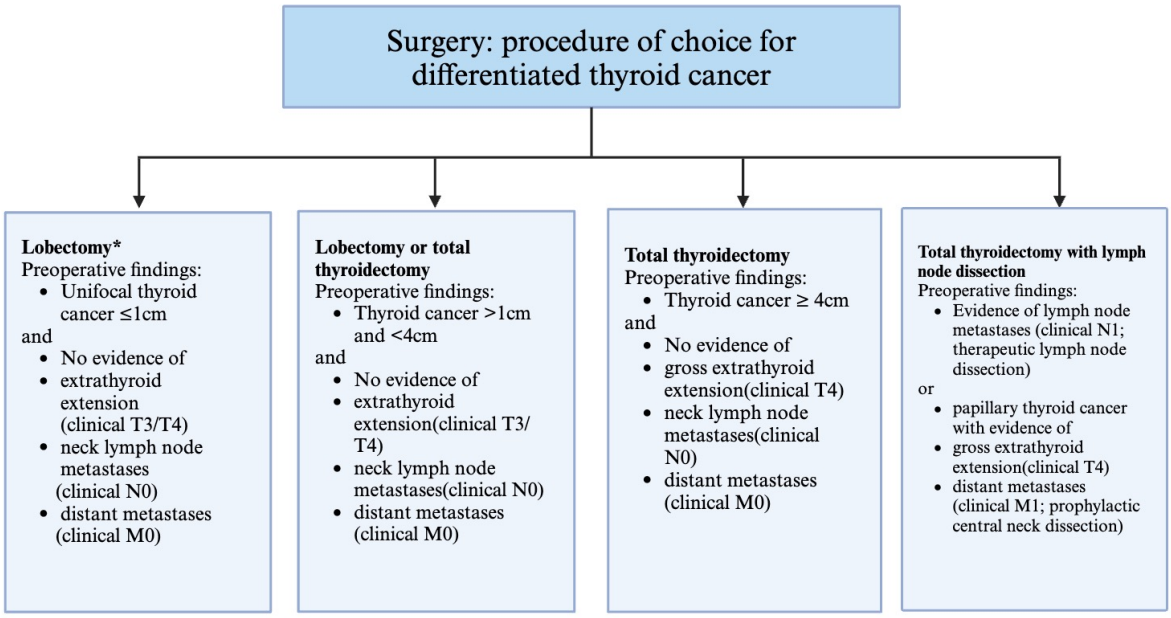


Figure 1. 10 Surgical treatment guidelines for differentiated thyroid cancer. **Patients with recognised risk factors for thyroid cancer, such as a history of head and neck radiation or a family history of thyroid carcinoma, should initially undergo a complete thyroidectomy as the surgical intervention. Figure adapted from (Cabanillas et al., 2016).*

1.2.4.3 Radioactive Iodine (RAI) Therapy

RAI therapy has been a cornerstone in the treatment of DTC since the mid-20th century (Seidlin et al., 1946). It is implemented following thyroidectomy to obliterate any remaining thyroid tissue and to tackle the residual or recurrent disease. RAI therapy serves three primary purposes: destroying benign residual thyroid tissue, treating microscopic residual disease to reduce the risk of subsequent recurrence, and treating known persistent, recurrent or metastatic disease (Pacini et al., 2022). Its application is guided by prognostic factors stratifying patients into risk categories for thyroid cancer-related outcomes. For high-risk groups, RAI significantly improves overall and disease-free survival. In intermediate-risk patients, its use is tailored to

individual risk factors, while low-risk individuals may forego RAI unless specific risk modifiers are present. The latest consensus recommends using recombinant human TSH stimulation before RAI and considering 1110 MBq as an effective dose for remnant ablation in low-risk cases if the patients are referred for thyroid remnant ablation. Diagnostic scans before RAI therapy are not routinely necessary, and the avoidance of iodine-containing drugs is advised to enhance treatment efficacy (Pacini et al., 2022). Additionally, MTC patients do not respond to RAI therapy because these neuroendocrine tumours lack NIS, which is essential for absorbing the radioactive compound (Wells et al., 2015).

RAI therapy plays a crucial role in the treatment of thyroid cancer. However, some patients exhibit resistance to radioiodine, rendering this approach ineffective for detecting or addressing distant diseases in their cases.

1.2.4.4 TSH Suppression Treatment

TSH is well-known to promote proliferation in normal thyroid cells and many thyroid cancer variants (Biondi et al., 2005). The normal reference range for TSH in the general population is approximately 0.4–4.0 mIU/L (Niafar et al., 2016). Therefore, postoperative management often includes thyroid hormone therapy at doses of levothyroxine that suppress TSH levels to decrease recurrence rates and mortality associated with DTC (Mazzaferri et al., 2001). The 2015 ATA guidelines for DTC represent a shift from the previous strict TSH suppression policy of the 2009 guidelines. The updated guidelines advocate for a more individualised approach to TSH suppression, tailored to the patient's initial risk of recurrence, response to therapy and

potential risks from thyroid hormone therapy. For low-risk and intermediate-risk patients who show an excellent response to treatment (such as negative imaging and undetectable suppressed thyroglobulin levels), the ATA recommends maintaining TSH levels between 0.5-2 mIU/L. High-risk patients who had an excellent response should aim for mild TSH suppression, maintaining TSH levels between 0.1-0.5 mIU/L. Similarly, mild TSH suppression is suggested for patients with a biochemically incomplete response. For patients with residual structural disease or a biochemically incomplete response who are young or at low risk of complications from exogenous subclinical hyperthyroidism, the ATA recommends more aggressive TSH suppression, targeting TSH levels below 0.1 mIU/L but not necessarily undetectable. This stratified approach aims to minimise the adverse effects of overtreatment while optimising therapeutic outcomes (Biondi et al., 2019; Haugen et al., 2016).

1.2.4.5 Molecular Targeted Therapies of Aggressive Thyroid Cancer

The essential role of RAI therapy in treating recurrent and metastatic thyroid cancer is well-established, particularly when tumours are capable of absorbing iodine. However, the challenge arises when certain cancers, like radioiodine-refractory differentiated thyroid cancer (RR-DTC), advanced PDTC and ATC, exhibit resistance to RAI, which is often linked to the poorest outcomes. This resistance highlights the pressing need to develop and integrate new treatments into therapeutic strategies (Ferrari et al., 2015; Leo et al., 2020). With the advancement in understanding the genetic landscape of thyroid cancer, there has been a significant diversification of therapies targeting aggressive thyroid cancers. These developments have greatly enhanced the strategic options available to combat this challenging condition.

1.2.4.5.1 Molecular Targeted Therapies for DTC

Multikinase inhibitors (MKIs) like sorafenib and lenvatinib, now approved by the US Food and Drug Administration (FDA) for RR-DTC, have shown improved progression-free survival. Sorafenib, which is a TKI, targets VEGFR 1-3, platelet-derived growth factor receptor (PDGFR), RET, FLT and c-kit. Lenvatinib targets VEGFR2, VEGFR3, EGFR, PDGFR, KIT, and RET. However, their side effects necessitate the exploration of more patient-tailored therapies (Al-Jundi et al., 2020). In 2021, a third MKI cabozantinib was approved by the FDA as a second-line treatment for advanced RR-DTC that had not responded to initial VEGFR targeted therapy. Its effectiveness against various tyrosine kinases, particularly VEGFR2, AXL, c-MET and RET, positions it as a strategic option, especially for patients resistant to antiangiogenetic treatments, but it does present a high incidence of side effects similar to those seen with other therapies of its class (Brose et al., 2022). MKIs have brought significant advancements in treating advanced RR-DTC by improving progression-free survival. However, their side effects and toxicological profiles can have a substantial impact on quality of life and necessitate frequent dose modifications or treatment pauses. Moreover, the eventual emergence of resistance to these treatments underscores ongoing research aims to find more tailored and less toxic therapeutic options.

Selective RET inhibitors, such as selpercatinib (LOXO-292) and pralsetinib (BLU-667), target specific genetic alterations in DTC and offer improved response rates with a better safety profile than traditional FDA-approved MKIs. In 2020, the FDA approved using selpercatinib and pralsetinib for managing DTC patients with RET gene fusions (Mansfield et al., 2022; Wirth et al., 2020).

Given the prevalence of $BRAF^{V600E}$ mutations in PTC, BRAF inhibitors like vemurafenib or dabrafenib are also utilised in treatment protocols of $BRAF^{V600E}$-positive RR-PTC. Furthermore, the necessity for combined RAF and MEK kinase inhibitors in thyroid cancer treatments stems from the innate resistance of these cancers to solo RAF inhibition, which is thought to be due to a lack of negative feedback suppression within the MAPK pathway (Al-Jundi et al., 2020). More recently, following the findings of the ROAR (NCT02034110) and NCI-MATCH trials, the combination therapy of dabrafenib and the MEK kinase inhibitor trametinib has been fast-tracked by the FDA for use in cases of metastatic or inoperable solid tumours with the $BRAF^{V600E}$ mutation. This approval, dated June 2022, encompasses patients who have exhausted previous treatment avenues (Salama et al., 2020; Subbiah et al., 2016). Additionally, in treating less differentiated DTC and PDTC, strategies that reactivate the ability of cancer cells to absorb iodine have proven beneficial. This involves MEK and BRAF inhibitors to upregulate NIS expression in cancers with BRAF mutations, followed by RAI therapy targeting the re-sensitised cancer cells (Leboulleux et al., 2023).

The discovery of ALK and NTRK fusions in DTC opens new therapeutic avenues, though these genetic alterations are uncommon. While no ALK inhibitors are approved for TC, NTRK inhibitors like larotrectinib and entrectinib have received FDA clearance for NTRK fusion-positive malignancies, regardless of their origin. This highlights their high efficacy and improved progression-free survival, offering a less toxic alternative compared to MKIs (Cabanillas et al., 2020; Marcus et al., 2021; Qin et al., 2022).

1.2.4.5.2 Molecular Targeted Therapies for MTC

The FDA has approved vandetanib and cabozantinib for metastatic and progressive MTC, and clinical trials have shown significant median progression-free survival improvements. However, as described before, their broad kinase targeting usually has severe adverse side effects (Elisei et al., 2013; Wang et al., 2023; Wells et al., 2012).

Selective inhibitors targeting the RET gene, such as selpercatinib and pralsetinib, have become pivotal for managing both hereditary and sporadic forms of MTC. Selpercatinib exhibits significant efficacy across various RET mutations and has demonstrated considerable antitumour effects. Pralsetinib surpasses traditional treatments such as vandetanib and cabozantinib in potency, particularly against RET mutation-positive MTC. Both pralsetinib and selpercatinib have received FDA approval for use in patients with advanced or metastatic MTC with RET mutations (Wang et al., 2023).

1.2.4.5.3 Molecular Targeted Therapies for ATC

ATC, while accounting for a minor fraction of TC cases, is recognised as the most lethal form. The American Joint Committee on Cancer categorised ATC as Stage IV thyroid cancer due to its severe aggressiveness and often metastatic state at diagnosis, regardless of the tumour size or the extent of lymph node and distant metastasis (Bible et al., 2021). Recently, genetic mutations in ATC have driven research into targeted therapies to enhance patient outcomes.

The FDA approval of dabrafenib and trametinib for treating $BRAF^{V600E}$ mutation-positive ATC offers a significant breakthrough for managing unresectable or metastatic ATC with no other options. This combination therapy addresses locally advanced and metastatic stages (Subbiah et al., 2018). Furthermore, the effectiveness of anti-PD-L1 antibody therapies, whether alone or combined with BRAF inhibitors, is an encouraging strategy for treating the ATC (Capdevila et al., 2020).

1.3 The Sodium/Iodide Symporter (NIS)

1.3.1 Physiological Function of NIS in Thyroid

The sodium/iodide symporter (NIS/SLC5A5), a solute carrier family 5A member, is an essential transmembrane glycoprotein predominantly studied and discussed within the thyroid gland. NIS plays an indispensable role in thyroid follicular cells by mediating iodide transport, a fundamental precursor in synthesising thyroid hormones. This iodide transport facilitated by NIS is pivotal for normal thyroid function, and also offers a strategic target for medical procedures. For instance, radioiodine therapy effectively employs radioactive iodine to image the gland in diagnostics or to ablate overactive thyroid tissue in conditions like Graves' disease. This method is also applied to target thyroid cancer cells that retain their iodine uptake ability, offering a therapeutic avenue for eliminating malignant cells and their potential spread (Dohán et al., 2003).

As introduced in the previous chapter (1.1.2), NIS facilitates the transport of iodide across the basolateral plasma membrane into thyroid follicular cells. Its function hinges on the sodium gradient established by the Na^+/K^+ ATPase pump, which maintains

higher sodium levels outside the cell which drives the active uptake of iodide. NIS operates by co-transporting two sodium ions with one iodide ion into the cell against the iodide gradient. This system is not only found in the thyroid gland but also operates in several extrathyroidal tissues, such as the salivary glands, stomach and mammary breast during lactation, and is observed in both primary and metastatic breast cancer cells (Tazebay et al., 2000; Wapnir et al., 2003). Initially thought to be thyroid-specific, NIS has shown its presence and functional potential in various extrathyroidal tissues. Gene therapy studies have successfully induced NIS-mediated iodide transport in diverse cell types, opening avenues for diagnosing and treating cancers outside the thyroid (Dohán et al., 2003).

NIS uniquely mediates the uptake of various anions and exhibits distinctive transport ratios. Specifically, iodide (I^-), thiocyanate (SCN^-) and chlorate (ClO_3^-) are translocated with a ratio of two sodium ions to one anion, exhibiting electrogenic properties. Conversely, perrhenate (ReO_4^-) and perchlorate (ClO_4^-) are shuttled in a one-to-one ratio with sodium, displaying an electroneutral mechanism. Moreover, previously identified as a competitive inhibitor, NIS also actively translocated perchlorate as a substrate (Dohán et al., 2007; Paroder-Belenitsky et al., 2011). Recently, this research has elucidated a crucial aspect of NIS functionality; its initial low iodide affinity is substantially enhanced in the presence of bound two Na^+ ions. After binding Na^+, NIS exhibits a 10-fold (Kd = 22.4 μM) increase in I^- binding efficiency, clarifying how effective I^- transport is achieved despite low serum I^- concentrations (Nicola et al., 2014).

1.3.2 Structural Insights into NIS: Understanding Its Mechanism of Action

The molecular exploration of NIS commenced in earnest in 1996 with the identification and isolation of the cDNA encoding rat NIS (rNIS), achieved through expression cloning in oocytes from Xenopus laevis, which utilised a cDNA library from the rat thyroid-derived FRTL-5 cell line. This pivotal development signalled the beginning of detailed studies into the molecular nature of NIS (Dai et al., 1996). Based on the cloned cDNA, the length of rNIS encoded a protein of 618 amino acids and was predicted to have 12 transmembrane segments, with both the NH_2 and COOH terminus located on the cytoplasmic side of the cell. This early model highlighted a significant hydrophilic region in the COOH terminus containing potential phosphorylation sites (Dai et al., 1996). The model was refined as research progressed to propose 13 transmembrane segments (Figure 1.11). The segment identified between positions 389-410 formed a new transmembrane segment (labelled X in Figure 1.11) between the original model's 9th and 10th segments. In the same year, Smanik et al. (1996) identified the human NIS (hNIS) gene. They revealed a 1929-nucleotide open reading frame (ORF) encoding a 643-amino-acid hNIS protein with a molecular weight of 87 kDa and 84 % identity and 93 % similarity to rNIS. Variations include a 5-amino-acid addition between hydrophobic domains and a 20-amino-acid extension at the C-terminal. Chromosomal mapping placed the hNIS gene on chromosome 19p13, with 15 exons and 14 introns (Smanik et al., 1997). This discovery and analysis of NIS across different species showed high sequence identity, underscoring the conserved nature of this transporter, which is crucial for iodine uptake in thyroid hormone synthesis.

Additionally, advanced immunofluorescence techniques supported the orientation of the NH2 terminus facing extracellular and the COOH terminus facing the cytoplasm. The consensus sequences for N-linked glycosylation at positions 225, 485 and 497 (Figure 1.11) suggest these are sites where carbohydrates are attached to the protein. However, N-linked glycosylation is not obligatory for iodide transport or protein stability (Levy et al., 1998). Conversely, the inhibition of NIS glycosylation has been implicated in impairing NIS translocation to the plasma membrane, resulting in decreased membrane NIS localisation and radioiodine uptake (Chung et al., 2015). Three charged amino acid residues (Asp16, Glu79, Arg208) are located in the transmembrane regions I, II, and VI, respectively. They are considered to be related to mediating iodine uptake (Vieja et al., 2000). It has also been confirmed that several hydroxyl-containing amino acid residues (Ser353, Thr354, Ser356 and Thr357) located in the transmembrane region IX are crucial for its function (Figure 1.11) as their mutations cause the loss of iodine uptake function (Levy et al., 1998). NIS dimerisation was hypothesised after detecting a high molecular weight band (135 kDa-180 kDa) in Western blots resulting from co-immunoprecipitation assays. Subsequently, experimental evidence has confirmed NIS dimerisation and identified three key residues: Y242, T243 and Q471 (Thompson et al., 2019).

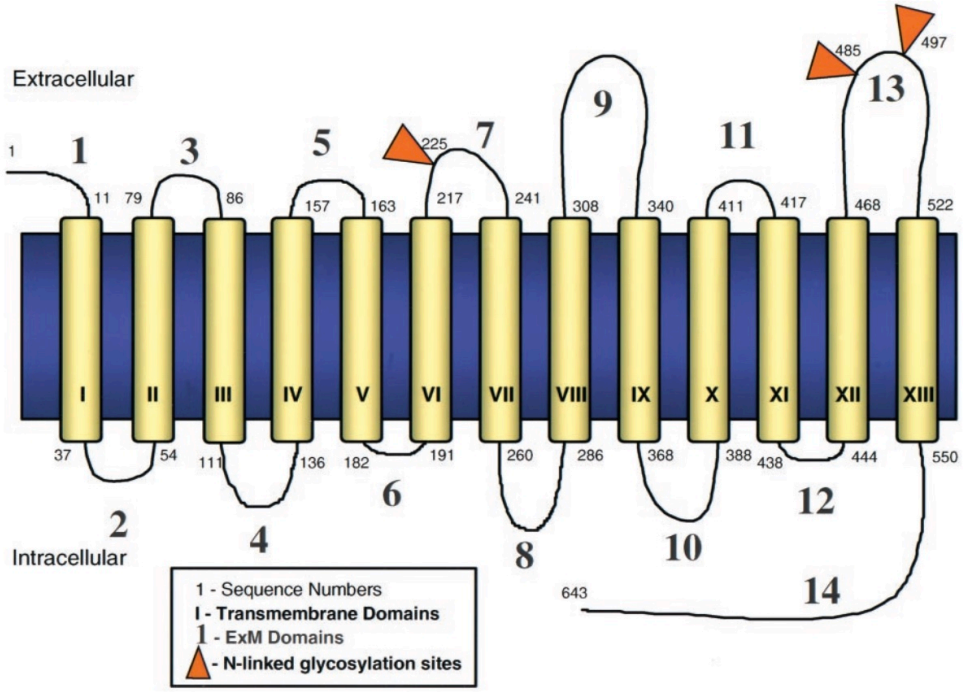


Figure 1. 11 Secondary structure of the sodium iodide symporter protein. *NIS comprises 13 transmembrane segments with a cytoplasmic C-terminal tail that is a binding site for various interacting proteins. The extracellular loops of NIS feature sites for N-terminal glycosylation. Figure adapted from (Spitzweg et al., 2001).*

1.3.3 Regulation of NIS Expression in Thyroid Gland

1.3.3.1 TSH

TSH is a glycoprotein with an approximate molecular weight of 30 kDa. It is synthesised in the anterior pituitary gland by basophilic cells called thyrotrophs (Pirahanchi et al., 2024). TSH is pivotal as the primary regulator of NIS expression in the thyroid gland. Through activation of TSHR, TSH triggers the adenylyl cyclase-Gs protein pathway, leading to cyclic AMP (cAMP) accumulation within thyroid follicular cells (Kogai et al., 2006). Elevating cAMP levels stimulates NIS transcription by engaging various signal pathways associated with cis-regulatory elements in the NIS

locus, especially the NIS upstream enhancer (NUE) (Riesco-Eizaguirre et al., 2021; Taki et al., 2002). The NUE is positioned between 9,242 and 9,300 base pairs upstream of the hNIS coding region, encompassing critical PAX8 and cAMP-response element (CRE) binding sites (Kogai et al., 2012). In thyroid follicular cells, cAMP activates the NUE via pathways involving protein kinase A (PKA) (J. Li et al., 2022). PKA phosphorylates the cAMP-responsive element binding protein (CREB) and other basic-leucine zipper (B-ZIP) proteins, facilitating their recruitment to the NUE element. PAX8 is crucial for thyroid-specific gene transcription, such as TSHR, Tg, TPO and NIS, binding to NUE upon TSH stimulation (Costamagna et al., 2004; Kambe et al., 1996; Ohno et al., 1999; Taki et al., 2002).

Additionally, in rNIS, the cascade reaction of the cAMP pathway also phosphorylates other thyroid-specific transcription factors, such as the thyroid-specific enhancer binding protein (NKX2-1), also known as thyroid transcription factor 1 (TTF-1), and the NIS TSH-responsive factor-1 (NTF-2). This phosphorylation further modulates the transcription of the rNIS gene through its proximal promoter (Dohán et al., 2003; Guan et al., 2021). Concerning the hNIS gene (Figure 1.12), two research groups have identified a thyroid-specific, TSH-responsive enhancer located upstream that shows high homology to the rat NUE. This enhancer contains potential binding sites for PAX8 and TTF-1, as well as a CRE-like sequence (Kogai et al., 2012; Kogai et al., 2006; Riesco-Eizaguirre et al., 2021). Through this intricate regulatory network, TSH regulates NIS transcription and biosynthesis in the thyroid gland.

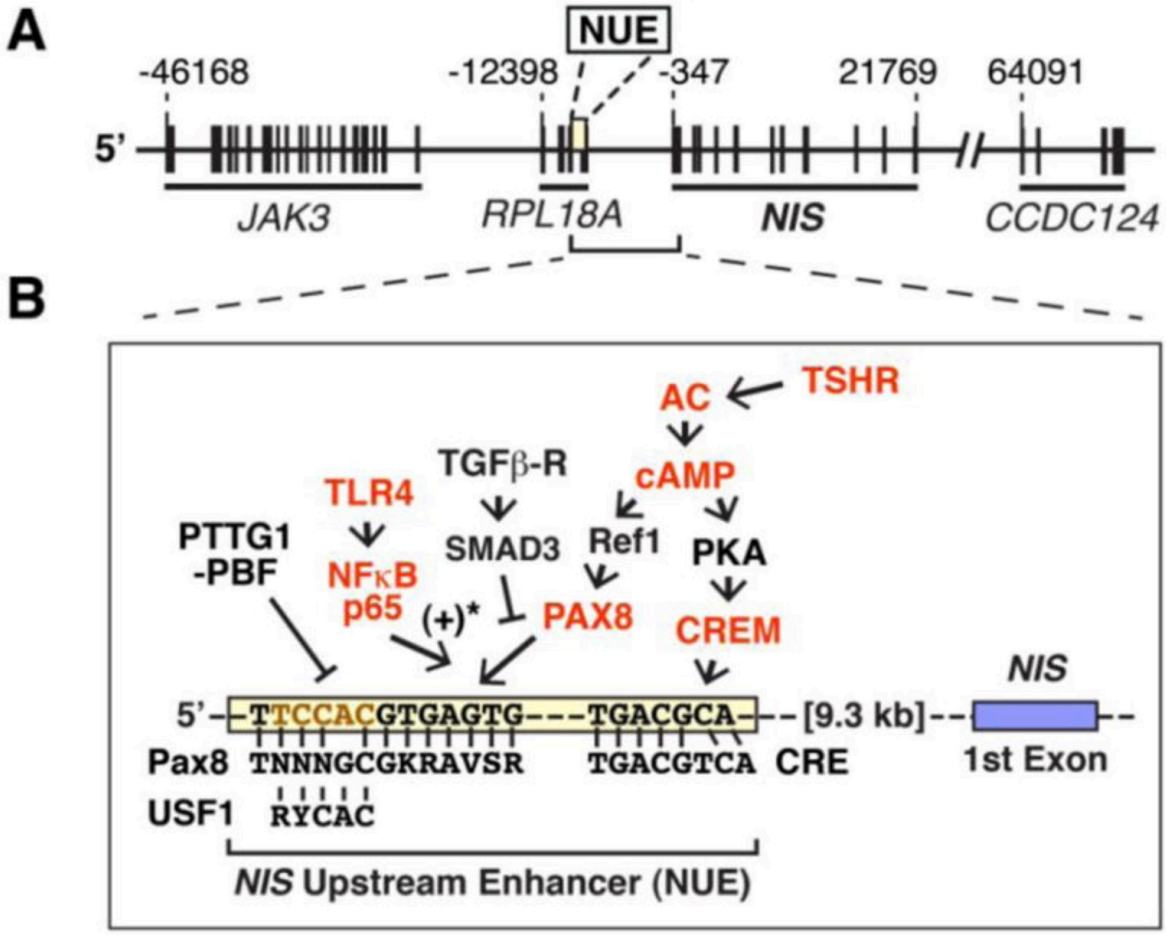


Figure 1. 12 Regulation of the NUE in Thyroid Cells. *(A) Overview of Human Chromosome 19p near the NIS Gene Locus. (B) TSHR Signalling Pathways to NUE: The expression of NIS in thyroid cells is primarily controlled through TSHR signalling to NUE. Studies involving the gain-of-function of the molecules, shown in red, have indicated enhanced activity of NUE. The consensus sequences for the cis-elements of PAX8, CRE, and USF1 are highlighted, along with the sequence of the human NUE. Figure adapted from (Kogai et al., 2012).*

Moreover, mechanisms independent of TSH additionally control the expression of NIS, chiefly through three signalling pathways that impact PAX8 binding to the NUE. Initially, within the transforming growth factor-β (TGFβ)-Smad signalling pathway cascade, TGFβ initiates Smad3 activity, which in turn impedes PAX8 from associating with NUE, leading to a notable reduction in NIS mRNA levels in thyroid follicular cells (Costamagna et al., 2004). Secondly, in the Toll-like receptor (TLR)-nuclear factor κ-

light-chain-enhancer of activated B cells (NF-κB) signalling pathway, the activation of TLR leads to subsequent activation of NF-κB, which interacts with PAX8 to initiate transcription of NIS via the NUE (Nicola et al., 2010; Nicola et al., 2009). Thirdly, in the complex involving the pituitary tumor-transforming gene-1 product (PTTG1) and the PTTG1 binding factor (PBF), PTTG1 and PBF disrupt the interaction between PAX8 and the NUE, thereby reducing NIS expression (Boelaert et al., 2007; Stratford et al., 2005).

TSH enhances NIS transcription and production and is crucial in targeting NIS translocation to, and retention in, the plasma membrane (J. Li et al., 2022). It was shown that when TSH is absent, NIS shifts from the basolateral plasma membrane to the cytoplasm, rendering it non-functional and leading to diminished iodide uptake. This process likely involves post-translational phosphorylation of NIS by cAMP-activated protein kinases upon TSH activation, influencing its plasma membrane trafficking or retention (Riedel et al., 2001). Crucially, NIS at the plasma membrane is vital for iodide uptake, a critical process for effective RAI therapy in treating thyroid cancer. The observed reduction in iodide absorption across most thyroid cancer cases can be attributed to reduced expression and disrupted positioning or maintenance of NIS at the plasma membrane. Hence, TSH is the foremost regulator of NIS within the thyroid gland, influencing both transcriptional and post-transcriptional aspects of NIS management (Riedel et al., 2001).

1.3.3.2 Regulation of NIS by Iodide

Iodide can exert an impact on NIS expression, with plasma levels modulating the accumulation and integration of iodide within the thyroid gland. Excess iodide consumption can negatively influence NIS expression, and large quantities of iodide in the plasma can hinder the synthesis of thyroid hormones by obstructing organification (Uyttersprot et al., 1997; Wolff et al., 1948). High concentrations of iodide exposure *in vivo* and *in vitro* lead to diminished iodide transport and organification, termed the Wolff-Chaikoff effect (Uyttersprot et al., 1997; Wolff et al., 1948). This effect involves the blockade of the organic binding of iodide in the thyroid when iodine levels reach a critical threshold, followed by an “escape” phenomenon restoring normal hormone biosynthesis (Wolff et al., 1949).

Research conducted on animal models demonstrated that increased iodine levels led to a decrease in the thyroid gland's ability to absorb iodine, and this phenomenon is independent of TSH (Socolow et al., 1968). Further studies indicated that excess iodine reduces both NIS mRNA and protein levels (Eng et al., 1999; Leoni et al., 2011). Interestingly, another study by Eng et al. (2001) revealed only a reduction in the NIS protein level but no decrease in the mRNA level after 24 to 48 hours of excess iodine exposure in FRTL-5 cells, suggesting post-transcriptional regulation of NIS expression by iodine (Eng et al., 2001). A more recent study showed that rats treated with NaI exhibited elevated iodine levels in urine, increased serum TSH levels, and decreased expression of NIS, TSHR and TPO mRNA and proteins levels, indicating primary thyroid dysfunction induced by chronic iodine excess (Calil-Silveira et al., 2016). These

findings underscore the intricate interplay between iodide levels and NIS activity, highlighting the multifaced regulatory mechanism involved.

1.3.3.3 Effect of Cytokines on NIS

Beyond TSH and iodide, cytokines significantly modulate NIS expression and function in thyroid cells, impacting iodine uptake critical for TH biosynthesis. In 1994, a study found that cytokines such as IL-1, TNF-alpha and IFN-gamma can significantly influence thyroid cell activity with their concentration-dependent effects. High levels of these cytokines generally inhibit the production of crucial thyroid components, potentially contributing to the decreased thyroid function seen in various thyroid inflammatory diseases (Rasmussen et al., 1994). Later, research using FRTL-5 cells showed that cytokines like TNF-alpha and IL-1 alpha inhibit both basal and TSH-stimulated NIS mRNA levels. However, IFN-gamma reduces TSH-induced NIS mRNA expression at higher concentrations. TNF-alpha, IL-1 alpha and IFN-gamma all influence iodide uptake negatively (Ajjan et al., 1998). Similarly, another study indicated that ageing, lower TSH levels, and increased TNF or TGF-β1 primarily reduced iodide uptake by diminishing NIS mRNA expression in the thyroid. Furthermore, TNF inhibits this expression via a protein synthesis-dependent activation of the sphingomyelinase (Pekary et al., 1998). The experiments from Spitzweg et al. (1999) demonstrated that specific cytokines, particularly IL-1β and TNF-α, significantly suppress NIS gene expression and function, leading to decreased iodide uptake in thyroid follicular cells, which may contribute to the reduced effectiveness of radioiodine uptake in thyroiditis.

1.3.4 Dysregulation of NIS in Thyroid Cancer

The activity or presence of NIS in thyroid cancer cells is essential for the success of RAI therapy in patients. Since 1996, the successful cloning of the NIS gene has allowed in-depth molecular analysis of the disrupted iodide accumulation process in thyroid cancer cells (Smanik et al., 1996). Multiple researchers have demonstrated that NIS gene expression is frequently reduced and/or exhibits impaired plasma membrane targeting (Spitzweg et al., 2001). Thus, therapeutic strategies to enhance NIS expression or its localisation to the plasma membrane hold promise for restating radioiodine uptake in thyroid tumours.

As mentioned in the previous section (1.3.3), in the normal thyroid gland, NIS expression and function are regulated by TSH and additional molecular pathways that ensure adequate iodide accumulation for TH production. However, in thyroid cancer, numerous signalling pathways, epigenetic alterations and aberrant molecular interactions contribute to NIS dysfunction, leading to the impaired radioiodine uptake characteristic of these malignancies.

1.3.4.1 MAPK Pathway in Thyroid Cancer and NIS Regulation

In thyroid cancer, the MAPK pathway often becomes constitutively activated due to mutations in genes such as BRAF, RAS or rearrangements involving RET/PTC. This aberrant activation leads to uncontrolled cell growth and a differentiated state where thyroid-specific genes, including NIS, are down-regulated (Zaballos et al., 2017). The constitutive signalling pathway through MAPK interrupts the regular transcriptional

programme maintained by thyroid-specific transcription factors, such as PAX8, NKX2-1 and FOXE1 (also known as TTF-2), which are crucial for gene transcription activity within thyroid follicular cells, thereby diminishing NIS expression and compromising iodide uptake (Frattini et al., 2004; Kimura et al., 2003; Soares et al., 2003). Recently, strategies to overcome this include using MEK inhibitors, which, combined with BRAF inhibitors such as vemurafenib, have shown potential in re-sensitising thyroid cancers to radioiodine by restoring NIS expression. This combination therapy aims to blunt the overactive MAPK signalling, thus allowing re-differentiation of thyroid cancer cells and re-establishment of their iodide-handling capabilities (H. Song et al., 2018).

1.3.4.2 PI3K/AKT Pathway in Thyroid Cancer and NIS Regulation

Aberrant activation of the PI3K/AKT pathway has been associated with advanced disease and radioiodine refractory states in thyroid carcinomas (Zaballos et al., 2017). For example, insulin-like growth factor 1 (IGF-1) has been shown to inhibit iodide uptake in TSH-stimulated thyroid cells by activating the PI3K/AKT pathway, which can suppress NIS gene expression (García et al., 2002). Importantly, inhibition of this pathway by using the PI3K inhibitor LY294003 appears to reverse the downregulation of NIS and enhance radioiodine uptake. Blockade of AKT, a critical downstream effector of PI3K, can increase NIS expression and its functional activity (Kogai et al., 2008). Furthermore, mutations in regulators like RasGRP3 have been identified in metastatic and radioiodine-refractory thyroid cancers, with mutant RasGRP3 reducing NIS and TSHR expression, and increasing AKT phosphorylation, suggesting that overactive AKT signalling pathway via such mutations could contribute to the failure of radioiodine therapy (J. Song et al., 2018).

Additionally, the mammalian target of rapamycin (mTOR), operating downstream of the PI3K/AKT signalling pathway, is a pivotal regulator of NIS expression, radioiodine uptake and cellular survival (Zaballos et al., 2017). Several studies have demonstrated that mTOR inhibitors, including Torin2 and rapamycin, significantly enhance the expression and functionality of NIS expression and other thyroid-specific genes, particularly in thyroid cancers with distinct genetic mutations (Plantinga et al., 2014; Tavares et al., 2018). This evidence highlights the essential role of mTOR signalling pathways in regulating NIS gene expression and influencing therapeutic responses in thyroid cancer.

1.3.4.3 Other Signalling Pathways

The Notch, TGF-β/Smad, NF-κB and Wntβ/-catenin signalling pathways are also integral components of the molecular landscape in thyroid cancer, influencing cellular functions and contributing to the dedifferentiation processes of the disease (Hao et al., 2019; Oh et al., 2021). Aberrant activation of these pathways can disrupt the expression and functionality of thyroid-specific genes, including NIS, thereby impairing the iodide accumulation capacity of thyroid cells (Oh et al., 2021).

1.3.4.4 DNA Methylation in Thyroid Cancer and NIS

DNA methylation is a prevalent epigenetic modification closely associated with the pathogenesis of various cancers, including thyroid cancer (Xing, 2013). The hNIS promotor contains CpG-rich regions critical for transcription and DNA methylation in these areas, which has been implicated in the altered expression of NIS (Zhao et al.,

2015). Decreased NIS mRNA expression in thyroid cancer is often attributed to hypermethylation of its promoter, with studies indicating a correlation between methylated NIS promoters and reduced iodide concentrating ability in PTC patients (Galrão et al., 2014; Venkataraman et al., 1999). Aberrant hypermethylation of the NIS gene and other thyroid-specific genes, like TSHR, Pendrin and NKX2-1, is common in various thyroid cancers. This hypermethylation is strongly associated with decreased expression of these genes, impairing crucial functions like iodide uptake, which is essential for effective RAI therapy (Kondo et al., 2009; Xing et al., 2003). Importantly, applying DNA demethylating agents has been shown to effectively reverse these epigenetic changes, thereby restoring gene function and improving radioiodine uptake, offering a potential therapeutic avenue for enhancing outcomes in thyroid cancer treatment (Galrão et al., 2014; Venkataraman et al., 1999).

1.3.4.5 Histone Modification

Histone modifications, especially acetylation and deacetylation, play critical roles in gene regulation and significantly affect thyroid cancer progression and treatment strategies (Chen et al., 2022; Russo et al., 2013). These modifications influence chromatin structure, alternately promoting gene activation or repression, and are crucial in the expression of thyroid-specific genes, including NIS. In thyroid cancer, alterations in histone acetylation patterns, particularly in lysine residues of histones H3 and H4, have been identified as early events in tumourigenesis, affecting NIS function and impacting the effectiveness of RAI therapy (Zhang et al., 2014). Recent studies have demonstrated that histone deacetylase inhibitors (HDAC inhibitors, HDACi) can significantly enhance the expression and functionality of NIS and other thyroid-specific

genes, such as PAX8, NKX2-1, FOXE1 and TSHR, thereby improving radioiodine uptake in thyroid cancer (Oh et al., 2021). Moreover, HDAC inhibitors induce histone acetylation, leading to chromatin relaxation and gene transcription activation, which promotes differentiation, apoptosis, and growth arrest of PTC cells. This advancement points to a promising therapeutic potential for HDAC inhibitors in promoting the redifferentiation of thyroid cancers, which is crucial for effectively managing the disease (Chen et al., 2022).

1.3.4.6 MicroRNAs

MicroRNAs (miRNAs) play pivotal roles in thyroid cancer by regulating gene expression at the post-transcriptional level, impacting both the initiation and progression of disease (Chou et al., 2017). miR-146-3p, which is highly prevalent and overexpressed in PTC, attaches to a unique site on the 3′ untranslated regions (3' UTR) of NIS, decreasing its expression. Crucially, miR-146-3p also targets three specific locations in the 3' UTR of PAX8, inhibiting its expression. Therefore, miR-146-3p suppresses NIS expression both directly and indirectly by downregulating PAX8 (Riesco-Eizaguirre et al., 2015). Consistent with this finding, blocking miR-146-3p in human thyroid cancer cells restored NIS-mediated iodine uptake (Hou et al., 2020; Li et al., 2015). Other miRNAs, such as miR-339-5p and miR-17-92, have been identified as repressors of NIS expression across different cell types, including thyroid and breast cancer cells (Fuziwara et al., 2020; Lakshmanan et al., 2015).

In summary, the complex interplay between disrupted signalling pathways, altered gene expression, epigenetic modifications, and microRNAs illustrates the multifaceted

nature of NIS dysfunction in thyroid cancer. This complexity underscores the necessity for a comprehensive, multi-targeted therapeutic approach to restore thyroid cell differentiation and function, enhancing treatment efficacy and improving patient outcomes. While not all are predominantly upregulated in thyroid carcinomas, their impact on NIS and related thyroid-specific genes like PAX8 highlight their essential role in modulating thyroid cell differentiation.

1.3.5 NIS Trafficking to the Plasma Membrane

NIS must be localised at the basolateral plasma membrane (PM) to transport iodide efficiently (Ahn, 2012). As mentioned above, TSH intricately regulates the trafficking of NIS to the cell surface, significantly influencing the expression, stability and localisation of the NIS protein (Riedel et al., 2001). In addition, the oncogenic $BRAF^{V600E}$ mutation also affects the expression and redistribution of NIS. This mutation was proven not only to disrupt the TSH/cAMP signalling pathway but also to stimulate TGF-β secretion, further inhibiting NIS transcriptionally and trafficking to PM (Riesco-Eizaguirre et al., 2009). Studies have found that in many cases of thyroid and breast cancers, while the expression of NIS may be normal or even at elevated levels, it often fails to facilitate iodide transport due to being retained within a cytoplasmic localisation (Wapnir et al., 2004). Therefore, while enhancing NIS transcription is crucial, it alone may be insufficient, and adequate therapeutic strategies must also ensure the correct basolateral PM localisation of NIS to reestablish its iodide transport function. Although the precise mechanisms of NIS subcellular trafficking are not fully understood, significant progress has been made in understanding the impact of post-transcriptional modifications such as glycosylation and phosphorylation. Glycosylation

at designated sites affects NIS functionality and stability: specific mannosidases may control its glycosylation and thereby influence its processing and localisation (Rathod et al., 2019). Furthermore, phosphorylation and interactions with clathrin adaptors, such as AP-1B subunit σ1, are crucial for properly targeting NIS to the appropriate membrane in polarised epithelial cells, ensuring its iodide uptake efficacy (Martín et al., 2019).

1.3.6 NIS Interactome: Its Interaction with PBF, Moesin and VCP

Recent discoveries have identified several additional proteins interacting with NIS, significantly impacting transcription and cellular localisation.

1.3.6.1 PBF

Pituitary tumor-transforming gene-binding factor (PBF), encoded by the PTTG1IP gene on chromosome 21q22.3 (Chien et al., 2000), is a multifunctional protein implicated in diverse cellular processes such as transcription regulation, proliferation and tumourigenesis.

1.3.6.1.1 PBF Structure and Function

PBF (Figure 1.13) comprises 180 amino acids and possesses an estimated molecular weight of 22 kDa (Yaspo et al., 1998). It is characterised by several domains and motifs essential for its varied biological functions, including an N-terminal region potentially containing a signal peptide within the first 32 amino acids and then a Plexin-

Semaphorin-Integrin (PSI) domain between residues 39-92, rich in cysteines and commonly found in membrane-associated proteins, which facilitates protein-protein interactions (Bork et al., 1999). Adjacent, a transmembrane domain between amino acids 95 and 122 suggests potential plasma membrane localisation. Within the segment spanning amino acids 94 to 150, a binding site for the p53 protein is present (Yaspo et al., 1998). Critically, amino acids 149 and 166 contain a bipartite nuclear localisation signal (NLS) near the C-terminus, suggesting its dual localisation in the nucleus and cytoplasm (Chien et al., 2000). A tyrosine-based sorting signal (YXXΦ motif) found at the C-terminal end (Y174 - F177) is crucial for internalisation and cellular trafficking (Smith et al., 2013). This motif includes a phosphorylation site at tyrosine 174, which is pivotal for the function of PBF in intracellular signalling and protein sorting. PBF also features two N-glycosylation sites at residues N45 and N54, which may influence protein folding, stability and function (Perez et al., 2023).

The protein-protein interaction between PBF and the pituitary tumor-transforming gene (PTTG1) is pivotal for their nuclear translocation and subsequent transcriptional regulation. The C-terminal domain of PBF is crucial for binding to PTTG1, anchoring it within the nucleus, where they collaboratively enhance the transcription of fibroblast growth factor-2 (FGF-2). FGF-2 is a potent angiogenic factor that modulates vascular endothelial growth factor (VEGF) expression and plays an essential role in tumour angiogenesis and metastatic potential, indicating that the PBF-PTTG1 complex plays a significant role in transformation, proliferation and tumourigenesis (Chien et al., 2000; McCabe et al., 2002; Saadeh et al., 2000; Zou et al., 1999). Furthermore, the interplay between PBF and PTTG1 is implicated in modulating the tumour suppressor protein p53, diminishing its stability and downstream DNA repair and apoptotic functions,

indicating PBF plays a significant role in a broad range of cancers, including those of the thyroid, breast and colorectum (Read et al., 2018). Regarding its physical structure, the proto-oncogene PBF influences cellular dynamics by modulating migration and invasion across various cancer cell types. Overexpression of PBF is observed across multiple endocrine malignancies and is linked with heightened tumour aggressiveness (Watkins et al., 2016).



Figure 1. 13 Structure of the PBF protein. *PBF initiates with a presumptive signal peptide at the N-terminus (amino acids 1-32). Between residues 39-92, a plexin-semaphorin-integrin (PSI) domain rich in cysteines follows. A transmembrane region (residues 95-122) is proximal to the PSI domain. From residues 149 to 166 is a bipartite nuclear localisation signal (NLS). The C-terminus of the protein comprises the final 30 residues, a tyrosine-based sorting signal (YXXΦ motif) found at the C-terminal end (Y174-F177), which is crucial for internalisation and cellular trafficking. Figure adapted from (Smith et al., 2009).*

1.3.6.1.2 PBF and NIS

PBF is upregulated in thyroid cancer and is a predictor of early tumour recurrence. Multiple studies have indicated that PBF is critical in thyroid tumourigenesis, inhibiting effective radioiodine treatment by repressing iodide uptake. This inhibition occurs through transcriptional suppression of NIS and post-transcriptional modifications affecting the NIS localisation (Smith et al., 2011).

PTTG1 and its binding factor PBF downregulate NIS mRNA and reduce iodide uptake in rat FRTL-5 and human primary thyroid cells. This process is partly mediated

influenced by FGF-2 and the suppression of promoter activity at the NUE region, particularly via a complex PAX8-upstream stimulating factor (USF1) response element (Boelaert et al., 2007). *In vivo*, studies utilising the PBF-Tg mouse model have confirmed that overexpression of PBF significantly suppresses NIS expression and function, where NIS mRNA levels and radioiodine uptake were reduced considerably in transgenic PBF-Tg mouse thyrocytes compared to wild type (Read et al., 2011). Furthermore, targeted siRNA-mediated PBF downregulation in primary thyroid cultures from transgenic mice and human cells effectively alleviates this suppression (Read et al., 2011). These findings demonstrated that PBF can downregulate NIS expression and its functional activity both *in vivo* and *in vitro*.

In addition to influencing transcription, PBF also suppresses NIS function through posttranslational modifications (Smith et al., 2009). This study first confirmed specific binding between PBF and NIS through pull-down and co-immunoprecipitation assays. Further, cell-surface biotinylation assays revealed that PBF transfection leads to a decreased presence of NIS on the plasma membrane compared to vector-only controls (Smith et al., 2009). This study also demonstrated that both PBF and NIS strongly colocalise with CD63 in late endosomes through a clathrin-pit-mediated internalisation pathway rather than associating with caveolin-1, which governs caveolar-dependent trafficking. The presence of a YXXΦ motif at the C-terminal of PBF, which has been demonstrated as an endocytosis motif, supports its involvement in this specific internalisation trafficking mechanism (Smith et al., 2013). This process crucially influences NIS localisation away from the PM (Smith et al., 2009).

Moreover, PBF was identified as being tyrosine phosphorylated via specific binding to the proto-oncogene tyrosine-protein kinase Src, leading to phosphorylation at residue tyrosine 174 (Y174) within the YXXΦ motif (Smith et al., 2013). It was also demonstrated that Y174 plays a pivotal role in mediating both PBF endocytosis and its interaction with NIS. Inhibition of this phosphorylation by the Src inhibitor PP1 resulted in enhanced iodide uptake into thyroid carcinoma cells and human primary thyroid cells (Smith et al., 2013). These findings suggest that targeting PBF phosphorylation at Y174 with tyrosine kinase inhibitors could serve as a promising therapeutic approach to improve the effectiveness of RAI therapy in thyroid cancer or other endocrine-related carcinomas.

Additionally, heightened expression of $BRAF^{V600E}$ in thyroid carcinoma cells corresponded to elevated PBF protein levels, along with poorer overall and disease-free survival rates in patients (Read et al., 2017).

1.3.6.2 VCP

Recent research has uncovered the involvement of another protein in NIS trafficking, particularly in thyroid and breast cancers. Fletcher et al. (2020) revealed that valosin-containing protein (VCP, also known as p97) exhibits a specific interaction with NIS. VCP/p97 and its yeast homologue Cdc48p belong to the type II class of the AAA (ATPase associated with various cellular activities) ATPase family and were initially identified as endoplasmic reticulum (ER) - associated proteins. VCP plays a critical role in ER and mitochondrial function. Dysregulation of VCP can disrupt protein

degradation, subcellular translocation, and calcium homeostasis, contributing to the pathogenesis of various diseases (Sun et al., 2020).

1.3.6.2.1 VCP Structure

Structurally, VCP comprises four distinct domains: a conserved N-terminal domain, two AAA ATPase domains (D1 and D2) and a C-terminal domain (Niwa et al., 2012). The D1 and D2 domains are arranged in a head-to-tail configuration, linked by a brief polypeptide connector. In contrast, a separate short linker connects the N-terminal domain to the D1 domain (Figure 1.14). In mammalian cells, VCP functions as a homohexamer (Xia et al., 2016), forming an active complex with a double-ring structure where the D1 and D2 domain is positioned on top of each other (Figure 1.14). Six subunits are organised to create a central channel through which proteins are transported and unfolded from their tertiary structure. Notably, the N-terminal domain of VCP plays a pivotal role in substrate recognition and cofactor interaction. Cofactors are believed to utilise shared binding regions located on the N-terminus and within the linker connecting the N and D1 domains of VCP monomers. This arrangement may prevent the simultaneous binding of multiple cofactors with conflicting functions (Niwa et al., 2012). The D1 and D2 domains exhibit homology in sequence and structure but perform different roles. The D2 domain is primarily responsible for significant ATPase activity, whereas the D1 domain contributes to hexamer assembly and less to ATPase activity (Tang et al., 2016). The C-terminal tail facilitates nuclear localisation through interactions with other proteins (Xia et al., 2016). Crucially, the linkers connecting domains are integral to the functions of the VCP (González-Pérez et al., 2012).

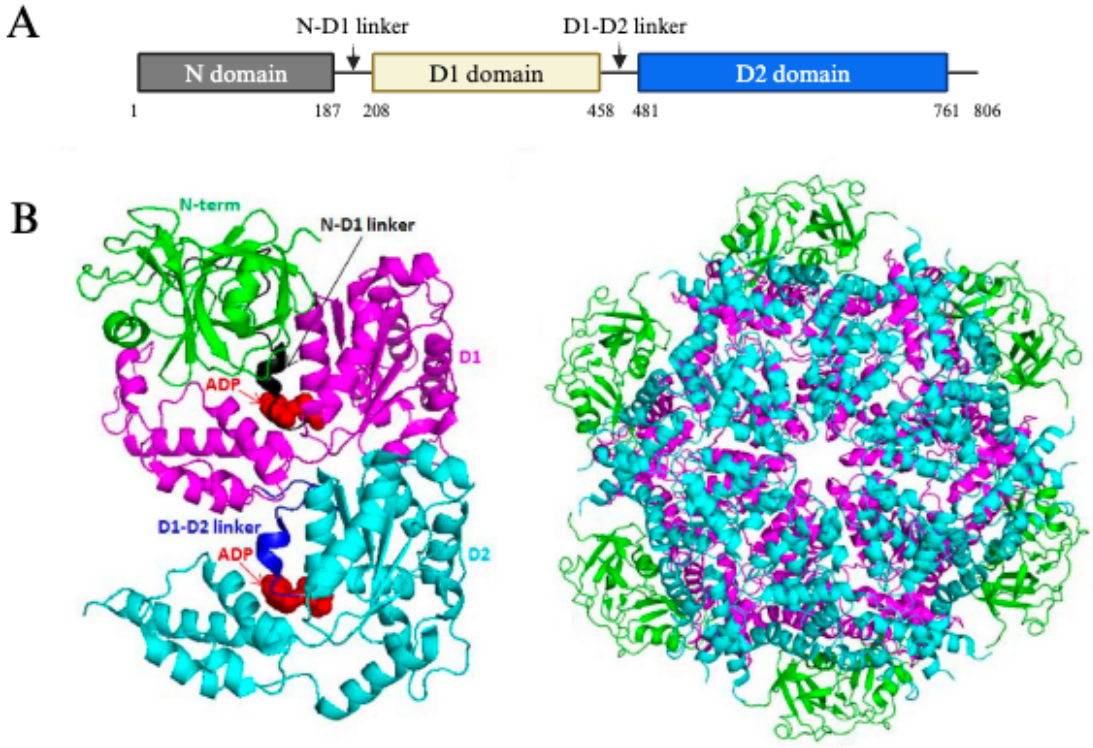


Figure 1. 14 2-D and 3-D structural of Valosin-containing protein (VCP). *(A) VCP comprises 806 amino acids and is organised into domains N, D1, and D2. Between the three domains, there are N-D1 linkers and D1-D2 linkers. (B) The atomic configurations of VCP are both a single monomer (left) and part of a hexametric assembly (right). The N-terminal domain is highlighted in green, the N-D1 liner in black, the D1 domain in magenta, the linker between D1 and D2 in blue and the D2 domain in cyan. Adenosine diphosphate (ADP) molecules are depicted as red spheres. Figure adapted from (Costantini et al., 2021; Xia et al., 2016).*

1.3.6.2.2 VCP Function

As a protein substrate, VCP plays various molecular biological roles in cell physiological and biochemical reactions. The diversity of VCP cell function is mainly related to the molecular function of protein quality and stability, which is associated with the transcriptional regulation of various cellular processes controlled by protein aggregates. Importantly, VCP/97 engages with numerous cofactors, contributing to various cellular processes crucial for the survival and aggressiveness of cancer cells.

Its overexpression in multiple cancer types, including thyroid cancer, has positioned VCP/p97 as a potential biomarker and therapeutic target in cancer research (Costantini et al., 2021).

1.3.6.2.2.1 Function of VCP Protein and Cofactor

VCP binds to and interacts with many cofactors, regulating their function by recruiting them into different cellular pathways, including endoplasmic reticulum-associated degradation (ERAD), chromatin-associated degradation, endosomal trafficking and autophagy. One of the critical functions of VCP is as a molecular chaperone within the ERAD pathway, a crucial quality control mechanism for maintaining protein homeostasis. Recruited to the ER membrane by adapters like nuclear protein localisation protein 4 (NPL4), p47 and UBX domain-containing protein 1 (UBXD1), VCP subsequently undergoes conformational changes upon ATP binding, facilitating the unfolding and subsequent extraction of target proteins. This process ensures the delivery of misfolded proteins to the proteasome for degradation, contributing to cellular homeostasis. Additionally, the NPL4-UFD1-VCP complex plays a role in cell cycle regulation, including extracting prereplication factors and Aurora B (Costantini et al., 2021).

1.3.6.2.2.2 VCP Degrades Endoplasmic Reticulum-Associated Proteins

Cells maintain protein homeostasis using highly efficient and sophisticated protein quality control systems, including facilitating the synthesis, folding, and transport of new peptide chains and mediating the degradation of misfolded or damaged proteins.

The ER is an essential site for synthesising and processing endocrine proteins in cells. Endoplasmic reticulum homeostasis imbalances induce ER stress responses (ERS) and the ERAD pathway, and initiate the unfolded protein reaction (UPR) (Walter et al., 2011). The UPR produced by ER stress is a complex process consisting of multiple signalling pathways (Hetz, 2012). When proteins are properly synthesised and processed, they are transported outside the endoplasmic reticulum through membrane vesicular transport. When misfolded proteins are produced, the endoplasmic reticulum stress response is induced, and the ERAD pathway is initiated so that the misfolded proteins are transported outside the membrane and degraded by the proteasome, thus maintaining protein homeostasis (Walter et al., 2011).

VCP plays an essential role in ERAD (Anderson et al., 2015). VCP is a recognition factor and pathological effector for abnormally folded proteins accompanying substrates from the endoplasmic reticulum to the cytoplasm through the ubiquitin-proteasome (Ub-Pr) pathway (Hirabayashi et al., 2001; Rao et al., 2004; Zhong et al., 2004). The Ub-Pr system is a protein degradation pathway in eukaryotic cells that mainly degrades ubiquitinated proteins. Ubiquitin binds substrate proteins through a series of catalytic steps involving ubiquitin-activate E1, ubiquitin-binding enzyme E2, and ubiquitin-ligase E3 to form a ubiquitin-substrate protein complex, which enables substrates to enter the 26S proteasome for ubiquitination and degradation (Leestemaker et al., 2017).

Cancer cells rely more on protein quality control systems including the ubiquitin-proteasome system (UPS) than normal cells to maintain protein homeostasis (Deshaies, 2014). This is because the rapid growth of tumours depends on high-speed

protein synthesis and folding ability. At the same time, the increase of genomic mutations in cancer cells leads to many mutant proteins that are difficult to fold correctly. The microenvironment is subject to hypoxia, REDOX imbalance, pH fluctuation and nutrient shortage. This situation can cause tumour cells to face a more severe protein-toxic pressure (Dufey et al., 2015). In tumour cells, UPS is often overactive to meet the need to degrade misfolded proteins, thereby relieving intracellular protein 'poisonous' stress. Once the UPS pathway is blocked, a significant accumulation of misfolded proteins in the cell leads to the death of oncogenic cells. Therefore, targeting the critical components of UPS, blocking the degradation of misfolded or damaged proteins, breaking the homeostasis of proteins in cancer cells, and inducing apoptosis have all become new directions of tumour therapy. The successful clinical application of proteasome inhibitors has confirmed the feasibility of targeting UPS in cancer treatment (Manasanch et al., 2017).

1.3.6.2.3 VCP and NIS

The McCabe group utilised diverse methodologies, including mass spectrometry, co-immunoprecipitation, and proximity ligation assays, to elucidate that VCP binds to NIS and plays a regulatory role in NIS trafficking (Fletcher et al., 2020). This study revealed that VCP overexpression correlates with decreased cytoplasmic and membrane-bound NIS levels, leading to impaired radioiodine uptake, suggesting that VCP has a potential role in modulating NIS expression at the PM. The typical function of VCP is to promote the extraction of misfolded proteins from the ER, which is a "separating enzyme" process that usually requires ATPase activity. However, abrogation of VCP ATPase in the D2 domain did not rescue NIS function, showing that VCP affected NIS

function in a way independent of the ATPase activity (Fletcher et al., 2020). Hence, it is unclear whether the functional association between NIS and VCP aligns with the conventional ERAD role of VCP, contingent on ATP hydrolysis, or if NIS engages with VCP through alternative pathways like autophagy.

Additionally, inhibiting VCP restored NIS function, enhancing radioiodine uptake in mouse and human thyroid models, suggesting a promising avenue for improving RAI therapy efficacy. Furthermore, analysis of The Cancer Genome Atlas (TCGA) data indicated that elevated VCP levels in PTC patients, particularly those with RET fusion, BRAF mutation or PAX8 fusion, correlated significantly with shorter disease-free survival and increased recurrence risk post-RAI treatment (Fletcher et al., 2020). Detailed examination of VCP inhibitors as a therapeutic approach to restore radioiodine uptake in thyroid and breast cancer cells will be extensively explored in Chapter 4.

1.3.6.3 Moesin

1.3.6.3.1 Moesin Structure and Function

Moesin, an ERM (ezrin-radixin-moesin) protein family member, was initially isolated from the bovine uterus and identified as a potential heparan sulfate receptor. Then, cDNA sequencing revealed a 577 amino acid protein encoded by a 4.2 kb mRNA MSN gene (Lankes et al., 1991). Structurally, the moesin protein (Figure 1.15) comprises a conserved N-terminal FERM domain responsible for interactions with plasma membrane proteins, an extended alpha-helical domain, and a C-terminal domain

facilitating binding to F-actin (Pearson et al., 2000). This configuration allows moesin to act as a molecular linker between the plasma membrane and the cytoskeleton, regulating diverse cellular processes such as cell motility, adhesion and signalling transduction (Bretscher et al., 2002; Fehon et al., 2010). The FERM domain of moesin comprises three subdomains (F1, F2 and F3), resembling a cloverleaf structure, with each subdomain displaying structural homology to distinct protein folds (Fehon et al., 2010). Moesin is characterised by masked binding sites resulting from intramolecular interactions in its dormant conformation, thereby maintaining its inactive status. This structure state hides crucial functional domains, such as the N-terminal and C-terminal interaction domains. Activation of moesin occurs via phosphorylation of a threonine residue (Thr558) in the C-terminal domain (Matsui et al., 1998), which exposes the actin-binding site to membrane proteins, whether integral or peripheral, via a FERM domain (Pearson et al., 2000). Moesin binds to the cytoplasmic domains of CD43, ICAM-2 and CD44 *in vitro*.

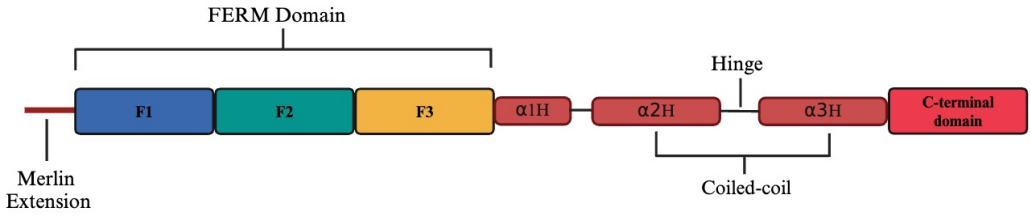


Figure 1. 15 Structure of Moesin. *Moesin comprises a conserved N-terminal FERM domain responsible for interactions with plasma membrane proteins, an extended alpha-helical domain, and a C-terminal domain facilitating binding to F-actin. Adapted from (Michie et al., 2019).*

It is well known that the ERM protein family plays a pivotal role in orchestrating fundamental cellular processes such as cell adhesion, migration and morphogenesis through regulating actin cytoskeleton dynamics (Fehon et al., 2010; Fiévet et al., 2007).

Many studies have demonstrated a correlation between upregulated levels of moesin protein expression and the advancement of malignancies in various cancer types, such as papillary thyroid carcinomas, glioblastoma tumours and breast cancers (Charafe-Jauffret et al., 2007; Tao et al., 2011; Zhu et al., 2013). One study indicated that in oral squamous cell carcinoma, the expression of moesin protein correlated with larger tumour size, lymph node metastasis and invasion (Kobayashi et al., 2004).

1.3.6.3.2 Moesin and NIS

The endocytosis process of NIS likely follows a clathrin-mediated pathway, wherein the internalised protein is directed to the early endosome for subsequent sorting, either for degradation, recycling back to the plasma membrane, or both (Fletcher et al., 2020). Moesin is essential to the clathrin-mediated internalisation pathway (Nomachi et al., 2013). Furthermore, unpublished findings from the McCabe research group reveal that thyroid cancer cells with moesin knockdown had significantly increased uptake of radioactive iodine, indicating increased PM expression of NIS protein. Additionally, evidence of an interaction between moesin and NIS was obtained through the NanoBiT assay (unpublished data from McCabe et al.).

1.4 NIS Importance in Breast Tissue

1.4.1 NIS Expression in Lactating Mammary Gland

NIS is expressed in the mammary gland during the lactation period and in both primary and metastatic breast cancer cells (Dohán et al., 2003). NIS plays a critical role in the

physiological mechanisms of iodide transport in the lactating mammary gland, facilitating the effective translocation of iodide from the bloodstream into milk (Ronga et al., 2007). This process is essential for providing approximately 150 μl/L of the iodine necessary for neonatal thyroid hormone synthesis, which is crucial for early development (Mulrine et al., 2010; Velasco et al., 2018). Conversely, immunoreactivity for NIS is absent in nonlactating mammary tissues, demonstrating that normal breast cells do not express NIS under typical physiological conditions (Tazebay et al., 2000).

Prolactin significantly stimulates iodide accumulation in cultured mouse mammary tissues (Rillema et al., 1996). This phenomenon indicated that the regulatory mechanisms modulating NIS expression in lactating mammary glands are distinct from those in thyroid tissues, and primarily influenced by hormonal changes associated with lactation (Tazebay et al., 2000). Increased levels of prolactin during lactation enhance NIS expression and activity (Rillema et al., 2000). Oxytocin has been shown to increase NIS expression and facilitate radioiodine uptake in mammary tissue, and oxytocin antagonists significantly reduce this effect (Cho et al., 2000). Estrogen also enhances the expression levels of NIS mRNA in the mammary gland (Tazebay et al., 2000). In mice undergoing ovariectomy, a coordinated increase in NIS expression is most notably induced by the combined action of estrogen, prolactin and oxytocin hormones (Tazebay et al., 2000).

These findings present a novel perspective on the hormonal control of iodide homeostasis, with significant implications for physiological lactation and breast cancer.

1.4.2 NIS in Breast Cancer

1.4.2.1 Overview of Breast Cancer

Breast cancer is the most commonly diagnosed cancer among women worldwide, with an estimated 2.3 million new cases reported annually as of 2020. In the UK, annual statistics show approximately 56,000 new breast cancer cases, with a projected increase to 69,000 by 2038-2040. Incidence rates have risen by about 5% over the past decade. Mortality trends reveal about 11,500 deaths per year, with a decline of 18 % over the last decade and a further 13 % decrease anticipated by 2040. Nearly half of all breast cancer deaths occur in individuals aged 75 or older (Cancer Research UK). The incidence of breast cancer is predominantly higher in women, with female cases being approximately 100 times more common than in males (Sun et al., 2017). Numerous risk factors are associated with an increased likelihood of developing breast cancer, such as biological sex, advancing age, prolonged exposure to oestrogen (e.g., early menarche, late menopause, hormone replacement therapy), familial history, genetic factors, and unhealthy lifestyle choices (Smolarz et al., 2022).

1.4.2.1.1 Type of Breast Cancer

Breast cancer classification reflects its complexity and diversity. According to histopathological findings, breast cancer is categorised broadly into non-invasive and invasive breast cancer forms (Miyazaki et al., 2022). Non-invasive types primarily include ductal carcinoma in situ (DCIS) and lobular carcinoma in situ (LCIS). DCIS is the most prevalent form accounting for about 90 % of all non-invasive breast cancer.

LCIS is less common and is mainly seen as a marker for increased risk of invasive cancer (Sharma et al., 2010). Invasive breast cancers break past the confines of ducts or lobules, with cancer cells extending into the adjacent fatty and connective tissue of the breast. The most common invasive breast cancer is infiltrating ductal carcinoma (IDC), which constitutes about 72-80 % of all invasive breast cancer cases. In contrast, infiltrating lobular carcinoma (ILC) accounts for 10-15 % of invasive cases and is more likely to metastasise (Arps et al., 2013). Other less common invasive types include medullary carcinoma, mucinous carcinoma and tubular carcinoma, each characterised by unique pathological features and generally associated with better prognoses (Chen et al., 2024; Marrazzo et al., 2020; Vo et al., 2007). Rare forms like inflammatory breast cancer and Paget's disease of the nipple are usually aggressive and fast-growing, though they comprise a small percentage of cases (Beňačka et al., 2022). Phylloides tumours are also part of invasive breast cancer, and their incidence is particularly rare (Sharma et al., 2010).

These cancers are further classified into three primary subtypes based on the presence or absence of receptors like estrogen (ER), progesterone (PR) and human epidermal growth factor receptor 2 (ERBB2 or HER2): (1) hormone receptor-positive but lacking ERBB2, which comprises approximately 70 % of cases; (2) ERBB2 positive, making up 15-20 % of cases; and (3) triple-negative, which accounts for 15 % of cases and is defined by the absence of all three vital molecular markers (ER, PR and ERBB2). This classification guides treatment decisions and prognosis (Waks et al., 2019).

1.4.2.1.2 Comprehensive Treatment Strategies for Breast Cancer

Breast cancer treatment is customised based on tumour type, stage and patient-specific factors, integrating surgical, radiological and pharmacological strategies to optimise outcomes. Surgical resection is typically the initial approach and is often complemented by radiation therapy to target residual cells. Chemotherapy is employed preoperatively or postoperatively to manage aggressive or advanced cancers, while hormonal therapy is crucial for hormone receptor-positive cancers, utilising agents like tamoxifen or aromatase inhibitors. Additionally, targeted therapies such as trastuzumab which is effective for ERBB2-positive cancers and emerging treatments like immunotherapy are being explored for particularly challenging cases like triple-negative breast cancer. Overall, this multi-modal approach is designed to maximise survival and quality of life for breast cancer patients (Smolarz et al., 2022; Waks et al., 2019).

1.4.2.2 Role of NIS in Breast Cancer

For over forty years, research has documented that radioiodide and $^{99m}TcO_4^-$ accumulate in many breast cancers, while these compounds are not typically concentrated in normal, non-lactating breast tissue (Cancroft et al., 1973; ESKIN et al., 1974). An initial study utilising immunohistochemical assays on human breast tissue specimens found that over 80 % of the breast cancer samples exhibited NIS expression, in contrast to its absence in normal breast tissues derived from reduction mammoplasties (Tazebay et al., 2000). The same research group later confirmed this finding through an expanded analysis involving a significantly larger cohort of breast

cancer samples (Wapnir et al., 2003). Concurrently, some studies have confirmed the presence of NIS mRNA in human breast cancer tissues (Kilbane et al., 2000; Upadhyay et al., 2003). These findings open up the potential for using radioiodide as an innovative treatment for breast cancer. However, the NIS protein is primarily localised within the cytoplasm in breast cancer cells, in contrast to its positioning on the basolateral membrane in lactating mammary glands (Wapnir et al., 2003; Yao et al., 2015). This suggests that breast cancer may not be as efficient as the thyroid gland in absorbing radioiodine.

Previous studies on NIS in metastatic breast cancer have shown limited functional expression. For instance, research involving various metastases such as bone, lung, liver and lymph nodes demonstrated NIS expression in a few cases, with even fewer exhibiting radioiodine uptake, indicating minimal functional activity (Wapnir et al., 2004). Additional analysis on brain metastases revealed cytoplasmic NIS presence in a significant portion of samples and only a minority of cases of NIS localised on the plasma membrane (Renier et al., 2010). These observations confirm that while NIS is present in some metastatic breast cancers, its functional contribution to iodide uptake is infrequent, suggesting targeted RAI therapy might only be viable for a select subset of patients.

Overall, recent research indicates that while NIS expression in breast cancers and their metastases is prevalent, its cytoplasmic localisation limits effective radioiodine uptake. Thus, enhancing the translocation of NIS to the plasma membrane could enable RAI therapy for breast cancer.

1.5 Aims and Hypothesis

Radioiodide therapy has long been a cornerstone treatment for thyroid cancer, particularly differentiated thyroid cancer (DTC). However, its effectiveness is significantly diminished in radioiodide-refractory thyroid cancer, largely due to the impaired expression and improper localisation of NIS away from the plasma membrane (PM). Additionally, although NIS is present in breast cancer, including triple-negative subtypes, its predominantly cytoplasmic localisation limits the potential effectiveness of radioiodine-based therapies. This underscores the need for strategies that enhance NIS function and ensure its proper localisation to the PM to improve therapeutic outcomes in both thyroid and breast cancer.

Understanding the role of VCP in NIS degradation has paved the way for identifying drug treatments that can potentially enhance radioiodide uptake. While several compounds with anti-VCP activity have been reported, achieving effective VCP inhibition *in vivo* has been challenging due to issues related to compound tolerability and bioavailability. Given VCP's role in cancer pathology, it remains an attractive target for anti-cancer therapies. The experiments in this thesis aim to improve VCP inhibition in the context of differentiated thyroid cancer through multiple pharmacological approaches.

This thesis investigates the molecular mechanisms underlying NIS function, with a particular focus on its endocytosis, trafficking and dimerisation. It examines the roles of key proteins such as AP2, PBF, moesin and VCP in regulating NIS stability, trafficking and degradation. The research also evaluates the potential of VCP inhibitors,

such as CB-5083 and CB-5339, along with novel clotrimazole and NMS-873 derivatives, to enhance radioiodide uptake by modulating these processes.

The central hypotheses of this thesis are:

1. NIS Endocytosis and Trafficking: It is hypothesised that further analysis of putative NIS interactors, previously identified through mass spectrometry, may reveal additional NIS-interacting proteins and improve our understanding of the post-translational processing of NIS in thyroid cancer. Proteins such as the AP2 adaptor complex, along with PBF and moesin, may play critical roles in NIS endocytosis and plasma membrane localisation. Disrupting these interactions could enhance NIS retention at the plasma membrane and improve iodide uptake.

2. VCP Inhibition: Specific VCP inhibitors, including newly developed clotrimazole and NMS-873 derivatives, can enhance NIS-mediated radioiodide uptake by reducing NIS degradation, thereby improving the efficacy of radioiodine therapy in thyroid and breast cancer.

3. NIS Dimerisation: Residues K554 and R555 within NIS are essential for its dimerisation, and mutations in these residues are hypothesised to disrupt NIS dimerisation, trafficking and function, resulting in reduced iodide uptake and improper localisation.

The primary aims of this thesis are therefore to:

1. Investigate the roles of AP2, PBF, moesin, and the newly identified endocytosis motifs within the NIS C-terminus in NIS endocytosis and trafficking, to identify potential therapeutic targets that could enhance NIS retention at the plasma membrane and improve the effectiveness of radioiodide therapy.

2. Evaluate the efficacy of VCP inhibitors, including CB-5083, CB-5339 and novel derivatives, in enhancing NIS-mediated radioiodide uptake in breast and thyroid cancer cell lines.

3. Assess the structural and functional significance of NIS dimerisation by studying the impact of mutations at residues K554 and R555 on NIS trafficking, plasma membrane localisation and iodide uptake.

Through these aims, this research seeks to provide a comprehensive understanding of the molecular mechanisms regulating NIS function and to develop novel therapeutic strategies that could significantly improve the outcomes of radioiodide therapy in cancer treatment.

CHAPTER 2 MATERIALS AND METHODS

2.1 Cell Culture

2.1.1 Source of Cell Lines

The cell lines used in this study include a variety of origins and genetic backgrounds. TPC-1 cells, sourced from an adult female with papillary thyroid cancer, are characterised by the RET-CCDC6 fusion, TERT promoter mutation C228T, and mutations in CDKN2A and STAG2. 8505C cells, obtained from an anaplastic thyroid tumour in a 78-year-old female, are homozygous for the $BRAF^{V600E}$ mutation and additional mutations in NF2, TP53 and TERT promoter region (Landa et al., 2019). L87-NIS cells, a subline of L87 mesenchymal stem cells derived from a 70-year-old male, are stably transfected with the NIS gene, facilitating studies on iodide uptake mechanisms. These cells were kindly donated by Professor Christine Spitzweg (Ludwig-Maximilians University, Munich), with special thanks to Nathalie Schwenk. MDA-NIS cells, derived from the MDA-MB-231 metastatic human breast adenocarcinoma cell line, were stably transfected with the NIS gene through lentiviral transduction performed by Dr. Martin Read and Dr Alice Fletcher, following the manufacturer's instructions (Fletcher et al., 2020). AU565 cells from the pleural effusion of a 43-year-old female with breast adenocarcinoma, and are estrogen and progesterone receptor-negative but HER2-positive. ZR-75-1 cells originate from an estrogen receptor-positive breast cancer. SUM-52 cells, notable for PPM1D gene amplification and TP53 mutations, provide a model for studying these alterations in breast cancer. SKBR3 cells, derived from a human breast adenocarcinoma, are ER-negative, PR-negative and HER2-positive (Neve et al., 2006). HeLa is a human epithelial adenocarcinoma cell line derived from biopsy samples of a 31-year-old

patient, Henrietta Lacks, who was treated for cervical cancer at Johns Hopkins University in 1951. HEK293 cells are human embryonic kidney cells transformed with sheared adenovirus 5 DNA.

2.1.2 Providers

TPC-1 and MDA-MB-231 cells were kindly provided by Dr. Rebecca Schweppe from the University of Colorado. 8505C cells were sourced from German Collection of Microorganisms and Cell Cultures GmbH (DSMZ), while HeLa and HEK293 cells were obtained from the European Collection of Authenticated Cell Cultures (ECACC). L87-NIS cells were generously contributed by Professor Christine Spitzweg (Ludwig-Maximilians University, Munich), with thanks to Nathalie Schwenk. Breast cancer cell lines AU565, SUM-52, ZR751 and SKBR3 were sourced from the American Type Culture Collection (ATCC).

Dr Martin Read and Katie Brookes (McCabe group) constructed the stable TPC1, 8505C cell lines expressing NIS (Read et al., 2024). To ensure the sustained expression of NIS in these cell lines, the culture medium was supplemented with 500 µg/ml geneticin (Gibco).

The cells were verified through short tandem repeat (STR) analysis (NorthGene) and screened for mycoplasma contamination by Katie Brookes using the EZ-PCR kit (Geneflow).

2.1.3 Growth Conditions and Media

TPC1-NIS, 8505C-NIS, L87-NIS, AU565, SUM-52 and ZR751 were maintained in the RPMI-1640 medium (Life Technologies). SKBR3 breast cancer cells were grown in McCoy's 5A medium (Gibco). In contrast, HeLa and HEK293 cell lines were cultured in DMEM (Sigma-Aldrich). All media were supplemented with 10 % foetal bovine serum (FBS), penicillin (10^5 U/l), and streptomycin (100 mg/l). The cells were incubated at 37°C with 5 % CO_2 in a humidified environment.

2.1.4 Cell Splitting and Seeding

Cells were cultured with low passage numbers (below passage 35) until reaching 80-90 % confluency in 75 cm^2 flasks before being passaged. The media was aspirated, and the cells were gently washed with 5 ml of sterile PBS. Subsequently, 1 ml of 0.25 % trypsin was added, and the flasks were incubated for 3-5 minutes at 37°C to facilitate cell detachment. After detachment, cells were resuspended in 9 ml of RPMI, DMEM, or McCoy's 5A media. Cell counts were then performed using a cytometer with a 10× objective lens. Specific seeding densities for 6-well or 24-well plates were calculated based on these cell counts, as detailed in Table 2-1.

plate	6-well plate			24-well plate		
Volume	2ml			500ul		
	72 hours siRNA knockdown	48 hours transfection	24hours drug treatment	72 hours siRNA knockdown	48 hours transfection	24hours drug treatment
TPC1-NIS	3×10^5	-	2.5×10^5	-	6.5×10^4	7.5×10^4
8505C-NIS	3.5×10^5	-	3×10^5	-	8×10^4	1×10^5
MDA-NIS	-	-	2.5×10^5	-	-	7.5×10^4
L87-NIS	-	-	2.5×10^5	-	-	7.5×10^4
Hela	3.5×10^5	3.5×10^5	-	-	6.5×10^4	-
Hek293	3.5×10^5	3.5×10^5	-	-	6.5×10^4	-
AU565	-	-	3.5×10^5	-	-	1×10^5
ZR-75-1	-	-	3.5×10^5	-	-	1×10^5
SUM-52	-	-	3.5×10^5	-	-	1×10^5
SKBR3	-	-	3.5×10^5	-	-	1×10^5

Table 2- 1 Seeding densities for each cell line used in experiments with 6-well and 24-well plates. *For experiments requiring extended incubation periods between seeding and harvesting, lower initial seeding densities were used to ensure that cells reached 90-100 % confluency by the final experimental time point.*

2.2 Primary Thyroid Culture

Primary thyroid tissues for culture were sourced from the Queen Elizabeth Hospital Birmingham via the Human Biomaterials Resource Centre (Project No. 17-291) following ethical approval and signed informed consent from patients. Initial tissue samples were finely minced and subjected to enzymatic dissociation in HBSS containing 0.2 % Type II collagenase (Worthington) over 12-16 hours using end-over-end rotation. After incubation, the material was strained to discard undigested debris and centrifuged at 300 g for three minutes. This washing step was repeated approximately six times to remove unwanted erythrocytes and thyroglobulin clusters. Cells were subsequently resuspended in Coon's Modified Ham's F12A medium supplemented with 4 % FBS, penicillin-streptomycin, L-glutamine, 2 mg/ml insulin (Sigma I6634) and 300 mU/ml TSH (Sigma T8931) and dispensed into 24-well plates

at 500 μl per well. After an initial 2-3 days of incubation, the culture medium was switched to an FBS-free Coon medium with insulin and TSH. Cells were then cultured under optimal conditions of 37°C, 5 % CO_2 and proper humidity for 5-6 days before any subsequent experimental assays were carried out. For TSH responsiveness, a subset of 12 wells was isolated and exposed to varying concentrations of TSH (0, 300 mU/L, 1 U/L, 10 U/L) after three days in TSH-free and serum-free conditions. Cells responsive to a TSH level of 300 mU/L were earmarked for subsequent analyses (Eggo et al., 1996).

2.3 Plasmid Preparation

2.3.1 Plasmid AP2σ2

The AP2σ2 cDNA ORF Clone was obtained from Sino Biological Europe GmbH (Catalog Number: HG16782-UT). To prepare the APσ2 plasmid, the vial containing the lyophilised plasmid was first centrifuged at 5000 g for 5 minutes to ensure the material settled at the bottom. After carefully unsealing the vial, 100 μl of sterilised water was added to dissolve the DNA. The vial was then resealed and incubated at room temperature for 10 minutes, followed by brief vortexing and quick centrifugation to collect the liquid at the bottom. The resuspended plasmid was stored at -20°C for future use.

The AP2σ2 cDNA sequence was cloned into the pcDNA3.1 (+) vector using a systematic approach. Initially, both the AP2σ2 cDNA sequence and the pcDNA3.1 (+) vector were digested with KpnI and XbaI restriction enzymes (Promega) in a 10×

MULTI-CORE buffer (Promega). The digested samples underwent agarose gel electrophores at 140 V for 30 minutes. The bands corresponding to the AP2σ2 coding sequence and the linearised pcDNA3.1 (+) vector were then isolated and purified using a gel purification kit (Qiagen). Ligation of the purified products was carried out using T4 DNA Ligase (NEB) in T4 DNA Ligase buffer (NEB) with nuclease-free water, and the mixture was incubated for two hours at room temperature. Successfully ligated constructs were subsequently transformed into DH5α competent E. coli cells. These prepared plasmids were then employed in various experiments, including restriction enzyme analysis, PCR validation, E. coli transformation and DNA sequencing.

2.3.2 Transformation of DNA into E. coli

Competent DH5α E.coli cells were utilised as the host for transforming multiple plasmids, including AP2σ2 and other relevant constructs. Approximately 10 ng of the selected plasmid DNA was combined with 45 μl of competent cells and incubated on ice for 5 minutes. This was followed by a heat shock at 42°C for 45 seconds to facilitate plasmid uptake. After the heat shock, the mixture was incubated on ice for 30 minutes. Then, 950 μl of SOC medium (Sigma) was added to the mixture and shaken horizontally at 37°C for one hour. Following this incubation, the cells were subjected to low-speed centrifugation at 400 g for 5 minutes, and the pellet was resuspended in 200 μl of SOC medium. The resuspended cells were plated onto agar plates containing the appropriate antibiotic (100 μg/ml of carbenicillin or 50 μg/ml of kanamycin) to ensure the selective growth of transformed cells.

2.3.3 Plasmid DNA Purification

2.3.3.1 Miniprep Purification

After cultivating bacterial colonies for 16 hours at 37°C on antibiotic-containing LB-agar plates, a single colony was chosen and placed in 10 ml of LB medium and incubated at 225 rpm and 37°C for 8 hours. Plasmid DNA extraction was performed using the Wizard SV Plus Miniprep System Kit (Promega) according to the manufacturer's instructions. Bacterial cells were harvested by centrifugation (13,000 rpm for 10 minutes) and resuspended in 250 μl of resuspension buffer. Cell lysis was achieved with 250 μl of lysis buffer and incubated for 4 minutes, followed by treatment with 10 μl alkaline protease for 4 minutes and neutralisation with 350 μl of neutralisation buffer. The lysate was clarified by centrifugation at 13,000 rpm for 10 minutes, and the supernatant was passed through a DNA-binding column. The column was washed with 96 % ethanol to enhance DNA adherence and then with a wash buffer to remove contaminants. Plasmid DNA was eluted with nuclease-free water. The concentration and purity of the extracted DNA were determined using a NanoDrop 1000, ensuring a 260/280 nm absorbance ratio of 2.1 or greater. Only DNA samples meeting these criteria were used for subsequent applications such as transfection or sequencing.

2.3.3.2 Maxiprep DNA Amplification

Maxiprep was performed using the EndoFree Plasmid Maxi Kit (QIAGEN) according to the manufacturer's instructions. A single bacterial colony was selected from an

antibiotic-containing LB-agar plate to inoculate a 2-5 ml LB medium starter culture, which was incubated at 37°C with shaking at 225-250 rpm for approximately 8 hours. This starter culture was then diluted and incubated in selective LB medium 150 ml for 12-16 hours under the same conditions. Following incubation, bacterial cells were harvested by centrifugation at 6000 g for 15 minutes at 4°C. The cell pellet was resuspended in 10 ml of buffer P1. Lysis was initiated by adding 10 ml of buffer P2, followed by thorough mixing and a 5-minute room temperature incubation. Subsequently, 10 ml of chilled buffer P3 was added and mixed vigorously, and the lysate was allowed to settle. The lysate was then poured into a QIA filter Cartridge and allowed to sit for 10 minutes at room temperature. A plunger was gently inserted into the QIAfilter Cartridge to filter the lysate into a 50 mL tube, mixed with 2.5 ml of buffer ER, and incubated on ice for 30 minutes. During this incubation, 10 mL of equilibration buffer QBT was added to the QIAGEN-tip 500 columns provided with the kit, and the buffer was allowed to pass through the columns by gravity flow without centrifugation. The lysate was applied to a pre-equilibrated QIAGEN-tip 500 column by gravity flow. The column was washed twice with 30 ml of buffer QC. Plasmid DNA was eluted with 15 ml buffer QN and precipitated with 10.5 ml of isopropanol. The DNA pellet was obtained by centrifugation at 15,000 g for 30 minutes at 4°C and washed with endotoxin-free 70 % ethanol by centrifugation at 15,000 g for 10 minutes. Afterwards, the ethanol was carefully removed, and the DNA pellet was left to air-dry at room temperature for 5 to 10 minutes. The dried DNA pellet was then dissolved in 100-300 µl of nuclease-free water and stored at -20°C.

2.3.4 Sequencing

For validating the genomic sequence of the plasmids used in this study, approximately 500 ng of isolated plasmid DNA was resuspended in 5 µl of nuclease-free water and sent to Source Bioscience, UK for Sanger sequencing. The sequencing was performed using the CMV Forward and BGH Reverse primers provided by Source Bioscience. The returned sequence data in .abi chromatogram files were meticulously analysed using SnapGene version 4.3.6. To further verify the sequencing results, the data were cross-referenced using the Basic Local Alignment Search Tool (BLAST) and its translated variant, blastx, hosted by the National Center for Biotechnology Information (NCBI) at https://blast.ncbi.nlm.nih.gov/Blast.cgi. The sequencing primers utilised in this thesis are listed below (Table 2-2).

Primer	Sequence(5' to 3')
CMV_Forward	CAACGCGACTTTCCAAAATG
BGH_Reverse	TAGAGGGCACAGTCGAGG

Table 2- 2 Oligonucleotides used for plasmid sequencing in this study, provided by Source Bioscience UK.

2.4 Site-Directed Mutagenesis of pcDNA3.1-Based Constructs

For the mutagenesis process, wild-type genes or genes tagged with SmBiT, LgBiT or Nluc at the C-terminus or N-terminus were used as the template DNA, all cloned within the pcDNA 3.1 (+) Vector. Mutations were generated using the Agilent QuikChange XL Site-Directed Mutagenesis Kit. Each reaction mixture comprised 2.5 µl of the provided

10× reaction buffer, 10 ng of template cDNA, and 125 ng of both forward and reverse primers (Sigma), as detailed in Table 2-3.

Target Mutation	Forward Primer (5' → 3')	Reverse Primer (5'→3')
NIS (L562A and L563A)	CCCCGGGAGCGGCGTGGTGGGAC	GTCCCACCACGCCGCTCCCGGGG
NIS (E578A and E579A)	GGATGGCCACTGCTGCCTTGGGG	CCCCAAGGCAGCAGTGGCCATCC
NIS^{K554A}-Nluc	TGCCTGACAGGCCCCACAGCGAGAAGCACACTGGCTCCAGG	CCTGGAGCCAGTGTGCTTCTCGCTGTGGGGCCTGTCAGGCA
NIS^{R555A}-Nluc	TGCCTGACAGGCCCCACAAAGGCGAGCACACTGGCTCCAGG	CCTGGAGCCAGTGTGCTCGCCTTTGTGGGGCCTGTCAGGCA
NIS$^{K554A/R555A}$-Nluc	TGCCTGACAGGCCCCACAGCGGCGAGCACACTGGCTCCAGG	CCTGGAGCCAGTGTGCTCGCCGCTGTGGGGCCTGTCAGGCA
NIS K554A or NIS^{K554A}-SmBiT	CAGGGTGCTGCGCGCGGTGGGGCCTGTC	GACAGGCCCCACCGCGCGCAGCACCCTG
NIS R555A or NIS^{R555A}-SmBiT	GCCAGGGTGCTGGCCTTGGTGGGGCC	GGCCCCACCAAGGCCAGCACCCTGGC
NIS K554A/R555A or NIS$^{K554A/R555A}$-SmBiT	GGGCCAGGGTGCTGGCCGCGGTGGGGCCTGTCA	TGACAGGCCCCACCGCGGCCAGCACCCTGGCCC
AP2σ2 V88D or LgBiT-AP2σ2^{V88D}	AGGCCATTCACAACTTCGACGAGGTCTTAAACGAATATTT	AAATATTCGTTTAAGACCTCGTCGAAGTTGTGAATGGCCT
AP2σ2 L103S or LgBiT-AP2σ2^{L103S}	CAATGTCTGTGAACTGGACAGCGTGTTCAACTTCTACAAG	CTTGTAGAAGTTGAACACGCTGTCCAGTTCACAGACATTG
LgBiT-Moesin^{T558D}	AAATACAAGGACCTGCGCCAGA	TCTGGCGCAGGTCCTTGTATTTGT
LgBiT-Moesin^{T558A}	AAATACAAGGCCCTGCGCCAGA	TGGCGCAGGGCCTTGTATTTGT

Table 2- 3 Primer sequences employed for mutagenesis in this study.

The mix also included 1 μl of dNTPs, 1 μl of Pfu Ultra HF DNA Polymerase, and nuclease-free water to a final volume of 50 μl. Thermal cycling parameters were as follows: initial denaturation at 95°C for 1 minute, followed by 18 cycles of denaturation at 95°C for 50 seconds, annealing at 60°C for 50 seconds, and elongation at 68°C for 8 minutes and 30 seconds. For Moesin and AP2σ2 constructs, the elongation time was adjusted to 7 minutes. The process concluded with a final extension at 68°C for 8 minutes. Post-cycling PCR products were immediately cooled on ice for 5 minutes before adding 1 μl of DpnI enzyme to digest the methylated, non-mutated template DNA. The reaction conditions are outlined in Table 2-4.

Cycles	Temperature	Time
1	95ºC	60s
18	95ºC	50s
	60ºC	50s
	68ºC	8 minutes 30 seconds (1 minute per kb length)
1	68ºC	7 minutes

Table 2- 4 PCR thermocycler conditions for gene mutagenesis.

The DpnI-treated PCR products were transformed into 50 μl of NEB 5α competent E. coli cells. Following gentle mixing and a 30-minute incubation on ice, the cells were heat-shocked at 42°C for 30 seconds and then cooled on ice. Subsequently, 950 μl of SOC medium was added, and the mixture was shaken at 225 rpm for 1 hour to facilitate recovery. The bacterial suspensions were then spread onto LB-agar plates containing carbenicillin and incubated overnight at 37°C.

Individual colonies were selected and subjected to plasmid extraction the following day using a standard miniprep protocol. The introduced mutations were verified via Sanger sequencing, conducted by Source Bioscience, Nottingham, UK, confirming the success of the mutagenesis procedure.

2.5 Transfection

2.5.1 Plasmids Transfection

In this study, cells were seeded in 6-well and 24-well plates at appropriate densities for transfection. For the 24-well plates, 0.5 μg of plasmid DNA was utilised per well. For the NanoBiT assays, cells were prepared in 6-well plates, with each well receiving 1.0 μg of total plasmid DNA. For the NanoBRET assays, cells were seeded in 6-well plates, with each well co-transfected with 10 ng/well NIS-Nluc and 100ng/well Venus or pcDNA3.1 (control). The DNA was first diluted in serum-free Opti-MEM Reduced Serum Medium (Invitrogen) and incubated at room temperature for 5 minutes. Simultaneously, Lipofectamine reagent TransIT-LT1 (Mirus) was used as the transfection reagent, mixed with the DNA at a 3:1 ratio (μl of Lipofectamine to μg of DNA). After a 25-minute incubation at room temperature to allow complex formation, 100 μl of the mixture was added to each well of the 6-well plates, and 25 μl was added to each well of the 24-well plates. The cells were then incubated at 37°C for 48 hours before further analysis.

2.5.2 siRNA Transfection

Small-interfering RNAs (siRNAs) were employed in this study to evaluate the downstream effects of mRNA knockdown on target genes, as detailed in Table 2-5. For siRNA-mediated gene silencing, lyophilised siRNA powders were reconstituted in 50 µl of nuclease-free water to prepare a 100 µM stocking solution. The solution was gently shaken for 30 minutes to ensure homogeneity before storage at -20°C. Cells were cultured in either 6-well or 24-well plates, reaching 70-80 % confluence before transfection. A transfection cocktail was prepared by combining Opti-MEM Reduced Serum Medium with Lipofectamine RNAiMAX Reagent at a ratio of 12 µl of RNAiMAX to 1 ml of Opti-MEM, followed by a 5-minute incubation at room temperature. The siRNA was then added to achieve a final concentration of 0.2 µM, and the mixture was incubated for an additional 20 minutes at room temperature. Subsequently, either 1.5 ml (6-well plates) or 375 µl (24-well plates) of the existing medium was removed from each well. The cells were treated with 0.5 ml (6-well plates) or 125 µl (24-well plates) of the prepared Opti-MEM, RNAiMAX and siRNA solution. The plates were then incubated at 37°C for 4-6 hours, after which the medium was replaced with the standard cell culture medium. At 72 hours post-transfection, assays were conducted to validate gene knockdown. Protein samples were collected for Western blotting or qPCR analysis to confirm the efficacy of the siRNA-mediated gene silencing.

Target Transcript	Source	Catalog ID
ON-TARGETplus Non-targeting Pool siRNA	Horizon Discovery	D-001810-10-05
ON-TARGETplus Human AP2α1 siRNA	Horizon Discovery	L-012492-00-0005
ON-TARGETplus Human AP2µ2 siRNA	Horizon Discovery	L-008170-00-0005
ON-TARGETplus Human AP2σ2 siRNA	Horizon Discovery	L-011833-01-0005
ON-TARGETplus Human PBF siRNA	Horizon Discovery	L-011820-00-0005
ON-TARGETplus Human Moesin siRNA	Horizon Discovery	L-011732-00-0005

Table 2- 5 Commercially sourced siRNA products utilised in this study.

2.6 Western Blotting

2.6.1 Protein Harvest

Cells were prepared for protein extraction at designated time points: 72 hours after siRNA transfection, 48 hours after plasmid transfection, and 24 hours after drug treatment. The culture medium was aspirated, and cells were gently washed with 1ml of phosphate-buffered saline (PBS) per well. Cells were then lysed in 150 µl of RIPA buffer (50 mM Tris-HCl, PH 8.0, 150 mM NaCl, 1 % NP-40, 0.5 % sodium deoxycholate and 0.1 % SDS), supplemented with a protease inhibitor cocktail at a 1:16.7 dilution ratio. The lysates were incubated at -20°C for 30 minutes to ensure efficient lysis and then thawed on ice. The lysates were collected by scraping, transferred into labelled microcentrifuge tubes and subjected to vortexing followed by centrifugation at 13,000

g for 20 minutes at 4°C. The supernatant containing soluble proteins was collected and quantified using BCA assay.

2.6.2 Determining Protein Concentration via BCA Assay

Protein quantification was conducted using a colourimetric BCA assay. The BCA working solution was prepared by mixing 20 μl of Pierce BCA Reagent B with 1 ml of Pierce BCA Reagent A. To ensure accuracy, both the BCA reagent and protein lysate samples were loaded and measured in duplicate. In a 96-well plate, 4 μl of each protein sample was added to the individual well, followed by 80 μl of the BCA working solution. The plate was then incubated at 37°C for 30 minutes. Post-incubation, the optical density was measured at 560 nm using a SpectraMAX ABS Plus microplate reader, and the data were analysed with SoftMAX Pro software. Protein concentrations were determined using a concurrently generated standard curve with bovine serum albumin standards ranging from 0 to 5 mg/ml.

2.6.3 Western blotting

Protein samples were quantified, and 40 μg aliquots were combined with a 5× loading buffer (0.25 M Tris, 57 % w/v glycerol, 10 % SDS, 0.02 % bromophenol blue and 12.5 % β-mercaptoethanol). NIS protein samples were denatured at 37°C for 30 minutes, while other proteins were denatured at 95°C for 5 minutes. Electrophoresis was performed using 10 % polyacrylamide gels, with gel types chosen based on the protein target. A specific voltage program was employed for optimal separation. Post-electrophoresis, proteins were transferred onto PVDF membranes activated in 100 %

methanol and a transfer buffer (25 mM Tris, 192 mM glycine, 20 % v/v methanol). The transfer was conducted at a constant current of 360 mA for 75 minutes. Membranes were blocked in 5 % milk in TBST (72 % H2O, 0.2 mM TRIS pH 7.6, 1 % w/v NaCl, 0.03 % Tween 80) for one hour, then incubated overnight at 4°C with primary antibodies. Following incubation, membranes were washed three times with TBST for 10 minutes each, then incubated with HRP-linked secondary antibodies for one hour at room temperature. The specific concentrations of secondary antibodies used are detailed after each relevant results chapter. After three additional washes with TBST, membranes were treated with PierceTM ECL chemiluminescent substrate for 5 minutes. Signals were detected and captured on X-ray films. Densitometric analysis of the bands was performed using ImageJ software, with β-actin or Na^+/K^+ ATPase used as the internal loading control for normalisation. The antibodies used in Western blotting are listed in Table 2-6.

Antibody	Source	Code	Species reactivity	Dilution
NIS	Proteintech	24324-1-AP	Rabbit	1:1000
Moesin	Proteintech	26053-1-AP	Rabbit	1:10000
VCP	Proteintech	10736-1-AP	Rabbit	1:1000
AP2α1	Signalway	43215	Rabbit	1:400
AP2μ2	Novus Biologicals	NBP1-32272	Rabbit	1:500
Na^+/K^+ ATPase	Cell Signaling Technology	3010	Rabbit	1:500
β-actin	Sigma-Aldrich	A1978	Rabbit	1:10000

Table 2- 6 Antibodies utilised in this study for Western blot analysis.

2.7 Radioiodide Uptake Assay

2.7.1 Preparation and Treatment of Cells

In plasmid transfection experiments, cells were seeded into 24-well plates at a density of 65,000 or 80,000 cells per well. Radioiodide uptake was measured 48 hours post-transfection. For drug treatment experiments, cells were initially seeded into 24-well plates at 65,000 or 80,000 cells per well, with drug application occurring 24 hours post-seeding, and radioiodide uptake was analysed 24 hours later. Across all experimental conditions, 100 μM sodium perchlorate ($NaClO_4$), a competitive inhibitor of NIS-mediated iodide uptake, was applied to designated wells for one hour at 37°C.

2.7.2 Radioiodide Uptake Measurement

After inhibitor treatment, ^{125}I was added to each well at a concentration of 1.2×10^5 counts per minute in a 5 μl volume, followed by an additional hour of incubation at 37°C. Subsequently, the medium was aspirated, and cells were washed with cold Hank's Balanced Salt Solution (HBSS) to halt iodide uptake and remove residual ^{125}I. Cells were lysed using a 2 % SDS solution, and lysates were collected in measureable tubes for gamma counting using a Berthold Gamma Counter LB2111. Concurrently, protein concentrations were determined using a BCA colourimetric assay. Radioiodide counts were normalised to protein content to calculate iodide uptake rates. Specific NIS-mediated iodide uptake was determined by subtracting counts from wells treated with sodium perchlorate from those of untreated wells.

2.8 Bioluminescence Resonance Energy Transfer (BRET) Assay

2.8.1 Introduction of NanoBRET Assay

The Promega®NanoBRET™ Assay is a real-time technique used to study protein-protein interactions within live cells. This method relies on the non-radiative transfer of energy from an energy donor to an energy acceptor protein tag when these tags are in close proximity, generally within 10 nm, as determined by the Förster distance. This proximity-based energy transfer allows BRET to function as a molecular ruler, capable of detecting protein-protein interactions, protein localisation and dynamics within this distance (Lan et al., 2012; Pfleger et al., 2006).

In a typical NanoBRET assay, as shown in Figure 2.1, one protein of interest is tagged with a highly efficient energy donor, Nanoluciferase (Nluc, around 19 kDa), while the interacting protein is tagged with the fluorescent energy acceptor (Venus). When these two tagged proteins are in close proximity (within 10 nm), energy transfer from the luminescent donor (Nluc) to the fluorescent acceptor occurs, resulting in a measurable emission signal from the acceptor. The intensity of this signal is proportional to the degree of interaction or proximity between the tagged proteins.

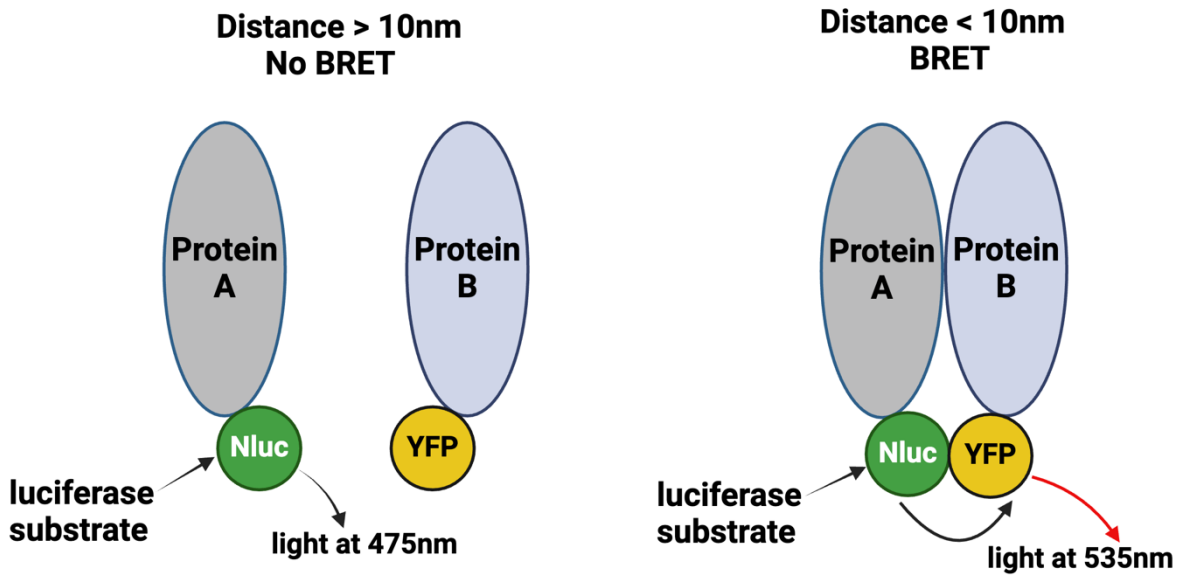


Figure 2. 1 Schematic representation of the NanoBRET assay. *NanoBRET relies on the proximity between the donor luciferase and the acceptor fluorophore. Adding the Nano-Glo luciferase substrate leads to the oxidation of the substrate to Furimazine, emitting light at 475 nm. When protein A and protein B interact, bringing the donor luciferase (Nluc) and the acceptor fluorophore (YFP) within close proximity (<10 nm), resonance energy transfer occurs, producing light at 535 nm. If the BRET tags are not close enough, only 475 nm light is emitted.*

In detecting NIS trafficking and subcellular localisation, the NanoBRET assay can be employed by tagging NIS with Nluc and co-expressing it with fluorescently tagged proteins like Venus-Kras, Venus-Rab or an empty vector (Tiulpakov et al., 2016). This setup allows for the visualisation and quantification of NIS localisation and movement within the live cell, providing valuable insights into mechanisms regulating NIS trafficking and localisation, as illustrated in Figure 2.2.

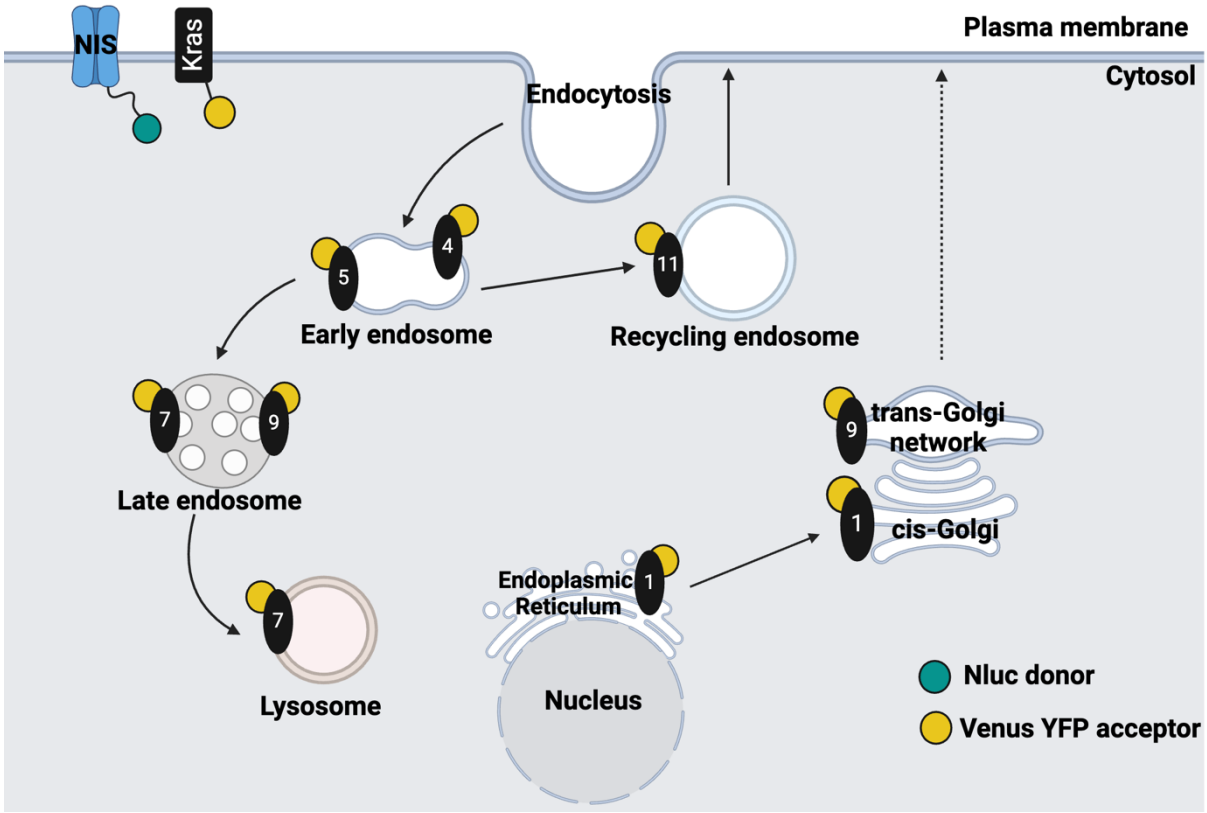


Figure 2. 2 A simplified schematic representation of the NanoBRET assay illustrating subcellular marker localisation and receptor trafficking. *Specific subcellular markers were used to identify subcellular compartments: Kras-Venus for plasma membrane localisation; Rab5-Venus for early endosomes; Rab4-Venus for early endosomes recycling; Rab11-Venus for recycling endosomes; Rab7-Venus for late endosomes/lysosomes; Rab9-Venus for late endosome trafficking to the trans-Golgi network and Rab1-Venus for endoplasmic reticulum trafficking to the cis-Golgi. Figure adapted from (Tiulpakov et al., 2016).*

2.8.2 Cell Preparation and Reverse Transfection

In the initial experiment, cells were seeded in 6-well plates at a density of 3.5×10^5 cells per well. After a 24-hour incubation period, siRNA transfection was performed. Following an additional 24 hours, the cells were trypsinised and resuspended in a white 96-well plate at a density of 3,000 cells per well for a reverse co-transfection. This process involved co-transfection NIS-Nluc constructs (10 ng/well) with 100 ng/well of Venus-tagged protein constructs (Kras, Rab4, Rab5, Rab7, Rab9 and

Rab11) or pcDNA 3.1 (+) vector. In the second experiment setup, cells were directly seeded into a white 96-well plate at a density of 2,600 cells per well and immediately subjected to reverse transfection. This setup included various NIS-Nluc constructs: NIS-Nluc, NIS^{K554A}-Nluc, NIS^{R555A}-Nluc or NIS$^{K554A/R555A}$-Nluc (10 ng/well), along with Venus-tagged protein constructs (Kras, Rab1 and Rab9) or pcDNA3.1 (+) vector (100 ng/well). The NIS-Nluc cDNA was synthesised and subcloned into pcDNA3.1 by GeneArt (ThermoFisher Scientific). The NanoBRET plasma membrane marker Kras-Venus, along with the Venus-tagged subcellular compartment markers Rab5, Rab7, and Rab11, were generously provided by Professor Nevin Lambert (Georgia Regents University) (Lan et al., 2012). Additionally, Venus-tagged markers Rab1, Rab4, Rab9 were graciously supplied by Professor Kevin Pfleger (University of Western Australia) (Tiulpakov et al., 2016). Tables 2-7 below are a comprehensive list of all the NanoBRET plasmids used in this study.

cDNA	Expression Vector	Source
Empty	pcDNA3.1 (+)	ThermoFisher Scientific (V79020)
NIS-Nluc	pcDNA3.1 (+)	ThermoFisher Scientific
NIS^{K554A}-Nluc	pcDNA3.1 (+)	Obtained by mutagenesis
NIS^{R555A}-Nluc	pcDNA3.1 (+)	Obtained by mutagenesis
NIS$^{K554A/R555A}$-Nluc	pcDNA3.1 (+)	Obtained by mutagenesis
Kras-Venus	pcDNA3.1 (+)	Nevin Lambert's lab
Rab1-Venus	pcDNA3.1 (+)	Kevin Pfleger's lab
Rab4-Venus	pcDNA3.1 (+)	Kevin Pfleger's lab
Rab5-Venus	pcDNA3.1 (+)	Nevin Lambert's lab
Rab7-Venus	pcDNA3.1 (+)	Nevin Lambert's lab
Rab9-Venus	pcDNA3.1 (+)	Kevin Pfleger's lab
Rab11-Venus	pcDNA3.1 (+)	Nevin Lambert's lab

Table 2- 7 Catalog and origin of all genes of interest utilised in the NanoBRET assay.

2.8.3 Luminescence Measurement and NanoBRET Analyses

Following reverse transfection and an appropriate incubation period for protein expression, the media in the wells were replaced with FluoroBrite DMEM phenol red-free complete media, supplemented with 10 % FBS and 2 mM L-Glutamine (Life Technologies), approximately 24 hours before substrate addition and luminescence measurement. This media change was crucial for optimising the conditions for the NanoBRET assay, and then furimazine substrate for NanoLuc luciferase was added to each well according to the manufacturer's instructions.

Luminescence signals were captured at 120-second intervals for 40 minutes using a PHERAstar FS microplate reader at donor wavelength 475-30 nm and acceptor wavelength 535-30 nm at 37°C. This setup was crucial for monitoring interactions between NIS-Nluc and the various Venus-tagged proteins. The NanoBRET ratio, indicating the proximity between NIS-Nluc and Venus-tagged proteins, was calculated by dividing the acceptor emission at 535 nm by the donor emission at 475 nm. This ratio quantitatively reflected the extent of interaction between the proteins within the live cellular environment.

2.8.4 Data Analysis of BRET Assay

Export the collected data into spreadsheet software to analyse the fluorescence and BRET data. The BRET ratio is determined by dividing the fluorescence signal by the luminescence signal, specifically using BRET readings at 535 nm and 475 nm. To calculate the net BRET, subtract the background luminescence (BRET readings from

cells expressing the donor with empty vector pcDNA3.1) from the initial BRET readings. Then, calculate the acceptor/donor ratio by dividing the initial fluorescence measurements at 535 nm by the luminescence measurements at 475 nm. The BRET ratios were carefully analysed to elucidate the interactions between NIS and Kras or Rab proteins. Particular emphasis was placed on understanding how these interactions might vary depending on the Kras or specific Rab protein involved, thereby shedding light on the functional dynamics of NIS in plasma membranes or different intracellular compartments.

2.9 Nanoluc Binary Technology (NanoBiT)

2.9.1 Introduction to The NanoBiT Assay

The NanoBiT assay, developed by Promega, is an advanced split-luciferase assay for detecting protein-protein interactions in live cells. This assay tags the protein of interest with two distinct luciferase subunits: Large BiT (LgBiT, 17.7 kDa) and Small BiT (SmBiT 1.3 kDa). Upon close proximity due to protein interaction, LgBiT and SmBiT combine to form an active luciferase enzyme, which oxidises the Nano-Glo substrate, generating a measurable luminescence signal as illustrated in Figure 2.3. This feature makes the NanoBiT assay an effective tool for studying protein-protein interactions within their native cellular environment, as demonstrated in several cellular protein-protein interactions (PPI) studies (Dixon et al., 2016).

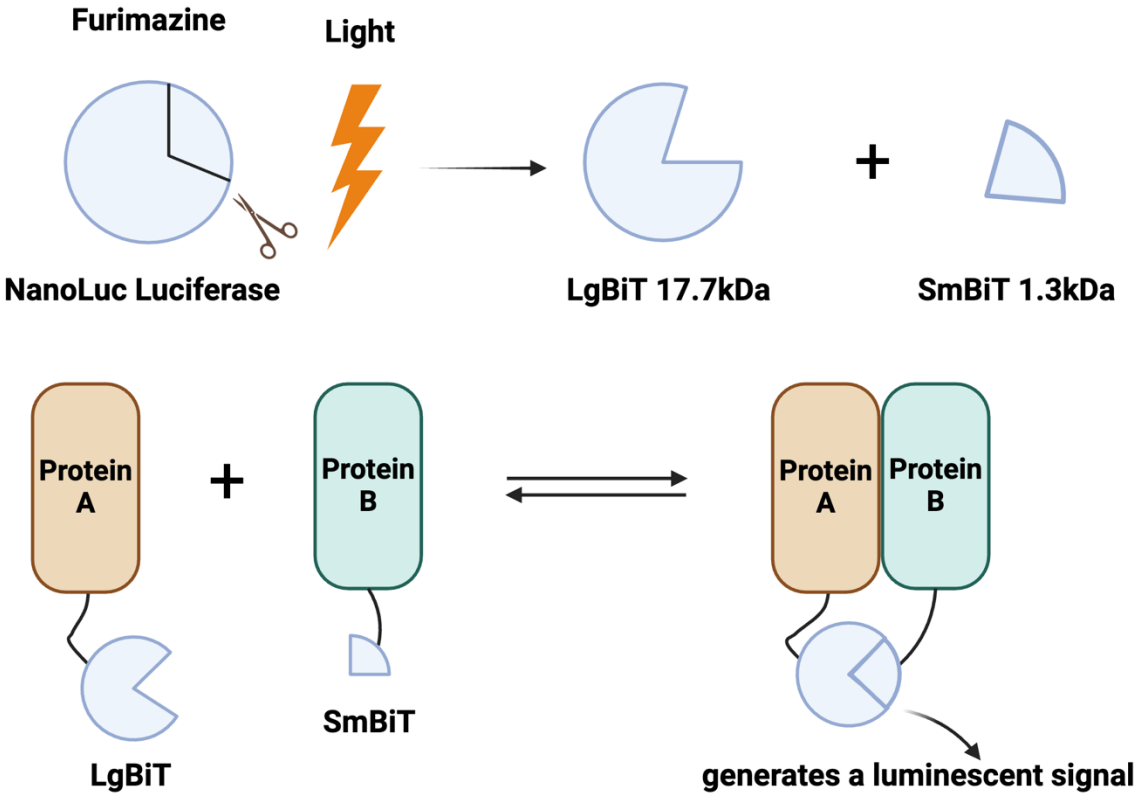


Figure 2. 3 The NanoBiT assay evaluated the interaction between LgBiT and SmBiT tags on two proteins. *Upon protein-protein binding, these tags combine to form an active luciferase enzyme. When the luciferin substrate is introduced, the enzyme oxidises the substrate, resulting in detectable luminescence. Conversely, if the tagged proteins do not interact, active luciferase is not formed, and no luminescence is observed.*

2.9.2 Synthesis of Luciferase-Fused Constructs for NanoBiT Assay

For the NanoBiT assay, Dr Caitlin Thornton (University of Birmingham) provided a pcDNA3.1 (+) vector carrying LgBiT and SmBiT tags. These components were foundational for creating fusion constructs to study protein-protein interactions.

For LgBiT tags, AP2σ2 and PBF coding sequences were amplified by PCR using Q5 High-Fidelity DNA polymerase (New England Biolabs), ensuring precise amplification. Post-amplification, the PCR products underwent electrophoretic separation, and the

target bands were excised following visualisation on a 1 % agarose gel. The extraction was accomplished using a Qiaquick Gel Extraction Kit, ensuring high-purity retrieval. The specific sequence of primers is outlined in Table 2-8. The PCR-amplified genes (AP2σ2 and PBF) and LgBiT-containing vector were linearised with KpnI/XbaI, purified via a 1 % agarose gel, and ligated with T4 DNA ligase at room temperature overnight.

Amplicon	Forward Primer (5'→3')	Reverse Primer (5'→3')
AP2S1(C) for LgBiT	GCCGGTACCACCATGATCCG CTTTATCCTC	GCCTCTAGACTCCAGGGA CTGTAGCAT
AP2S1(N) for LgBiT	GCCGGTACCATCCGCTTTAT CCTCATC	GCCTCTAGATCACTCCAGG GACTGTAG
PBF (C) for LgBiT	GCCGGTACCACCATGGCGC CCGGAGTGGC	GCCTCTAGAGTTGTTTTCA AATCTAGC
PBF (N) for LgBiT	GCCGGTACCGCGCCCGGAG TGGCCCG	GCCTCTAGATTAGTTGTTTT CAAATCT

Table 2- 8 PCR primers for amplifying genes of interest before insertion into pcDNA3.1 (+) with LgBiT tags were designed as follows: *Primers for C-terminal tagging excluded the stop codon of the gene of interest, while primers for N-terminal. Tagging excluded the start codon. All primer pairs included restriction sites for the KpnI and XbaI enzymes.*

The primers amplified AP2σ2 and PBF tagged with SmBiT directly through PCR (Table 2-9). The PCR products were purified through 1 % agarose gels, extracted using the QIAquick Gel Extraction Kit, and digested with KpnI/XbaI. The empty pcDNA3.1 (+) vector was linearised with KpnI/XbaI, purified via a 1 % agarose gel, and ligated tags and vectors using the T4 ligase enzyme.

Amplicon	Forward Primer (5'→3')	Reverse Primer (5'→3')
AP2S1(C) for SmBiT	GCCGCCGCCGCCGGTACCACCATGATCCGCTTTATCC	GCCTCTAGATTACAGAATCTCCTCGAACAGCCGGTAGCCGGTCACCTCCAGGGACTGTAGC
AP2S1(N) for SmBiT	GCCGGTACCACCATGGTGACCGGCTACCGGCTGTTCGAGGAGATTCTCATCCGCTTTATCCTCA	GCCGCGCCGCCGCCTCTAGATCACTCCAGGGACTGT
PBF (C) for SmBiT	GCCGCCGCCGCCGGTACCACCATGGCGCCCGGAGTG	GCCTCTAGAGAGAATCTCCTCGAACAGCCGGTAGCCGGTCACGTTGTTTTCAAATCTAG
PBF (N) for SmBiT	GCCGGTACCACCATGGTGACCGGCTACCGGCTGTTCGAGGAGATTCTCGCGCCCGGAGTGGCCC	GCCGCGCCGCCGCCTCTAGATTAGTTGTTTTCAAATC

Table 2- 9 PCR primers for amplifying SmBiT tag onto gene interest. *Each primer pair included restriction sites for XbaI and KpnI to facilitate insertion into the empty pcDNA3.1 (+) vector.*

The ligation products were transformed into DH5α competent E. coli cells, and plasmids were purified using a miniprep protocol. Source Bioscience, UK, verified the correct plasmid constructs via Sanger sequencing.

2.9.3 NanoBiT Assay for Investigating the Interaction between NIS, PBF, AP2σ2 and Moesin

The NanoBiT assay was employed to probe interactions between NIS, PBF, AP2σ2 and Moesin, including various mutants of NIS, AP2σ2 and Moesin. AP2 subunits were silenced using siRNA techniques to elucidate their role in the NIS-PBF interaction.

2.9.4 Cell Culture and Transfection

HeLa or HEK293 cells were seeded at 3.5×10^5 cells per well in 6-well plates. After 24 hours, cells were transfected with LgBiT and SmBiT-tagged constructs corresponding to NIS, PBF, APσ2, Moesin or their respective mutants. In some experiments, cells were treated with siRNA-targeting genes. Following siRNA transfection, cells were transfected with LgBiT and SmBiT-tagged NanoBiT constructs.

2.9.5 Cell Harvesting and Assay Preparation

Two days following the initial siRNA transfection or 24 hours post-NanoBiT constructs transfection, cells were detached using trypsin, neutralised with phenol-red-free DMEM, and then aliquoted in 100 μl volumes reseeding into white 96-well flat-bottom plates in duplicate.

2.9.6 NanoBiT Luminescence Measurement

After a 24-hour period post-reseeding, the Nano-Glo Live Cell reagent (Promega) was prepared by mixing 19 volumes of dilution buffer with 1 volume of the substrate. Twenty-five microliters of this mixture were added to each well, and the plates were gently mixed by hand. Luminescence was recorded at two-minute intervals over 40 minutes (20 cycles) at 37°C using a PHERAstar plate reader.

2.9.7 Data Transformation and Analysis

To address experimental variability due to factors like passage number, transfection efficiency and cell confluency, luminescence readings were normalised to help standardise the data across multiple experimental repeats. A representative measurement was selected at 20 minutes (the tenth cycle), twenty minutes after adding the luminescent substrate, where luminescence typically stabilises. Values obtained at this time point from at least three independent experiments facilitated statistical analysis to validate the interactions between interesting proteins.

2.10 Cell Surface Biotinylation Assay

The Cell Surface Biotinylation Assay was conducted using the Thermo Scientific™ Pierce™ Cell Surface Protein Isolation Kit, designed for the biotinylation and subsequent isolation of cell surface proteins for Western blot analysis.

First, cells were grown to 90-95 % confluence in 6-well plates. Two wells were used per condition. The culture media was aspirated, and cells were washed twice with 1 ml of ice-cold PBS per well to remove residual media. The cells were then incubated with a 2 ml biotinylation solution (dissolving one vial of Sulfo-NHS-SS-Biotin in 48ml of PBS) per well for 30 minutes at 4°C on a rocking platform to ensure uniform biotinylation. After biotinylation, the reaction was quenched by adding 100 μl of Quenching Solution to each well and gently swirling to ensure even coverage. Cells were then scraped off the wells using a cell scraper and collected into 50 ml centrifuge tubes. The collected cells were centrifuged at 500 g for 3 minutes, the supernatant

was discarded, and the cell pellet was washed twice with 5 ml of cold TBS to remove unreacted biotin. The cells were lysed by resuspending the pellet in 200 μl per condition of Lysis Buffer containing a protease inhibitor cocktail. The lysates were then incubated on ice for 30 minutes, with brief vortexing every 5 minutes to facilitate complete cell lysis. Following lysis, the cell debris was removed by centrifugation at 10,000 g for 2 minutes at 4°C, and the supernatant containing the cell surface proteins was carefully transferred to fresh 1.5 ml microcentrifuge tubes. A total of 100 μl of each condition lysate was set aside as a total protein for Western blot analysis. The remaining lysates were used in equivalent protein amounts to isolate the biotinylated proteins.

To isolate the biotinylated proteins, NeutrAvidin™ Agarose slurry was prepared according to the manufacturer's instructions. A total of 150 µL of the slurry was added to the column after 3 times wash with Wash Buffer, which was then centrifuged at 1,000 g for 1 minute. Subsequently, 150 µL of the prepared slurry was combined with the cell lysate, and the mixture was incubated at room temperature for 1 hour with end-over-end mixing. Following incubation, the agarose beads were centrifuged at 1,000 g for 1 minute, and the supernatant was discarded. The column was then washed three times with Wash Buffer, each followed by centrifugation to ensure the removal of non-bound proteins. Finally, the biotinylated proteins were eluted from NeutrAvidin Agarose by adding 100 μl of Elution Buffer (SDS-PAGE Sample buffer containing 50 mM DTT). The mixture was incubated for 1 hour at room temperature to facilitate the release of the bound proteins. The eluted proteins were then collected by centrifugation at 1,000 g for 2 minutes and transferred to a new collection tube. The

eluates were either analysed immediately by Western blot or stored at -20°C for future use. Add a trace amount of 5× loading buffers to the eluates before the Western blot.

2.11 Statistics

Data were analysed using IBM SPSS Statistics (Version 29) and GraphPad Prism (Version 10.2.3). The Shapiro-Wilk normality test was employed to verify that the data confirmed a Gaussian distribution before further analysis using either Student's t-test or one-way analysis of variance (ANOVA) followed by Dunnett's or Tukey's post-hoc test. Student's t-test was applied to compare two independent data groups, while one-way ANOVA was utilised to compare three or more independent groups. All statistical analysis was performed on datasets with a minimum of three replicates, and significance was determined at $P < 0.05$.

CHAPTER 3 ENHANCING RADIOIODIDE UPTAKE BY ADDRESSING THE MECHANISM OF SODIUM/IODIDE SYMPORTER (NIS) ENDOCYTOSIS

CHAPTER 3 ENHANCING RADIOIODIDE UPTAKE BY ADDRESSING THE MECHANISM OF SODIUM/IODIDE SYMPORTER (NIS) ENDOCYTOSIS

3.1 Introduction

3.1.1 Introduction to the Mechanisms of Sodium/Iodide Symporter (NIS) Endocytosis

β-emitting radioiodide (^{131}I) therapy has been a critical treatment for more than eighty years in thyroid cancer, which targets and eliminates residual cancer cells post-surgery and distant metastatic disease (Nguyen et al., 2015). However, in cases of radioiodide refractory thyroid cancer, especially those with recurrence or distant metastases, the prognosis is poor, with a 10-year survival rate falling below 10 % (Pitoia et al., 2022). Diminished RAI uptake is observed in 25-50% of thyroid cancer patients, primarily due to reduced NIS expression and its mislocalisation away from the plasma membrane, resulting in the loss of its ability to transport radioiodide effectively (Read et al., 2024). The presence of NIS mRNA in human breast cancer tissues has previously indicated the potential for using RAI as a treatment for breast cancer (Kilbane et al., 2000; Upadhyay et al., 2003). However, NIS protein is primarily localised within the cytoplasm in breast cancer cells, which limits the use of RAI therapy (Yao et al., 2015).

NIS must be located at the plasma membrane of cells to function effectively. Its activity and localisation are regulated through a combination of transcriptional, post-transcriptional, and post-translational mechanisms, including endocytosis and recycling back to the plasma membrane. Understanding the mechanisms controlling NIS endocytosis could lead to new therapeutic strategies to enhance NIS expression and localisation at the plasma membrane, thereby improving the uptake of therapeutic radioisotopes. However, relatively little is known about NIS trafficking and endocytosis.

Previously, studies have shown that PBF interacts with NIS and enhances its endocytosis. This effect is mediated by a tyrosine-based endocytosis motif (YXXΦ motif) in the C-terminus of PBF. Altering this motif or modulating the phosphorylation state of PBF can restore NIS membrane localisation and increase RAI uptake (Smith et al., 2011; Smith et al., 2009; Smith et al., 2013). Clathrin-mediated endocytosis (CME) is the predominant endocytotic mechanism in eukaryotic cells, and the adaptor protein complex 2 (AP2) is crucial in this process (Brodsky et al., 2001). The internalisation of NIS from the plasma membrane and its subsequent routing to late endosomes for degradation is believed to predominantly occur via CME (Smith et al., 2013).

Additionally, the COOH terminus of NIS includes key sorting signals crucial for its cellular trafficking, such as a PDZ target motif at T616, N617 and L618, which interacts with PDZ domain-containing proteins to regulate membrane retention and endocytosis in non-neoplastic cells (Martín et al., 2021). Furthermore, a dileucine motif (L557 L558) and multiple acidic dipeptide motifs (E573 D574, E579 E580, E587 D588) within the C-terminus may facilitate the interaction with clathrin-coated vesicles and manage the retrieval or retention of NIS, ensuring its proper localisation and function (Hingorani et al., 2010). However, there is no overall consensus on how NIS is endocytosed, how this might be disrupted in cancer and how best to manipulate the retention of NIS at the PM.

In this chapter, NanoBiT and CSBA assays, as well as other subcellular techniques, were used to understand the roles played by PBF, AP2, and moesin in the endocytosis

of NIS, and to explore the function of newly identified potential endocytosis motifs located within the C-terminal region of NIS.

3.1.2. The Adaptor Protein 2 (AP2) Complex: Structure, Function, and Involvement in Protein Endocytosis

CME is crucial for the internalisation of most cell surface proteins. During CME, clathrin adaptors that bind to the plasma membrane recruit and polymerise clathrin, forming clathrin-coated pits (CCPs) where cargo is sorted. AP2 is the most prevalent adaptor in this process and plays an essential role in CME (Brodsky et al., 2001).

AP2 is a critical link between clathrin and ligand-receptor complexes, playing an essential role in clathrin-mediated endocytosis. This heterotetrameric complex is composed of four subunits (Figure 3.1): two large subunits, alpha (α) and beta-2 (β2), each ranging from 100 to 130 kDa; a medium subunit, mu-2 (μ2), approximately 50 kDa; and a small subunit, sigma-2 (σ2), between 17 and 20 kDa. This arrangement facilitates the efficient packaging and transport of cellular cargo (Traub et al., 1999). The two large subunits of AP2 each comprise a trunk region (70~75 kDa) and an appendage (~30 kDa) connected by a hinge susceptible to proteolytic hydrolysis. Two positively charged sites capable of binding PIP2 have been identified, one on the trunk domains of α and the other on the μ2 subunits, which can allosterically activate AP2 and play an essential role in clathrin vesicle formation. The primary site on the α subunit is particularly crucial in the initial docking of AP2 onto PIP2 and targeting it to cargo-riched plasma membranes (Collins et al., 2002). AP2 interacts with clathrin through the LΦD/EΦD/E (Φ representing a bulky hydrophobic residue) clathrin box

motifs in the β2 hinge and the appendage domains (Collins et al., 2002). The appendage domains also engage various regulatory and accessory proteins (such as AP180) through diverse motifs and facilitate complex functionality (Praefcke et al., 2004).

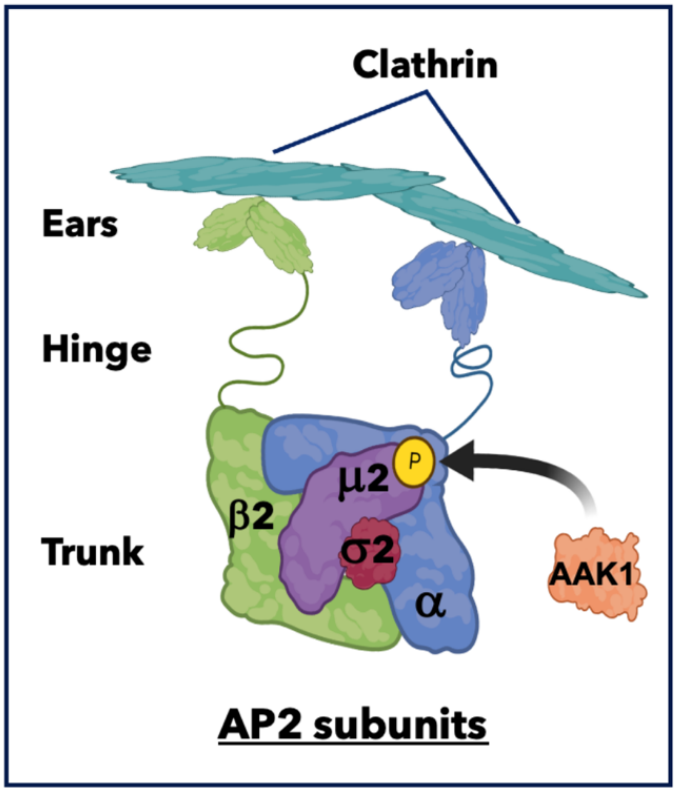


Figure 3. 1 Schematic illustrating AP2 subunits and interaction with clathrin and the kinase AAK1. *Figure adapted from (Read et al., 2024).*

The core of AP2 is constituted by the N-terminal domains of α and β2 subunits along with the entire μ2 and σ2 subunits. The C-terminal of μ2 subunit specifically recognises and binds to the endocytic motif "YxxΦ" tyrosine-based sorting signal found in the intracellular tails of cargo proteins, clustering them into clathrin-coated pits (CCPs) and mediating their endocytosis. Additionally, the D/ExxxLL or "acidic dileucine" internalisation motifs on transmembrane cargo proteins interact with the σ2 subunit (Collins et al., 2002; Ohno et al., 1996). When AP2 is inactive, its clathrin binding site

remains shielded within the core (Kelly et al., 2014). Interaction with the membrane cargo triggers a conformational shift from a “locked” to an “open” state in AP2, catalysing the initiation of CCP formation. However, the exact mechanism remains unclear (Beacham et al., 2019). Meanwhile, phosphorylation of the μ2 subunit is essential for the subsequent maturation and functionality of CCPs (Kelly et al., 2014) (Figure 3.2).

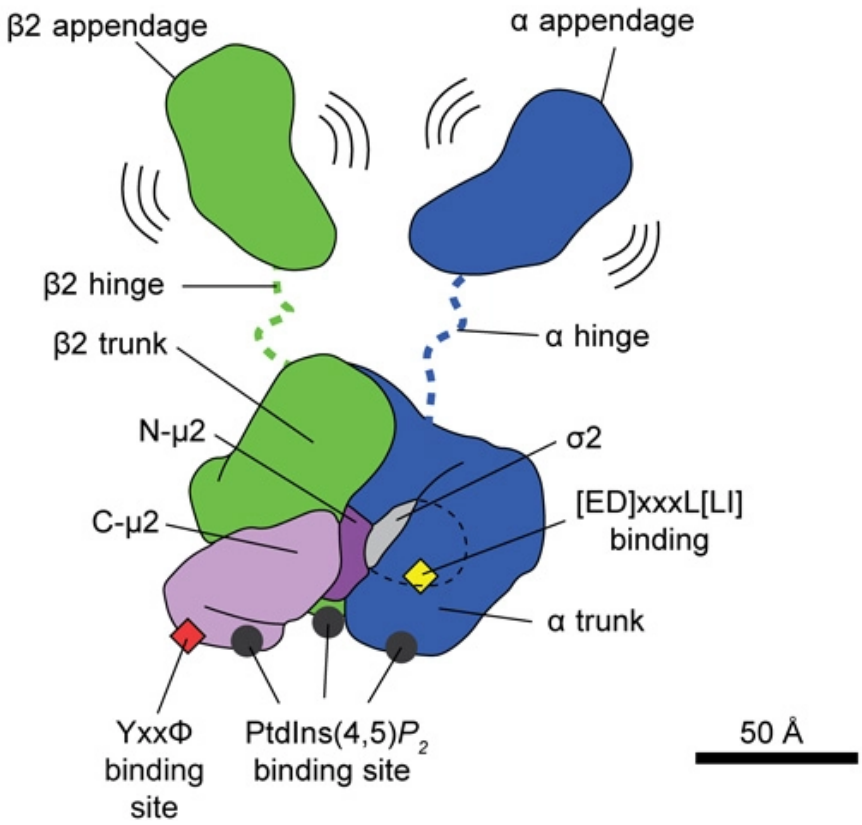


Figure 3. 2 The structure of AP2. *AP2 plays an important role in CME by interacting with cargo proteins, clathrin, and other regulatory/accessory proteins. Adapted from (Kovtun et al., 2020).*

The initial stage of AP2 activation involves its recruitment to the plasma membrane and interactions with PIP2 on the membrane. This allosteric activation reveals cargo-binding sites on the μ2 and σ2 subunits (Jackson et al., 2010). In addition, the μ2 subunit interacts with the tyrosine sequence on the cargo protein, anchoring the allosteric-activated AP2 to the cell membrane for specific cargo selection (Höning et

al., 2005). Upon cargo binding, AP2 enters a fully open and active conformation, exposing clathrin binding sites on the hinge domain of its β2 subunit and binding with clathrin, thereby forming a complex of cargo protein, AP2 and clathrin. This interaction facilitates the formation of early CCPs (Kadlecova et al., 2017).

In a recent study from our laboratory, mass spectrometry and pathway analysis identified AP2 as a potential interactor of NIS. A siRNA screen showed that reducing AP2 subunits α1 and μ2 and AP2-associated kinase 1 (AAK1) significantly enhanced RAI uptake in NIS-expressing thyroid cancer cells (Read et al., 2024). Previous studies have shown that the AP2σ2 subunit, encoded by AP2S1, binds cargo proteins with acidic dileucine endocytic motifs (Kelly et al., 2008). We therefore hypothesised that AP2σ2 may bind to NIS, promoting its endocytosis through the CME pathway, and sought to challenge this notion.

3.2 Materials and Methods

3.2.1 Cell Culture

Thyroid cancer cell lines (TPC1-NIS and 8505C-NIS) were cultured in RPMI-1640, while HeLa and HEK293 cell lines were cultured in DMEM. Culture media were supplemented with 10 % FBS, penicillin (10^5 U/l) and streptomycin (100 mg/l). All cell lines were maintained at 37˚C in a humidified environment with 5 % CO_2.

3.2.2 siRNA Transfection

TPC1-NIS, 8505C-NIS, HeLa, HEK293 and primary human thyrocytes were subjected to siRNA treatment targeting three specific sequences of the target genes, along with a non-targeting control, as detailed in Section 2.5.2. Follow-up analyses were conducted 72 hours post-transfection.

3.2.3 Plasmid Preparation and Transfection

The AP2σ2 (AP2S1) and PBF cDNAs were cloned into the pcDNA3.1-containing LgBiT plasmid, or amplified with the SmBiT tag, before being inserted into pcDNA3.1. AP2σ2 and PBF were tagged at the C- and N-termini with LgBiT and SmBiT tags, as described in Section 2.9.2, to analyse protein-protein interactions. In contrast, NIS was tagged with LgBiT or SmBiT exclusively at the C-terminus, as previous in-house research has indicated that tagging NIS at the N-terminus disrupts its function by hindering its transport to the plasma membrane. The NIS-NanoLuc (Nluc) cDNA was synthesised and subcloned into pcDNA3.1 by GeneArt (ThermoFisher Scientific). Two NIS mutants (L562A/L563A and E578A/E579A), as well as two mutants of AP2σ2 (V88D and L103S), were created using the Agilent QuikChange XL Site-Directed Mutagenesis Kit, following the protocol in Section 2.4. Professor Nevin Lambert (Georgia Regents University) generously provided the NanoBRET PM marker Kras-Venus, along with the Venus-tagged subcellular compartment markers Rab5, Rab7, Rab9 and Rab11. The Venus-tagged markers Rab1, Rab4 were kindly provided by Professor Kevin Pfleger (University of Western Australia). Plasmid DNA transfections

were performed using TransIT-LT1 (Mirus Bio) according to standard protocols and the manufacturer's guidelines, as detailed in Section 2.5.1.

3.2.4 Western blotting, CSBA and RAI uptake

Western blotting, CSBA and radioactive iodine (^{125}I) uptake assays are described in Section 2.6, Section 2.10 and Section 2.7. The blots were probed using specific antibodies against NIS (1:1000), AP2α1 (1:400), AP2μ2 (1:500), Na^+/K^+-ATPase (1:500) and β-actin (1:10,000). HRP-conjugated secondary antibodies targeting rabbit IgG were utilised at a 1:2000 dilution for NIS, AP2μ2, Na^+/K^+-ATPase, and β-actin, and at a 1:8000 dilution for AP2α1. Additionally, HRP-conjugated secondary antibodies targeting mouse IgG were utilised at a 1:2000 dilution for β-actin.

3.2.5 NanoBiT

The NanoBiT assay comprises two subunits: a large Bit (LgBiT, 17.7 kDa) and a small Bit (SmBiT, 1.3 kDa). When 2 proteins of interest interact, interaction between the SmBiT and LgBiT tags is made possible, forming a complete luciferase enzyme and producing a quantifiable luminescent signal.

The manufacturer provided a positive control, LgBiT-PRKAR2A and SmBiT-PRKACA, encoding two subunits of a cAMP-dependent protein kinase that naturally interact within cells. The assay also includes a HaloTag-SmBiT negative control, a modified haloalkane dehydrogenase designed to bind only to synthetic ligands. Additionally, to

offer a more assay-specific negative control, NIS-SmBiT and LgBiT-PRKAR2A were co-transfected.

Figure 3.3 (from McCabe group unpublished data) illustrates a typical and robust luciferase emission over 20 cycles in the positive control wells while showing minimal emission over time in both the HaloTag-SmBiT negative control and the assay-specific NIS-SmBiT and LgBiT-PRKAR2A negative control. The luciferase signals increased over roughly ten cycles in all measurements, aligning with the luciferase substrate's movement from the media across the cell membranes towards equilibrium. Consequently, the luminescence reading at cycle ten was used for paired statistical analysis. The luminescent signal after ten cycles can be attributed to partial signal degradation.

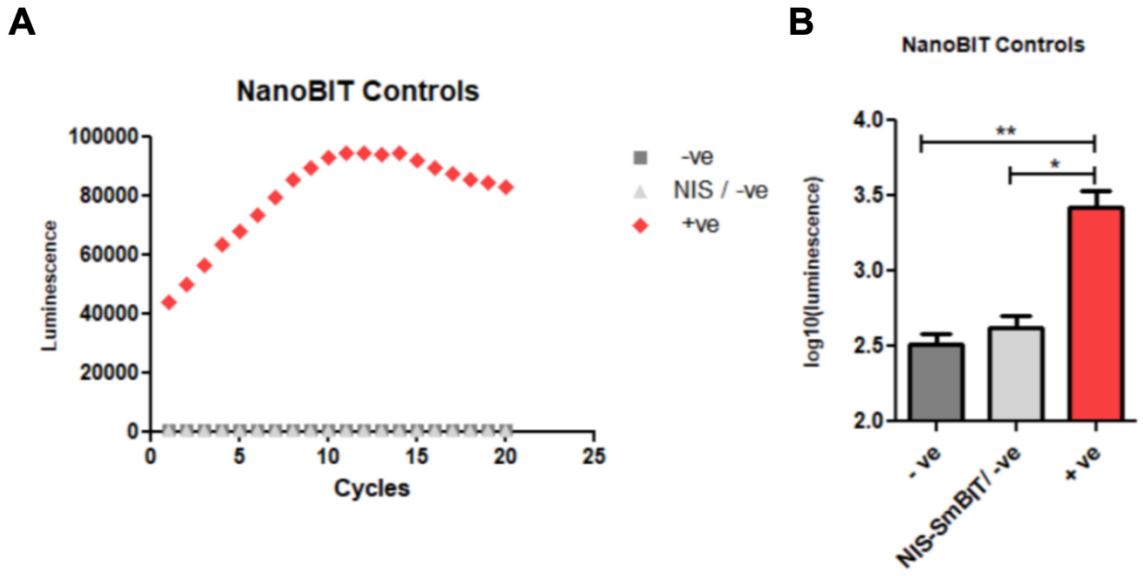


Figure 3. 3 NanoBiT assay control analysis and validation. *(A) Luminescence profiles show a clear peak for the positive control (+ve), while negative controls (-ve and NIS/-ve) maintain low luminescence, confirming assay specificity. (B) Quantification of luminescence indicates significantly higher levels for the positive control compared to both negative controls. Statistical analysis was performed using paired, two-tailed t-tests. Data are presented as mean ± SEM (n = 3), with significance levels: * = P < 0.05; ** = P < 0.01. Figure adapted from McCabe group's unpublished data.*

HeLa and HEK293 cells were prepared as described in Section 2.1.4. Table 3-1 details the transfection combinations used for the NanoBiT assay. Each experiment included two technical replicates per condition. Following the manufacturer's guidelines, only the inner 60 wells of the 96-well plate were used to minimise edge effects and thermal gradients. Luminescence was measured every two minutes for a total of 20 cycles using a PHERAstar luminescent plate reader.

Plasmid 1	Plasmid 2	Control or Experimental
Halotag-SmBiT	None	Manufacturer supplied negative control
SmBiT-PRKACA	LgBiT-PRKAR2A	Manufacturer supplied positive control
NIS-SmBiT	LgBiT-PRKAR2A	Assay specific negative control
NIS-SmBiT	NIS-LgBiT	Assay specific positive control
NIS-SmBiT	PBF-LgBiT	Experimental
NIS-SmBiT	LgBiT-PBF	Experimental
NIS-SmBiT	AP2S1-LgBiT	Experimental
NIS-SmBiT	LgBiT- AP2σ2	Experimental
NIS EE-SmBiT	LgBiT- AP2σ2	Experimental
NIS LL-SmBiT	LgBiT- AP2σ2	Experimental
NIS-SmBiT	LgBiT- AP2σ2	Experimental
NIS-SmBiT	LgBiT- AP2σ2 V88D	Experimental
NIS-SmBiT	LgBiT- AP2σ2 L103S	Experimental

Table 3- 1 Transfection combinations for the NanoBiT assay.

In addition, a NanoBiT reverse assay was conducted to validate the observed interactions further. The transfection combinations for the reverse assay are specified in Table 3-2.

Plasmid 1	Plasmid 2	Control or Experimental
Halotag-SmBiT	None	Manufacturer supplied negative control
NIS-SmBiT	LgBiT-PRKAR2A	Assay specific negative control
NIS-LgBiT	NIS-SmBiT	Assay specific positive control
NIS-LgBiT	PBF-SmBiT	Experimental
NIS-LgBiT	SmBiT-PBF	Experimental
NIS-LgBiT	AP2S1-SmBiT	Experimental
NIS-LgBiT	SmBiT-AP2S1	Experimental

Table 3- 2 Transfection combinations for the reverse NanoBiT assay.

3.2.6 NanoBRET Live Cell Assay

HEK293 and HeLa cells were seeded in 6-well plates at a density of 3.5×10^5 cells per well and co-transfected with 10 ng/well NIS-Nluc and 100 ng/well Venus or pcDNA3.1 (control). After 24 hours of transfection, the cells were harvested and reseeded into white 96-well plates using phenol-red-free DMEM. Nano-Glo reagent was added to each well following the instructions (detailed in section 2.8). BRET measurements were recorded using a PHERAstar FS microplate reader at donor wavelength 475-30 nm and acceptor wavelength 535-30 nm. The BRET ratio (acceptor/donor) was calculated for each time point. Readings were taken every 2 minutes for up to 40 minutes.

3.2.7 Statistical Analysis

Statistical analyses were performed using GraphPad Prism (Version 10.2.3) and Microsoft Excel. Results were derived from biological replicates performed at least in triplicate. Data were assessed with the t-test to compare the two groups, and for multiple groups, one-way ANOVA was used with Dunnett's post-hoc test.

3.3 Results

3.3.1 NanoBiT Assay for Detecting NIS-AP2S1 Interactions

To determine whether tagging the NIS constructs with LgBiT, SmBiT, or Nluc at the C-terminus for subsequent NanoBiT or NanoBRET assays altered intrinsic radioiodide uptake activity, radioiodide uptake assays were carried out (Figure 3.4). Data were compared to NIS tagged at the C-terminus with HA, the standard NIS control construct used in the McCabe group's iodide uptake assays.

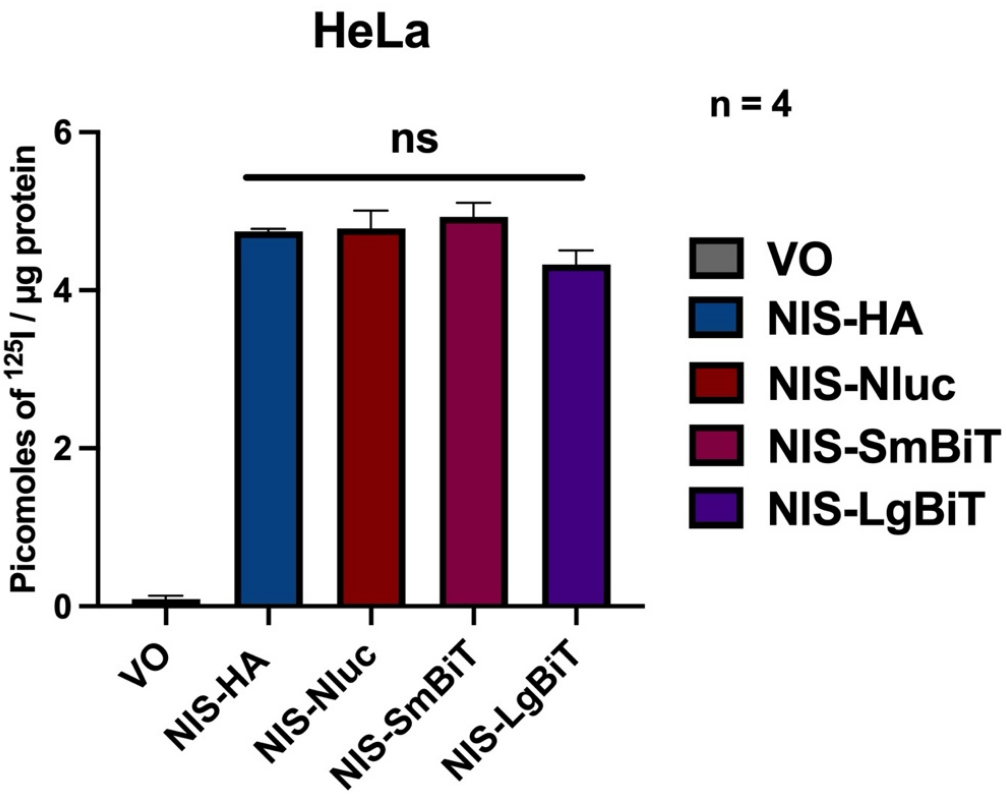


Figure 3. 4 Iodide uptake assessment in HeLa cells with NIS constructs. *Cells were transfected with various NIS constructs with Nluc, SmBiT and LgBiT tags in HeLa cells. After 48 hours post-transfection, no significant differences in iodide transport were observed, compared to NIS-HA. N=4, analysed by one-way ANOVA followed by Tukey's post hoc test (ns, not significant).*

No significant impact was observed on iodide uptake, indicating that these tags for NanoBiT or NanoBRET assays did not impair NIS functionality.

Additionally, Western blot analysis was performed to verify the expression of NIS with various tags in HeLa and HEK293 cells following transfection. VO served as a control indicating the baseline expression without exogenous NIS. Protein samples were harvested 48 hours post-transfection, allowing sufficient time to express NIS constructs. The resulting Western blots (Figure 3.5) confirmed that each variant of tagged NIS was expressed at comparable levels. A consistent band for NIS ranging

between 75-100 kDa was observed across the tagged constructs, confirming successful transfection and expression, supporting their use in subsequent NanoBRET and NanoBiT assays.

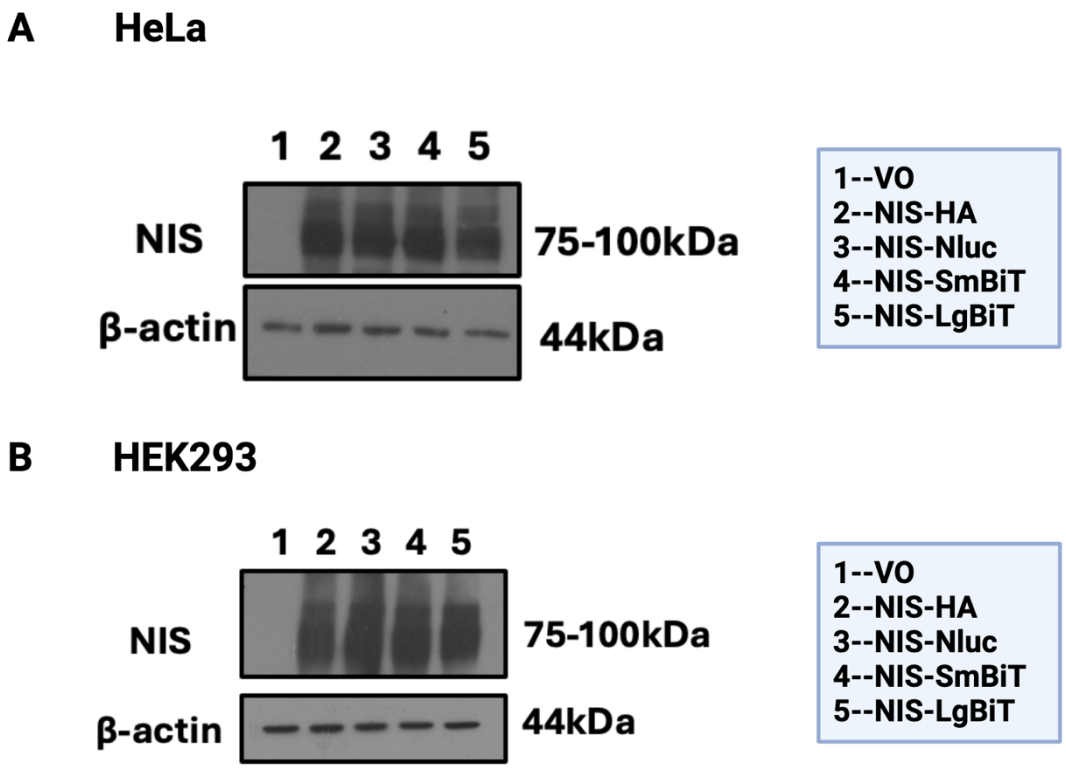


Figure 3. 5 Western blot analysis of NIS expression with various tags in HeLa (A) and HEK293 (B) cell lines. *NIS expression was detected using antibodies specific to NIS, with β-actin as a loading control. This experiment was performed once (n = 1).*

Consequently, the NanoBiT assay was employed to investigate the interactions between NIS and PBF, as well as NIS and AP2σ2.

First, the putative interaction between NIS and AP2σ2 was tested via NanoBiT. The assay-specific negative control combining NIS-SmBiT with LgBiT-PRKAR2A (NIS/-ve) was included in all experiments. The luminescence data indicated a direct and significant interaction between NIS-SmBiT and AP2σ2-LgBiT or LgBiT-AP2σ2 (Figure 3.6 A), with luminescence levels statistically higher than those observed in the

negative control. To further substantiate this interaction, reverse NanoBiT assays were conducted using LgBiT-tagged NIS and SmBiT-tagged AP2σ2, further confirming the interactions between NIS and AP2σ2 (Figure 3.6 B).

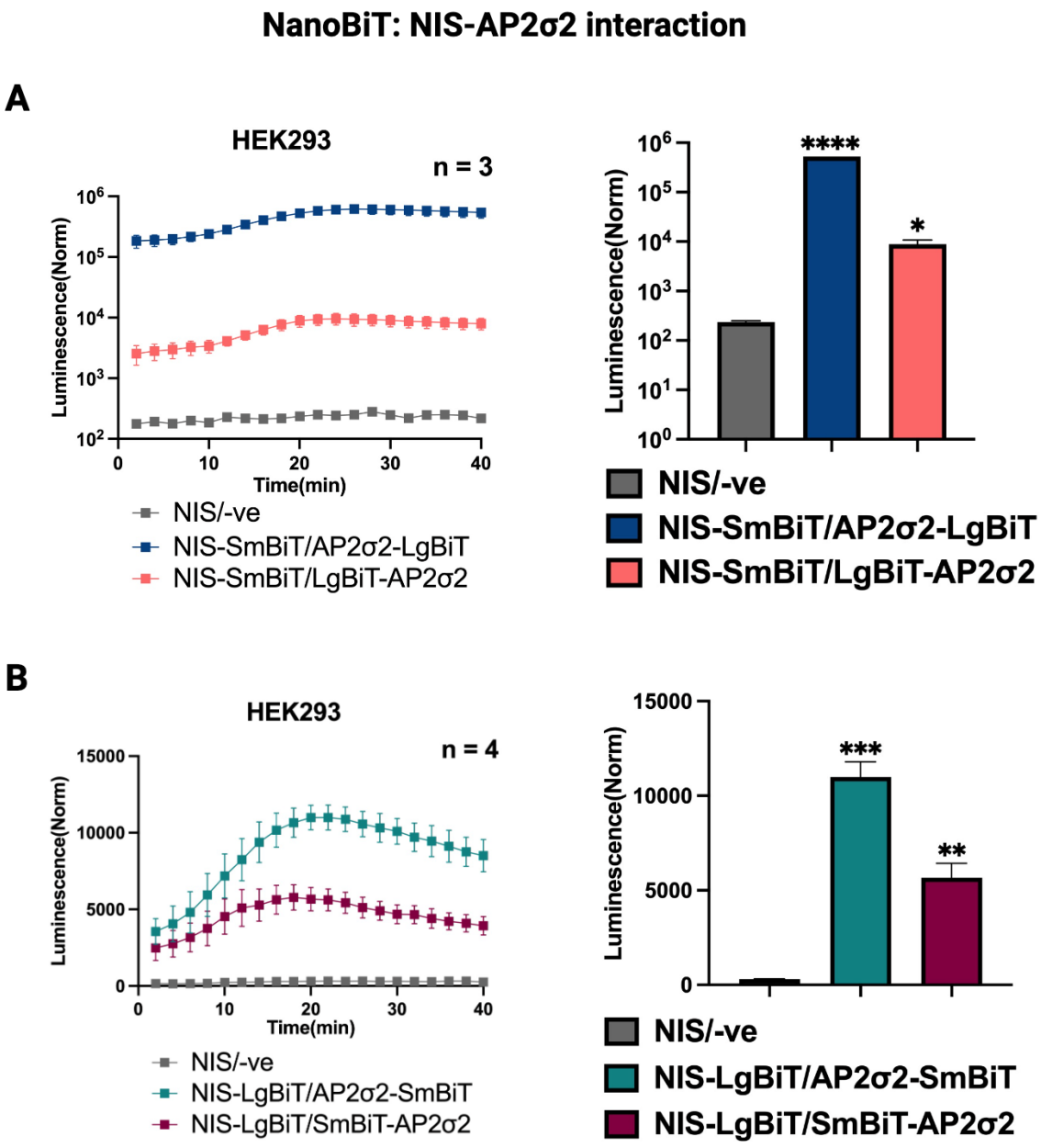


Figure 3. 6 Evaluation of NIS and AP2σ2 interaction using NanoBiT Assays in HEK293 cells. *(A) Left: Real-time kinetic measurements were conducted via the NanoBiT assay. Right: results from the NanoBiT assay 20 minutes (10 cycles) after adding the Nano-Glo substrate. (B) Reverse NanoBiT assay with NIS tagged with LgBiT and AP2σ2 tagged with SmBiT. The data are expressed as the mean ± SEM from n=3-4 biological replicates, with statistical significance determined using a paired, two-tailed t-test against the assay-specific negative control. Significance levels are denoted as *P<0.05, **P<0.01, ***P<0.001, and ****P<0.0001).*

The consistency of these binding interactions was subsequently verified in HeLa cells (Figure 3.7).

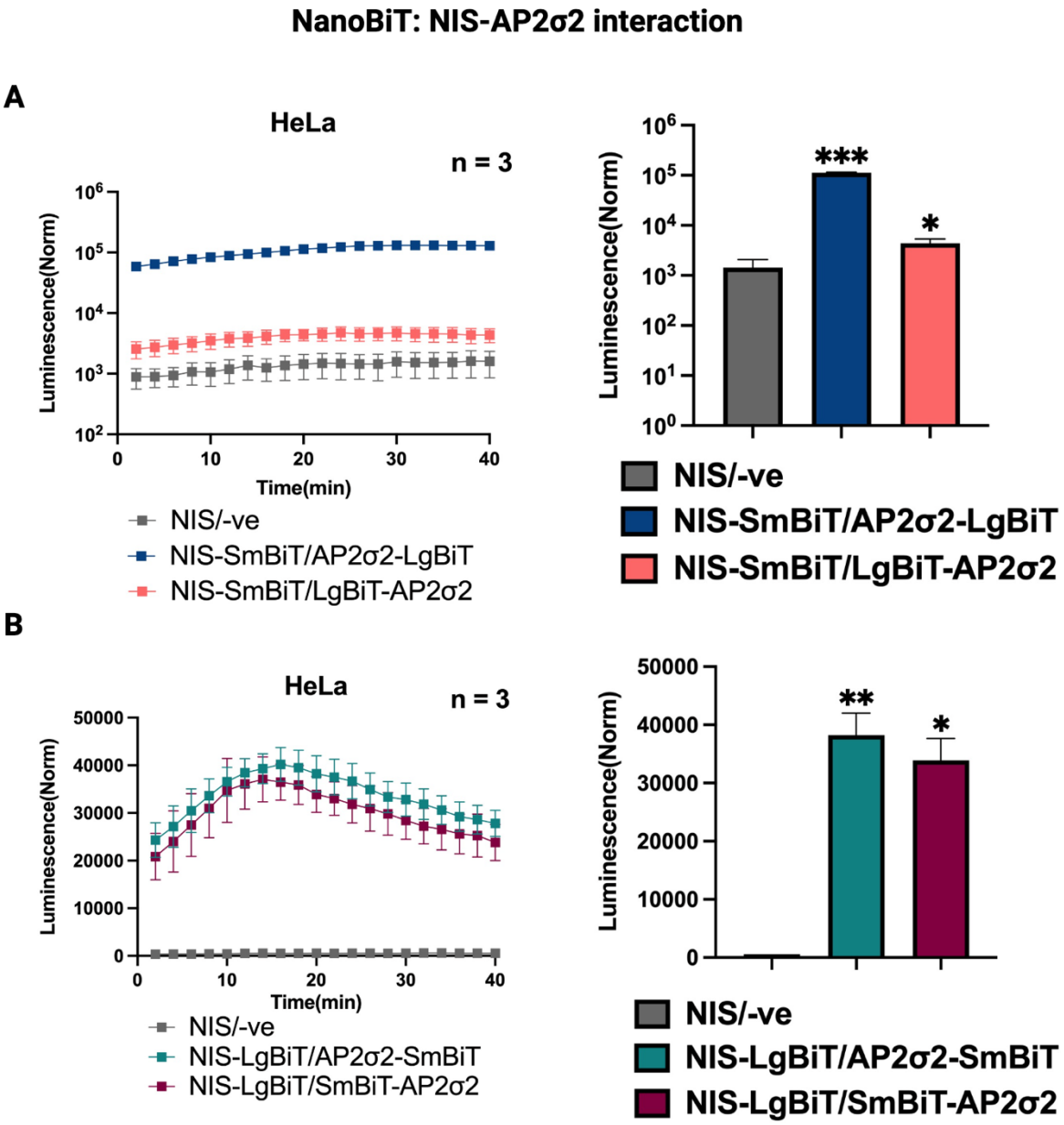


Figure 3. 7 NanoBiT Assay Analysis of NIS and AP2σ2 interaction in HeLa cells. *N=3. *P<0.05, **P<0.01, ***P<0.001.*

In some cases, the measurable degree of interaction was affected by the specific end of the interacting protein tagged with LgBiT. Nonetheless, the luminescent signals from all interactions between NIS and AP2σ2 consistently exceeded the negative control

by more than tenfold, highlighting the robustness of the binding irrespective of the tagging orientation.

3.3.2 Exploring the Interaction Dynamics of NIS with AP2σ2

3.3.2.1 RAI Uptake in C-Terminal NIS Mutants

The C-terminal region of hNIS contains several putative and poorly characterised regulatory sites, such as phosphorylation, di-acid, di-leucine, and PDZ-binding motifs, which may potentially participate in protein-protein interaction and be essential for symporter function (Hingorani et al., 2010; Huc-Brandt et al., 2011). To identify specific motifs that might interact with the AP2 endocytic machinery, dileucine (562LL563) and diacidic (578EEVAIL583) motifs within the intracellular C-terminus of NIS were examined, given that they share structural similarities with the well-known endocytosis motif of the protein VMAT2 (EEKMAIL), known to bind AP2σ2 (H. Li et al., 2005).

Comparative species analysis revealed high conservation of the L and E residues (Figure 3.8 A). The independent abrogation of each motif (L562A/L563A (‘dileucine mutant’) and E578A/E579A (‘diacidic mutant’)) statistically affected NIS function. Specifically, the dileucine mutant showed significantly reduced iodide uptake in HeLa cells, being 79.9 % decreased compared to wild-type NIS. In contrast, the diacidic mutant significantly increased iodide uptake in HeLa cells, yielding a 52.3 % enhancement over wild-type NIS (Figure 3.8 B). At the same time, NIS protein expression was assessed by Western blotting (Figure 3.8 C).

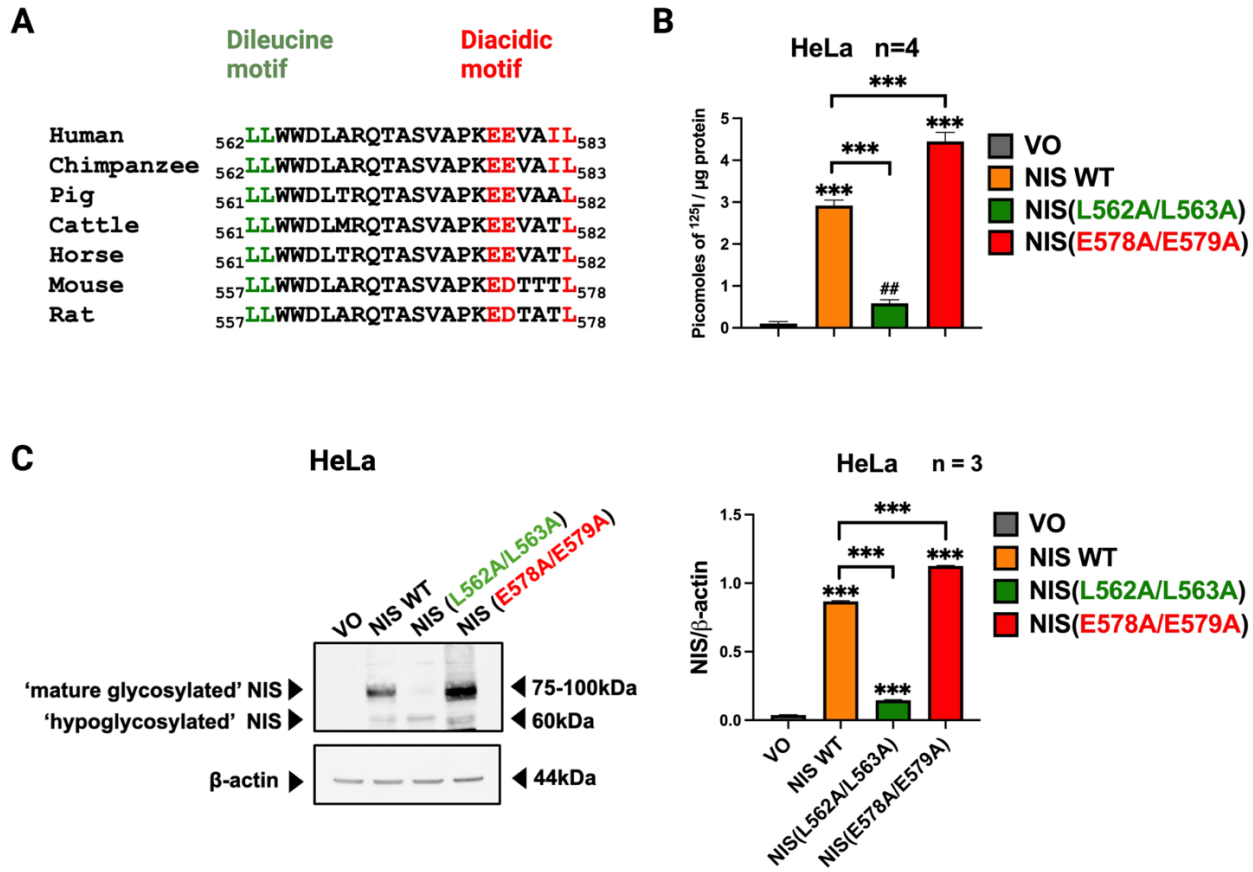


Figure 3. 8 Functional implications of putative C-terminal motifs in NIS. *(A) Conservation of the NIS C-terminal region spanning amino acids 562 to 583 across several species. (B) Radioiodide uptake in empty vector (VO), wild-type (WT) NIS, NIS mutant L562/L563A or NIS mutant E578A/E579A transfected HeLa cells (n=4 biological replicates). (C) Western blot analysis delineating the glycosylation profiles of NIS in HeLa cells, comparing wild-type NIS with mutants L562A/L563A and E578A/E579A (left). Densitometric analysis (right) quantified the relative abundance of NIS variants against β-actin, used as a loading control. Data are presented as mean ± SEM for n=3 or 4 experiments. Statistical significance was determined using one-way ANOVA with Tukey's post hoc test for multiple comparisons (***P<0.001) or unpaired two-tailed t-test (##P<0.01).*

Western blot analysis showed that wild-type NIS is fully glycosylated, whereas the dileucine mutant was only partially glycosylated, and was expressed at lower levels. The diacidic mutant, on the other hand, appeared to be fully glycosylated, showing both immature and mature glycosylated forms (Figure 3.8 C). These findings suggest

differences in the processing and cellular targeting of these NIS mutants, resulting in altered expression and hence altered function.

3.3.3.2 Characterising the Putative Interaction Site between NIS and AP2σ2 Subunit

3.3.3.2.1 NIS C-terminal Dileucine and Diacidic Endocytosis Motifs are Essential for Interaction with AP2σ2.

The AP2σ2 subunit has been shown to interact with the dileucine and diacidic motifs of multiple membrane proteins as a prerequisite for initiating endocytosis (Collins et al., 2002). These residues were substituted with neutral alanines in the NIS SmBiT plasmids (NIS (L562A/L563A)-SmBiT and NIS (E578A/E579A)-SmBiT) to investigate their impact on the interaction between NIS and AP2σ2. Importantly, NanoBiT assay results showed that both NIS-SmBiT LL or EE mutants decreased binding affinity to AP2σ2 compared to wild-type NIS-SmBiT in live cells (Figure 3.9). Importantly, NIS LL/EE-SmBiT and LgBiT-AP2σ2 interaction remained significantly higher than the assay-specific negative control. These results indicate that mutations did not entirely abrogate binding but resulted in a 55 % and 51 % reduction in the interaction strength between NIS and AP2σ2, respectively. This partial retention of binding capability underscores that while the EE/LL mutations diminish the interaction efficiency, they do not entirely disrupt the molecular association between NIS and AP2σ2 under experimental conditions.

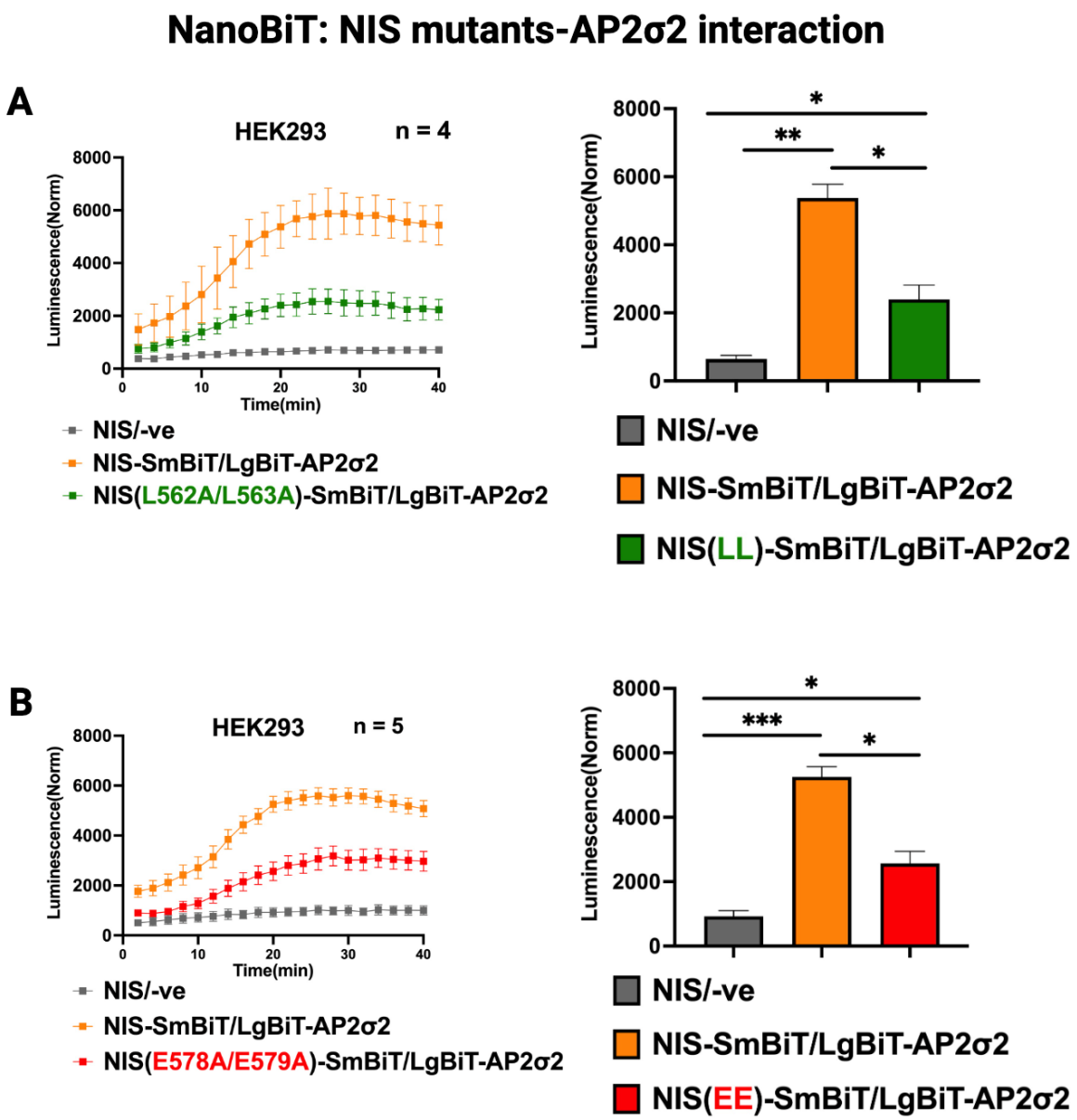


Figure 3. 9 Impact of NIS dileucine and diacidic mutations on AP2σ2 binding. *NIS mutants L562A/L563A (A) and E578A/E579A (B) demonstrated a statistically significant reduction in binding affinity for AP2σ2 compared to wild-type NIS, as indicated by the luminescence measurements over 40 minutes, summarised in the corresponding bar charts. The results were analysed by paired, two-tailed t-test. *P<0.05; **P<0.01, ***P<0.001.*

However, this reduction in binding affinity highlights these motifs' critical functional roles in mediating effective interactions between NIS and AP2σ2. The observed decrease in interaction strength suggests that these specific mutations might alter the

structural or electrostatic properties necessary for optimal binding, thus providing valuable insights into the molecular mechanism for NIS protein recruitment and internalisation processes facilitated by AP2 in cellular endocytosis.

3.3.3.2.2 AP2σ2 Mutations Impair the Interaction with NIS and Increase NIS Expression

Mutations in AP2σ2, specifically V88D and L103S, have been shown to markedly reduce the binding capacity of the recombinant AP2 core complexes to dileucine and diacidic motifs (Kelly et al., 2008). NanoBiT constructs LgBiT-AP2σ2 V88D and LgBiT-AP2σ2 L103S were therefore generated to explore this effect further. Data from Figure 3.10 demonstrated that these mutations resulted in significantly decreased binding affinity to NIS, as evidenced by NanoBiT assays performed in both HEK293 and HeLa cell lines. AP2σ2 V88D and L103S reduced luminescence emitted by 2.15-fold and 2.11-fold, respectively.

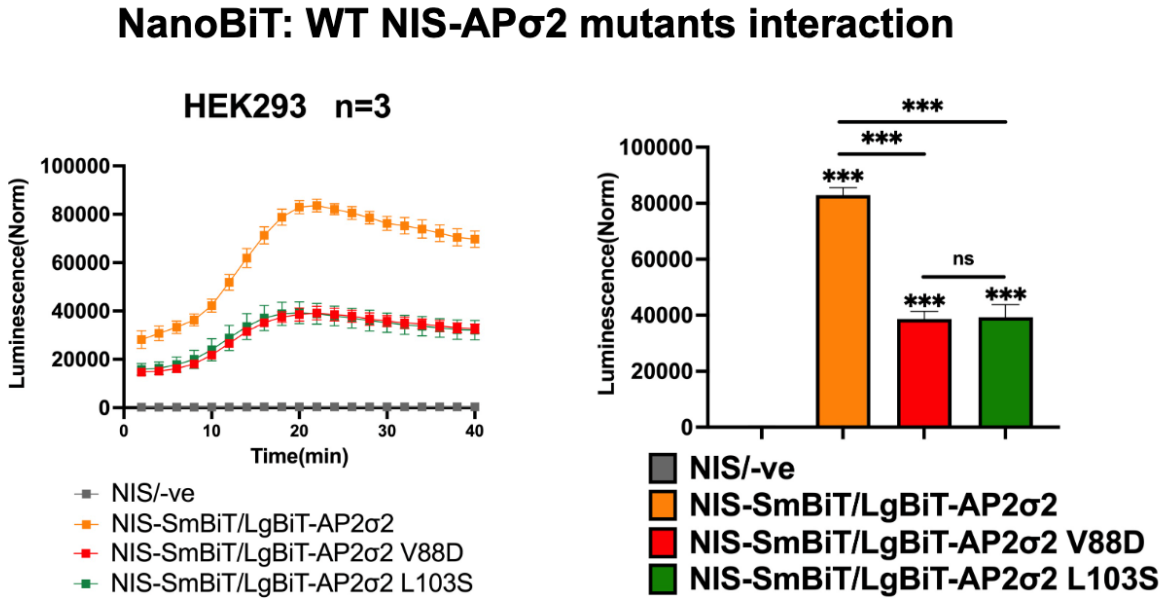


Figure 3. 10 Influence of AP2σ2 Mutations on NIS Interaction. *Left: the diminished luminescence indicative of reduced interaction between NIS and AP2σ2 mutants V88D and L103S in comparison to wild-type AP2σ2. Right: differences in binding were statistically analysed using one-way ANOVA followed by Tukey's post hoc test, revealing a significant decrease in interaction (ns, not significant; ***P<0.001).*

The NanoBiT assay thus demonstrated that residues V88 and L103 in AP2σ2 are crucial for interacting with NIS. Radioiodide uptake assays were conducted to explore the functional implications of these interactions. The overexpression of wild-type AP2σ2 and AP2σ2 mutations V88D and L103S were analysed in thyroidal TPC1-NIS and 8505C-NIS cell lines. As depicted in Figure 3.11, both the V88D and L103S mutants of AP2σ2 resulted in enhanced RAI uptake compared to wild-type AP2σ2. This enhancement suggests that overexpressing AP2σ2 variants with reduced NIS binding affinity may competitively inhibit the activity of endogenous wild-type AP2σ2 within the AP2 heterotetramer. This competitive inhibition likely leads to sustained increased localisation of NIS at the plasma membrane, subsequently elevating RAI uptake.

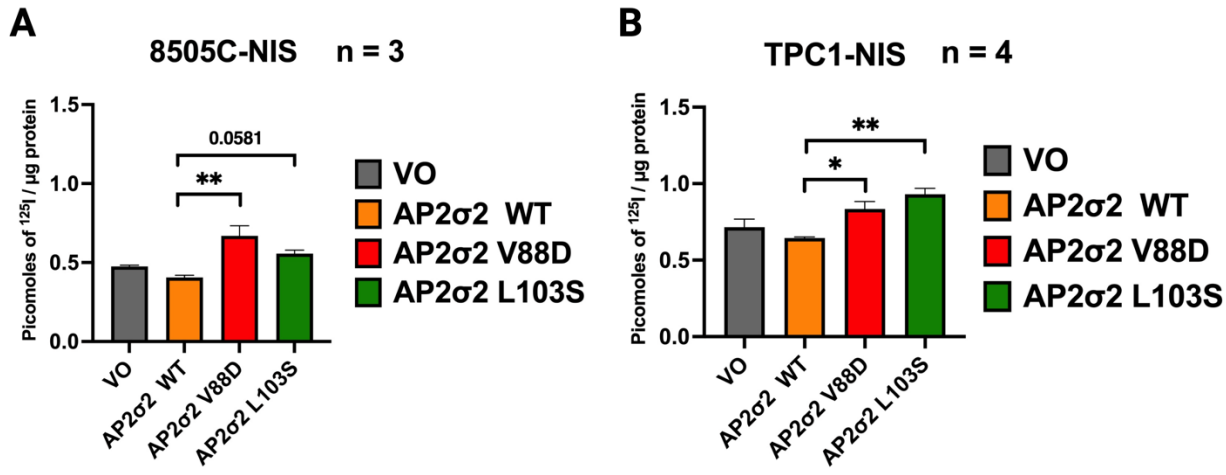


Figure 3. 11 Overexpression of WT AP2σ2, AP2σ2 mutant V88D, and AP2σ2 mutant L103S by exogenous transfection affects radioiodide uptake in 8505C-NIS (A) and TPC1-NIS (B) cells. *Data were analysed by one-way ANOVA followed by Tukey's post hoc test (ns, not significant; *P<0.05, **P<0.01).*

3.3.3 The Effect of AP2 on Radioiodide Uptake

The impact of siRNA-mediated knockdown of AP2α1, AP2μ2, and AP2σ2 on radioiodide uptake was assessed in TSH-responsive human primary thyrocytes. The knockdown of all three subunits led to a statistically significant increase in NIS-mediated radioiodide uptake (Figure 3.12). Specifically, the knockdown of AP2α1 resulted in a 26 % increase in primary thyrocytes, while AP2μ2 knockdown led to a 138 % increase in radioiodide uptake in primary thyrocytes. AP2σ2 knockdown also enhanced radioiodide uptake by 93 %. However, it should be noted that NIS protein content in primary thyrocytes may be relatively low, and cell numbers are limited, which made it difficult to probe via Western blot.

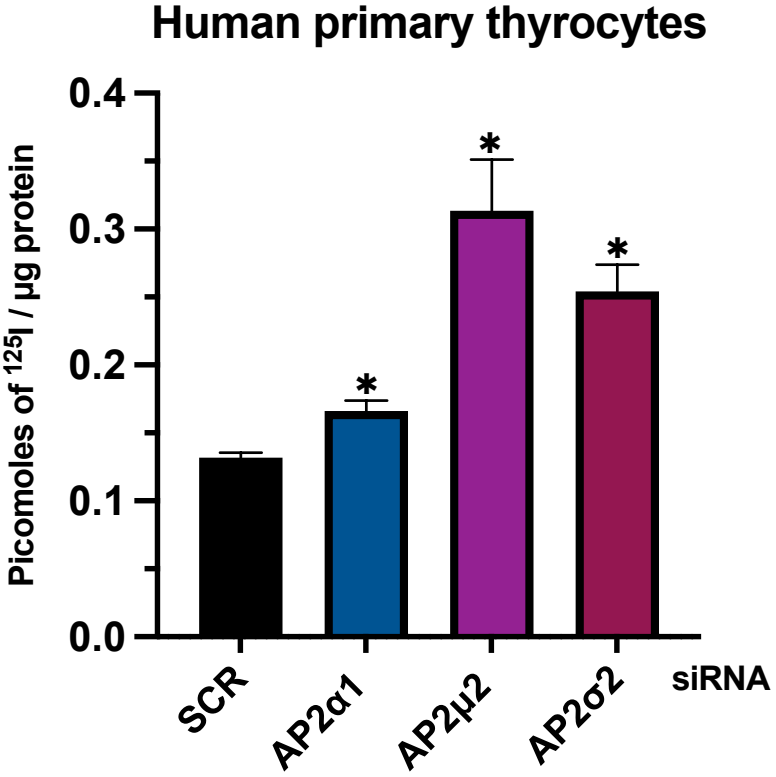


Figure 3. 12 The effect of siRNA transfection on RAI uptake in human primary thyrocytes was assessed for the specified AP2 genes. *Statistical significance was determined using a paired t-test, * indicates $p<0.05$.*

3.3.4 AP2 Alters NIS Subcellular Localisation

3.3.4.1 CSBA

To assess the role of AP2α1 on the subcellular localisation and expression of NIS, cell surface biotinylation assays (CSBA) were employed in TPC-1-NIS and 8505C-NIS cells following transient transfection with scrambled or AP2α1 siRNA, using Na^+/K^+ ATPase as a loading control. Total NIS protein levels were assessed by Western blot, with β-actin serving as the loading control. In this way, the presence of NIS at the plasma membrane and in total cell lysates was analysed to determine the specific effects of AP2α1 knockdown.

For the biotinylation assay, biotinylated plasma membrane proteins were isolated using streptavidin beads, with results compared against scrambled siRNA-transfected cell protein lysates (Figure 3.13).

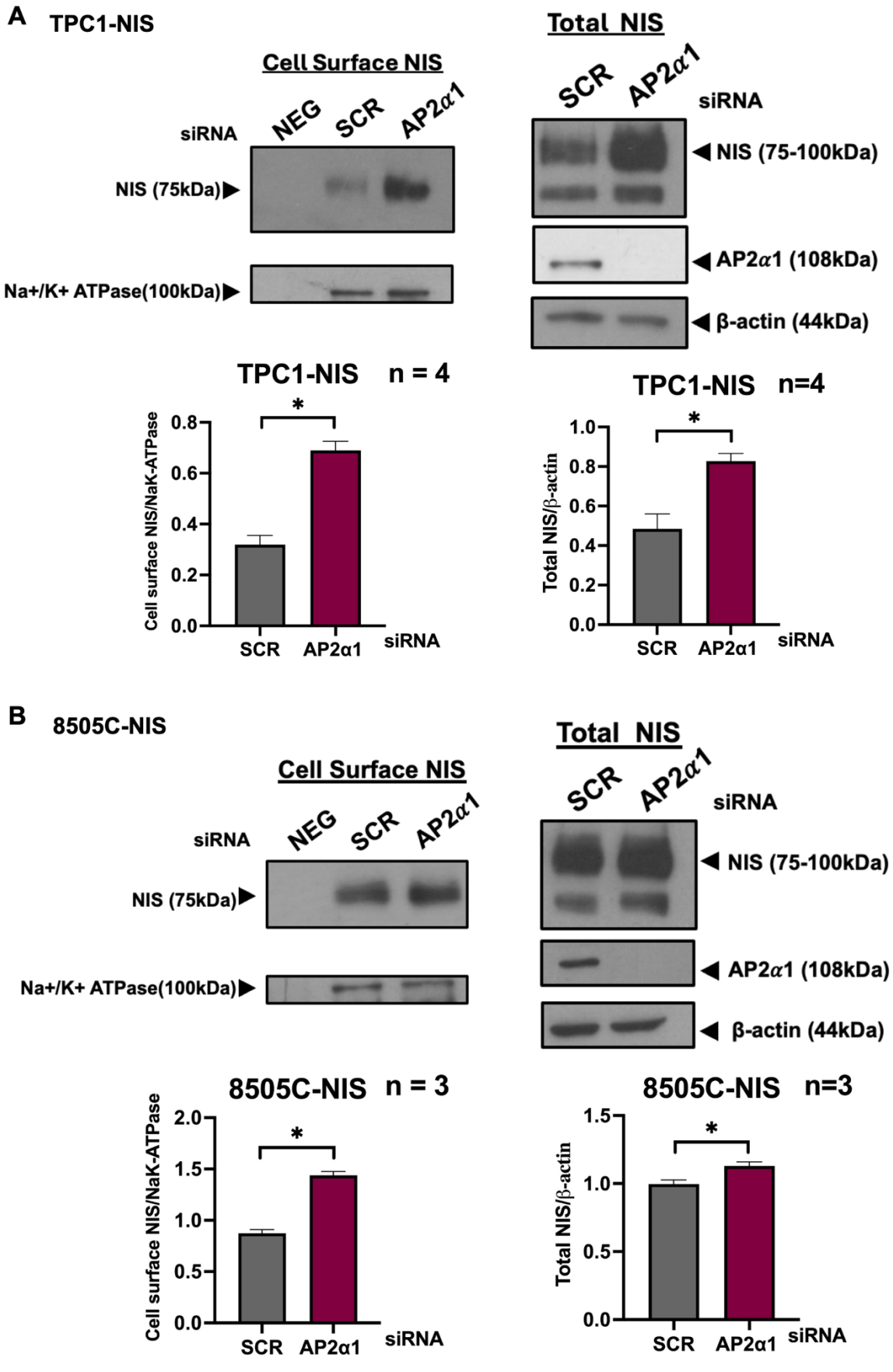

A
TPC1-NIS
Cell Surface NIS
siRNA
NEG
SCR
AP2α1
NIS (75kDa)
Na+/K+ ATPase(100kDa)
Total NIS
SCR
AP2α1
siRNA
NIS (75-100kDa)
AP2α1 (108kDa)
β-actin (44kDa)
TPC1-NIS n = 4
Cell surface NIS/NaK-ATPase
0.0
0.2
0.4
0.6
0.8
*
SCR
AP2α1
siRNA
TPC1-NIS n=4
Total NIS/β-actin
0.0
0.2
0.4
0.6
0.8
1.0
*
SCR
AP2α1
siRNA
B
8505C-NIS
Cell Surface NIS
siRNA
NEG
SCR
AP2α1
NIS (75kDa)
Na+/K+ ATPase(100kDa)
Total NIS
SCR
AP2α1
siRNA
NIS (75-100kDa)
AP2α1 (108kDa)
β-actin (44kDa)
8505C-NIS n = 3
Cell surface NIS/NaK-ATPase
0.0
0.5
1.0
1.5
2.0
*
SCR
AP2α1
siRNA
8505C-NIS n=3
Total NIS/β-actin
0.0
0.5
1.0
1.5
*
SCR
AP2α1
siRNA

Figure 3. 13 Effect of AP2α1 ablation on the cell surface and total NIS protein levels in TPC1-NIS (A) and 8505C-NIS (B) thyroid cancer cell lines. *Left: representative cell surface NIS protein expression. Right: total NIS protein expression. The densitometry analysis (bottom left) shows cell surface NIS protein relative to Na^+/K^+ ATPase protein expression. Densitometry analysis (bottom right) shows total NIS protein relative to β-actin expression. Data presented as mean ± SEM from three or four independent experiments. Statistical analysis was performed using a paired student's t-test. *p<0.05.*

In the AP2α1 siRNA experiments, there was a significant increase in the amount of NIS localised at the plasma membrane. Specifically, TPC1-NIS and 8505C-NIS cells showed increases of 115.79 % and 64.67 %, respectively, compared to the control group. Interestingly, the ablation of AP2α1 was also correlated with an increase in total NIS protein expression in both TPC1-NIS (70.74 %) and 8505C-NIS (13.31 %), as shown in Figure 3.13. Western blot analysis was conducted to verify the successful knockdown of AP2α1 in TPC1-NIS and 8505C-NIS cells (Figure 3.13). Overall, AP2α1 knockdown significantly boosted both cell surface and total NIS protein levels in thyroid cancer cell lines.

To better understand the interaction between the dileucine (562LL563) and diacidic (578EE579) motifs of NIS with the AP2 complex, HeLa cells were subjected to AP2α1 gene knockdown using siRNA, with scrambled RNA (SCR) serving as the control. Cells were transfected with vector-only, wild-type NIS, and both mutants and NIS localisation were assessed via CSBA.

After AP2α1 gene knockdown, total NIS protein levels increased only in the wild-type NIS transfected cells, with no significant increase observed in cells transfected with the E578A/E579A mutant (Figure 3.14). The L562A/L563A mutant showed no

detectable NIS expression of the 75-100 kDa glycosylated form, even after AP2α1 knockdown. Similar trends were observed in the cell surface biotinylation assays (Figure 3.14, right). NIS WT showed a significant increase in cell surface expression following AP2α1 knockdown, while the E578A/E579A mutant showed no noticeable increase. The L562A/L563A mutant showed no glycosylated NIS expression on the cell surface, and no change was observed after AP2α1 knockdown. In the absence of AP2α1 knockdown, the expression of the EE mutant NIS was higher than that of the wild-type, both in total protein levels and at the cell surface. The absence of the AP2α1 band confirmed successful knockdown.

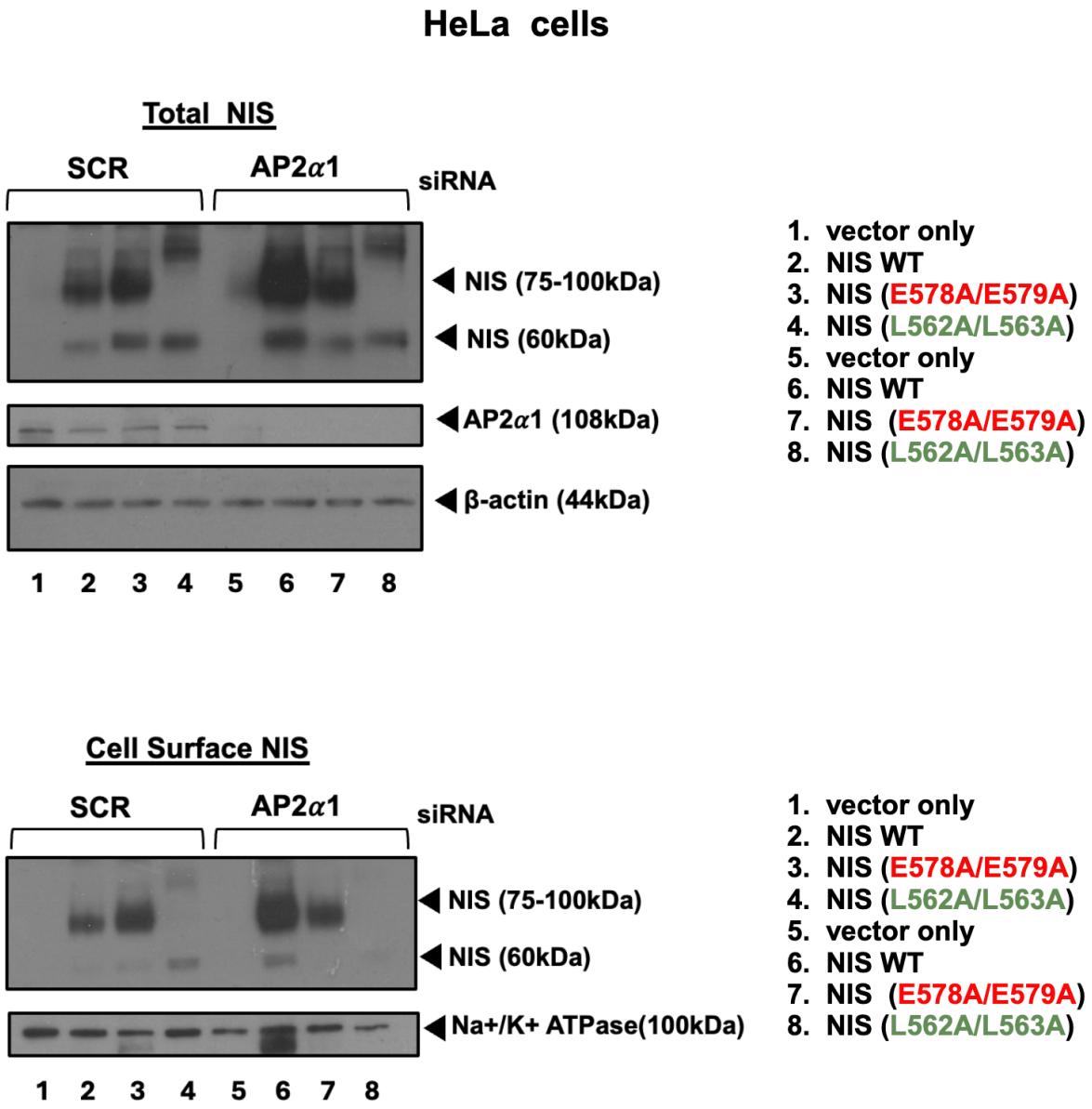


Figure 3. 14 Total NIS protein (top) and cell surface NIS protein (bottom) in HeLa cells after AP2α1 knockdown and transfection with VO, NIS WT, NIS(E578A/E579A) and NIS (L562A/L563A). *β-actin was the loading control for total protein content, and Na^+/K^+ ATPase was the loading control for cell surface proteins.*

These results indicate that AP2α1 knockdown significantly increases total and cell surface NIS protein levels in wild-type NIS-expressing cells but not in cells expressing the L562A/L563A and E578A/E579A mutations. This suggests that the AP2 complex may play a critical role in regulating NIS expression and localisation and that specific mutations in NIS can abrogate this regulatory effect.

3.3.4.2 NanoBRET: Evaluating the Impact of AP2 Subunit Depletion on NIS Trafficking and Localisation

To further challenge the effects of AP2 subunit depletion on NIS trafficking and localisation, the NanoBRET assay was utilised to measure protein interactions in live cells, focusing on the dynamics between NIS tagged with C-terminal nanoluciferase (NIS-Nluc) and multiple membrane markers tagged with Venus. These included Kras (a plasma membrane marker), Rab4 (early endosomes recycling marker) and Rab5 (early endosomes marker), Rab7 (late endosomes/lysosomes marker), Rab9 (late endosomes trafficking to the trans-Golgi network marker) and Rab11 (recycling endosomes marker) (Tiulpakov et al., 2016). Interactions were analysed under conditions where siRNAs targeting AP2α1 and AP2μ2 were applied. NanoBRET, which exploits Bioresonance Energy Transfer (BRET), was used to gain a detailed view of the molecular dynamics influencing NIS trafficking and localisation across different cellular compartments, thereby offering more profound insights into the role of the AP2 complex in membrane protein regulation within live cells.

3.3.4.2.1 AP2α1 Knockdown Impairs NIS Internalisation and Increases NIS Cell Surface Expression

Initial measurements established baseline BRET ratios in SCR siRNA-treated cells. Upon siRNA-mediated knockdown of AP2α1, AP2μ2, and AP2σ2, a notable increase in BRET ratios between NIS-Nluc and Venus-Kras was observed compared to the control group, suggesting enhanced localisation of NIS at the plasma membrane (Figure 3.15).

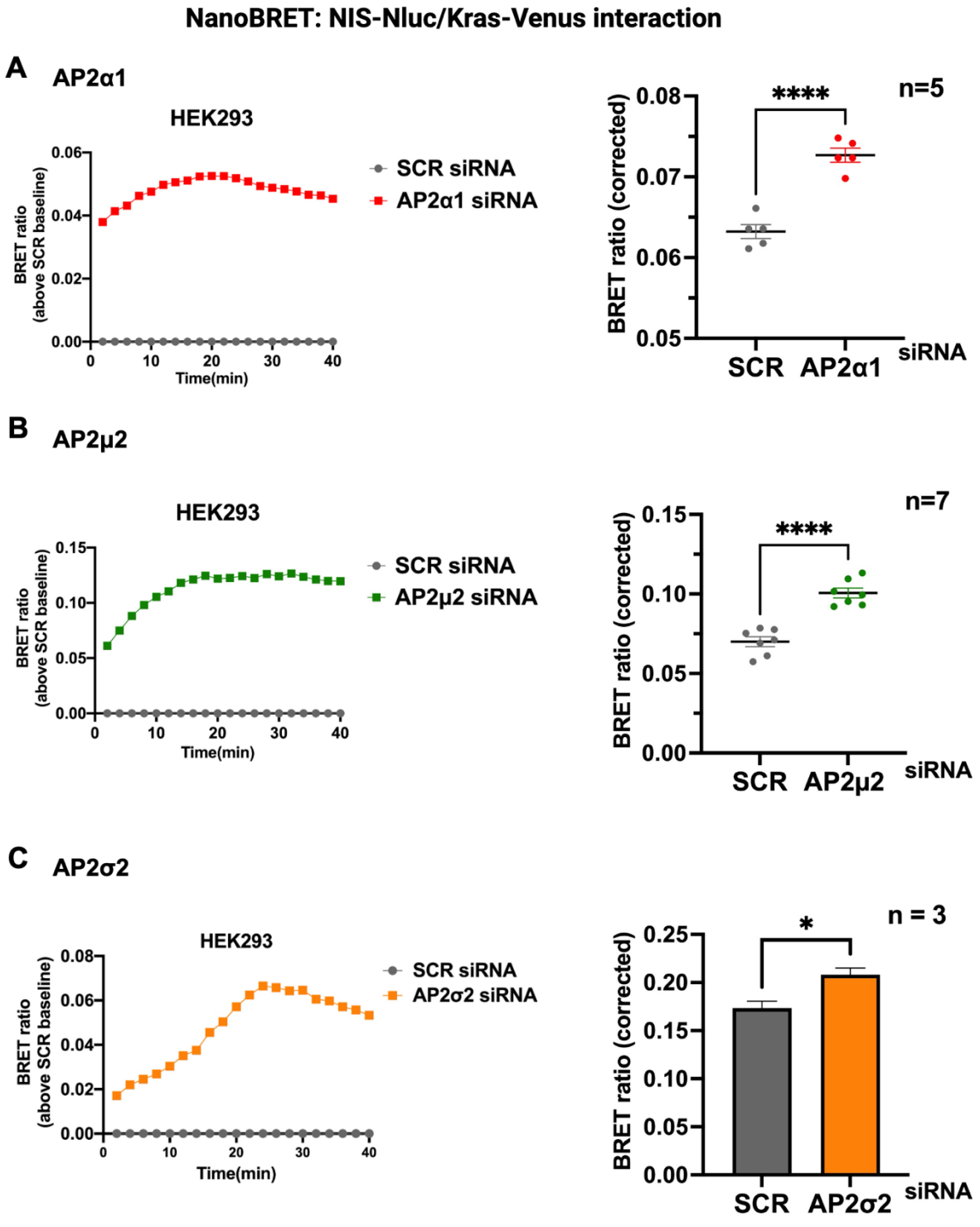


Figure 3. 15 Differential effects of AP2 subunit knockdown on NIS plasma membrane localisation in HEK293 cells. *The left graph in each panel represents the time-course BRET ratios curve measured in HEK293 cells, specifically for the interaction between NIS-Nluc and Venus-Kras over a 40-minute period following treatment with specific siRNAs targeting different AP2 subunits. NanoBRET assay results at 20 minutes post-addition of Nano-Glo luciferase are shown on the right. Data*

*are presented as mean ± SEM; statistical analyses were conducted using an unpaired t-test for each set of conditions (*P<0.05, ****P<0.0001).*

The results of the NanoBRET assays provided additional support, as ablation of AP2α1, AP2μ2, and AP2σ2 led to an enhanced localisation of NIS at the plasma membrane. This was corroborated by a more robust BRET signal observed in live cells, indicating a more pronounced interaction at the plasma membrane. The results were further validated using HeLa cell lines (Figure 3.16).

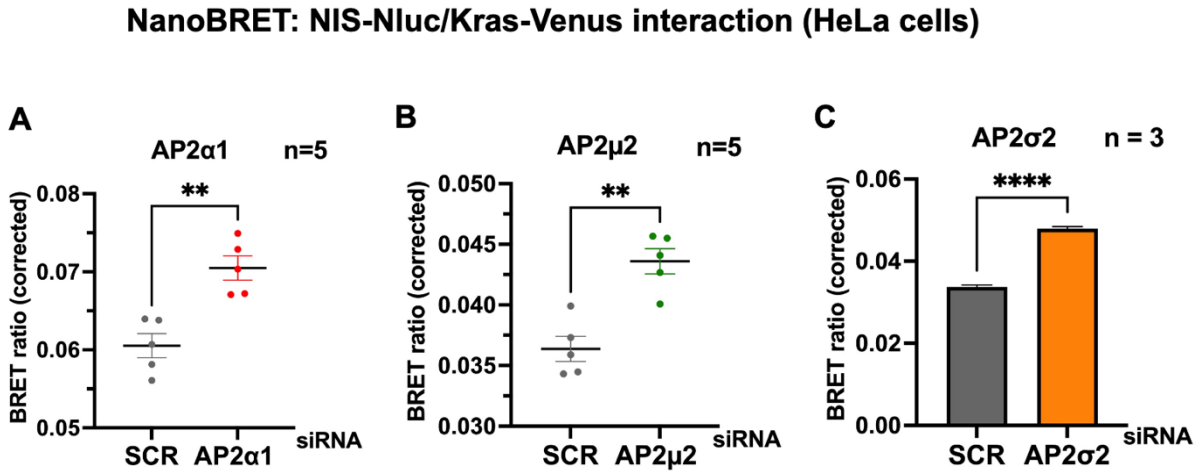


Figure 3. 16 NanoBRET analysis of the NIS-Kras interaction in HeLa cells following AP2 subunit knockdown. *Similar to observations in HEK293 cells, the BRET ratios indicate significantly increased plasma membrane localisation of NIS upon knockdown of AP2α1, AP2μ2, and AP2σ2 compared to the SCR control.*

3.3.4.2.2 Impact of AP2α1 Knockdown on NIS Trafficking and Subcellular Localisation

To further elucidate the impact of AP2 subunit knockdown on NIS endocytosis, NanoBRET measurements were carried out between NIS and venus-tagged markers representative of various subcellular compartments. This approach allowed for a

precise assessment of the spatial dynamics of NIS in response to the depletion of the AP2 subunits.

Figure 3.17 presents the results from a series of experiments assessing the effects of AP2α1 knockdown on the trafficking of NIS through various subcellular compartment pathways. Using NanoBRET assays, interactions between NIS and different Rab proteins (Rab4, Rab5, Rab7, Rab9 and Rab11) were measured in conditions of SCR siRNA (control) and AP2α1 siRNA (knockdown).

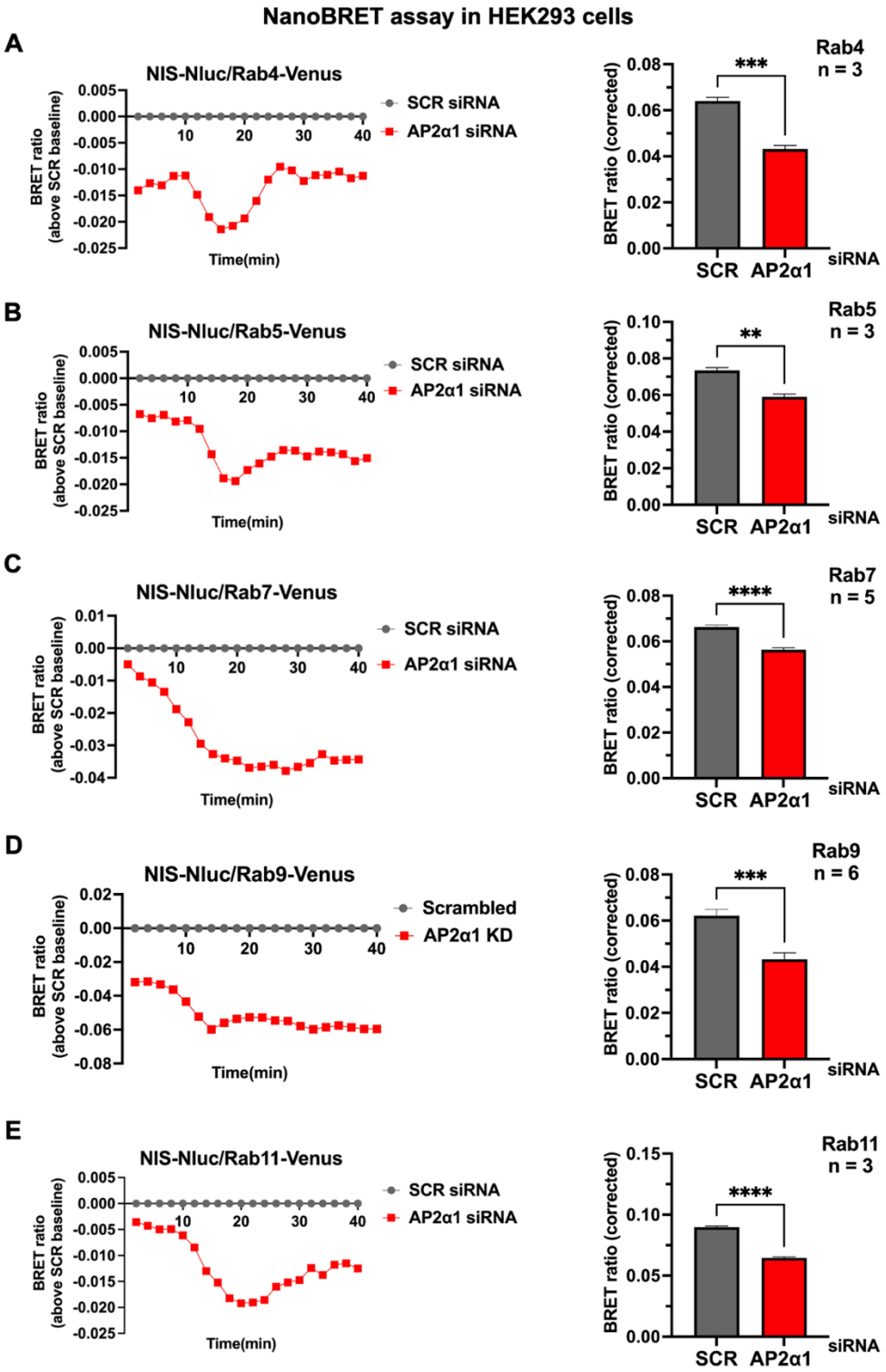


Figure 3. 17 Differential Impact of AP2α1 knockdown on NIS trafficking across subcellular compartments in HEK293 cells. *NanoBiT assays quantifying the interaction dynamics between NIS-Nluc and multiple Venus-tagged Rab proteins following AP2α1 knockdown in HEK293 cells. (A) Venus-Rab4 (early endosomes), (B) Venus-Rab5 (early endosomes), (C) Venus-Rab7 (late endosomes and lysosomes), (D) Venus-Rab9 (late endosomes), (E) Venus-Rab11 (recycling endosomes) across various biological replicates). Unpaired t-test (**P<0.01, ***P<0.001, ****P<0.0001).*

The results consistently showed a significant decrease in BRET ratios in AP2α1 knockdown condition across all Rab markers compared to the control. This demonstrates a reduced interaction of NIS with these subcellular compartments upon AP2α1 depletion and is indicative of impaired NIS internalisation through early endosome, late endosome, and recycling pathways.

3.3.5 Real-Time Validation of NIS-PBF Interaction

Previous co-immunoprecipitation assays revealed that PBF interacts with NIS and influences its subcellular localisation (Smith et al., 2009). NanoBiT assays in the current study now confirm the interaction between NIS and PBF in living cells and in real-time. Figures 3.18 and 3.19 illustrate robust luciferase emissions over twenty cycles and significant increases in luminescence compared to the assay-specific negative control in both HEK293 and HeLa cells, confirming the binding interaction between NIS and PBF.

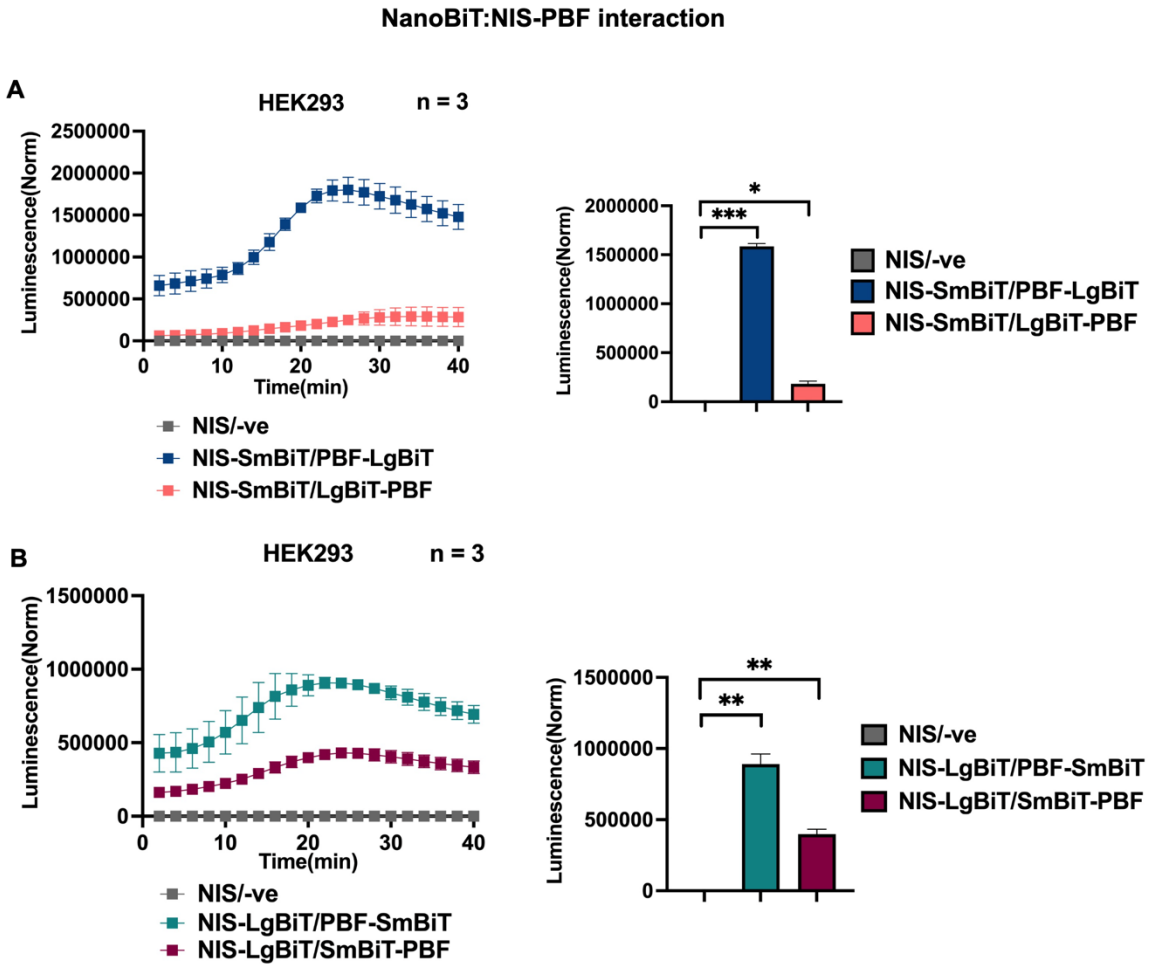


Figure 3. 18 Assessment of NIS-PBF interaction in HEK293 cells using NanoBiT assay. *(A) Interaction combinations (NIS-SmBiT/PBF-LgBiT and NIS-SmBiT/LgBiT-PBF) exhibited enhanced kinetic luminescence data over 40 minutes. The right bar chart quantifies these interactions at 20 minutes. (B) Reverse NanoBiT assays where NIS is tagged with LgBiT and PBF is tagged with SmBiT in the C-terminus or N-terminus. Statistical analysis was performed across three biological replicates, paired t-test, with significance indicated (*P<0.05; **P<0.01, ***P<0.001).*

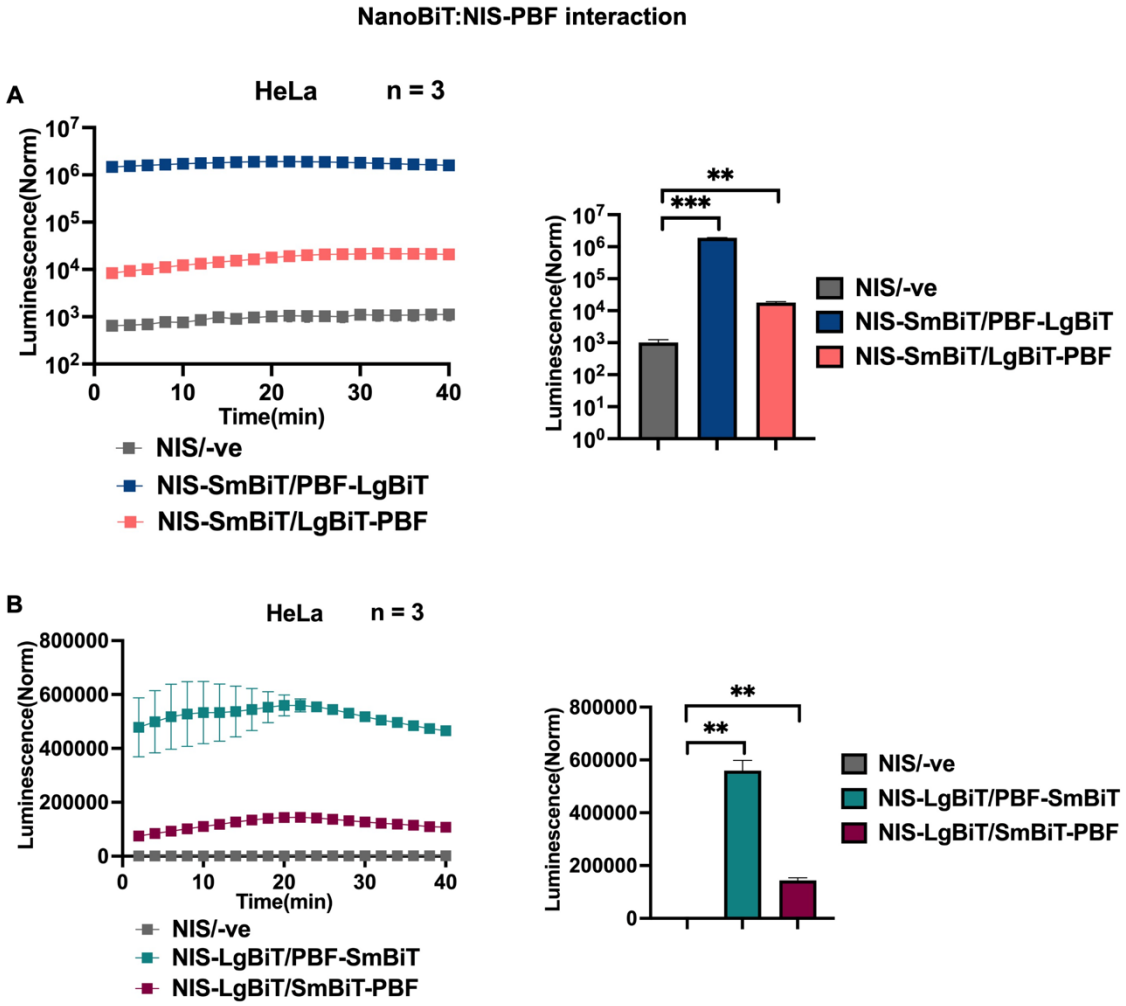


Figure 3. 19 Examination of NIS-PBF interaction in HeLa cells using NanoBiT assay. *Similar to HEK293 cells, results from NanoBiT assays assessing the binding between NIS and PBF in HeLa cells. Data represent mean ± SEM from three biological replicates (*P<0.05; **P<0.01).*

Previous research has identified PBF as a critical interacting partner of NIS, facilitating its endocytosis through a canonical YXXΦ tyrosine-based endocytosis motif (Smith et al., 2009; Smith et al., 2013). The current NanoBiT assays confirmed the binding of NIS and PBF in living cells, and was subsequently employed to investigate how the AP2 adaptor complex influences the dynamic interaction between NIS and PBF. Significantly, the transient knockdown of AP2 subunits α1, μ2 and σ2 in HEK293 cells

led to a substantial increase in NIS-PBF interactions, as evidenced by enhanced binding (Figure 3.20).

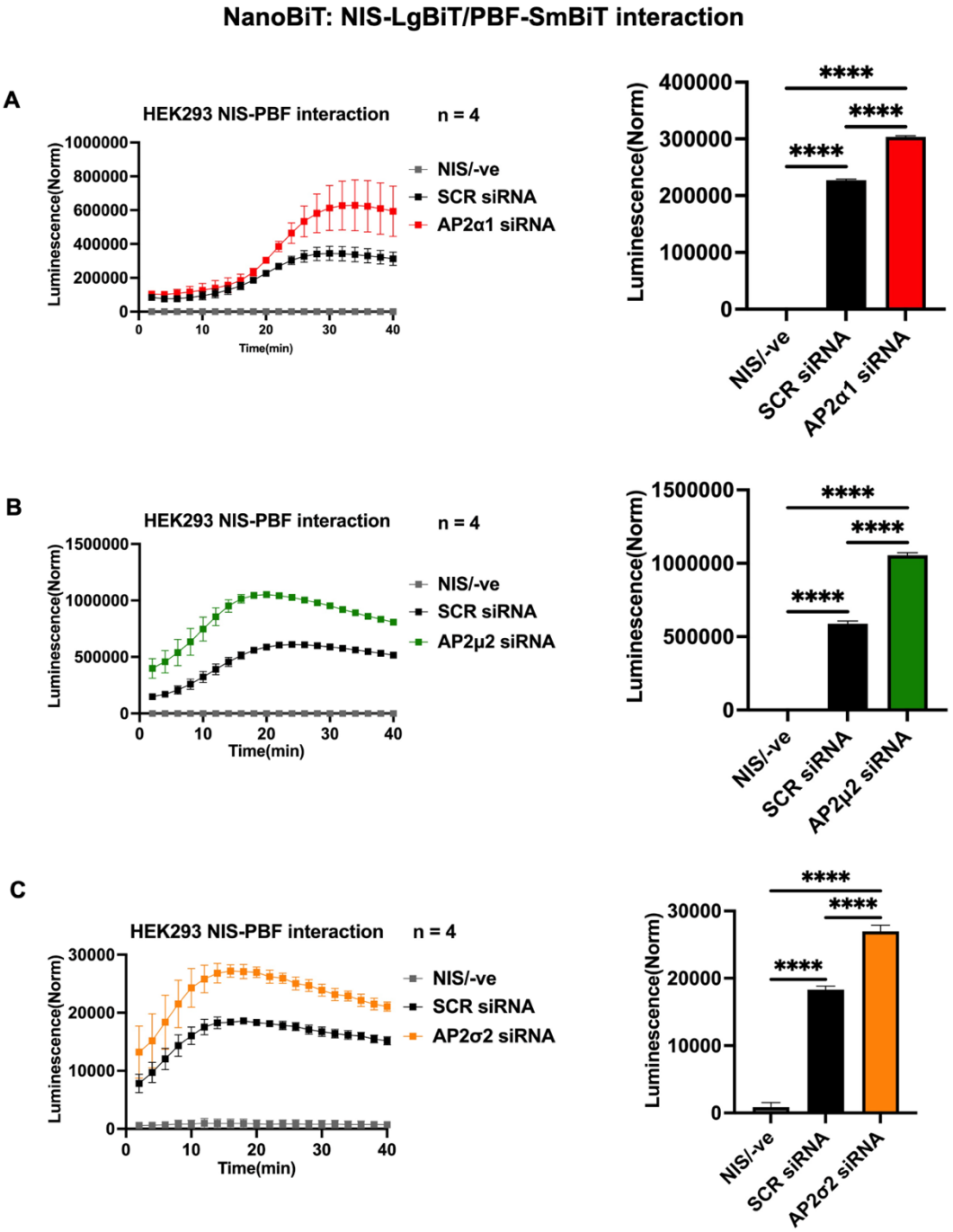


Figure 3. 20 Impact of AP2 subunit ablation on NIS-PBF interaction in live HEK293 cells. *Left: interaction between NIS and PBF in live HEK293 cells following transfection with siRNAs for AP2α1, AP2μ2 and AP2σ2. Right: NanoBiT data were measured at 20 munites after adding the Nano-Glo live cell substrate, with data from four biological replicates combined (n=4, analysed by one-way ANOVA followed by Tukey's post hoc test (****P<0.0001).*

These studies revealed significant changes in the interaction between NIS and PBF upon the knockdown of various AP2 subunits. Validation of successful knockdown via Western blotting is presented later in this chapter. Specifically, ablation of the AP2α1 gene brought out a 33.6 % increase in luminescence, indicative of enhanced interaction between NIS and PBF. Similarly, the knockdown of the AP2μ2 gene resulted in a mean 79 % increase in the binding affinity between these two proteins in live cells, and knockdown of the AP2σ2 gene was associated with a 47.2 % increase in the interaction between NIS and PBF.

Further supporting these observations, the knockdown of AP2 subunits also intensified the NIS-PBF interaction in HeLa cells (Figure 3.21).

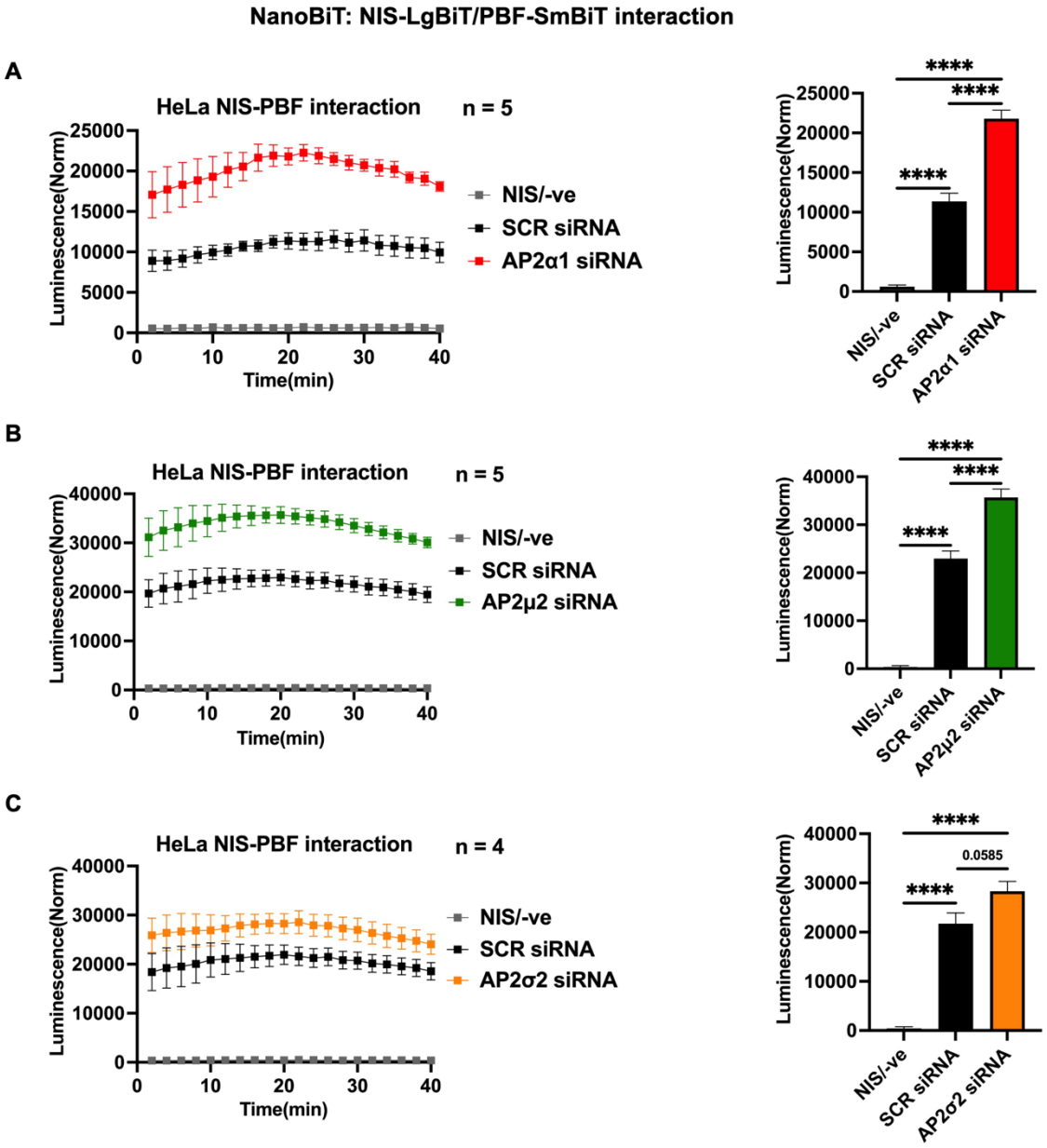


Figure 3. 21 NanoBiT assays in HeLa cells transfected with AP2α1, AP2μ2 and AP2σ2 siRNA.

3.3.6 Validation of AP2 Subunit Knockdown

To verify the successful ablation of AP2 subunits through siRNA-mediated transfection, Western blot and qPCR analyses were conducted in HEK293 and HeLa cells. Figure 3.22 demonstrates that these experiments confirmed the knockdown of the targeted

subunits, although due to technical issues with the AP2σ2 antibody, knockdown of this subunit was assessed via TaqMan RT-PCR rather than Western blotting.

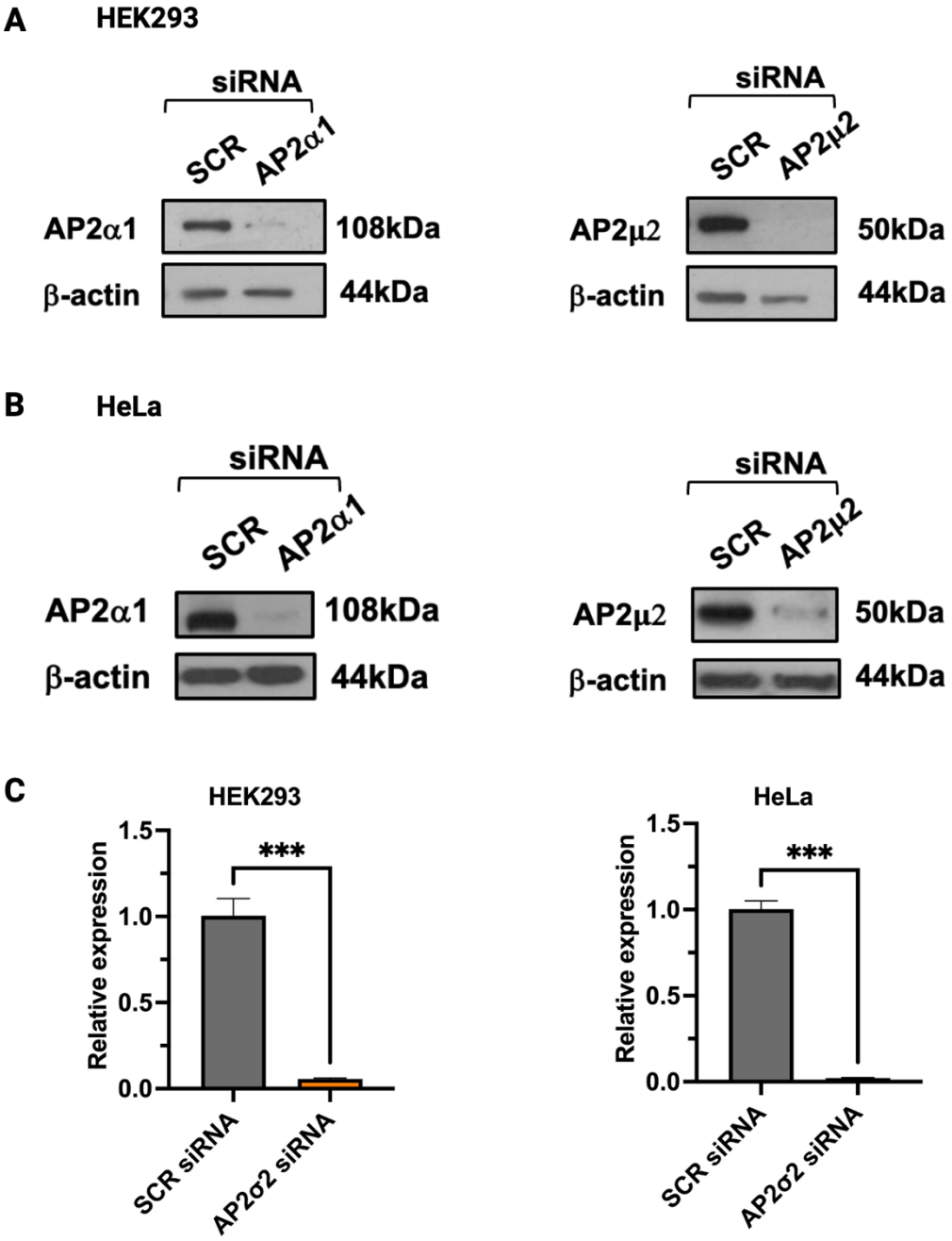


Figure 3. 22 Validation of AP2 subunit knockdown in HEK293 and HeLa cells. *In HEK293 (A) and HeLa (B) cells were transfected with siRNAs targeting AP2α1 and AP2μ2 or with control siRNA (SCR). Quantitative PCR (C) was employed to measure the knockdown of AP2σ2 in HEK293 (left) and HeLa (right) cells (qPCR data provided by Katie Brookes from the McCabe group).*

3.4 Discussion

3.4.1 Interaction Dynamics of NIS and AP2

This chapter aimed to investigate the interaction dynamics between NIS and AP2.

The studies used the NanoBiT assay, a technique for real-time analysis of protein-protein interactions in living cells, to confirm a direct and robust interaction between NIS and the AP2σ2 subunit. Additionally, the data indicated that tagging the N-terminus and C-terminus of AP2σ2, as well as the C-terminus of NIS proteins, did not disrupt these protein-protein interactions. (Figures 3.6 and 3.7). The plasmids used in this assay were transfected with the gene of interest driven by the CMV promoter. As CMV promoters achieve high levels of construct expression, it is important to consider whether system overload could lead to non-specific interactions between NIS-SmBiT and LgBiT-tagged proteins. In this context, the NIS-SmBiT and LgBiT-PRKAR2A negative control was utilised to assess the presence of non-specific interactions, which were absent. In addition, previously published studies have confirmed NIS and PBF interaction via alternative techniques such as co-immunoprecipitation.

A distinct dileucine sequence (562LL563) has been identified as pivotal for the basolateral localisation of NIS. Research by Koumarianou and colleagues highlighted that this dileucine motif within the C-terminal of NIS is crucial for its interaction with the AP1μ1A subunit, facilitating the targeted delivery of NIS to the basolateral plasma membrane (Koumarianou et al., 2022). Furthermore, the amino acids E578 and L583 are recognised to form a conserved monoleucine-based sorting motif, also integral for

transporting NIS to the basolateral membrane (Koumarianou et al., 2022; Martín et al., 2019). Here, further insights were gained through mutational analysis. NanoBiT assays indicated that the AP2σ2 subunit exhibits reduced binding efficiency to the modified dileucine and diacidic NIS mutants compared to the wild type (Figure 3.9), suggesting that these motifs significantly influence not only AP1 but also AP2 binding with NIS, given that modifications in the C-terminal dileucine (L562A/L563A) and diacidic (E578A/E579A) motifs of NIS altered its interaction with AP2σ2 (Figure 3.9).

Interestingly, NIS dileucine mutant protein was only observed at around 60 kDa, a size thought to represent a hypoglycosylated protein form, and which is considered to represent protein in the endoplasmic reticulum lumen (Chung et al., 2015; Feng et al., 2018; Thompson et al., 2019) (Figure 3.8). This suggests that the NIS dileucine mutant (L562A/L563A) showed altered trafficking, being retained intracellularly, and showing reduced iodide uptake capabilities. Conversely, the NIS diacidic mutant (E578A/E579A) increased NIS protein expression and radioiodide uptake. NanoBiT assays indicated reduced interaction between NIS (L562A/L563A)-SmBiT and AP2σ2-LgBiT, potentially due to diminished expression of the NIS protein rather than decreased binding affinity to AP2σ2 per se.

In contrast, both radioiodide uptake and Western blot analyses confirmed that the diacidic mutant had enhanced functionality and expression levels. Combined with the NanoBiT assay results, which show decreased interaction with AP2σ2-LgBiT, these findings suggest that the diacidic mutation’s impaired binding with AP2σ2 reduces its endocytic routing and lysosomal degradation, residing longer at the plasma membrane and hence transporting more iodide.

CSBA results (Figure 3.14) further support the hypothesis that the NIS diacidic motif (E578/E579) is a critical binding site for the AP2 complex and crucial for NIS endocytosis. In both total and cell surface protein analyses, NIS wild type expressing cells showed increased NIS protein expression following AP2 subunit knockdown, indicating that the AP2 complex negatively regulates NIS protein levels under normal conditions, presumably via endocytic sorting into lysosomal vesicles. In support of this, there was no significant increase in NIS protein expression after AP2 subunit knockdown, suggesting that the regulatory effect of AP2 on NIS expression is disrupted when the diacidic motif is mutated. The lack of response in the diacidic motif to AP2 subunit knockdown implies that the influence of the AP2 complex on NIS expression and translocation is mediated through its interaction with this region.

Notably, AP2σ2 mutations such as V88D and L103S diminished the binding affinity between NIS and AP2σ2 (Figure 3.10). Previous research (Kelly et al., 2008) suggested that these residues are crucial for the interaction between AP2 core complexes and motifs such as dileucine and diacidic motifs. This study highlights the critical nature of valine at position 88 and leucine at position 103 in maintaining the structural integrity necessary for the effective binding of AP2σ2 to NIS. The introduction of an aspartic acid at position 88 and a serine at position 103 likely causes conformational alterations that interfere with the binding interface, leading to significantly reduced affinity.

Overall, these studies demonstrated that NIS and AP2σ2 interact, and that mutations of the diacidic motif in NIS or V88 and L103 in AP2σ2 impair this binding. Moreover, the EE motif crucially influences NIS endocytosis and surface expression. In contrast,

mutations in the dileucine motif (562LL563) led to impaired glycosylation and intracellular intention of NIS.

3.4.2 Functional Impact of AP2 on NIS Localisation and Functionality

NanoBRET assays were used to understand multiple NIS trafficking destinations, including the plasma membrane (Kras), early endosomes (Rab5), late endosomes (Rab9), lysosomes (Rab7), and both the Rab4 and Rab11 recycling endosomes. However, future studies would require alternative approaches (subcellular imaging, etc.) in addition to NanoBRET to independently verify these data.

NanoBRET results revealed that siRNA-mediated knockdown of the three AP2 subunits (α1, μ2 and σ2) markedly enhanced the interaction between NIS and Kras (Figure 3.15 and Figure 3.16). This finding suggests that NIS is increasingly retained at the cell surface upon AP2 knockdown. Correspondingly, the interaction between NIS and various subcellular compartment markers was significantly reduced (Figure 3.17), putatively reflecting lower rates of NIS internalisation from the PM. Again, future studies would need to employ additional molecular or microscopy techniques to independently challenge these assertions.

Upon siRNA-mediated knockdown of the AP2α1 gene, an increase in NIS localisation on the cell surface – as well as total protein expression – was observed in TPC1-NIS, 8505C-NIS, and HeLa cell lines via CSBA (Figure 3.13 and Figure 3.14). These observations suggest a diminished NIS internalisation pathway, indicating a disruption in the endocytic pathway traditionally facilitated by the AP2 complex.

Further reinforcing these results, radioiodide uptake assays performed in primary thyrocytes demonstrated that the reduction or functional inhibition of AP2 subunits leads to an elevated accumulation of iodide (Figure 3.12). This suggests that the decreased endocytosis of NIS due to impaired AP2 complex function promotes increased iodide uptake due to prolonged NIS presence at the plasma membrane.

Mutations within the AP2 complex were engineered to elucidate the molecular mechanism underlying these observations further. Specifically, the V88D and L103S mutations in the AP2σ2 subunit, which as above disrupted its interaction with NIS, were overexpressed via exogenous transfection in thyroid cancer cell lines TPC1-NIS and 8505C-NIS. The results demonstrated significant increases in radioiodine uptake compared to the wild type. This supports the premise that weakening the interaction between AP2σ2 and NIS enhances its availability at the plasma membrane, thereby boosting its functional activity in iodide transport.

The present study advances the understanding of NIS regulatory mechanisms, particularly through the lens of the AP2 adaptor complex, an essential mediator in clathrin-dependent endocytosis. The alteration of AP2 expression or function affects not only the expression and localisation of NIS but also its iodide uptake capacity, confirming the pivotal role of the AP2 complex in modulating NIS trafficking. These findings suggest that strategies which modulate the interaction between AP2 and NIS could represent a novel approach to enhance the efficacy of radioiodine therapy in thyroid cancer.

3.4.3 AP2 and PBF Mediate NIS Endocytosis through the Clathrin-Mediated Pathway

The AP2 complex, a heterotetramer comprising the N-terminal domains of its α and β2 subunits along with the complete μ2 and σ2 subunits, orchestrates clathrin-mediated endocytosis by interacting directly with clathrin through its α and β2 subunits. The μ2 subunit specifically binds to the "YXXΦ" tyrosine-based sorting signal in cargo proteins, clustering them into clathrin-coated pits for endocytosis, while the σ2 subunit interacts with dileucine or diacidic motifs crucial for transmembrane protein internalisation (Collins et al., 2002; Ohno et al., 1996). Recent findings indicate that the disruption of the AP2μ2 subunit leads to a significant increase in the proto-oncogene PBF at the plasma membrane (Tobys et al., 2021). NanoBiT assays in live cells confirmed the direct interaction between NIS and PBF (Figure 3.18 and Figure 3.19). This interaction was notably enhanced upon the knockdown of AP2 subunits (Figure 3.20 and Figure 3.21), suggesting that the reduction of AP2 complex expression delays the endocytosis of NIS and PBF, enhancing their availability at the plasma membrane, accompanied by increased interaction detected via NanoBiT. The NanoBiT assay does not specify the precise cellular location of these interactions. Nevertheless, the significantly higher luciferase luminescence observed for the NIS-PBF interaction following the inhibition of AP2 subunits, compared to the control group, suggests that NIS may primarily bind to PBF near the membrane. Indeed, the knockdown of AP2μ2 not only enriched PBF presence at the plasma membrane by 9.6-fold (Tobys et al., 2021), but also implied less efficient recruitment of NIS into the endocytic pathway. However, these suppositions would need to be challenged directly via additional methodologies such as advanced microscopy.

In recent research from the McCabe group, it was observed that the disruption of AP2 subunits α1 and μ2, alongside AAK1, significantly increased RAI uptake in TPC1-NIS and 8505C-NIS thyroid cancer cell lines, while knockdown of AP2σ2 did not enhance RAI uptake (Read et al., 2024). However, the depletion of AP2σ2 results in a significantly increased RAI uptake in primary thyrocytes (Figure 3.12). This discrepancy prompts a hypothesis that other endocytic accessory factors may exhibit partial redundancy with AP2σ2, compensating for its absence in thyroid cancer cells (Read et al., 2024), and that cancer cells may have altered expression of these factors compared with untransformed human thyrocytes.

Combining insights from current and previous investigations, it is hypothesised that the AP2 heterotetramer effectively interacts with NIS at the plasma membrane in a stable conformation. This stabilisation primarily involves a direct interaction between the AP2σ2 subunit and NIS, which plays a fundamental role in the initial docking of NIS at the membrane for further endocytic signalling. Progression of this mechanism heavily relies on the engagement between the AP2μ2 subunit and the YXXΦ motifs of PBF as an endocytic trigger, which acts as an essential endocytic accessory factor (EAF). This interaction is crucial for initiating clathrin-mediated endocytosis, leading to the internalisation of NIS. Based on current understanding, a putative model is proposed to illustrate the interaction of NIS, PBF, and the AP2 adaptor complex in regulating NIS endocytosis and trafficking (Figure 3.23).

Future investigations are necessary to explore the hypothesis that a network of redundant EAFs could mitigate the effects of AP2σ2 ablation in cancer cells. Further, future studies would need to define the exact order and timeframe of events which

govern NIS endocytosis. This future research will help delineate the specific roles of different AP2 subunits and their interactions with EAFs in modulating NIS functionality and RAI uptake, which may be crucial for the targeted treatment of thyroid cancer using radioiodine therapy.

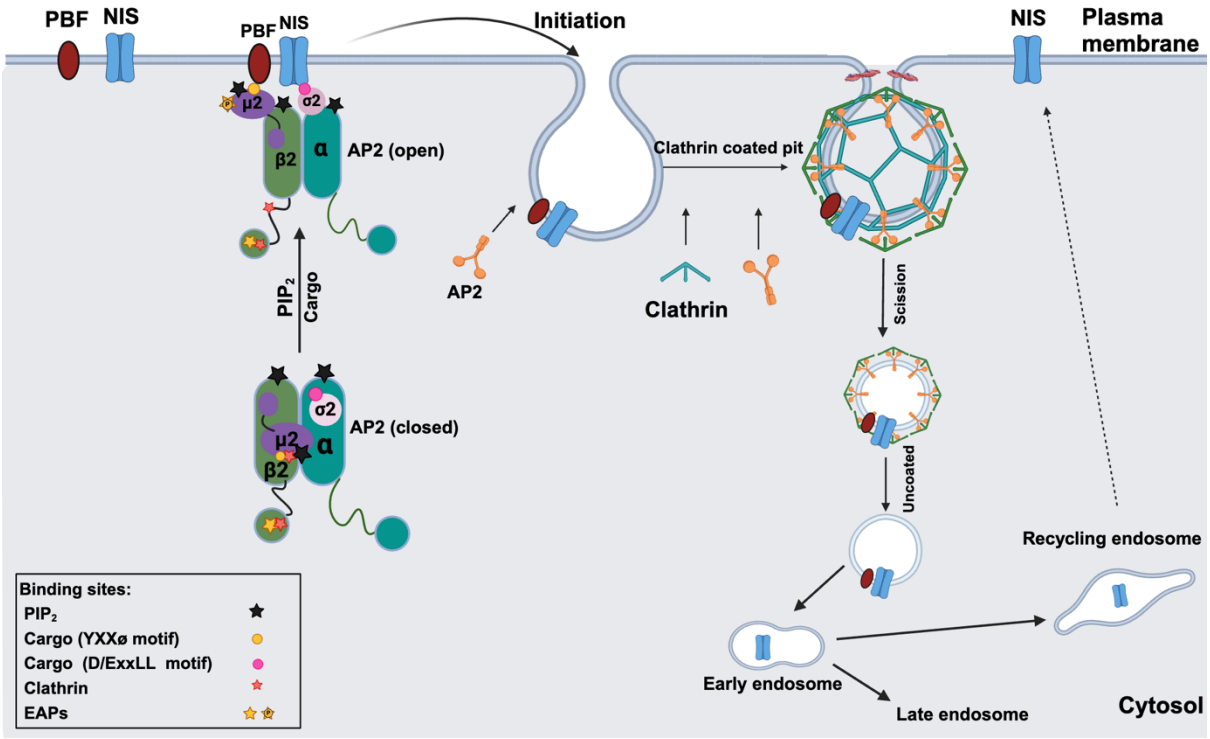


Figure 3.23 Proposed Model of NIS Endocytosis Regulated by PBF and AP2 Complex. *NIS, initially located at the plasma membrane for iodide uptake, NIS undergoes internalisation triggered by PBF. PBF promotes recruitment of the AP2 complex in its open conformation, which binds to NIS-specific motifs and interacts with PIP_2, transitioning AP2 into its closed conformation. This stabilises clathrin interaction, leading to clathrin-coated pit formation and vesicle budding. The vesicles then enter the endocytic pathway, delivering NIS to early endosomes for sorting. NIS is either recycled back to the plasma membrane to sustain iodide uptake or directed to late endosomes and lysosomes for degradation. However, the recycling route remains uncertain, as indicated by the dotted line in the schematic.*

CHAPTER 4 MOESIN MODULATES CLATHRIN-MEDIATED NIS INTERNALISATION

CHAPTER 4 MOESIN MODULATES CLATHRIN-MEDIATED NIS INTERNALISATION

4.1 Introduction

Moesin is a protein previously implicated in the progression of thyroid cancer. Recent in-house studies using mass spectrometry have identified moesin as an interactor with NIS, highlighting the potential of moesin as a therapeutic target (Fletcher et al., 2020).

Importantly, moesin is upregulated in papillary and follicular thyroid cancers, making it a potential biomarker for distinguishing malignant from benign thyroid nodules (Brown et al., 2006; Ciregia et al., 2013). Inhibiting moesin function has been shown to increase NIS protein levels and enhance iodide uptake (McCabe group unpublished data). Moreover, unpublished data from NanoBiT assays have confirmed that NIS and moesin interact in live cells, further validating the significance of their interaction.

As detailed in Chapter 3, the endocytosis of NIS protein involves AP2 and PBF in clathrin-mediated pathways. Jonathan et al. (2009) provided critical insights into the role of moesin in the trafficking of clathrin-coated vesicles (CCVs). Moesin co-distributes with components of clathrin-coated structures (CCSs) in a PIP2-dependent manner, regulates the lateral motility and clustering of CCSs, and is essential for the proper trafficking of nascent rab5-positive endocytic vesicles. Therefore, this chapter focuses on elucidating the specific role of moesin in the endocytosis of NIS, in addition to the AP2-mediated mechanisms described in Chapter 3.

4.2 Materials and Methods

4.2.1 Transient Transfection and siRNA Knockdown

Transient transfection of plasmid DNA was conducted using TransIT-LT1 at a 3:1 ratio (LT1: DNA), as specified in Section 2.5.1. For siRNA transfection knockdown experiments, transient transfection of siRNA was performed according to the protocol detailed in Section 2.5.2. Analyses were carried out 48 hours post-transient transfection and 72 hours post-siRNA transfection to assess the effects.

4.2.2 Plasmid Preparation

Mutants including LgBiT-Moesin^{T558D} and LgBiT-Moesin^{T558A} were generated using the Agilent QuikChange XL Site-Directed Mutagenesis Kit, as detailed in Section 2.4

4.2.3 NanoBiT Analyses

NanoBiT assay was performed as described previously (Section 2.9).

4.2.4 Statistical Analysis

All results were derived from at least three independent biological experiments. Comparisons between two groups were performed using the student's t-test, while one-way ANOVA followed by Dunnett's post-hoc test was employed for multiple group comparisons. Statistical significance was defined as $P < 0.05$.

4.3 Results

4.3.1 The Effect of AP2 on NIS-Moesin Interaction

The impact of AP2 subunits on the NIS-moesin interaction was assessed using the NanoBiT assay in HeLa cells. Knockdown of individual AP2 subunits—AP2α1, AP2μ2, and AP2σ2—revealed their distinct contributions to NIS-moesin binding.

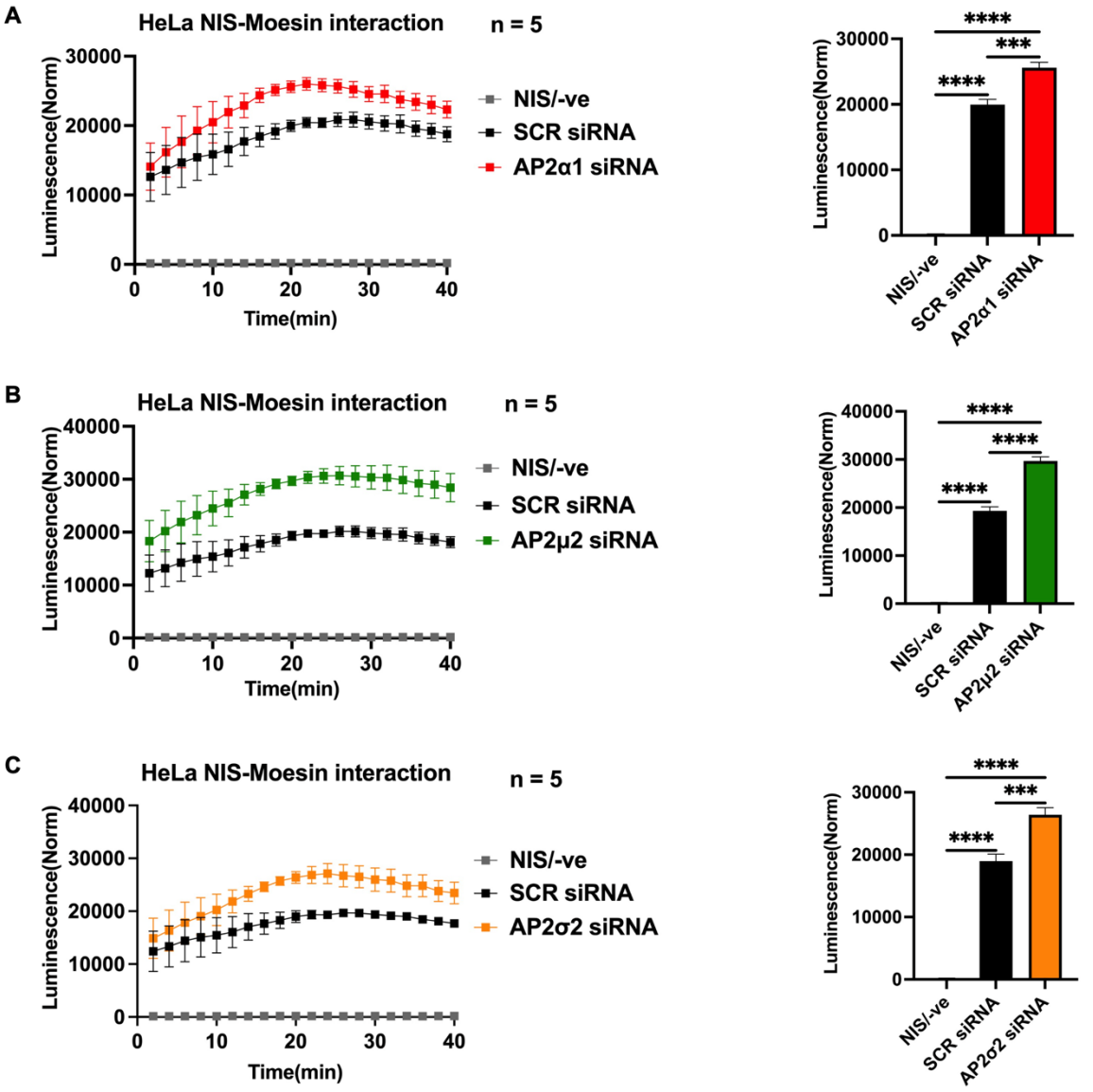


Figure 4. 1 Impact of AP2 subunit knockdown on NIS-moesin interaction in HeLa cells. *HeLa cells were transfected with individual siRNAs targeting AP2α1 (A), AP2μ2 (B) and AP2σ2 (C) subunits. Left: The NanoBiT assay measured the interaction between NIS and moesin for 40 minutes after the addition of the Nano-Glo live cell substrate. Right: results from the NanoBiT assay quantified at 20 minutes (10 cycles) after adding the Nano-Glo substrate, normalised and averaged from five biological replicates. Statistical significance was determined using one-way ANOVA followed by Dunnett's post-hoc test (***P<0.001, ****P<0.0001).*

Knockdown of the APα1 subunit (verified in Section 3.3.6) resulted in a 28.1 % increase in luminescence, indicating enhanced NIS-moesin binding (Figure 4.1). Similarly, ablation of the AP2μ2 subunit led to a 53.7 % increase in the interaction,

highlighting its potential regulatory role. Additionally, the knockdown of the AP2σ2 subunit resulted in a 39.1 % increase in NIS-moesin interaction. These findings align with previous results regarding the NIS-PBF interaction, where the knockdown of AP2 subunits also enhanced binding affinity. The consistent increase in interactions across different partners implies that the AP2 complex is involved in NIS: moesin interaction, with potential implications for the broader regulation of NIS endocytosis.

4.3.2 PBF Knockdown Decrease NIS-Moesin Interaction

Next, changes in NIS-moesin interaction dynamics following the silencing of PBF via siRNA were investigated, with the aim of providing further insights into the molecular mechanisms regulating NIS endocytosis.

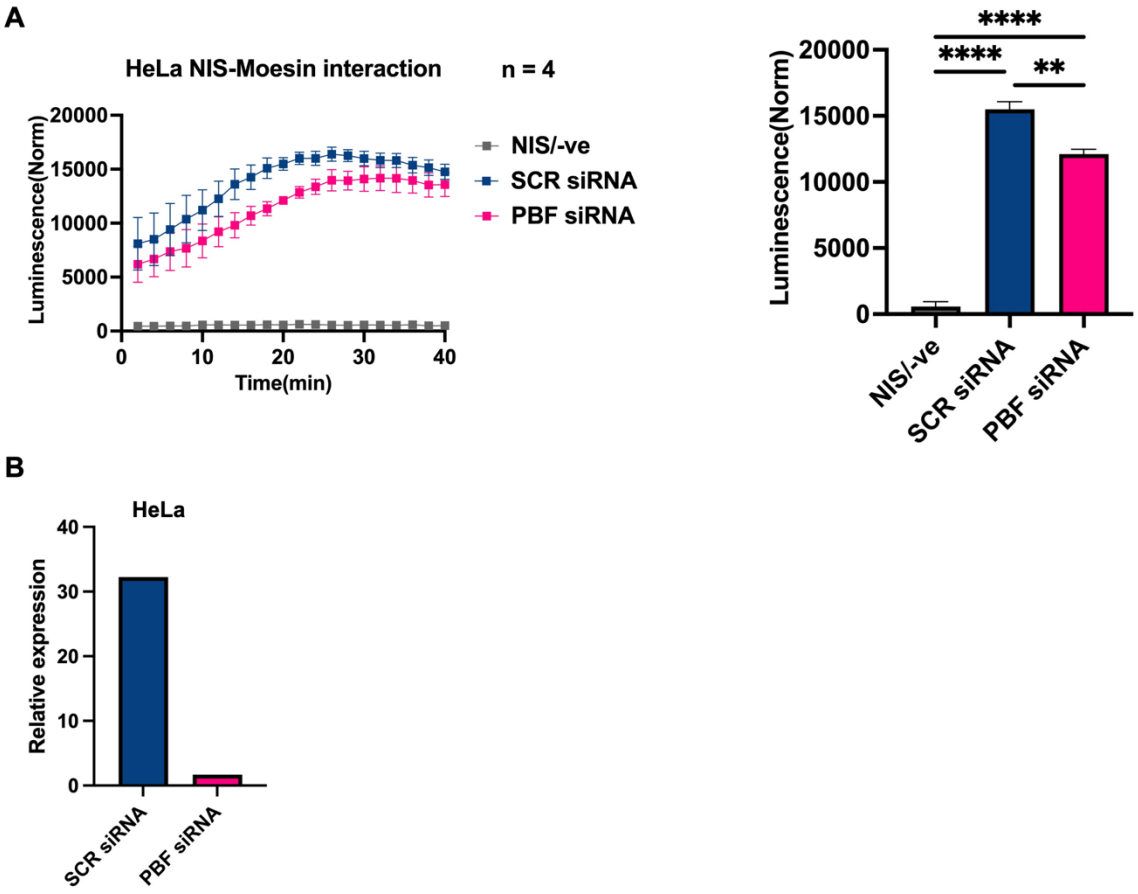


Figure 4. 2 PBF knockdown reduces NIS-moesin interaction in HeLa cells. *(A) HeLa cells were transfected with siRNAs targeting PBF. Data are from four biological replicates (n=4) (****P<0.0001, **P<0.01). Quantitative PCR (B) was employed to measure the knockdown of PBF in HeLa cells (qPCR data provided by Merve Kocbiyik from the Vicki Smith group).*

PBF knockdown led to a significant reduction in NIS-moesin interaction (Figure 4.2). Specifically, cells treated with an siRNA targeting PBF exhibited 21.8 % lower luminescence levels compared to those treated with scrambled (SCR) siRNA control, indicating diminished interaction.

4.3.3 Moesin Knockdown Increases NIS-PBF Interaction

To further elucidate the relationship between PBF, moesin and the AP2 complex in the clathrin-mediated endocytosis pathway, NanoBiT assays were used to investigate the impact of moesin knockdown on NIS-PBF interaction.

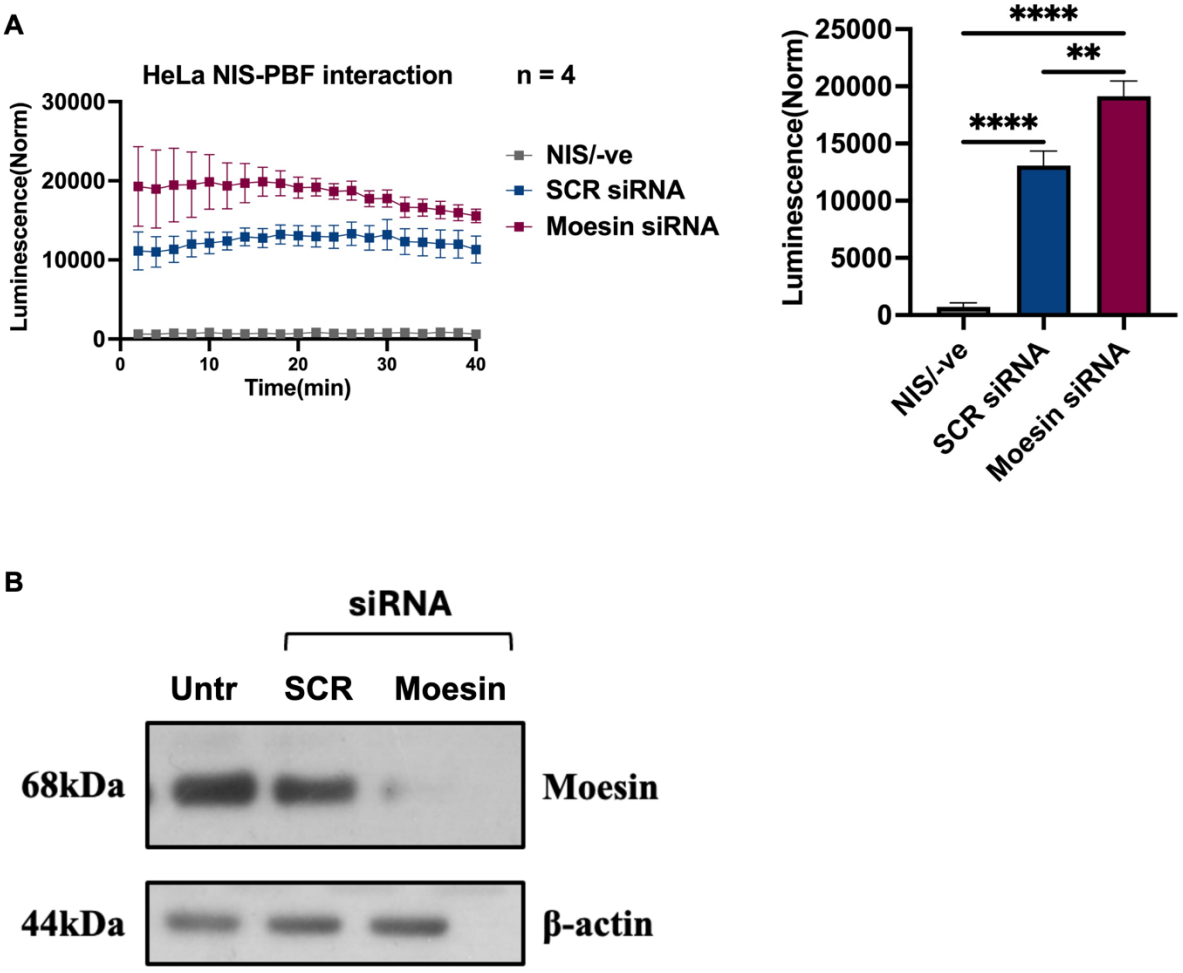


Figure 4. 3 Moesin knockdown increases NIS-PBF interaction. *HeLa cells were transfected with siRNAs targeting moesin. (A) Moesin knockdown leads to a significant increase in NIS-moesin interaction. (B) Confirmation of moesin knockdown by Western blotting.*

Silencing moesin expression significantly enhanced the interaction between NIS and PBF. Specifically, cells treated with an siRNA targeting moesin exhibited 46.4 % higher

luminescence levels compared to those treated with scrambled (SCR) siRNA, indicating an increased interaction.

4.3.4 Effect of Moesin Phosphorylation on Interaction with NIS

To elucidate the impact of moesin phosphorylation on its interaction with NIS, NanoBiT assays were used in cells transfected with wild-type moesin and its phosphorylation site mutants (T558A and T558D) in HeLa and Hek293 cells. These mutants, which have been previously characterised, modulate the phosphorylation status of moesin, with T558A being non-phosphorylatable and T558D acting as a phosphomimetic variant (Huang et al., 1999; Li et al., 2022).

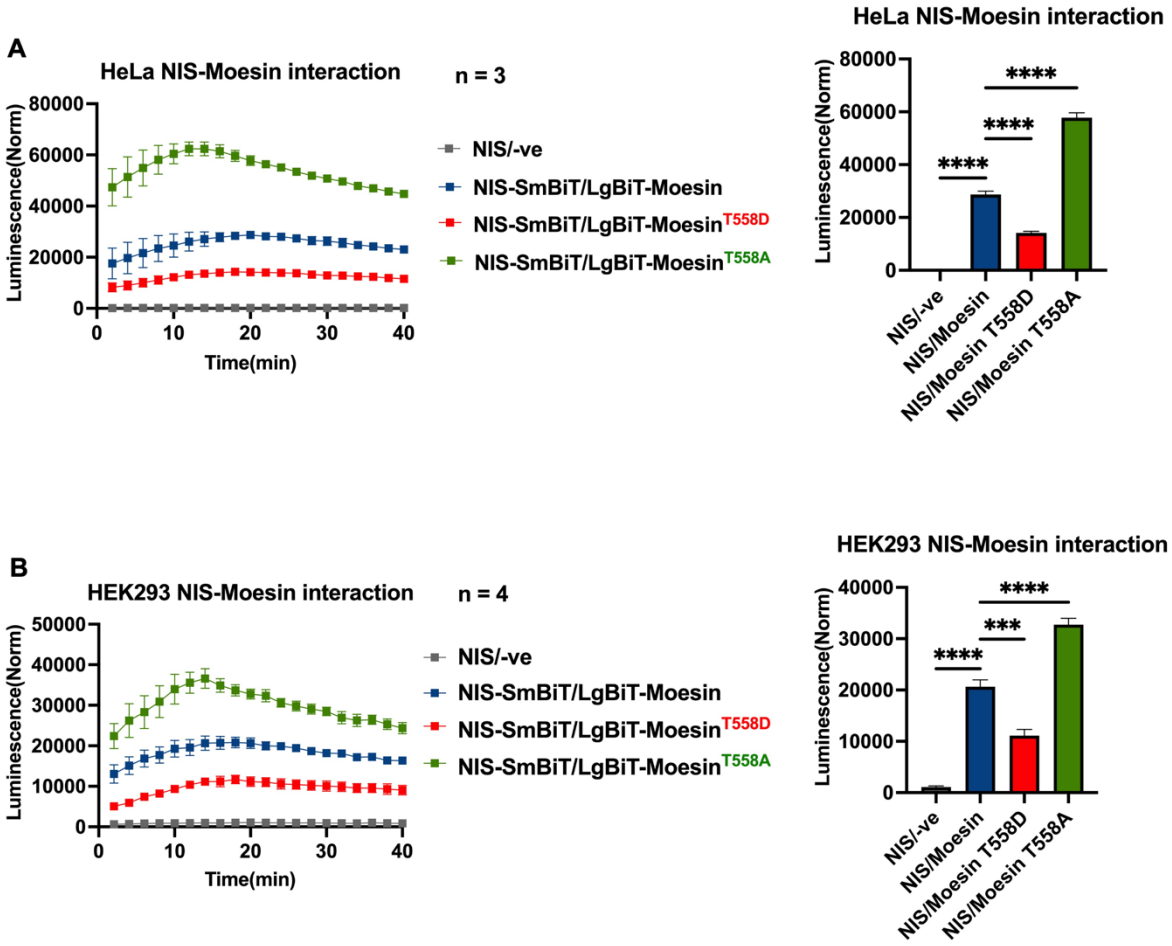


Figure 4. 4 Interaction of NIS with wild-type and phosphorylation site mutant moesin (T558A and T558D) in HeLa and HEK293 cells. *HeLa (A) and HEK293 (B) cells were co-transfected with NIS and wild-type moesin, phosphorylation mutant moesin (T558D) or non-phosphorylatable mutant moesin (T558A) NanoBiT constructs. Data based on three or four independent experiments.*

In HeLa cells (Figure 4.4 A), the interaction between NIS and wild-type moesin (NIS-SmBiT/LgBiT-Moesin) generated a significant luminescence signal, indicating a quantifiable interaction. The phosphomimetic mutation of moesin (NIS-SmBiT/ LgBiT-Moesin^{T558D}), showed a marked reduction in luminescence. Conversely, the non-phosphorylatable mutant moesin treatment group (NIS-SmBiT/LgBiT-Moesin^{T558A}) displayed significantly higher luminescence, indicating enhanced interaction. Consistent results were observed in HEK293 cells (Figure 4.4).

4.4 Discussion

4.4.1 Key Findings

This chapter elucidated an additional potential regulator of NIS endocytosis, which had been identified previously in preliminary data via mass spectrometry as a novel interactor of NIS protein (Fletcher et al., 2020). Interestingly, knockdown of 3 critical AP2 subunits (α1, μ2, and σ2) significantly increased the interaction between NIS and moesin, suggesting that moesin plays a direct or indirect role in regulating NIS surface levels. Conversely, PBF knockdown decreased NIS-moesin interaction, further implicating moesin in the overall process of facilitating NIS endocytosis. Additionally, silencing moesin expression enhanced the interaction between NIS and PBF, indicating potentially competitive and regulatory dynamics among the three proteins.

4.4.2 Mechanistic Insights

The results suggest a complex regulatory network involving moesin, the AP2 complex and PBF in mediating NIS endocytosis. Previous data from the McCabe group demonstrated that moesin knockdown resulted in increased radioiodide uptake in TPC1-NIS and 8505C-NIS cell lines (Figure 4.5). Additionally, cell surface biotinylation assays quantitatively confirmed that PBF overexpression leads to a reduction in the plasma membrane expression of NIS (Smith et al., 2009). The observed increase in NIS-moesin interaction following AP2 subunit knockdown (Figure 4.1) implies a degree of competitive binding between NIS, moesin and various AP2 subunits. This highlights the importance of considering competitive and cooperative interactions within this network. This is consistent with the established role of AP2 in clathrin-coated vesicle (CCVs) formation, an essential step in endocytosis.

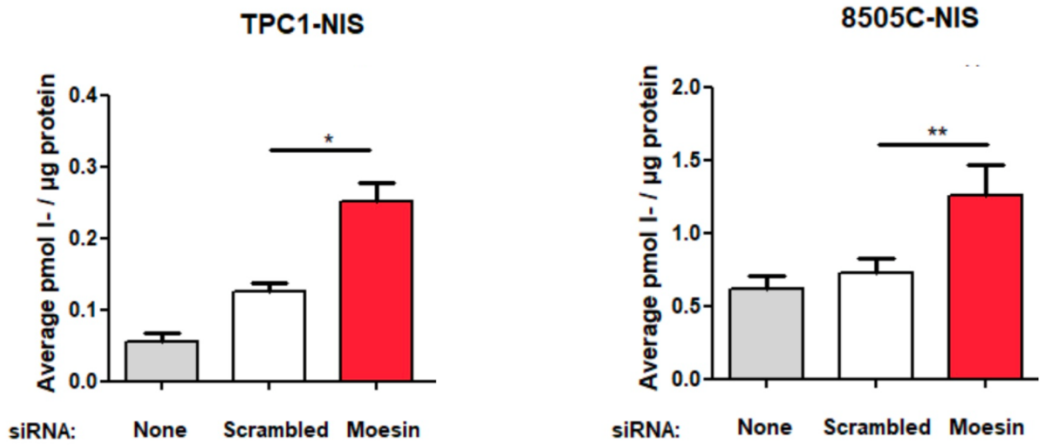


Figure 4. 5 siRNA-mediated silencing of moesin resulted in significant increases in radioiodide uptake in TPC1-NIS and 8505C-NIS cell lines. ** p<0.05, ** p<0.01 (Figure adapted from McCabe group's unpublished data).*

Reduction in NIS-moesin interaction upon PBF knockdown indicates that PBF may act as an accessory or 'pioneer' factor, promoting the initial stages of NIS internalisation.

Increased NIS-PBF interaction upon moesin gene silencing suggests moesin may be a clathrin-coated vesicle ‘linker’ that drives NIS trafficking, with PBF potentially taking precedence in initiating endocytosis.

The analysis of moesin phosphorylation mutants (T558D and T558A) using NanoBiT assays provided further insights into the regulatory mechanisms involved. The results indicated that NIS and the T558A mutant exhibited increased interaction, while the T558D mutant displayed a reduced luminescence signal, suggesting a decreased interaction with NIS. However, it is crucial to approach these interpretations with caution, as NanoBiT assays measure whole-cell protein-protein interactions and do not provide detailed information about the distribution of NIS within various cellular organelles or the specific levels of protein expression.

Based on these observations, the hypothesis is that phosphorylation of moesin at threonine 558 induces a conformational change from the closed, autoinhibited state to an open, active state. This conformational change likely occurs due to increased repulsive interactions between the FERM domain and the C-terminal domain, driven by the addition of the negatively charged phosphate group. In this active conformation, moesin's interaction sites for both F-actin and PIP2 at the plasma membrane are unmasked, enhancing its binding affinity to the membrane and actin cytoskeleton. This enhanced interaction facilitates the recruitment of NIS into clathrin-coated vesicles, thereby promoting NIS endocytosis. Conversely, the T558A mutant, which cannot undergo this phosphorylation, remains in a more closed, autoinhibited conformation. This state likely impairs moesin’s ability to interact with the plasma membrane and actin, thereby reducing NIS endocytosis and increasing its retention on the cell surface.

Additionally, the study by Barroso-González et al (2009) demonstrated that moesin co-distributes with plasma membrane-derived clathrin-coated structures (CCSs) in a predominantly PIP2-dependent manner. Moesin regulates the lateral motility, cellular distribution and trafficking of a subset of nascent Rab5-positive CCVs and likely facilitates CCV recycling. This research supports the role of moesin in the clathrin-mediated endocytosis pathway. Nevertheless, these conclusions are speculative and require further validation. Due to NanoBiT assays providing valuable interaction insights, they do not directly measure endocytosis rates, protein levels, or the subcellular distribution of NIS; additional experiments are necessary to rigorously test this hypothesis and fully comprehend the role of moesin phosphorylation in NIS endocytosis. These should include direct measurements of NIS endocytosis and protein levels using complementary techniques such as fluorescence microscopy and NanoBRET to visualise subcellular localisation and biotinylation assays to quantify the impact of these mutations on NIS surface levels. Furthermore, functional assays to measure iodide uptake in cells expressing different moesin mutants would provide more direct evidence of the role of moesin phosphorylation in NIS regulation.

4.4.3 Therapeutic Implications

The identification of moesin as a regulator of NIS endocytosis may present an additional therapeutic target for enhancing iodide uptake in radioiodide refractory thyroid cancer cells. Inhibiting moesin or modulating its interaction with NIS could increase NIS surface levels, improving the efficacy of radioiodide therapy in thyroid cancer treatment. While this study provides significant insights, it is limited by the need for a broader range of experimental approaches and the use of additional cell line

models. However, based on current understanding, a putative model of moesin action is shown in Figure 4.6.

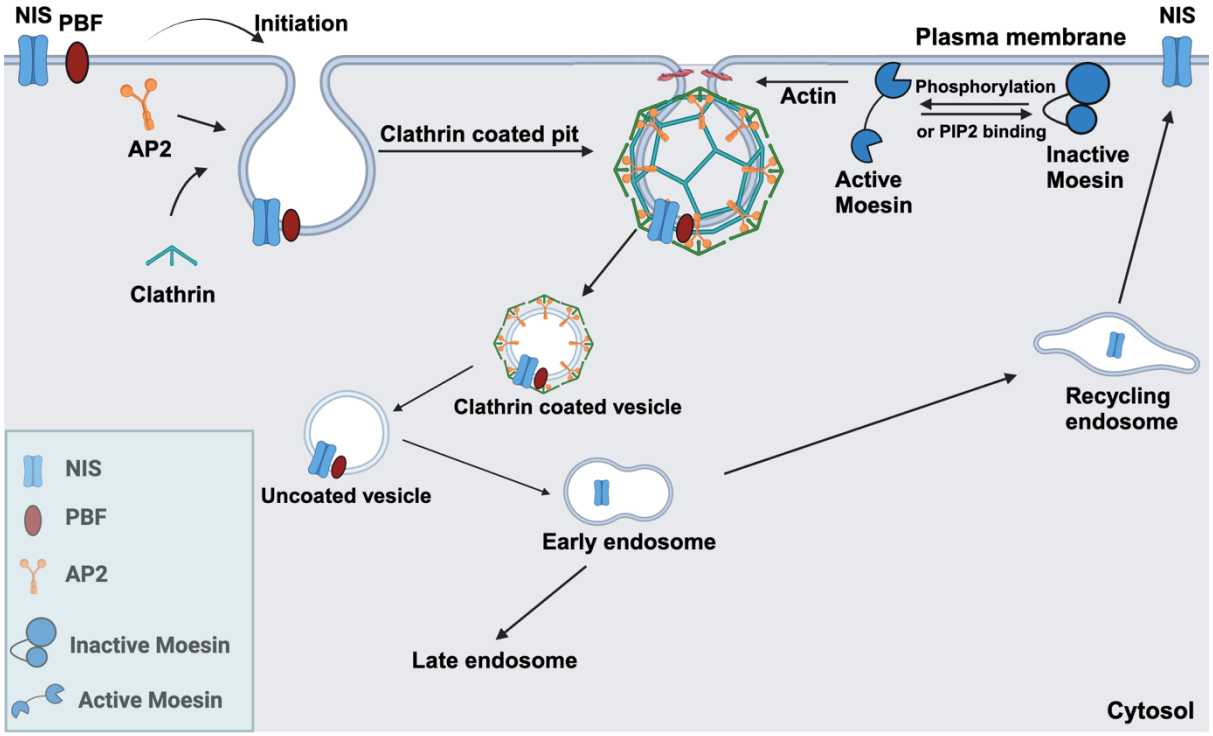


Figure 4. 6 Putative model of the endocytotic processing of NIS.

The model illustrates the sequential events in the endocytosis of NIS. Initially, NIS is located at the plasma membrane, facilitating iodide uptake into thyroid cells. The adaptor protein complex AP2 is recruited to the plasma membrane, recognising and binding to specific motifs on NIS, which initiates the formation of clathrin-coated pits. The binding of AP2 facilitates the recruitment of clathrin, leading to the assembly of clathrin-coated vesicles. Moesin, an ERM family protein, interacts with NIS and the clathrin-coated structures; its phosphorylation at threonine 558 may regulate its activity and interaction with F-actin and NIS, scissoring the CCPs from the plasma membrane, and facilitating their internalisation. The clathrin-coated vesicles containing NIS are internalised into the cell through the invagination of the plasma membrane and the release of the vesicle into the cytoplasm. PBF acts as an accessory or pioneer factor

in the initial stages of NIS internalisation, possibly interacting with both NIS and the clathrin-coated vesicles. Once internalised, the vesicles are transported to early endosomes, where NIS is sorted for either recycling back to the plasma membrane or degradation in lysosomes. The dynamic balance between endocytosis, recycling, and degradation determines the surface levels of NIS, thereby regulating iodide uptake efficiency. This model highlights the regulatory mechanisms that may involve proteins like AP2, clathrin, moesin, and PBF in controlling NIS endocytosis, providing insights into potential therapeutic targets for enhancing iodide uptake in thyroid cancer treatment.

CHAPTER 5 THE IMPACT OF VCP INHIBITION ON RAI-UPTAKE IN CANCER CELLS VIA 3 ALTERNATIVE STRATEGIES: (I) CB-5083 AND 5339, (II) CLOTRIMAZOLE ANALOGUES, AND (III) NMS-873 DERIVATIVES

CHAPTER 5 THE IMPACT OF VCP INHIBITION ON RAI-UPTAKE IN CANCER CELLS VIA 3 ALTERNATIVE STRATEGIES: (I) CB-5083 AND 5339, (II) CLOTRIMAZOLE ANALOGUES, AND (III) NMS-873 DERIVATIVES

5.1 The Effect of CB-5083 and CB-5339 on Radioiodide Uptake in Breast Cancer Cells

5.1.1 Introduction

Breast cancer is the most commonly diagnosed cancer among women worldwide (Lima et al., 2021). The presence of NIS in breast cancers, including triple-negative breast cancers and their metastases, is well-documented. However, its primarily cytoplasmic localisation restricts the efficacy of radioiodine-based therapies. Enhancing the plasma membrane translocation of NIS in tumour cells could significantly improve the effectiveness of radioiodine therapy for breast cancer (Knostman et al., 2007; Renier et al., 2009; Tazebay et al., 2000; Wapnir et al., 2003). VCP/p97 belongs to the type II class of the AAA (a broad family of ATPases involved in diverse cellular functions) and was revealed to be significantly overexpressed in breast cancer tissues compared to normal tissues (Cui et al., 2015); furthermore, elevated VCP levels are associated with metastasis and poor prognosis in breast cancer (Costantini et al., 2021). Importantly, VCP has been shown to influence NIS trafficking. The inhibition of VCP function blocks NIS proteasomal degradation and then restores NIS functionality in thyroid cancer cells, offering a potential strategy to enhance the efficacy of radioiodine therapy (Fletcher et al., 2020). These previous findings suggested that VCP could be a valuable target for therapeutic strategies and might improve NIS expression at the plasma membrane, thereby achieving therapeutically effective levels of radioactivity uptake.

The introduction of VCP inhibitors, particularly CB-5083 and CB-5339, has opened new avenues for targeting VCP-mediated pathways. CB-5083, a potent VCP inhibitor derived from earlier compounds such as ML240 and structurally related to the drug DBeQ, is a relatively recent VCP inhibitor targeting the D2 ATPase domain and demonstrating significant specificity and effectiveness (Chou et al., 2014; Zhou et al., 2015). An earlier study in rodent cancer xenograft models with high VCP levels indicated that CB-5083 could markedly reduce tumour growth and progression (Le Moigne et al., 2017). Based on these findings, Cleave Therapeutics Inc. initiated a Phase I study of CB-5083 with 84 participants with solid tumours and multiple myeloma. This clinical study was halted due to unintended side effects impacting visual function (Leinonen et al., 2021). Although the trial did not meet its primary goal, it showed that CB-5083 is generally safe and well tolerated at lower doses. The doses were below the therapeutic level needed for cancer treatment but might still help treat VCP-related diseases (Cheng et al., 2022).

Cleave Therapeutics has recently advanced drug development with the introduction of CB-5339, a second-generation analogue of CB-5083. CB-5339 is designed to be a potent VCP inhibitor with reduced side effects in normal tissues, showing improved specificity and higher bioavailability in pre-clinical studies across various species. CB-5339 has advanced to Phase I clinical trials to treat advanced solid tumours and lymphomas, as listed on ClinicalTrials.gov under trial number NCT04372641 (Kilgas et al., 2023; Roux et al., 2021). The McCabe research group recently utilised the NanoBiT assay to demonstrate that CB-5083 directly influences the interaction between VCP and NIS. This study established that increasing doses of CB-5083 alter the interaction dynamics between VCP and NIS (Read et al., 2022).

Unpublished data from the McCabe group have further shown that the VCP inhibitors CB-5083 and CB-5339 can enhance iodide uptake *in vitro* (Figure 5.1). Given these results, investigating the effects of these VCP inhibitors in breast cancer cell lines is a logical next step. By reducing NIS degradation, VCP inhibitors might potentially enhance radioiodine therapy in breast cancer, representing a feasible and innovative therapeutic approach.

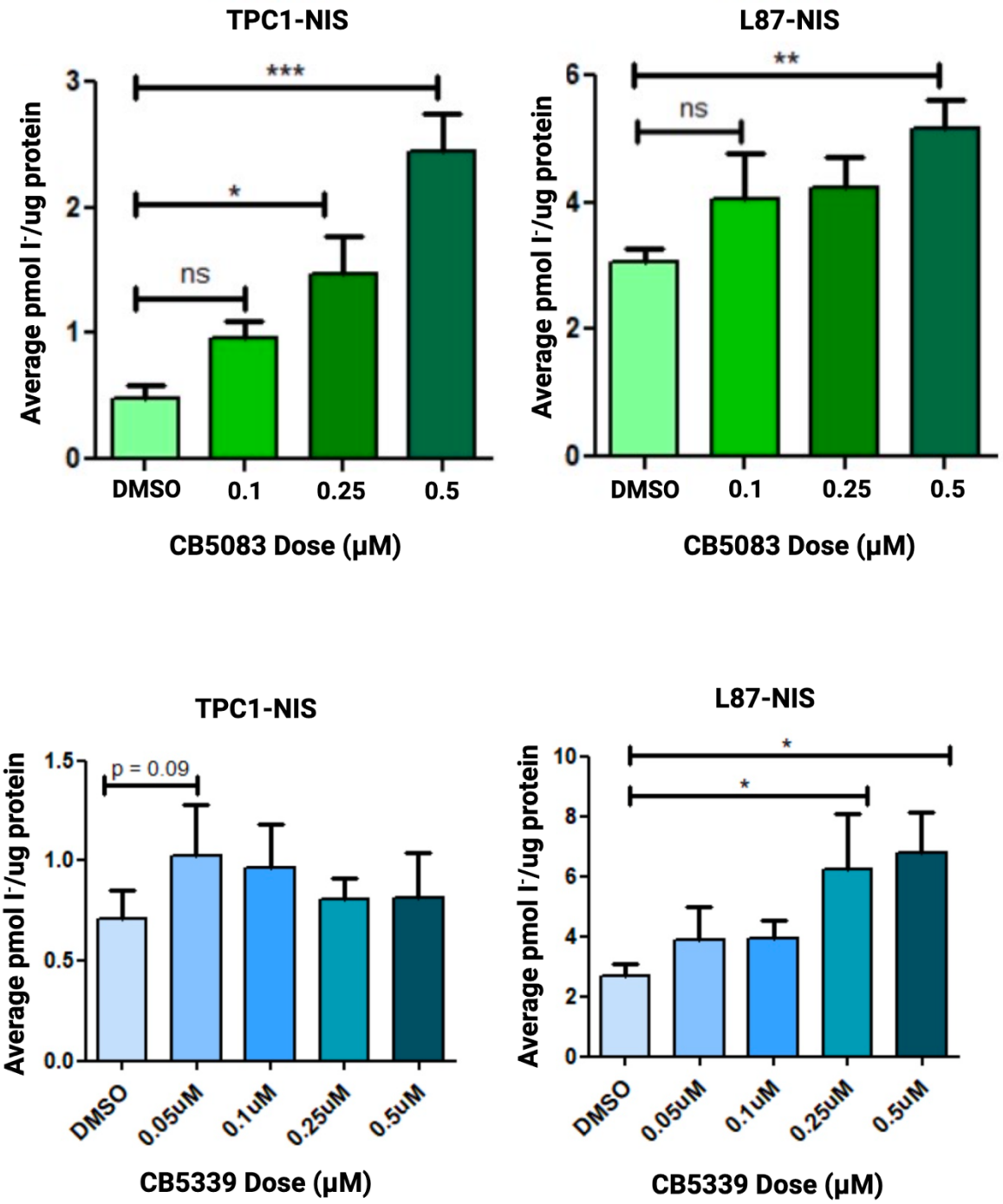


Figure 5. 1 The VCP inhibitors CB-5083 and CB-5339 increase radioiodide uptake in TPC1-NIS thyroid cells and L87-NIS cells. *(adapted from the McCabe group unpublished data).*

This chapter explored the effect of CB-5803 and CB-5339 on radioiodide uptake in breast cancer cells, investigating whether inhibiting VCP function can enhance NIS

translocation to the plasma membrane and improve the therapeutic potential of radioiodine treatment in breast cancer.

5.1.2 Materials and Methods

5.1.2.1 Cell Culture

Breast cancer cell lines (AU565, SUM-52, ZR751) were cultured in the RPMI-1640 medium (Life Technologies), whereas SKBR3 breast cancer cells were grown in McCoy's 5A medium (Gibco). All media were enriched with 10 % fetal bovine serum (FBS), penicillin (10^5 U/l), and streptomycin (100 mg/l). The cell lines were incubated at 37°C with 5 % CO_2 in a humidified incubator. These cell lines were sourced from the American Type Culture Collection (ATCC).

5.1.2.2 Drug Treatments

CB-5083 was sourced from Cayman Chemical (Catalog#19311), and Cleave Therapeutics generously provided CB-5339. Both agents were dissolved in DMSO to create a stock solution of 10mM. On treatment days, these stock solutions were further diluted in RPMI cell culture medium to achieve a working concentration of 10 μM, and cells were treated at doses of 0.05, 0.1, 0.25, 0.5, 0.75 and 1.0 μM. DMSO was used as vehicle control and was adjusted to match all dosing levels.

5.1.2.3 Radioiodide Uptake Assay

For each experimental condition, there were six replicates, with two wells pre-treated with sodium perchlorate for one hour before the introduction of radioiodide. Radioactivity levels ranging from 1×10^5 to 1.2×10^5 counts per minute of ^{125}I were added to each well and incubated at 37°C for one hour. Post-incubation, cells were washed with cold HBSS and lysed using a 2 % SDS buffer. The radioactivity in the lysates was quantified using a gamma counter, and protein concentrations were determined through a BCA assay. The complete methodology for the radioiodide uptake assay is detailed in Section 2.7. Statistical analyses were conducted on data from at least three independent experiments.

5.1.2.4 Western Blot

Western blot analysis was as outlined in Section 2.6.3. TPC1-NIS extracts acted as the positive control for this assay. Membranes were incubated with antibodies at 4°C overnight, followed by detection using a chemiluminescent substrate and x-ray film. The specific antibodies utilised were NIS, VCP and β-actin, with further details provided in Section 2.6.

5.1.2.5 Statistical Analyses

Statistical analyses were performed using GraphPad Prism (Version 10.2.3) and Microsoft Excel. Results were derived from biological replicates performed at least in triplicate. Radioiodide uptake assays assessing the dose response to CB-5083 and

CB-5339 in breast cancer cells were analysed using ANOVA, followed by Dunnett's post-test, with the DMSO-treated condition as the reference control.

5.1.3 Results

5.1.3.1 The VCP Inhibitor CB-5083 Does Not Modify Radioiodide-Uptake in Breast Cancer Cells

The effect of the VCP inhibitor CB-5083 on radioiodide uptake and NIS expression was evaluated in four breast cancer cell lines: AU565, SKBR3, SUM-52 and ZR-75-1. Various concentrations of CB-5083 (ranging from 0.05 μM to 1.0 μM) were tested for their impact on iodide uptake. In control experiments of every condition, cells were treated with 100 μM sodium perchlorate ($NaClO_4$) for 1 hour before the assay to inhibit NIS-mediated radioiodide uptake and, therefore, gauge the specificity of any impact on NIS function. Notably, at a dose of 1.0 μM, CB-5083 was cytotoxic, reducing cell viability by approximately 50 %, which precluded the testing of higher doses.

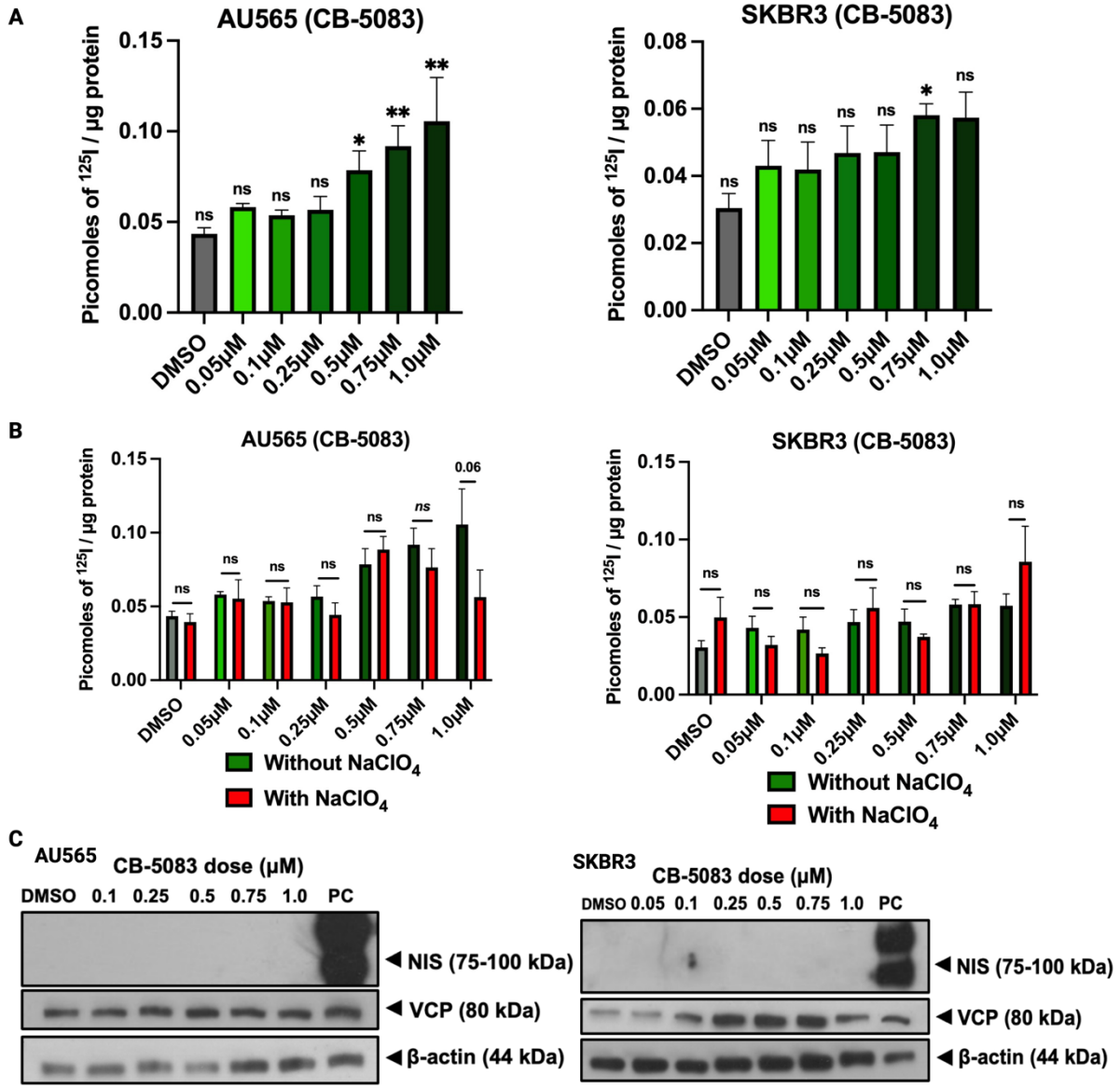


Figure 5. 2 Effect of the VCP inhibitor CB-5083 on radioiodide uptake and protein levels of NIS in breast cancer lines. *(A) Radioiodide uptake in AU565 (left) and SKBR3 (right) cells after 24 hours of CB-5083 treatment at increasing concentrations (0.05-1.0 µM). Statistical significance is indicated for dose-dependent changes in uptake compared to DMSO-treated controls. (B) Radioiodide uptake in AU565 (left) and SKBR3 (right) cells with and without the NIS inhibitor sodium perchlorate ($NaClO_4$), demonstrating specificity of NIS-mediated uptake. (C) Western blot analysis of NIS and VCP protein expression in AU565 (left) and SKBR3 (right) cells after 24 hours of CB-5083 treatment at increasing concentrations. β-actin is the loading control, and TPC1-NIS protein lysate is the positive control (PC). One-way ANOVA analysed data across n = 3 to n = 6 experimental repeats. Statistical significance is denoted as ns (not significant), *P < 0.05, **P < 0.01.*

In the AU565 cell line (Figure 5.2 left), CB-5083 treatment resulted in a dose-dependent increase in iodide uptake. Significant increases were observed at concentrations of 0.5 μM ($P < 0.05$), 0.75 μM ($P < 0.01$) and 1.0 μM ($P < 0.01$) compared to vehicle control. However, when compared with the $NaClO_4$-treated control group, these differences were not statistically significant at any dose. For the SKBR3 cells (Figure 5.2 right), a modest increase in iodide uptake was noted at 0.75 μM ($P < 0.05$). Nonetheless, no significant difference was observed between the CB-5083 treated cells with and without $NaClO_4$ groups across all concentrations, indicating that any increases in uptake are not due to NIS-specific mechanisms CB-5083 on induced uptake.

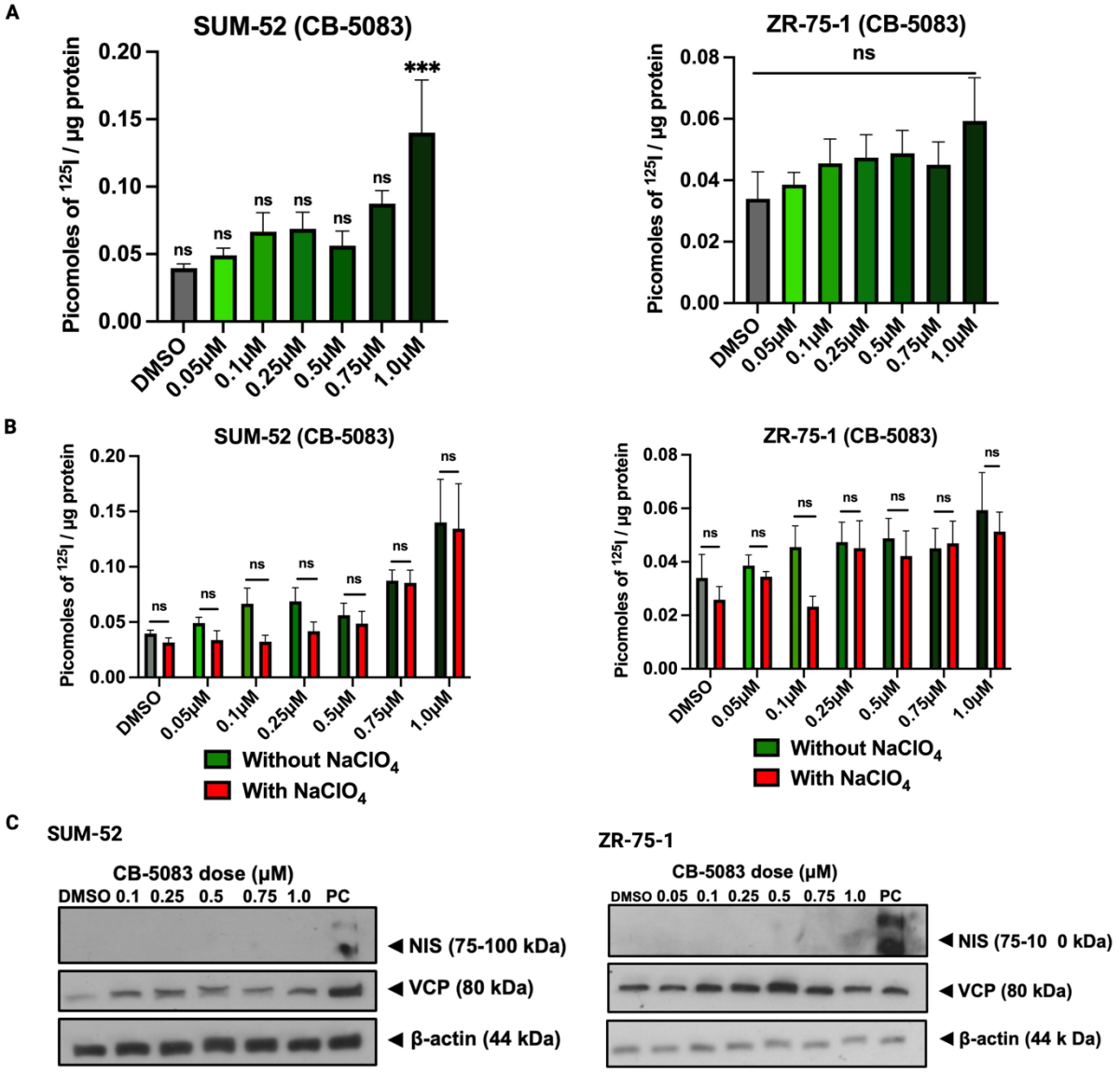


Figure 5. 3 Effect of the VCP inhibitor CB-5083 on radioiodide uptake and NIS and VCP protein levels in SUM-52 (left), ZR-75-1 (right) cells after 24 hours of treatment. *(A) Radioiodide uptake shows a dose-dependent increase in SUM-52 cells but no significant changes in ZR-75-1 cells. (B) Uptake specificity is confirmed by $NaClO_4$. (C) Western blot analysis shows NIS and VCP protein levels after CB-5083 treatment, with β-actin as a loading control and TPC1-NIS lysate as the positive control (PC). Statistical analysis (one-way ANOVA, n = 3–6) indicates ns (not significant), ***P < 0.001.*

In the SUM-52 cell line (Figure 5.3 left), a significant increase in iodide uptake was seen at 1.0 μM ($P < 0.001$). Despite this, no significant differences were observed when compared with the $NaClO_4$-treated cells at this concentration. The ZR-75-1 cells

(Figure 5.3 right) exhibited no significant changes in radioiodide uptake across all tested doses of CB-5083. Furthermore, there were no significant differences between the CB-5083 treated with and without $NaClO_4$ groups.

Overall, the data indicated that CB-5083, a VCP inhibitor, can increase radioiodide uptake in particular breast cancer cell lines at higher concentrations. However, this increase is abolished in the presence of $NaClO_4$, suggesting that the observed increase in radioiodide uptake at higher doses of CB-5083 is not due to increased NIS function. Western blot analysis further supports the radioiodide uptake results, with the NIS band being very low to undetectable in the assay and indicating minimal NIS protein levels across all four breast cancer cell lines.

5.1.3.2 The VCP Inhibitor CB-5339 Does Not Affect Radioiodide Uptake in Breast Cancer Cell Lines

CB-5339 is a second-generation VCP inhibitor based on the structure of CB-5083. Its effect on radioiodide uptake was assessed in the same breast cancer cell lines as CB-5083: AU565, SKBR3, SUM-52, and ZR-75-1. Various doses of CB-5339 (ranging from 0.05 to 0.75 μM) were tested. In AU565 Cells (Figure 5.4A), CB-5339 treatment resulted in a significant increase in radioiodide uptake at 0.5 μM ($P < 0.001$). There were no statistical differences when comparing the CB-5339 treated cells with and without NaClO4, suggesting that $NaClO_4$ eliminated the CB-5339-induced uptake — further indicating that this apparent increase is not NIS-mediated. SKBR3 cells (Figure 5.4B) exhibited a significant enhancement in iodide uptake at 0.75 μM ($P < 0.01$).

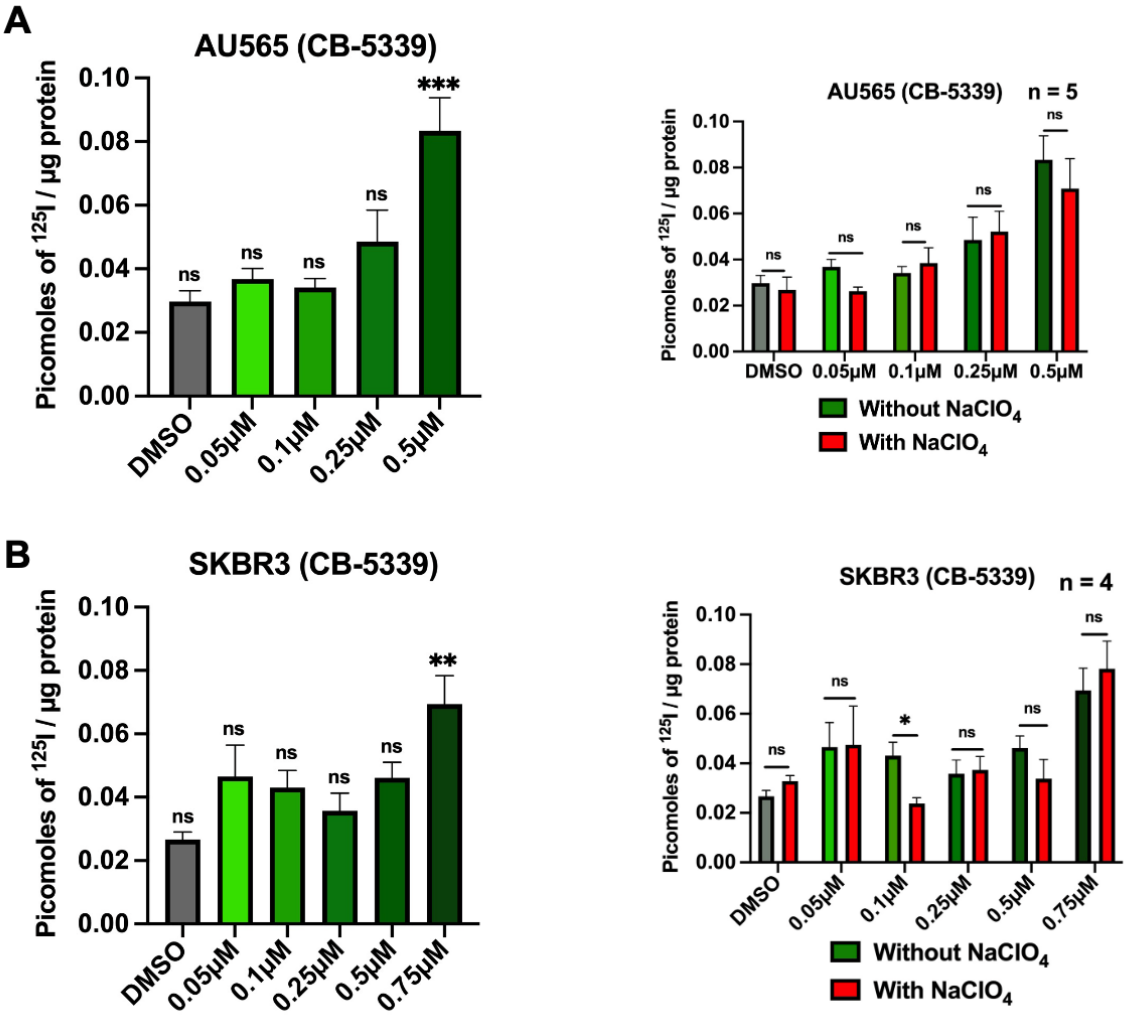


Figure 5. 4 Effect of the VCP inhibitor CB-5339 on radioiodide uptake in breast cancer lines after treatment for 24 hours. *(A, left) AU565 cells show a significant dose-dependent increase in radioiodide uptake at 0.5 µM CB-5339 (P < 0.001). (A, right) $NaClO_4$ inhibition assays demonstrate no statistical differences between treated cells with or without $NaClO_4$. (B, left) In SKBR3 cells, a significant enhancement in radioiodide uptake is observed at 0.75 µM CB-5339 (P < 0.01). (B, right) $NaClO_4$ inhibition assays confirms no statistical differences between treated cells with or without $NaClO_4$. Data are presented as mean ± SEM, with n = 3 to 5 biological replicates. Statistical analysis was performed using one-way ANOVA, with significance indicated as ns (not significant), **P < 0.01, ***P < 0.001.*

However, once again, no significant difference was observed between with and without $NaClO_4$ at this concentration. A considerable increase was observed at the 0.5 µM concentration in the SUM-52 cell line (Figure 5.5 A). Despite this, there were no

differences in iodide uptake between the $NaClO_4$ treated or untreated groups. For ZR-75-1 cells (Figure 5.5 B), no significant changes in radioiodide uptake were observed across all tested doses of CB-5339.

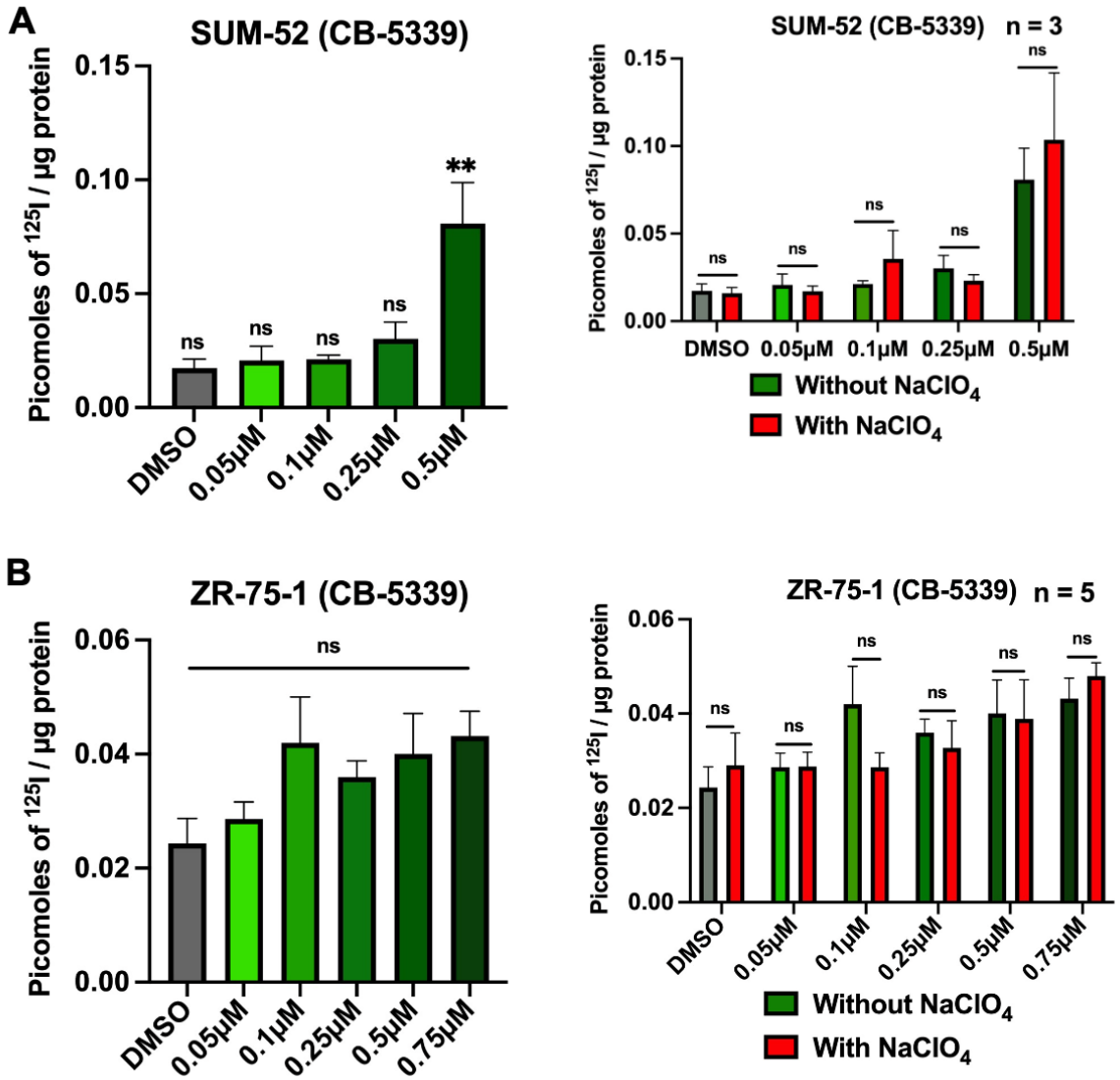


Figure 5. 5 Effect of the second-generation VCP inhibitor CB-5339 on radioiodide uptake in SUM-52 and ZR-75-1 breast cancer cell lines after 24 hours of treatment. *(A, left) In SUM-52 cells, CB-5339 treatment significantly increased radioiodide uptake at 0.5 µM (P < 0.01). (A, right) $NaClO_4$ inhibition assays showed no statistical differences between treated cells with or without $NaClO_4$, indicating the increase was not NIS-mediated. (B, left) ZR-75-1 cells exhibited no significant increase in radioiodide uptake across all tested doses of CB-5339. (B, right) $NaClO_4$ inhibition assays confirmed no differences between treated cells with or without $NaClO_4$. Data are presented as mean ± SEM, with n = 3 to 5 biological replicates. Statistical analysis was performed using one-way ANOVA: ns (not significant), **P < 0.01.*

The data (Figure 5.4 and Figure 5.5) suggest that CB-5339 can potentially modify radioiodide uptake in breast cancer cell lines; however, after comparing the $NaClO_4$ control group, this increase is unlikely to involve direct modulation of NIS function.

5.1.4 Discussion

This first section of Chapter 5 evaluated the impact of the FDA-approved VCP inhibitors CB-5083 and CB-5339 on radioiodide uptake in breast cancer cell lines. While these inhibitors demonstrated potential in enhancing NIS function and radioiodide uptake in thyroid cancer models *in vitro*, the results indicate limited efficacy in breast cancer cell lines due to inherently low NIS expression levels (Figure 5.2 and Figure 5.3). Even though CB-5083 treatment resulted in a dose-dependent increase in iodide uptake in AU565, SKBR3 and SUM-52 cell lines, these increases were not eliminated in the presence of $NaClO_4$, suggesting that the observed effects were not mediated through the increase of NIS function. Similarly, CB-5339 significantly enhanced iodide uptake in AU565, SKBR3 and SUM-52 cell lines, yet these effects were also not negated by $NaClO_4$, indicating a non-NIS mediated mechanism. Western blot analysis corroborated radioiodide uptake results, showing low to undetectable levels of NIS protein across all tested breast cancer cell lines in different conditions and emphasising the limitation posed by low baseline NIS expression even when VCP inhibitors act via inhibiting proteasomal degradation.

The increase in radioiodide uptake observed in the presence of CB-5083 and CB-5339, despite the lack of NIS involvement, raises the hypothesis that other iodide transporters may be contributing to this effect. In particular, the roles of SMCT (sodium-

coupled monocarboxylate transporter) and pendrin in iodide transporter should be considered (Gupta et al., 2006; Rodriguez et al., 2002; Scott et al., 1999; Thangaraju et al., 2006). For example, studies have demonstrated pendrin expression in MCF7 breast cancer cells, and its involvement in iodide transport has been demonstrated. In these cells, radioiodide uptake was reduced by the inhibitor DIDS, but not by sodium perchlorate or ouabain, suggesting that pendrin, rather than NIS, was responsible for the iodide transport observed (García-Solís et al., 2005; Rillema et al., 2003). However, this is a hypothesis that requires further investigation to be proven.

The low endogenous NIS expression in breast cancer cells suggests that strategies focusing solely on the post-translation process, such as inhibiting NIS degradation, may be insufficient. Future research should explore alternative approaches to upregulate NIS expression, such as transcriptional activators and combinatorial treatments that simultaneously enhance NIS expression at the plasma membrane and inhibit its degradation. Additionally, alternative approaches might be explored to manipulate the subcellular localisation of NIS. This shift in focus could lead to more effective treatments and improved outcomes for patients with NIS-expressing breast cancer.

5.2 Inhibiting VCP Function by Modifying the Structure of Clotrimazole to Improve its Solubility and Effectiveness

5.2.1 Introduction

A second strategy to inhibit VCP activity in thyroid cancer cells was next appraised. As mentioned previously, VCP/p97 is crucial in the ER-associated degradation pathway. Importantly, VCP/p97 was found to be essential for NIS protein processing, highlighting its potential as a therapeutic target in radioiodide-refractory thyroid cancer (Fletcher et al., 2020). A study utilising a combined approach of structure-based virtual screening and chemical genomics identified and experimentally validated clotrimazole, an FDA-approved antifungal agent, as an effective and allosterically direct VCP/p97 inhibitor through cell-based and ATPase assays (Segura-Cabrera et al., 2017). Clotrimazole significantly increased radioiodide uptake and NIS protein levels in TPC1-NIS cells, and mouse and human primary thyrocytes. Importantly, no induction of RAI uptake was observed in VCP-ablated TPC1-NIS cells, confirming that the effectiveness of clotrimazole on NIS function is dependent on the presence of VCP (Fletcher et al., 2020). SAHA (suberoylanilide hydroxamic acid) is a known histone deacetylase inhibitor that enhances NIS function in vitro by increasing NIS gene transcription and protein expression, improving iodide uptake in thyroid cancer cells (Hou et al., 2010). In this chapter, SAHA will be employed in the experimental design both as a positive control for assessing NIS functionality and as a means to enhance NIS expression. This dual role of SAHA allows for a more sensitive evaluation of treatments that target the post-translational activity of NIS, providing a robust framework for appraising the efficacy of novel VCP inhibitors.

5.2.1.1 Development of Clotrimazole Analogues and the Final Compound GB002

Despite its efficacy and safety profile as an FDA-approved topical agent, clotrimazole is poorly water-soluble with high partition coefficients (logP), limiting its bioavailability

for *in vivo* applications. The logP value measures the lipophilicity of the compound by indicating its distribution between hydrophobic (lipid) and hydrophilic (water) environments. It affects the absorption and bioavailability of a drug, with an optimal logP value below 3 for orally administrated drugs (Bergström et al., 2018). An *in vivo* study with clotrimazole showed no significant change in thyroidal iodide uptake in wild-type mice, likely due to poor bioavailability and insufficient accumulation in the thyroid (McCabe group, unpublished data). Due to the limited bioavailability of clotrimazole, a computational iterative drug design approach was employed to develop 21 analogues (C1-C21) with improved physicochemical properties, particularly aqueous solubility. Dr Giovanni Bottegoni (University of Birmingham, UK) utilised UCSG Chimera to model the binding of clotrimazole to an allosteric site on VCP, based on the cryo-EM resolved structure of VCP complexed with the allosteric inhibitor UPCDC30245. The model was optimised by comparing the binding conformations of clotrimazole and UPCDC30245, focusing on a common basic nitrogen atom that forms hydrogen bonds with Glu-498 within the D1-D2 linker of VCP. The modified compounds were synthesised through the alkylation of imidazole or related heterocycles with functionalised triaryl and benzyl substituents, particularly the debulking of the two aryl groups in clotrimazole to enhance solubility and improve logP values.

Through three iterations of modifications to clotrimazole's structure, the aim was to improve compound bioavailability and enhance NIS activity (McCabe group, unpublished data). In the first iteration, changes were made to the chloro-substituted aryl ring (R1) to assess its impact on VCP binding and logP values. The second iteration included modifications to the imidazole ring (R2) and the removal of aryl substituents (R3) to reduce logP values further and improve water solubility. Notably,

compounds 11 and 12 showed significant increases in iodide uptake when co-treated with SAHA in 8505C-NIS cells (McCabe group, unpublished data). The third iteration combined these successful modifications, leading to the development of compound-17, demonstrating significant iodide uptake in TPC1-NIS cells and human primary thyrocytes, indicating its potential efficacy (Figure 5.6).

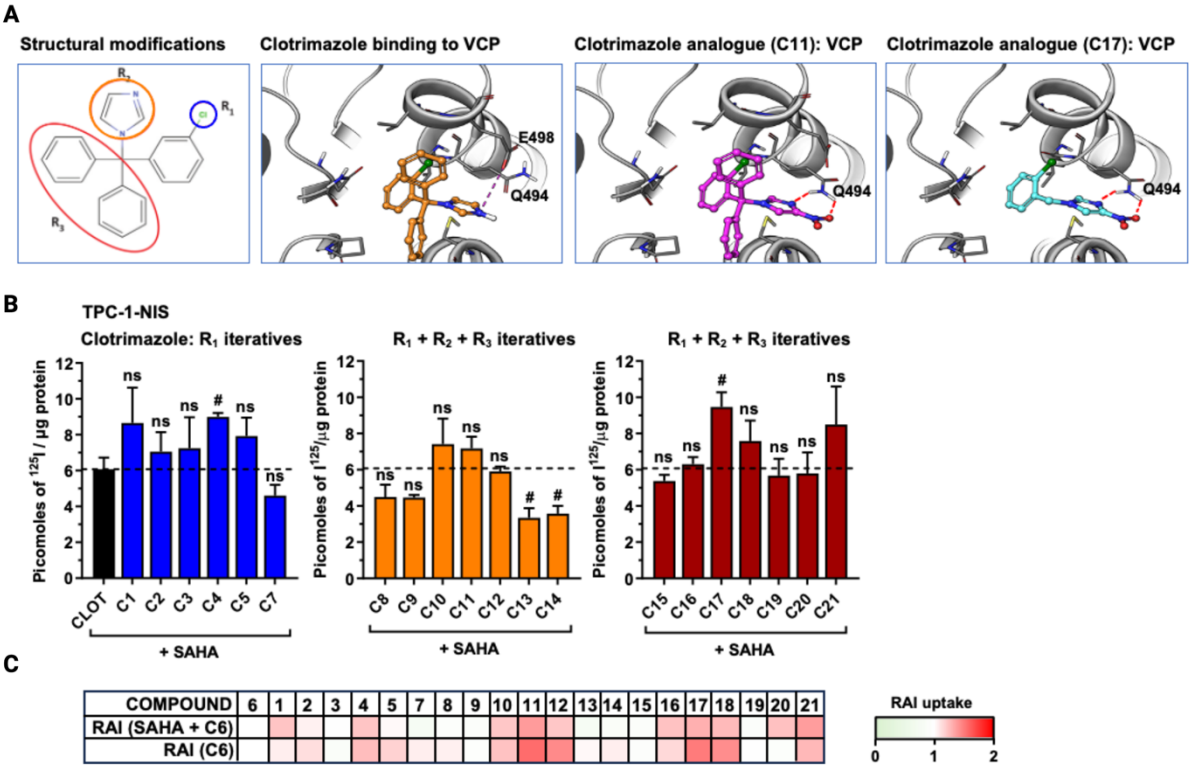


Figure 5. 6 Modification of clotrimazole and impact on RAI uptake. *(A) Modelling the binding of clotrimazole, compound C11 and compound C17 to VCP. Dashed lines show predicted hydrogen bonds with residues Q494 and E498. (Left) Chemical structure of clotrimazole highlighting modifications at the chloro-substituted aryl ring (R1), imidazole ring (R2) and two aryl substituent groups (R3). (B) RAI uptake in TPC1-NIS cells treated with 21 compounds (C1-C21; 12 hours) in combination with SAHA. The dashed line indicates normalised RAI uptake with CLOT + SAHA. (C) Heat map of mean RAI uptake in TPC1-NIS and 8505C-NIS cells treated with 21 compounds versus combination with SAHA. Notably, compound C6 in the heat map represents clotrimazole. Data are mean± SEM, analysed by one-way ANOVA with Dunnett's post hoc test (ns, not significant; *P<0.05, **P<0.01; ***P<0.001), or unpaired two-tailed t-test (#P<0.05). Figure adapted from McCabe group unpublished data.*

Computational modelling further refined compound-17 by suggesting adding a fluoroindole group designed to enhance interactions within the VCP pocket seen with the known VCP inhibitor UPCDC30425. This led to the design of GB002, which has a predicted logP value of 2.80 (Figure 5.7).

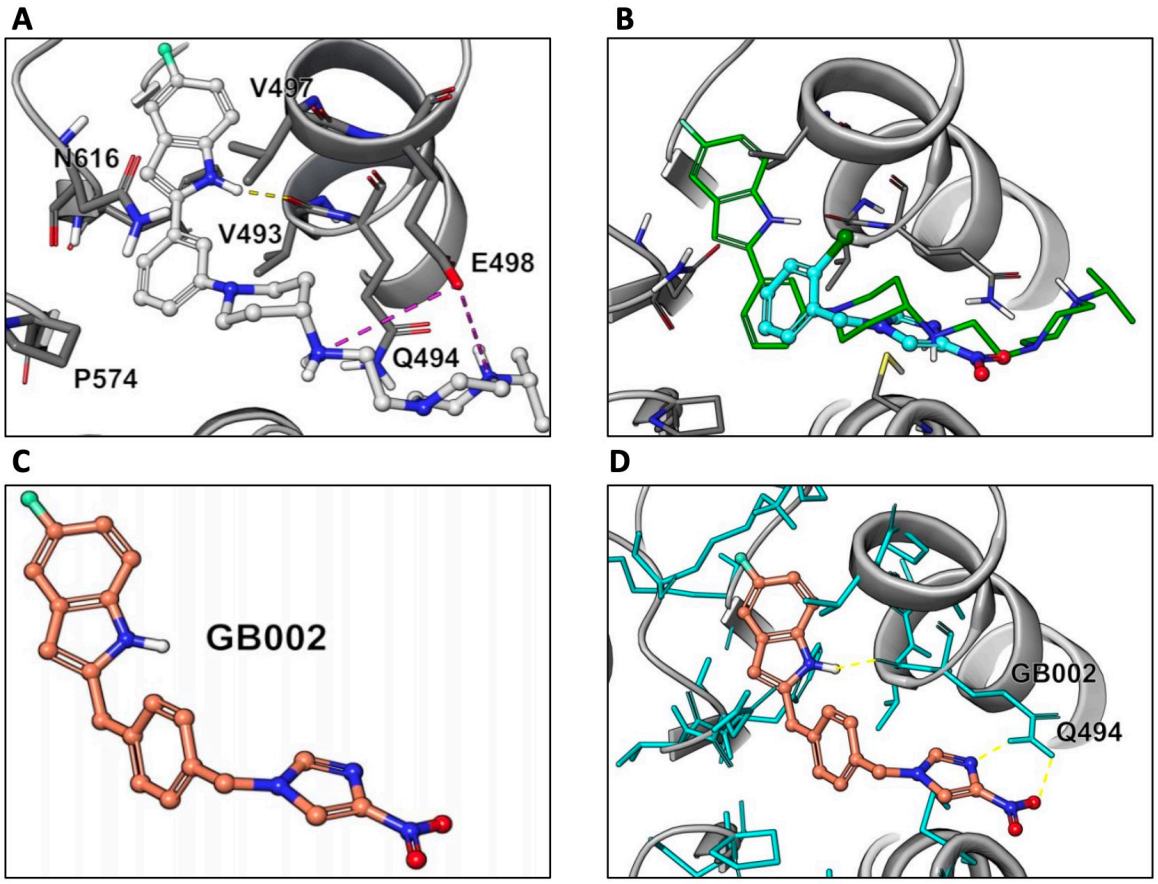


Figure 5. 7 Redesign of compound-17 into GB002 using an overlapping model with the VCP inhibitor UPCDC30425. *(A) UPCDC30425 in the VCP allosteric binding pocket interacts with E498 via a basic nitrogen atom (Banerjee et al., 2016). The piperazine tail extends further than in compound-17, as shown by the overlap in (B). (C) and (D) show that GB002, a modified compound-17, mimics the piperazine tail to capture additional interactions with VCP residues. Blue ion=Nitrogen; Red ion=Oxygen; Green ion= Fluorine; Yellow dashes=hydrogen bonds; Pink dashes= predicted hydrogen bonds between compound-17 and VCP, sterically excluded in UPCDC30425 and VCP. Modelling and images provided by Dr Giovanni Bottegoni, University of Birmingham.*

5.2.1.2 Modification to the Structure of NMS873

The specific VCP inhibitors CB-5083 and CB-5339 (detailed in 4.1.1) showed promising results in inducing NIS functions in thyroid cancer cells and human primary thyrocytes. However, CB-5083 did not induce thyroidal uptake of ^{99m}Tc in wild-type BALB/c mice (McCabe group, unpublished data). Several other types of VCP inhibitors have been reported as additional choices for cancer therapy. Interestingly, the allosteric inhibitor Nerviano Medical Sciences-873 (NMS-873), which is a potent and selective VCP inhibitor that allosterically binds to a site within the D2 ATPase domain, showed good activity for both specific VCP inhibition and anti-proliferation and thus could be considered a promising lead compound for further new VCP inhibitor development (S. Li et al., 2022; Wang et al., 2020).

Previous studies have shown that NMS-873 can modulate NIS protein expression and enhance iodide uptake in the TPC1-NIS thyroid cancer cell line, with significant effects observed at a concentration of 5 μM following 24 hours of treatment. However, NMS-873, like clotrimazole and UPCDC30425, shows a logP value indicative of poor bioavailability. The logP values of established VCP inhibitors are presented in Figure 5.8. An optimal logP value below 3.0 is necessary for orally administered drugs to achieve over 80 % bioavailability, which the majority of VCP inhibitors fail to meet.

Drug	Predicted logP
Clotrimazole	5
Ebastine	7.2
Astemizole	6
CB-5803	3.1
CB-5339	4.1
UPCDC30425	4.7
NMS-873	4.9
Eeyarestatin I	4.2
DBeQ	5.3

Figure 5. 8 Predicted logP values of various VCP inhibitors. *LogP values were obtained from PubChem and computed using the XLogP3 3.0 algorithm, based on the October 14, 2021, release, except for Eeyarestatin I, which was calculated using the May 7, 2021, release.*

More recently, a CryoEM structure was published that revealed – for the first time – the docking of NMS-873 into the VCP protein (Liu et al., 2022). Interestingly, NMS-873 interacts in a region similar to UPCDC30245 (Figure 5.9). This significant finding prompted us to redesign potential drugs targeting this structure. We hypothesised that, based on the chemical structure of NMS-873, it is possible to develop modified NMS-873 compounds that function with improved bioavailability, given NMS-873's high logP score. This chapter therefore appraised a number of novel compounds with the potential to inhibit VCP, with the aim of identifying new pharmacological strategies of improving radioiodide uptake *in vitro* and *in vivo*.

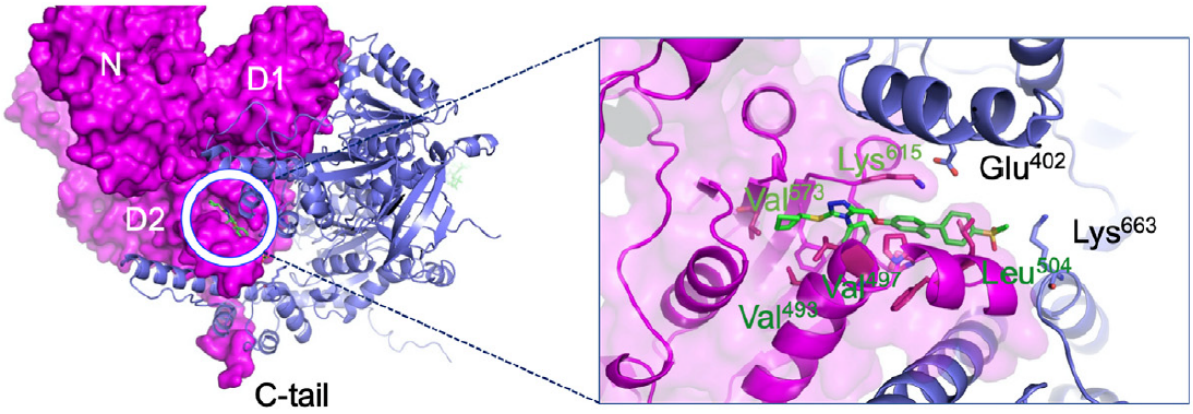


Figure 5. 9 CryoEM of NMS873 docking to VCP. *NMS-873 in its bound form with VCP, illustrating its precise interaction at the D1/D2 interface. The binding of NMS-873 at this interface is characterised by critical interactions with residues such as Glu-402, Val 493, Val 497, Lys-504 and Val-573. Figure adapted from (Liu et al., 2022).*

5.2.2 Materials and Methods

5.2.2.1 Cell Culture

Thyroid cancer cell lines (TPC-1, 8505C, TPC1-NIS and 8505C-NIS) and the L87-NIS mesenchymal stem cell line were cultured as described in Chapter 2.1

5.2.2.2 Drug Treatment and Radioiodide Uptake Assay

GB002 was provided by Dr Holly Adcock (University of Birmingham, UK) and dissolved in DMSO to create a 10 mM stock solution stored at -20°C. NMS-873-derived compounds (C22-C25) were synthesised by SIA Enamine (Latvia) and dissolved in DMSO to form 10 mM stock solutions. Before cell treatment, all drugs were diluted 1:100 in the RPMI-1640 medium. TPC1-NIS, 8505C-NIS and L87-NIS cells were seeded as previously described. Upon reaching approximately 80 % confluence after

24 hours, cells were treated with varying concentrations of GB002 (0.05 μM, 0.1 μM, 0.25 μM, 0.5 μM, 1.0 μM, 2.0 μM, 5.0 μM) or a DMSO control. Following a 24-hour incubation, radioiodide uptake assays were performed, as detailed in Section 2.7. The DMSO vehicle control was standardised across all treatment doses. Four compounds (C22-C25) were tested as single-agent treatments or combined with 2.5 μM SAHA for 24 hours. Following treatment, radioiodide uptake assays were performed.

5.2.2.3 Drugs in Silico Modelling

Acting in collaboration with our research group, Dr Giovanni Bottegoni (University of Birmingham, UK) employed the UCSF Chimera Program to model the predicted binding of both clotrimazole and NMS-873-derived compounds to allosteric sites on VCP. Using 3D coordinates from the cryo-EM resolved structures of VCP in complex with allosteric inhibitors UPCDC30245 and NMS-873, accessed via the Protein Data Bank, the models were refined through structure comparisons with other VCP-compounds, confirming the positioning of critical functional groups within the VCP binding pocket (Pettersen et al., 2004; Plantinga et al., 2016). For clotrimazole, the optimised model highlighted a common basic nitrogen atom shared with UPCDC30245, forming hydrogen bonds with Glu-498 in the D1-D2 linker region. In UPCDC30245, this nitrogen is part of a piperidine-4-amino group, whereas clotrimazole is part of the imidazole ring structure (Alverez et al., 2015). The cryo-EM structure revealed that NMS-873 molecules were distinctly visible at the D1/D2 interface of the VCP complex. Additionally, NMS-873 binds in a region similar to that of UPCDC30245, indicating a common binding site within the VCP allosteric pocket (Liu et al., 2022).

5.2.2.4 NanoBiT Live Cell Assay

NanoBiT was carried out as described in Chapter 2.9.

5.2.2.5 Statistical Analyses

Unless stated otherwise, all data were derived from triplicate independent biological experiments. Radioiodide uptake assays assessing the dose response for C22-25 in NIS-expressing cells were analysed using ANOVA, followed by Dunnett's post-test. For multiple-group comparisons in the NanoBiT assay, one-way ANOVA was employed, followed by Dunnett's post-hoc test.

5.2.3 Results

5.2.3.1 GB002 Does Not Significantly Improve RAI Uptake *in Vitro*

Clotrimazole has previously been shown to induce NIS-mediated radioiodide uptake at least two-fold *in vitro* (Fletcher et al., 2020). However, its poor bioavailability likely hindered its efficacy *in vivo*. As described above, a new version of clotrimazole with improved bioavailability, designated GB002, was developed. Following 24 hours of GB002 treatment, NIS function was analysed using an RAI uptake assay in three different NIS-expressing cell lines: TPC1-NIS, 8505C-NIS and L87-NIS. Each experimental group was treated with the same concentration of DMSO for the same duration as the control group. Despite the improved bioavailability of GB002, it did not

broadly enhance iodide uptake in these cell lines at the concentrations tested (Figure 5.10).

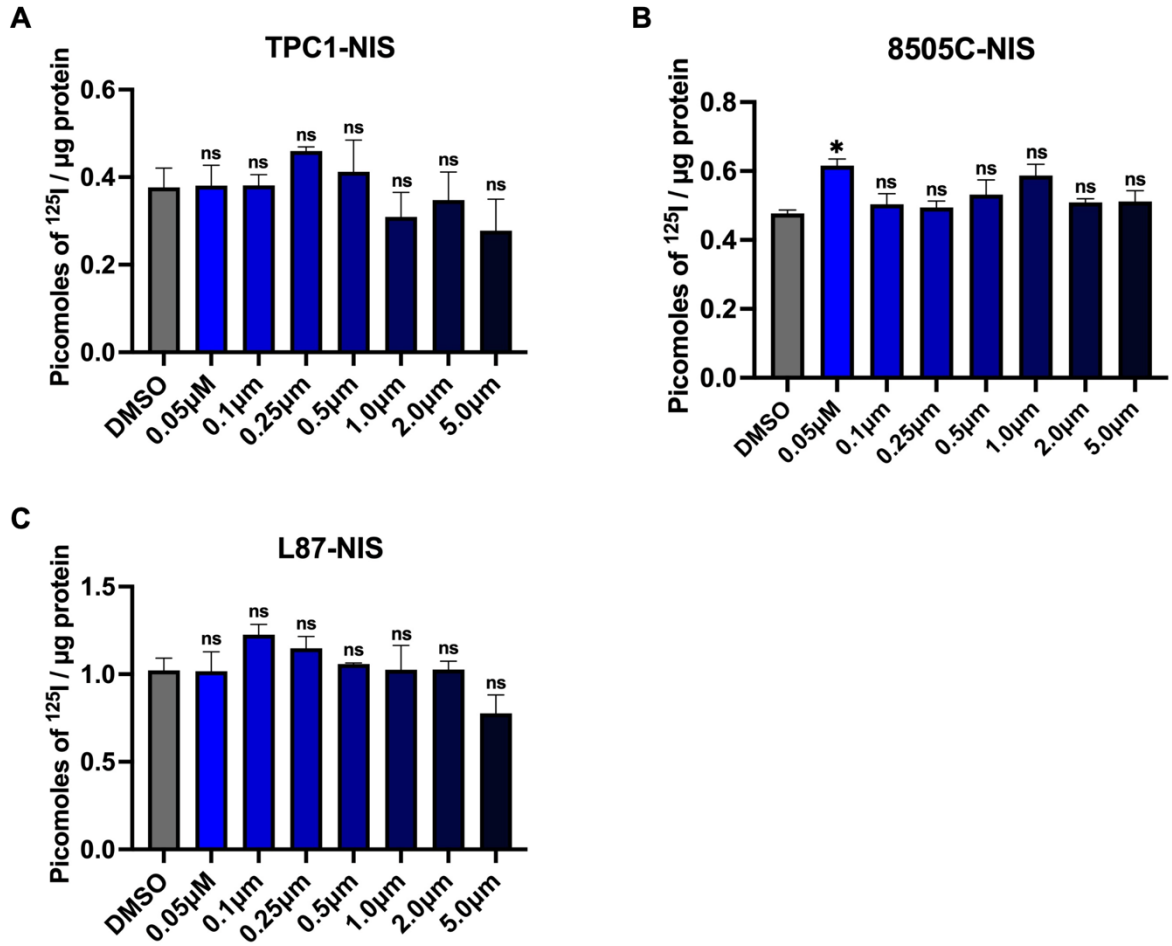


Figure 5. 10 Effects of GB002 on radioiodide uptake in NIS-expressing cell lines. *TPC1-NIS (A), 8505C-NIS (B) and L87-NIS (C) were treated with various doses of GB002, with DMSO serving as the control. N=3 biological replicates.*

Given that GB002 did not induce a marked enhancement in NIS-mediated iodide uptake in any of the three tested cell lines, further analysis via Western blot was deemed unnecessary.

5.2.3.2 Development and Evaluation of Derivation Compounds Based on NMS-873

Recent advancements in cryo-EM analysis guided the design of new derivative compounds based on the structure of NMS-873, aimed at enhancing bioavailability and VCP interaction. These de novo derivatives, Compounds 22-25, are depicted in Figure 5.11.

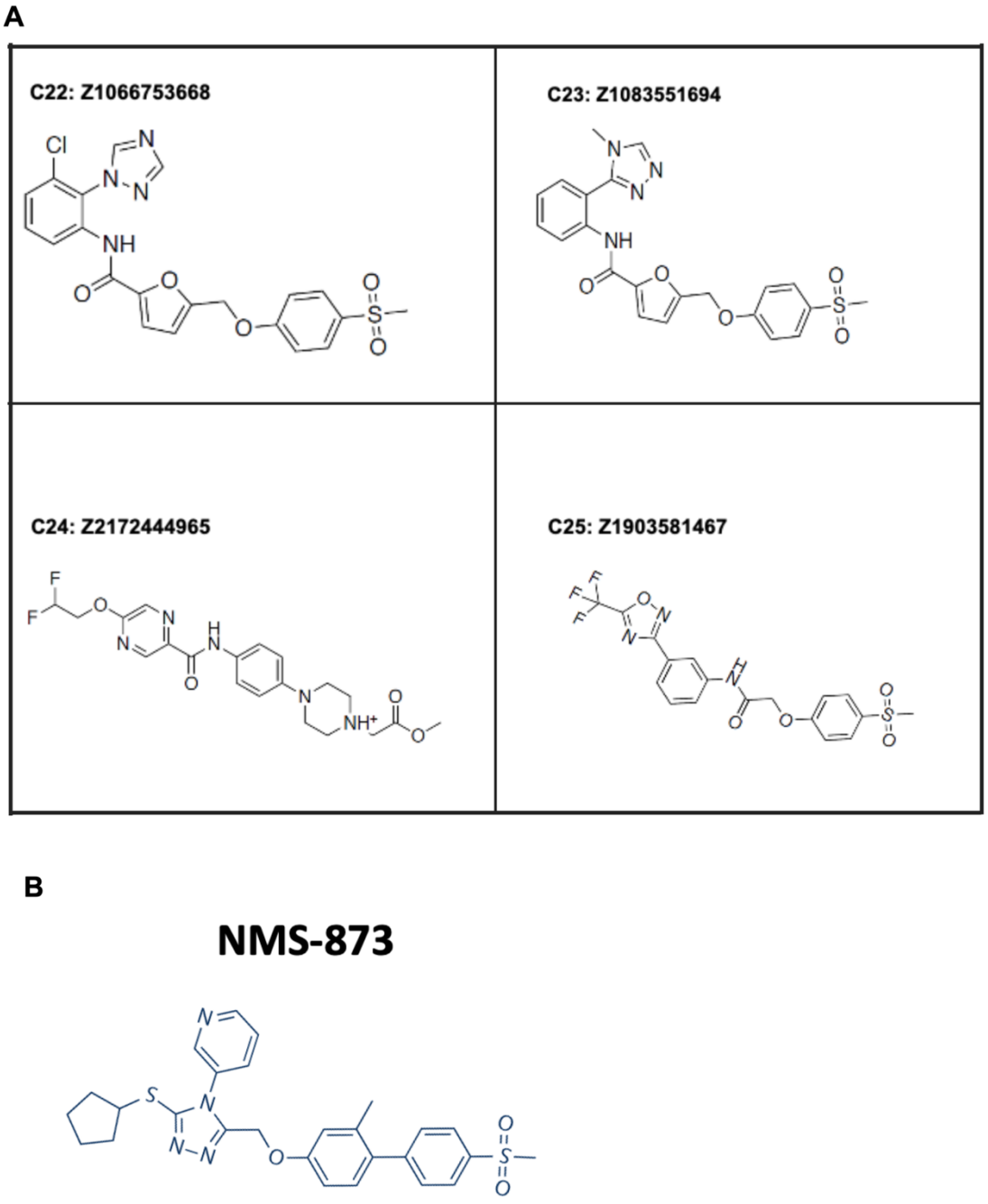


Figure 5. 11 Modification to the structure of NMS-873 resulted in new compounds. *Changes were designed to various parts of the original structure, leading to compounds C22, C23, C24 and C25. These compounds were designed in collaboration with Dr Giovanni Bottegoni (University of Birmingham, UK).*

Fletcher et al. (2020) demonstrated that iodide uptake in stable NIS-expressing thyroid (TPC-1) and breast (MDA-MB-231) cells increased after 24-hour treatment with VCP

inhibitors such as clotrimazole, astemizole and ebastine. Subsequently, we evaluated the effects of novel NMS-873 derivatives on radioiodide uptake in 8505C-NIS, TPC1-NIS and MDA-NIS cell lines. In the initial round of screening, compounds 22 to 25 (C22-25) were tested alone at various doses (0.05 μM, 0.1 μM, 0.25 μM, 0.5 μM, 1.0 μM, 2.5 μM, 5.0 μM) for 24 hours. The inclusion of SAHA (2.5 μM) acts both as a positive control for NIS functionality, but also to boost NIS expression.

The results showed no significant changes in NIS-mediated iodide uptake in TPC1-NIS and MDA-NIS cell lines across the tested doses compared to the DMSO control group (Figure 5.12, Figure 5.14). However, in the 8505C-NIS cell line (Figure 5.13), small improvements were observed with two specific compounds: Compound-22 at 0.5 μM resulted in a 24.3 % increase in iodide uptake compared to the DMSO control ($P < 0.05$). Compound-25 at 0.25 μM resulted in a 33.7 % increase in iodide uptake compared to the control ($P < 0.05$).

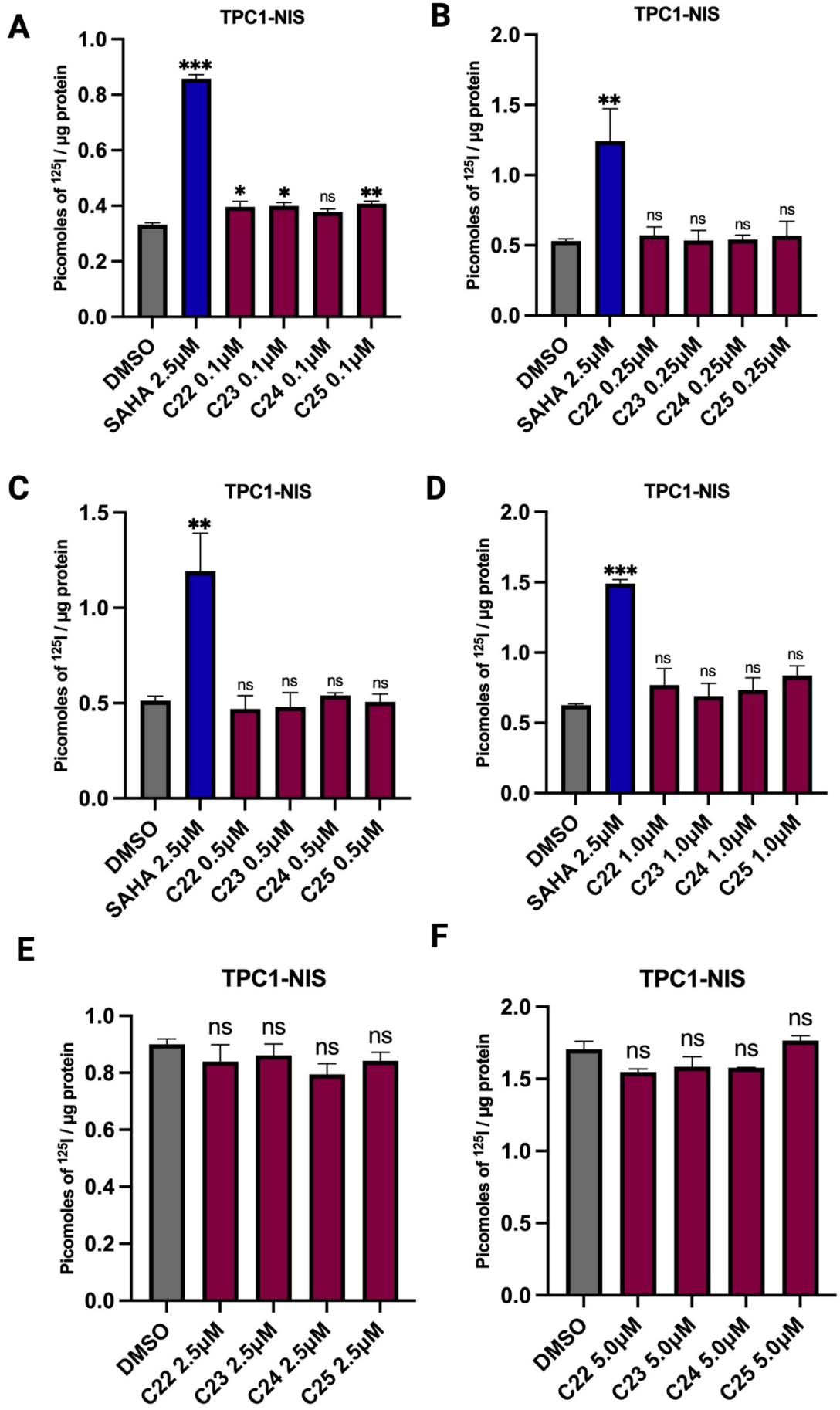

A
TPC1-NIS
Picomoles of 125I / µg protein
1.0
0.8
0.6
0.4
0.2
0.0
***
*
*
ns
**
DMSO
SAHA 2.5µM
C22 0.1µM
C23 0.1µM
C24 0.1µM
C25 0.1µM
B
TPC1-NIS
Picomoles of 125I / µg protein
2.0
1.5
1.0
0.5
0.0
**
ns
ns
ns
ns
DMSO
SAHA 2.5µM
C22 0.25µM
C23 0.25µM
C24 0.25µM
C25 0.25µM
C
TPC1-NIS
Picomoles of 125I / µg protein
1.5
1.0
0.5
0.0
**
ns
ns
ns
ns
DMSO
SAHA 2.5µM
C22 0.5µM
C23 0.5µM
C24 0.5µM
C25 0.5µM
D
TPC1-NIS
Picomoles of 125I / µg protein
2.0
1.5
1.0
0.5
0.0
***
ns
ns
ns
ns
DMSO
SAHA 2.5µM
C22 1.0µM
C23 1.0µM
C24 1.0µM
C25 1.0µM
E
TPC1-NIS
Picomoles of 125I / µg protein
1.0
0.8
0.6
0.4
0.2
0.0
ns
ns
ns
ns
DMSO
C22 2.5µM
C23 2.5µM
C24 2.5µM
C25 2.5µM
F
TPC1-NIS
Picomoles of 125I / µg protein
2.0
1.5
1.0
0.5
0.0
ns
ns
ns
ns
DMSO
C22 5.0µM
C23 5.0µM
C24 5.0µM
C25 5.0µM

Figure 5. 12 Effect of compounds 22–25 and SAHA on radioiodide uptake in TPC1-NIS cells after 24 hours of treatment. *(A–F) Dose-response curves for compounds 22-25 and SAHA, showing radioiodide uptake across tested doses (A: 0.1 μM, B: 0.25 μM, C: 0.5 μM, D: 1.0 μM, E: 2.5 μM, F: 5.0 μM). No significant changes in radioiodide uptake were observed at any dose for compounds 22–25 compared to the DMSO control group, while the SAHA group served as a positive control. Data represent mean ± SEM from n = 3 biological replicates. Statistical analysis was performed using one-way ANOVA, followed by Dunnett's post-test: ns (not significant), **P < 0.01, ***P < 0.001.*

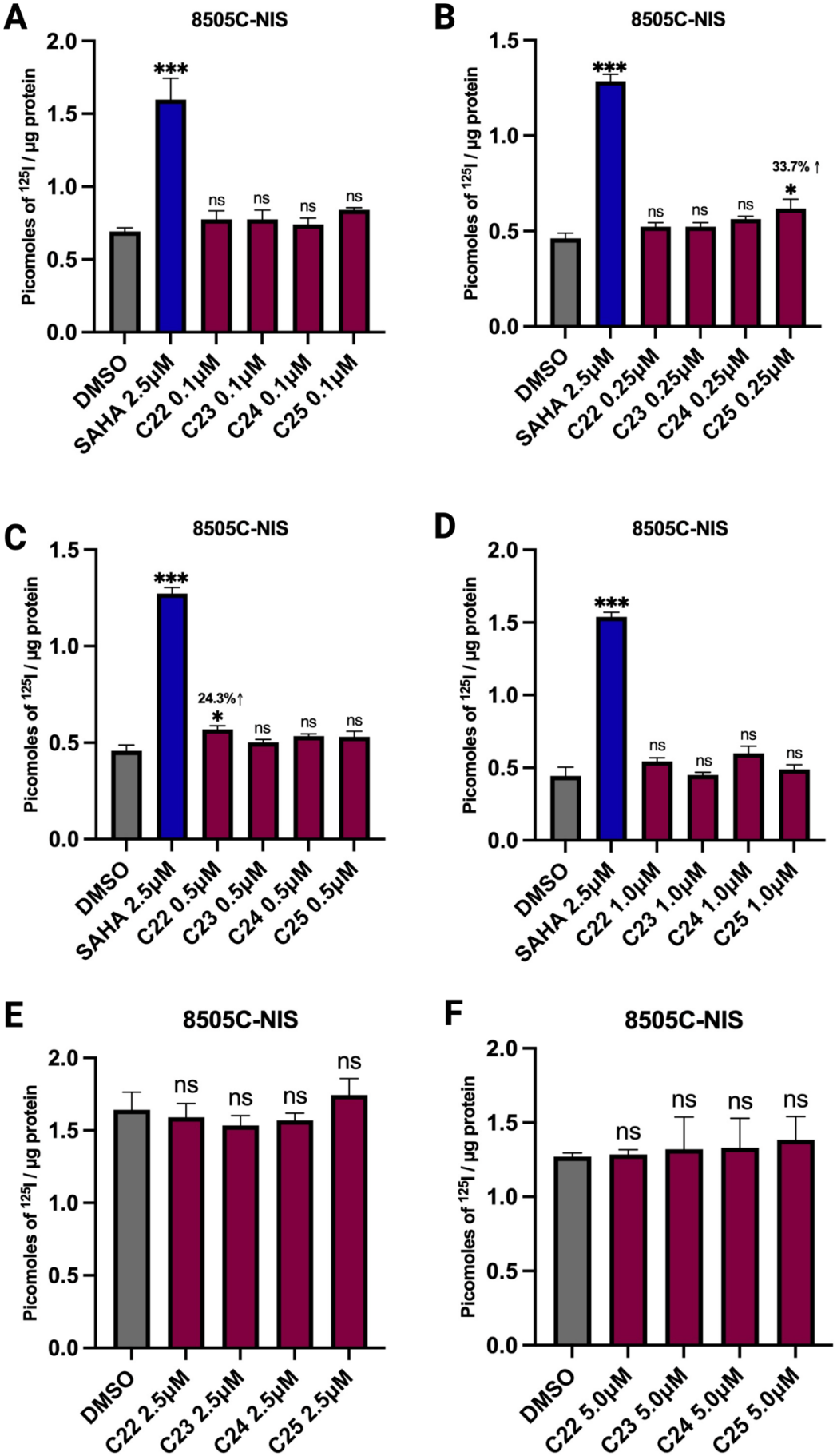

A
8505C-NIS
Picomoles of 125I / µg protein
2.0
1.5
1.0
0.5
0.0
***
ns
ns
ns
ns
DMSO
SAHA 2.5µM
C22 0.1µM
C23 0.1µM
C24 0.1µM
C25 0.1µM
B
8505C-NIS
Picomoles of 125I / µg protein
1.5
1.0
0.5
0.0
***
ns
ns
ns
33.7% ↑
*
DMSO
SAHA 2.5µM
C22 0.25µM
C23 0.25µM
C24 0.25µM
C25 0.25µM
C
8505C-NIS
Picomoles of 125I / µg protein
1.5
1.0
0.5
0.0
***
24.3%↑
*
ns
ns
ns
DMSO
SAHA 2.5µM
C22 0.5µM
C23 0.5µM
C24 0.5µM
C25 0.5µM
D
8505C-NIS
Picomoles of 125I / µg protein
2.0
1.5
1.0
0.5
0.0
***
ns
ns
ns
ns
DMSO
SAHA 2.5µM
C22 1.0µM
C23 1.0µM
C24 1.0µM
C25 1.0µM
E
8505C-NIS
Picomoles of 125I / µg protein
2.0
1.5
1.0
0.5
0.0
ns
ns
ns
ns
DMSO
C22 2.5µM
C23 2.5µM
C24 2.5µM
C25 2.5µM
F
8505C-NIS
Picomoles of 125I / µg protein
2.0
1.5
1.0
0.5
0.0
ns
ns
ns
ns
DMSO
C22 5.0µM
C23 5.0µM
C24 5.0µM
C25 5.0µM

Figure 5. 13 Effect of NMS-873 analogues on iodide uptake in 8505C-NIS cells after 24 hours of treatment. *(A–F) Dose-response curves for NMS-873 analogues across tested doses (A: 0.1 μM, B: 0.25 μM, C: 0.5 μM, D: 1.0 μM, E: 2.5 μM, F: 5.0 μM). No significant changes in iodide uptake were observed at any dose compared to the DMSO control group, while the SAHA group served as a positive control. Data represent mean ± SEM from n = 3 independent experiments. Statistical analysis was performed using one-way ANOVA, followed by Dunnett's post-test: ns (not significant), ***P < 0.001.*

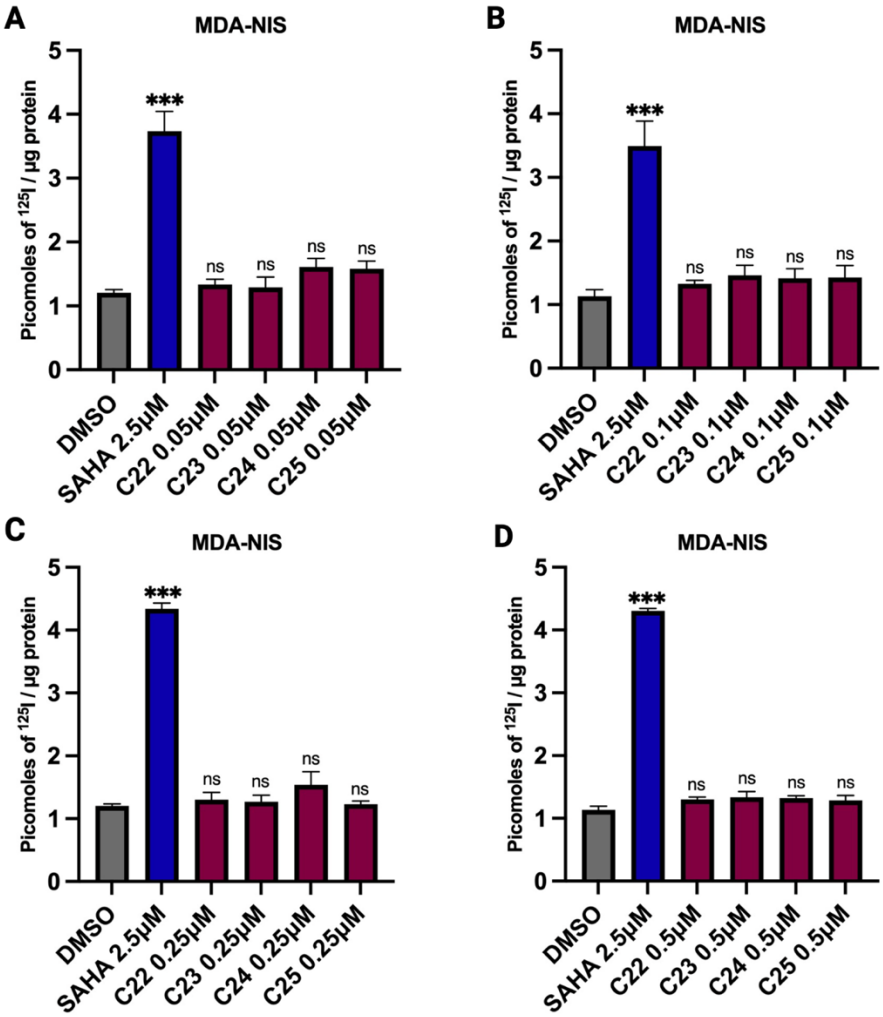


Figure 5. 14 Effect of compounds 22–25 on radioiodide uptake in MDA-NIS cells after 24 hours of treatment. *(A–D) Dose-response analysis for compounds 22, 23, 24, and 25 at increasing concentrations (0.05 μM, 0.1 μM, 0.25 μM, 0.5 μM). No significant changes in radioiodide uptake were observed at any dose for compounds 22–25 compared to the DMSO control group. The SAHA-treated group (2.5 μM) served as a positive control, showing a significant increase in radioiodide uptake. Data represent mean ± SEM from n = 3 biological replicates. Statistical analysis was performed using one-way ANOVA, followed by Dunnett's post-test: ns (not significant), ***P < 0.001.*

Further experiments were conducted to evaluate the combination of compounds 22-25 at a concentration of 0.25 μM with SAHA (2.5 μM) for 24 hours to potentially enhance both NIS expression and function. Each experimental group was treated with the same concentration of SAHA (2.5 μM) alone for the same duration as the control group. The results show that co-treatment with compounds C22-25 did not modify iodide uptake in TPC1-NIS (Figure 5.15 B) and MDA-NIS (Figure 5.15 C) cells compared to the SAHA alone group. The only exception to this was that the 8505C-NIS cell line showed a 29.6 % increase in iodide uptake with C25 co-treatment compared to SAHA alone (Figure 5.15 A).

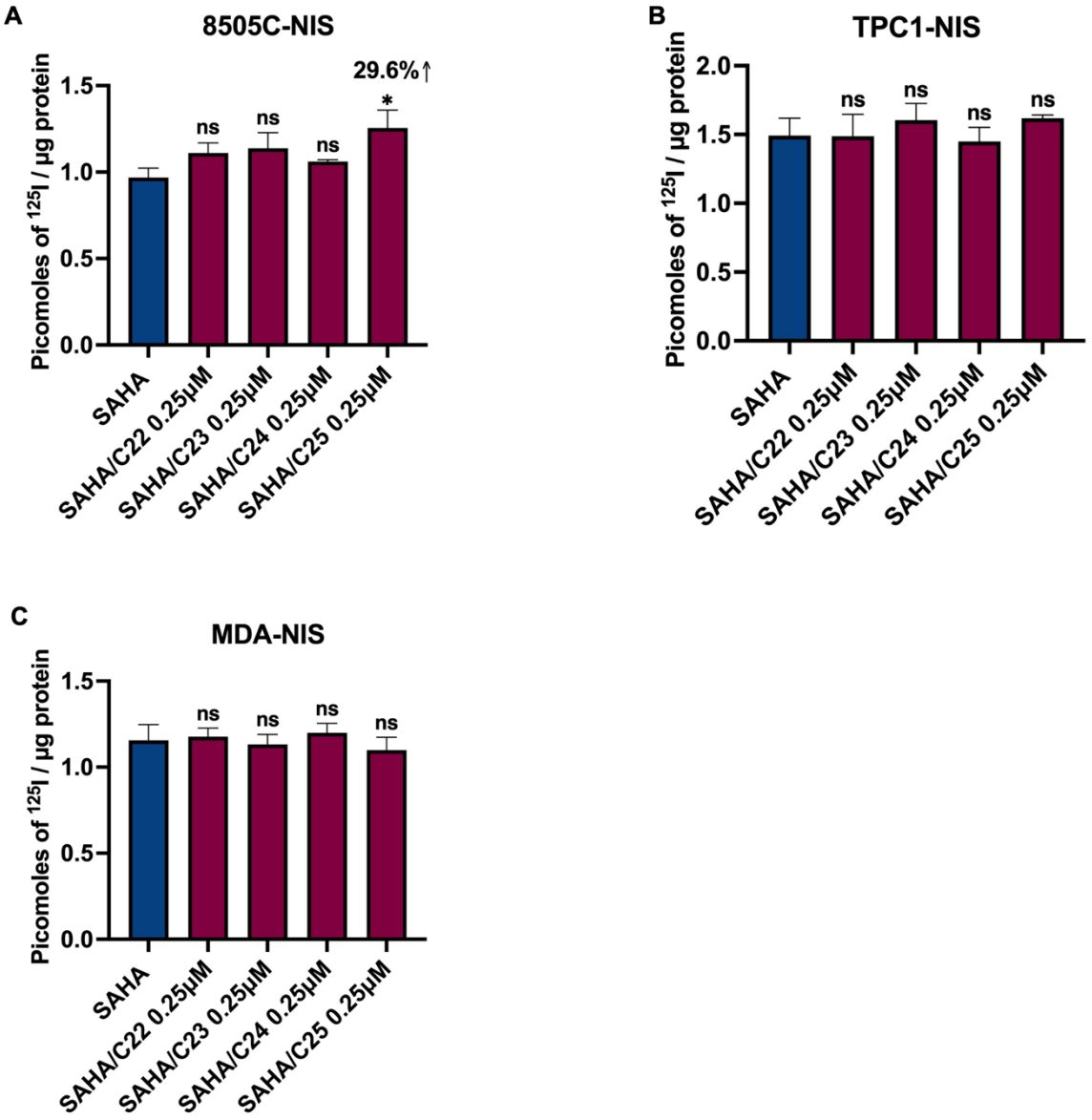


Figure 5. 15 Effects of compounds 22–25 on radioiodide uptake in NIS-expressing cell lines in combination with SAHA (2.5 µM) or SAHA alone after 24 hours of treatment. *(A) In 8505C-NIS cells, SAHA + C22-25 (0.25 µM) increased uptake compared to SAHA alone, while other combinations showed no significant changes. (B) TPC1-NIS cells showed no significant changes with any treatment. (C) MDA-NIS cells also showed no significant differences for SAHA + compounds 22–25 compared to SAHA alone. Data represent mean ± SEM from n = 3 biological replicates. Statistical analysis: one-way ANOVA, followed by Dunnett's post-test: ns (not significant), *P < 0.05.*

Previous unpublished research from the McCabe group detected a reduction in VCP-NIS interaction in the presence of VCP inhibitors like CB-5083 and CB-5339.

Additional experiments were therefore performed using the NanoBiT assay to examine whether compounds 22-25 could alter the affinity of NIS-VCP interaction. In this study, HEK293 cells co-transfected with LgBiT-VCP and NIS-SmBiT constructs were treated with compounds 22-25 at a concentration of 0.25 μM. 24 hours post-treatment, luminescence was measured to evaluate the interaction. C22, C23, and C25 significantly disrupted the physical interaction between NIS and VCP, reducing luminescence emitted by approximately 40 % (Figure 5.16).

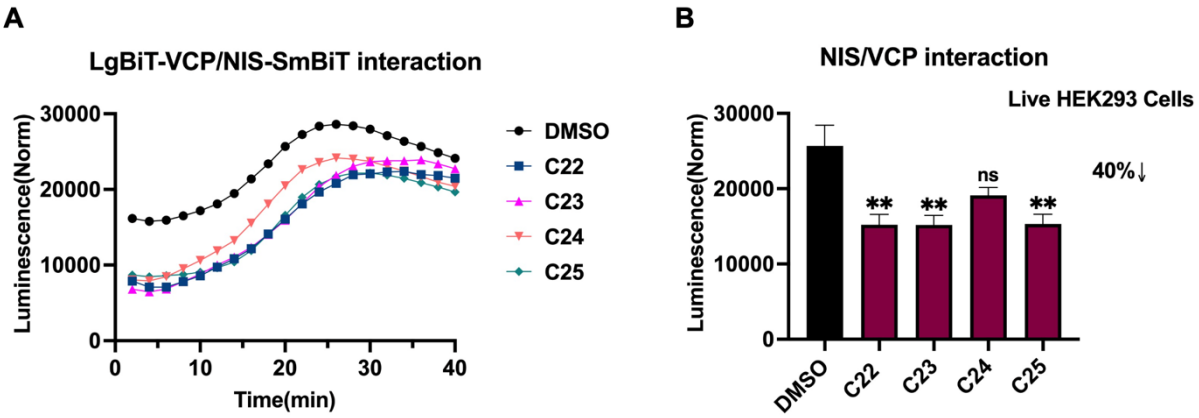


Figure 5. 16 Effects of compounds 22-25 on NIS-VCP interaction. *(A) time-course analysis of VCP-NIS interaction in HEK293 cells treated with DMSO or compounds 22-25. (B) Quantitative analysis of VCP-NIS binding at the 20-minute timepoint. The data from four independent experiments were analysed by one-way ANOVA.*

5.2.4 Discussion

5.2.4.1 Efficacy of Modified Clotrimazole Analogue (GB002)

The second strategy of Chapter 5 - to improve the potency and solubility of clotrimazole via the novel analogue GB002 failed to significantly enhance iodide uptake in TPC1-NIS and L87-NIS cells at the tested concentrations. The primary endpoint of this investigation was radioiodide uptake, an indirect measure of VCP

inhibitor activity. This assay relies on disrupting the functional interaction between VCP and NIS, theoretically preventing the endoplasmic reticulum degradation of NIS and enhancing its activity. The results suggest that while GB002 may have some effect, it is insufficient to induce a marked enhancement in NIS-mediated iodide uptake.

5.2.4.2 Development and Evaluation of Derivative Compounds Based on NMS-873

The third and final strategy of Chapter 5, following the limited success of GB002, was to design additional derivatives based on the known VCP inhibitor NMS-873, which is unsuitable for *in vivo* work given its poor bioavailability. Compounds 22-25 were evaluated for their effects on radioiodide uptake in NIS-expressing cell lines alone or combined with SAHA. The results showed no significant changes in TPC1-NIS and MDA-NIS cells, although a modest improvement was observed in 8505C-NIS cells with compound 22.

In parallel, the impact of compounds 22-25 on VCP-NIS interaction was assessed using the NanoBiT assay. The results demonstrated that C22, C23 and C25 significantly disrupted the binding between NIS and VCP, as evidenced by a reduction in luminescence by approximately 40 % (Figure 5.16). However, this reduction was lower than the 1.5-fold reduction with CB5083 and 2.4-fold reduction with CB-5339 previously reported (Read et al., 2022), likely explaining the correspondingly modest increase in radioiodide uptake observed in compounds 22-25.

SAHA, an FDA-approved HDAC inhibitor, has been shown to robustly increase NIS mRNA expression in thyroid cells, leading to enhanced NIS protein levels and improved radioiodide uptake (Cheng et al., 2016; Wächter et al., 2018). However, SAHA and similar HDACi have not been successful when used alone in clinical trials. Previous studies from the McCabe group demonstrated that combining VCP inhibitors with SAHA significantly increases iodide uptake in thyroid cancer cells. When combined with VCP inhibitors, such as ebastine, astemizole, clotrimazole or NMS-873, there were further increase in radioiodide uptake, which suggests an additive effect where SAHA-induced NIS expression benefits from the inhibition of VCP-mediated ERAD, thereby preserving NIS protein levels (Read et al., 2022). Interestingly, in 8505C-NIS cells, co-treatment with compound 25 and SAHA resulted in a 29.6 % increase in iodide uptake compared to the SAHA alone group. However, whilst these data circumstantially support the idea that VCP inhibitors block VCP-dependent proteasomal degradation pathways, which control the subsequent processing and degradation of NIS, mechanistic endpoints such as these were not pursued given the lack of pronounced impact on radioiodide uptake.

5.2.4.3 Conclusion

The 3 parallel strategies explored in this Chapter (established FDA inhibitors; clotrimazole analogues; de novo compounds based on NMS-873) all failed to dramatically enhance radioiodide uptake *in vitro*. Future work would need to explore other methods of effective allosteric inhibition of VCP *in vivo* with realistic bioavailabilities.

CHAPTER 6 FURTHER INVESTIGATION INTO NIS DIMERISATION

6.1 Introduction

The subcellular localisation and trafficking of many membrane proteins are functionally regulated through dimerisation, and circumstantial evidence suggests that NIS may also dimerise (Bocharov et al., 2008; Maurel et al., 2008; Vidi et al., 2008). For instance, freeze-fracture electron microscopy of NIS-expressing oocytes revealed intramembrane particles that were too large to be monomers (Eskandari et al., 1997). Huc-Brandt et al. conducted the most comprehensive evaluation of NIS dimerisation potential (2011). Electrophoresis patterns indicated dimerisation, and both size exclusion chromatography and light scattering analyses supported the likelihood of NIS dimerisation *in vitro*.

More recent studies (Thompson et al., 2019) have confirmed that NIS exists as a dimer. The dimerisation process appears to be essential particularly for the maturation and trafficking of the NIS protein. This research used a homology model based on the structure of the sodium/galactose transporter (vSGLT). Several key residues involved in NIS dimerisation were identified, including D237, Y242, T243, F244, Q471, A525, K554, and R555, which form two distinct putative dimerisation interfaces (Figure 6.1). Interestingly, mutational analyses have shown that while individual mutations in these residues do not significantly disrupt dimerisation, combinations of mutations can severely impair NIS monomer interaction. However, the precise function of NIS dimerisation is not fully defined and requires further insight.

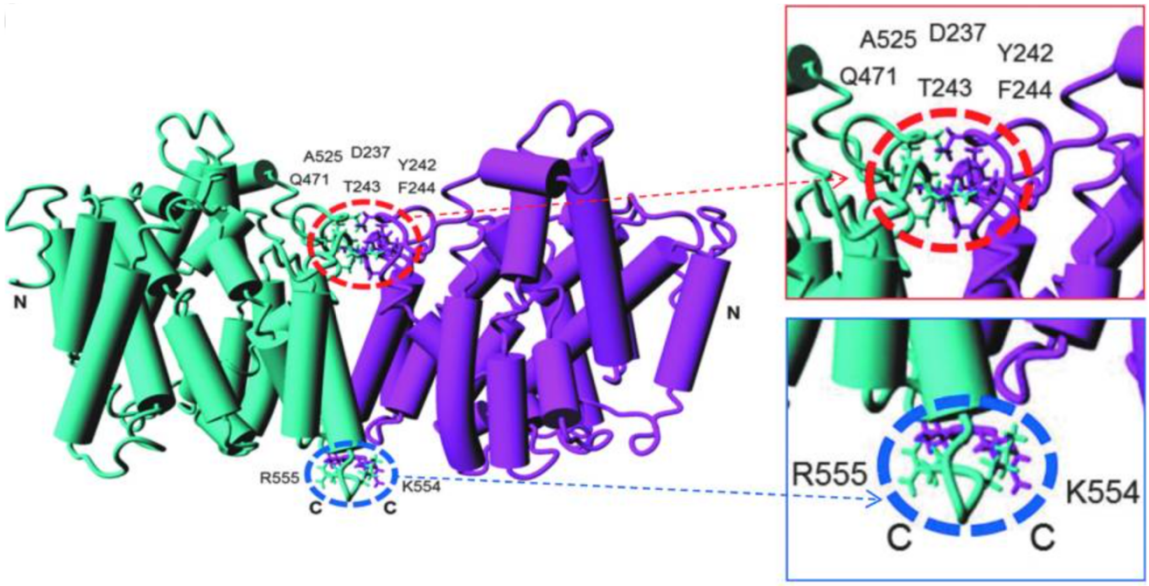


Figure 6. 1 Using the refined NIS homology model, eight novel residues were identified as potentially involved in NIS dimerisation. *Forming two distinct putative dimerisation interfaces, a larger "primary" region (circled in red) and a smaller "secondary" region (blue) have been proposed. Figure adapted from (Thompson et al., 2019).*

Given the investigations of this thesis into NIS function, protein: protein interaction and endocytosis, this Chapter challenged the notion that NIS dimerises, applying the approaches established in previous chapters to shed new light on the process.

6.2 Materials and Methods

6.2.1 Plasmid Preparation

The NIS coding sequences were tagged exclusively at the C-terminus with SmBiT, LgBiT and Nluc for NanoBiT and NanoBRET protein-protein interaction assays. Mutants including NIS^{K554A}, NIS^{R555A}, $NIS^{K554A/R555A}$, NIS^{K554A}-SmBiT, NIS^{R555A}-SmBiT, $NIS^{K554A/R555A}$-SmBiT, NIS^{K554A}-LgBiT, NIS^{R555A}-LgBiT, $NIS^{K554A/R555A}$-LgBiT, NIS^{K554A}-

Nluc, NIS^{R555A}-Nluc, $NIS^{K554A/R555A}$-Nluc were generated using the Agilent QuikChange XL Site-Directed Mutagenesis Kit, as detailed in Section 2.4.

6.2.2 NanoBRET and NanoBiT Assays

NanoBRET and NanoBiT assays were performed as described previously (Section 2.8 and Section 2.9). Cells were seeded in 6-well plates at a density of 3.5×10^5 cells per well and transfected with plasmid DNA as before.

6.2.3 Western Blot

Cells were lysed in RIPA buffer supplemented with a protease inhibitor cocktail. Western blot was conducted as previously described in Section 2.6. The primary antibodies used included rabbit polyclonal anti-NIS (1:1000), rabbit monoclonal anti-HA Y-11 (1:1000) and mouse monoclonal β-actin AC-15 (1:10000).

6.2.4 Radioiodide Uptake

Each condition included six replicates, with two replicates treated with sodium perchlorate for one hour before adding radioiodine. Approximately 1.2×10^5 counts per minute of ^{125}I were added to each well and incubated at 37°C for one hour. The lysate activity was measured with a gamma counter and protein quantification was performed using a BCA assay.

6.2.5 Statistical Analysis

Data were analysed using one-way ANOVA followed by Dunnett's multiple comparison test to compare against the wild type (WT). Significance was considered at $P < 0.05$. Statistical analysis was performed on a minimum of n = 3 independent experiments.

6.3 Results

6.3.1 Impact of K554A and R555A Mutations on NIS Dimerisation Assessed by NanoBiT Assay

To investigate the impact of mutations K554A and R555A on NIS dimerisation, NanoBiT assays were performed in HEK293 and HeLa cell lines. The results are presented in Figure 6.2.

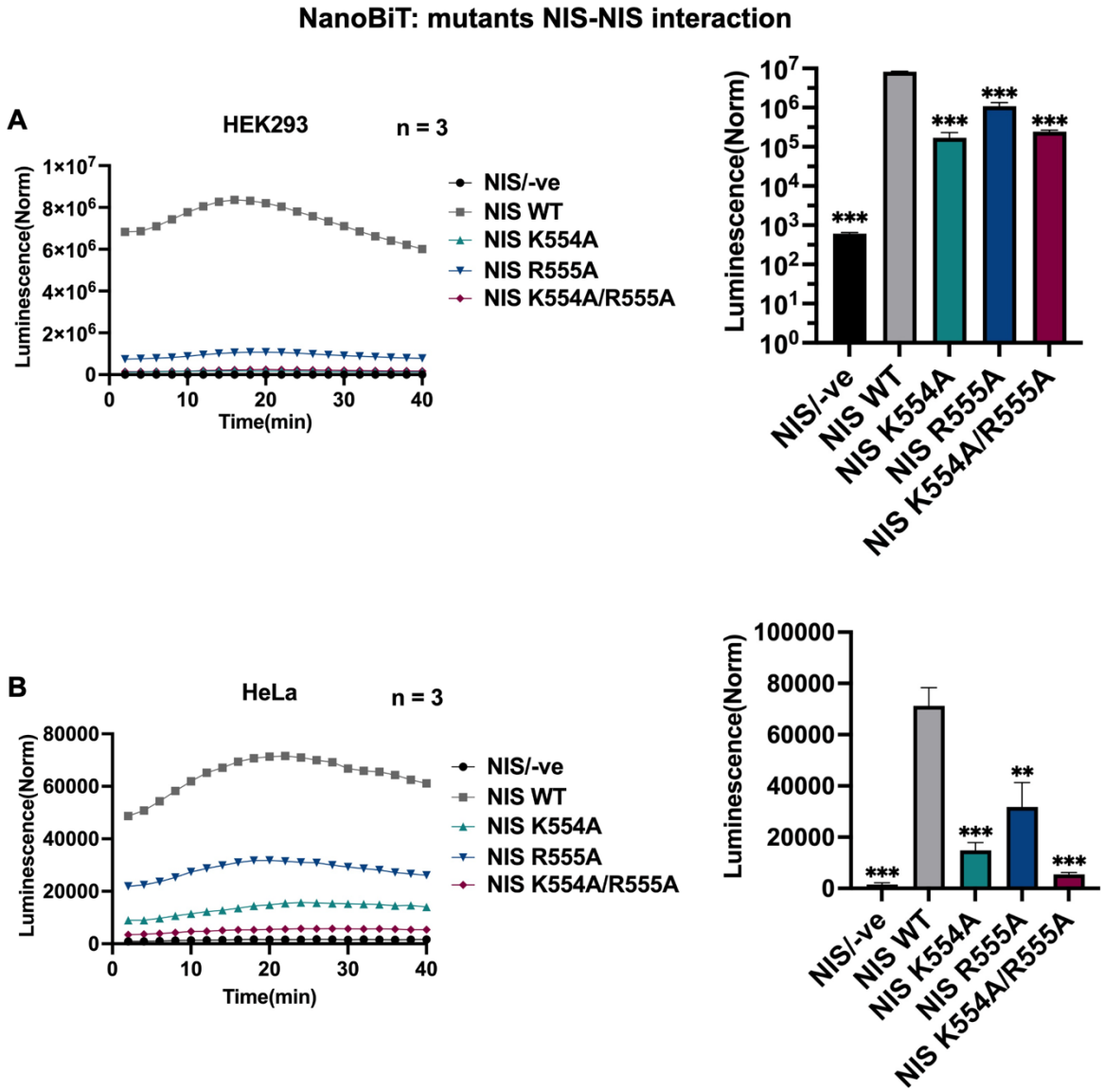


Figure 6. 2 The influence of putative dimerisation motifs on NIS dimerisation was assessed via NanoBiT assays. *Mutations NIS K554A, NIS R555A and NIS K554A/R555A showed significant reductions in luminescence compared to wild type. Statistical analysis was performed using one-way ANOVA, with **P<0.01 and ***P<0.001.*

In both HEK293 (Figure 6.2 A) and HeLa (Figure 6.2 B) cells, wild type (NIS WT) exhibited significant interaction signals, as detected via normalised luminescence. This independently supports the previous data via different methodologies that NIS can dimerise. The negative control (NIS/-ve) displayed minimal luminescence, as

expected. Mutations K554A and R555A, along with the double mutation K554A/R555A, resulted in markedly reduced luminescence compared to the wild type, with levels approaching the negative control. Specifically, in HEK293 cells, K554A reduced luminescence by 97 %, R555A by 86 % and the K554A/R555A double mutation by 97 %. In HeLa cells, K554A reduced luminescence by 80 %, R555A by 55 % and K554A/R555A by 92 %. These reductions in luminescence indicate a clear impairment in dimerisation capability.

6.3.2 Mutating Residues of Putative Dimerisation Interface Impairs NIS Function

To assess if NIS function was affected by mutating amino acids putatively involved in dimerisation, radioiodide uptake assay analyses were conducted in HEK293 and HeLa cell lines following transfection with the relevant constructs. One-way ANOVA followed by Dunnett's multiple comparison tests were conducted to determine significant differences in uptake compared to the wild type (WT).

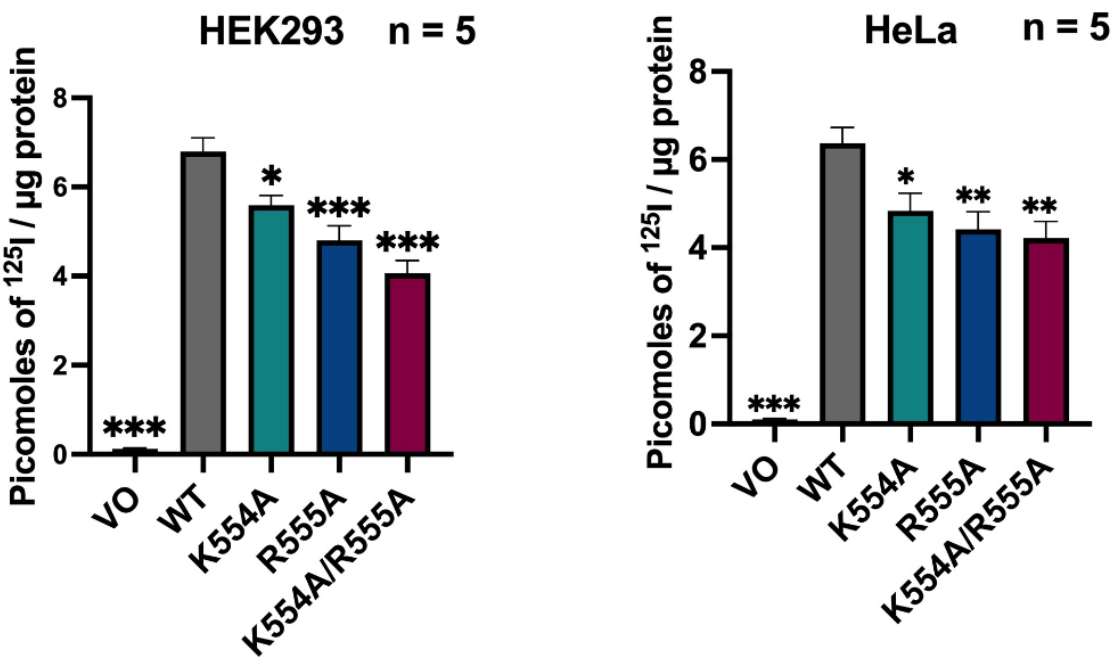


Figure 6. 3 Radioiodide uptake assay for NIS mutations. *Radioiodide uptake was significantly reduced when residues K554 and R555 within the putative dimerisation interface were mutated in both HEK293 (left) and HeLa cells (right) compared to the WT. *p<0.005, **p<0.01 and ***p<0.001 compared with WT (n=5 biological replications).*

In HEK293 cells, the K554A mutation resulted in an 18 % decrease in radioiodide uptake relative to WT, while the R555A mutation led to a 30 % reduction. The double mutant K554A/R555A exhibited a more pronounced effect, with a 49 % reduction in iodide uptake compared to WT. In HeLa cells, the K554A mutation caused a 24 % decrease in iodide uptake relative to WT. The R555A mutation resulted in a 30 % reduction, consistent with the HEK293 cells. The double mutant K554A/R555A showed a 34 % reduction in iodide uptake compared to WT. Thus, mutations at residues K554 and R555 partially decrease NIS-mediated radioiodide uptake rather than completely abolishing it. The combination of both mutations (K554 and R555) further impairs the function of NIS but does not abolish it entirely.

6.3.3 Impact of K554A and R555A Mutations on NIS Protein Expression.

Western blot analysis was performed on lysates from HEK293 and HeLa cells expressing either wild-type or mutant NIS constructs, aiming to determine if mutations within the putative dimerisation interface influence NIS protein expression (Figure 6.4).

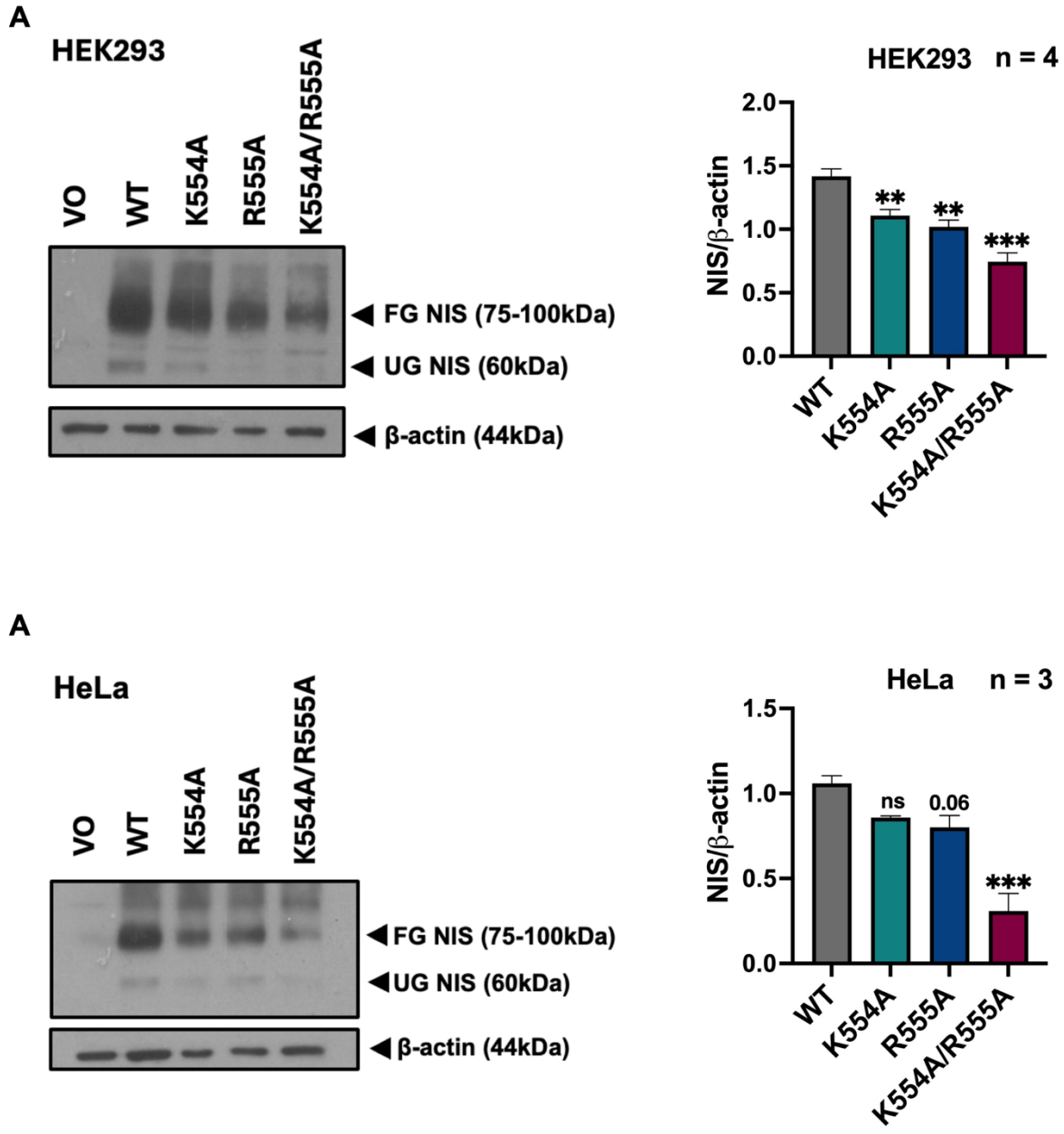


Figure 6. 4 Mutating residues within the putative dimerisation interface alters NIS expression. *HEK293 (A) and HeLa (B) cells were transfected with empty pcDNA3.1 (+) vector (VO), wild-type NIS (WT) or NIS constructs with mutations in the*

putative dimerisation interface (K554A, R555A, and K554A/R555A). Western blot analysis was conducted using a rabbit NIS primary antibody. The band observed at 75-100 kDa corresponds to the fully glycosylated, mature form of NIS, whereas the band at approximately 60 kDa represents the unglycosylated, immature form of NIS. β-actin was used as a loading control (n=3 or 4).

In both HEK293 and HeLa cells, WT NIS and three mutants appeared fully glycosylated. However, the K554A, R555A and K554A/R555A mutants had reduced the expression of the fully glycosylated (70-100 kDa) NIS protein isoform. Statistical analysis of the Western blot data revealed that single amino acid mutation (K554A or R555A) had marginal reductions in NIS protein expression compared to the WT. However, the double mutant K554A/R555A showed a significantly lower expression level than the WT: 1.9-fold lower in HEK293 cells and 3.4-fold lower in HeLa cells.

These findings are consistent with the results from the radioiodide uptake assay depicted in Figure 6.3, which demonstrated that a single mutation in the putative dimerisation interface modestly affects NIS activity. In contrast, double mutations significantly impair both NIS function and expression. This suggests that while these residues significantly impact protein: protein interaction, dimerisation is not imperative for proper functionality.

6.3.4 Mutating Residues of Putative Dimerisation Interface Affects NIS Plasma Membrane Localisation

Next, NanoBRET assays were used to evaluate the impact of mutations K554A and R555A on NIS plasma membrane (PM) localisation in both HEK293 and HeLa cell lines. The assay involved co-transfecting cells with Kras-Venus and NIS-Nluc or Kras-

Venus and mutants of the NIS-Nluc construct (NIS^{K555A}-Nluc, NIS^{R555A}-Nluc or NIS$^{K554A/R555A}$-Nluc). The results are shown in Figure 6.5 and Figure 6.6.

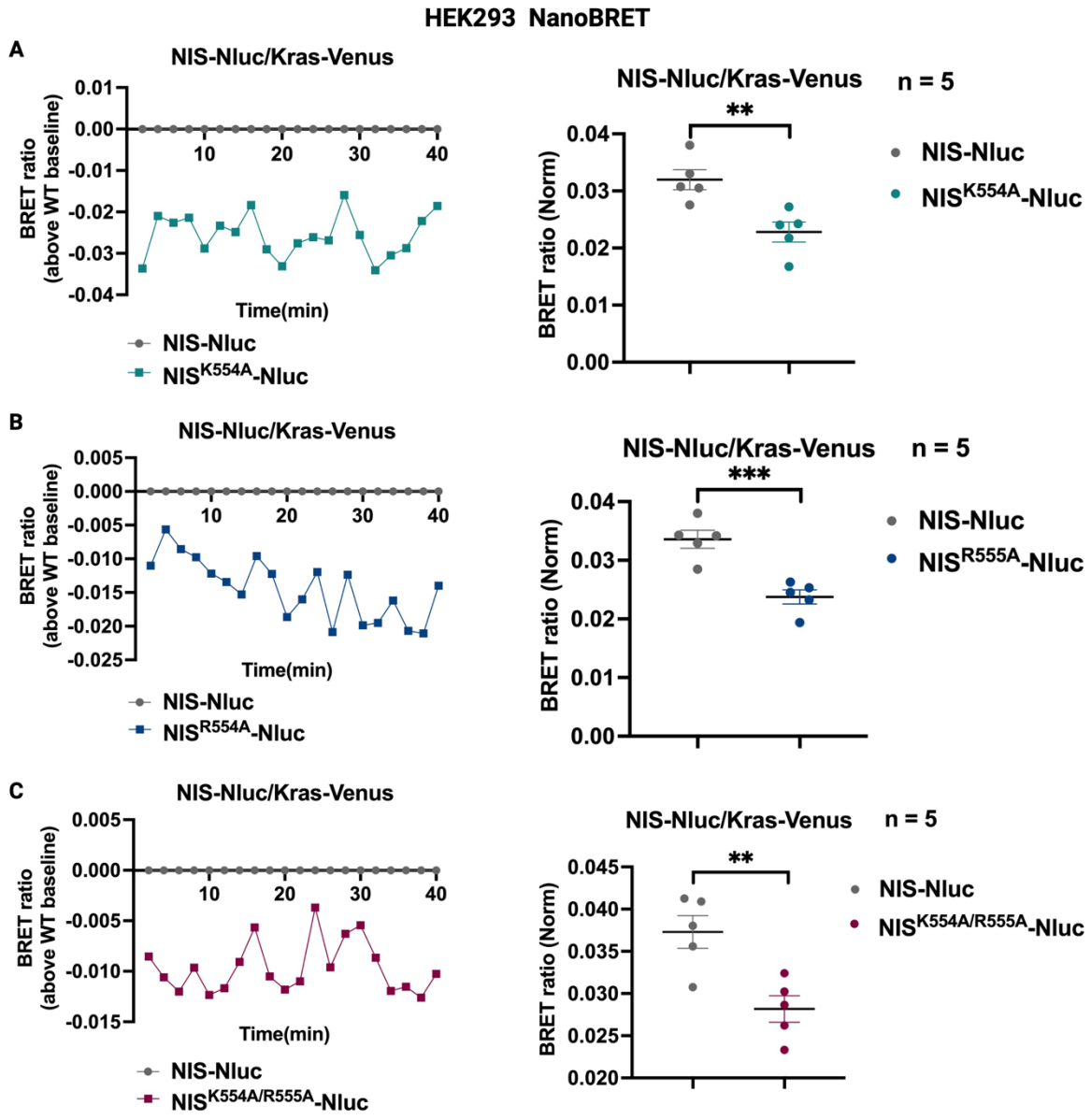


Figure 6. 5 Live cell kinetic measurement of NIS-Kras interaction in HEK293 cells. *NanoBRET was used to evaluate the proximity between NIS and Kras in HEK293 cells transfected with wild-type NIS or each NIS mutant (left). Assay results are shown at 20 minutes post-addition of Nano-Glo substrate (right). Data are presented as mean ± SEM; statistical analyses were conducted using an unpaired t-test for each set of conditions.*

In HEK293 cells (Figure 6.5), wild-type NIS (NIS-Nluc) demonstrated a detectable BRET signal, indicative of localisation at PM. In contrast, the K554A, R555A and K554A/R555A mutants exhibited a significantly reduced BRET ratio, reflecting a diminished presence at the PM compared to the wild type ($P < 0.01$ for K554A and K554A/R555A, $P < 0.001$ for R555A).

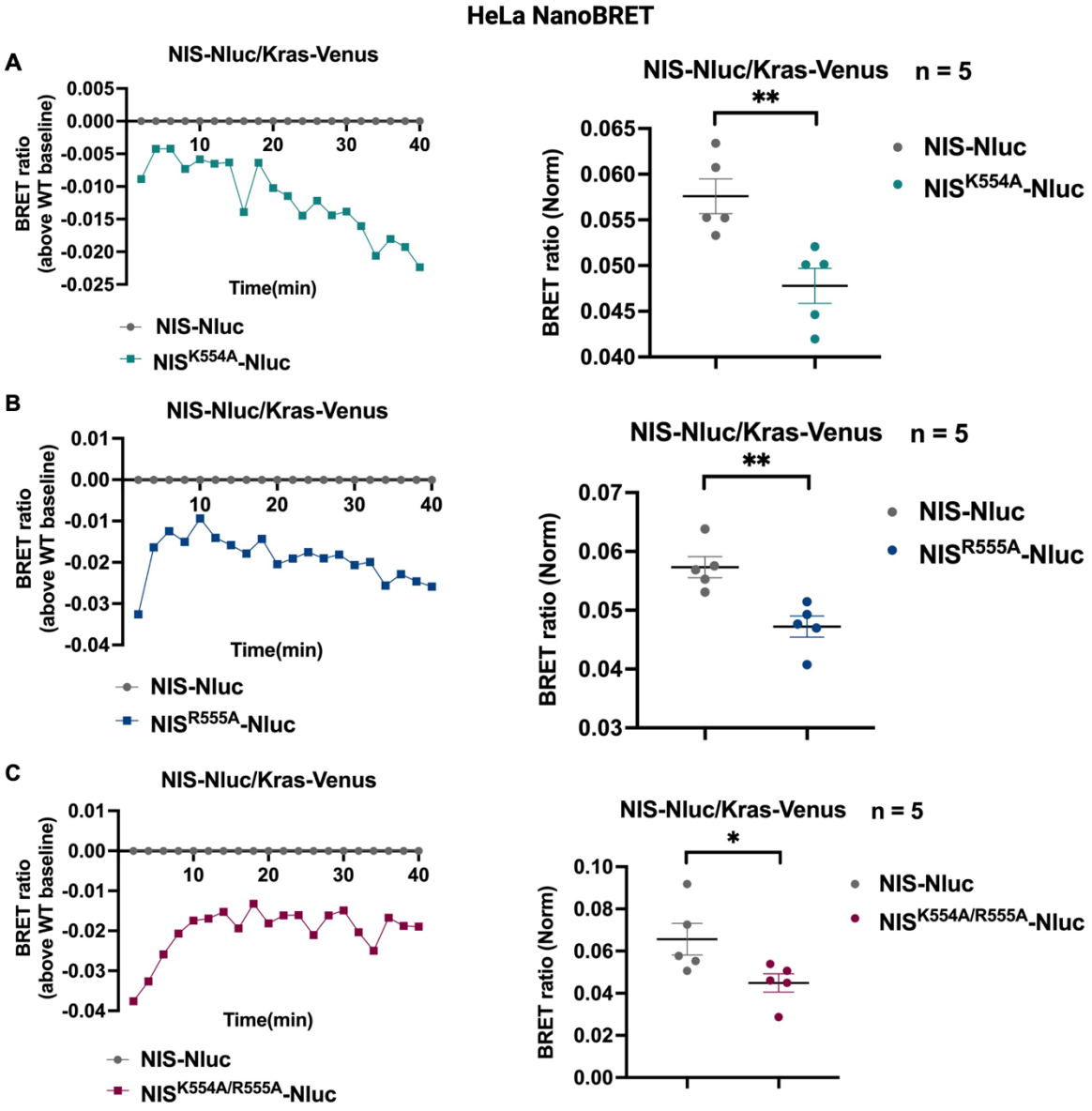


Figure 6. 6 Live cell kinetic measurement of NIS-Kras interaction in HeLa cells. *(A) BRET ratio over time for NIS-Nluc and NIS^{K554A}-Nluc interactions with Kras-Venus, showing reduced interaction for the K554A mutant. (B) BRET ratio over time for NIS-Nluc and NIS^{R555A}-Nluc interactions with Kras-Venus, indicating reduced interaction for the R555A mutant. (C) BRET ratio over time for NIS-Nluc and NIS$^{K554A/R555A}$-Nluc*

*interactions with Kras-Venus, showing significantly reduced interaction for the double mutant. Left panels display time-dependent BRET ratios, while right panels present normalized BRET ratios from five biological replicates (n = 5). Statistical analysis was performed using one-way ANOVA: *P < 0.05, **P < 0.01. Data are presented as mean ± SEM.*

Consistent with the results in HEK293 cells, HeLa cells co-transfected with wild-type NIS displayed a BRET signal, indicating PM localisation (Figure 6.6). Mutations K554A, R555A and K554A/R555A resulted in a significantly weaker BRET signal, suggesting the essential role of these residues in NIS trafficking and membrane localisation ($P < 0.01$ for K554A and R555A, $P < 0.05$ for K554A/R555A, all compared to WT).

These results demonstrate that both single and double mutations of K554A and R555A significantly disrupt NIS localisation at the PM in live cells, highlighting the importance of these residues in maintaining proper NIS function and membrane localisation.

6.3.5 Impact of K554A and R555A Mutations on NIS Trafficking and Subcellular Localisation

Previous studies have indicated that mutations within the putative dimerisation interface impair the localisation of the NIS protein to PM (Thompson et al., 2019). To further elucidate the impact of mutating these residues on NIS trafficking and localisation, this study employed NanoBRET assay subcellular markers to measure interactions between NIS and Venus-tagged markers representative of various subcellular compartments in live cells. In these additional NanoBRET assays, Rab1 (endoplasmic reticulum marker, ER) and Rab9 (trans-Golgi network maker) were

evaluated as essential markers for transport from the trans-Golgi network to the plasma membrane (Tiulpakov et al., 2016) (Figure 6.7).

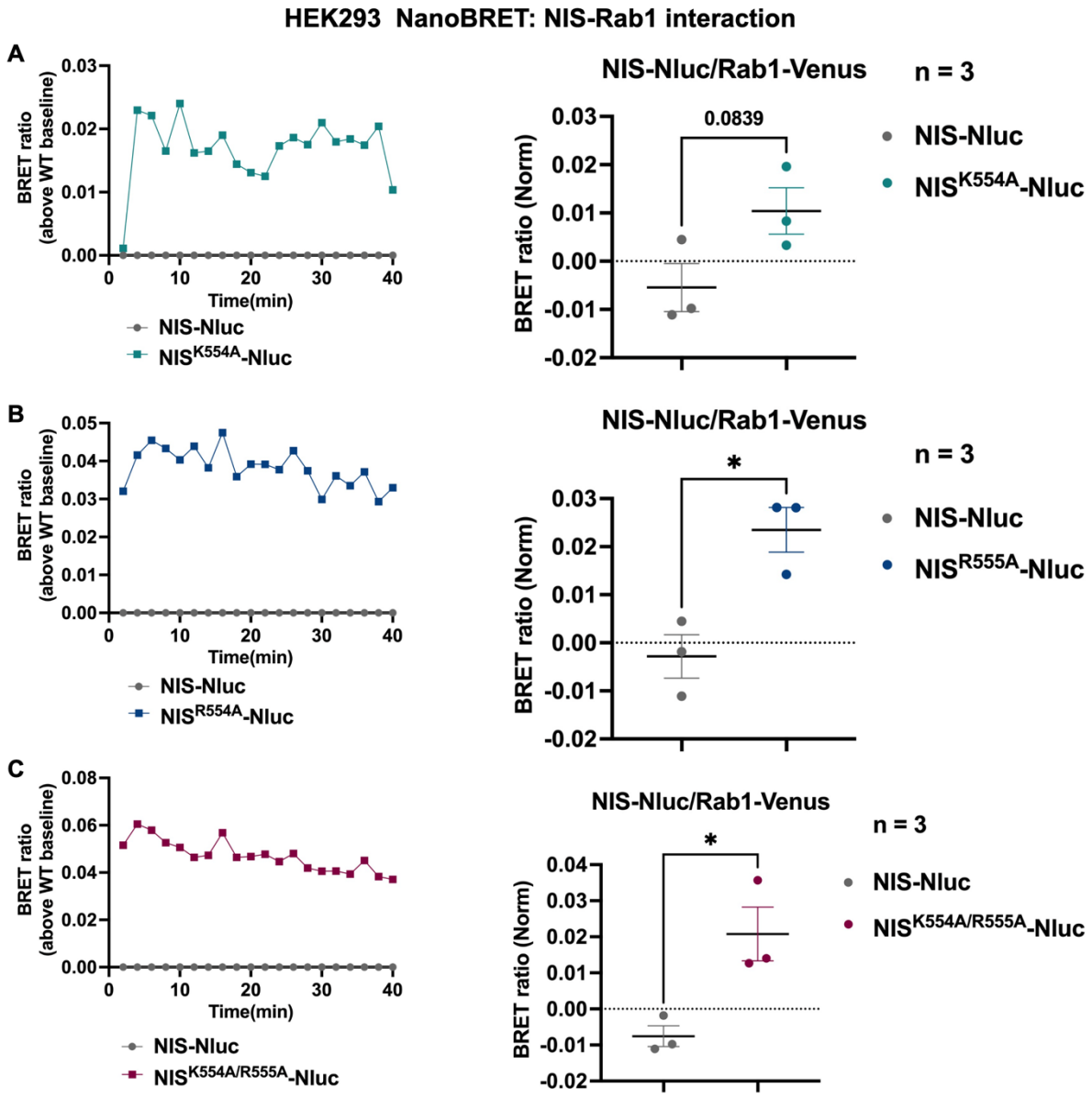


Figure 6. 7 NanoBRET analysis of NIS-Rab1 interaction in HEK293 cells (A for K554A, B for R555A, C for K554A/R555A). *Live cell kinetic measurement using the NanoBRET signal to evaluate the binding between NIS and Rab1 in HEK293 cells co-transfected with wild-type NIS or each NIS mutant and Rab1-Venus (left). This NanoBRET assay results at 20 minutes post-addition of Nano-Glo substrate (right). N=3 biological replicates. Data are presented as mean ± SEM; statistical analyses were conducted using an unpaired t-test for each set of conditions.*

All three mutations increased the BRET ratio compared to wild-type NIS-Nluc, suggesting a higher interaction level with Rab1-Venus, with the R555A mutant and K554A/R555A mutants exhibiting statistically significantly increased BRET ratios ($P < 0.05$).

Additionally, the reliability of these binding interaction trends was confirmed through experimental repetitions in HeLa cell lines (Figure 6.8)

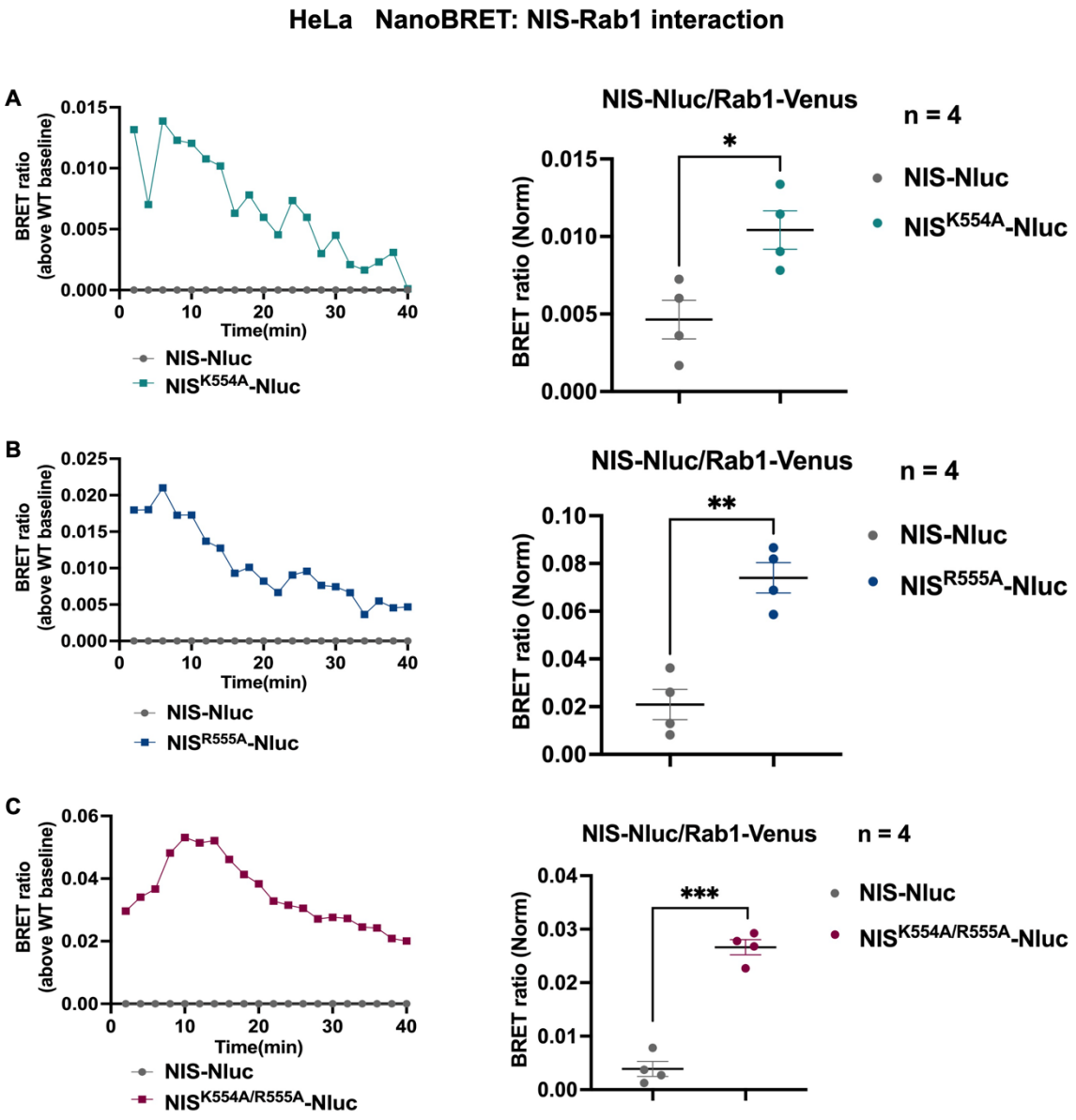


Figure 6. 8 NanoBRET analysis of NIS-Rab1 interaction in HeLa cells. *(A) BRET ratio for NIS-Nluc and NIS^{K554A}-Nluc interactions with Rab1-Venus, showing increased interaction for the K554A mutant. (B) BRET ratio for NIS-Nluc and NIS^{R555A}-Nluc interactions, indicating increased interaction for the R555A mutant. (C) BRET ratio for NIS-Nluc and NIS$^{K554A/R555A}$-Nluc interactions, showing significantly increased interaction for the double mutant. Left hand is time-dependent BRET ratios, while scatter plots on the right display normalised BRET ratios from four biological replicates (n = 4). Statistical analysis was performed using one-way ANOVA: *P < 0.05, **P < 0.01, ***P < 0.001. Data are presented as mean ± SEM.*

To further elucidate the impact of NIS mutations on its trafficking and localisation, the interaction between NIS and the trans-Golgi network marker Rab9 was investigated using the NanoBRET assay in HEK293 cells (Figure 6.9).

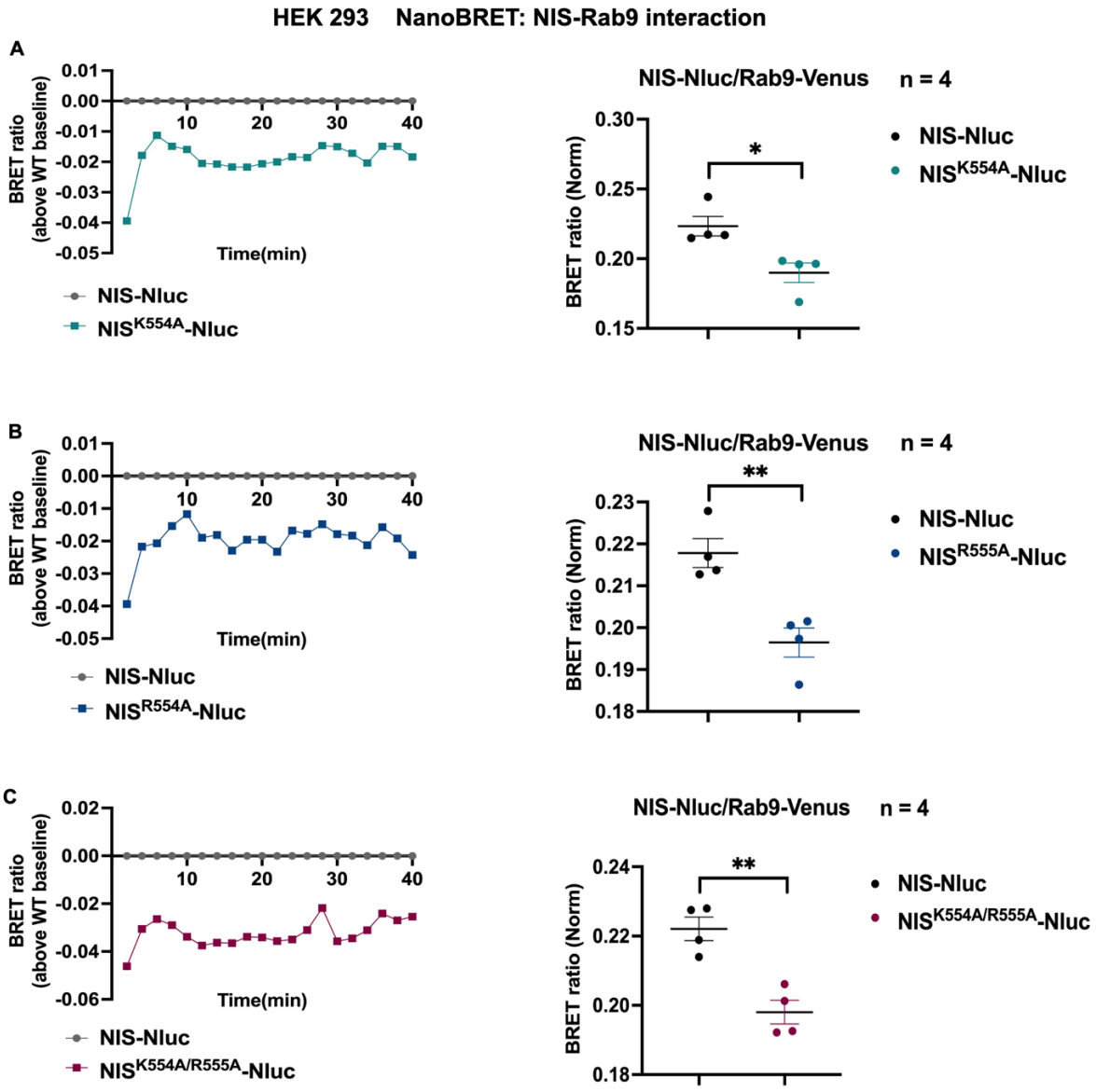


Figure 6. 9 Impact of NIS mutations on interaction with Rab9 in HEK293 cells. *(A) BRET ratio for NIS-Nluc and NIS^{K554A}-Nluc interactions with Rab9-Venus, showing reduced interaction for the K554A mutant. (B) BRET ratio for NIS-Nluc and NIS^{R555A}-Nluc interactions, indicating reduced interaction for the R555A mutant. (C) BRET ratio for NIS-Nluc and NIS$^{K554A/R555A}$-Nluc interactions, showing significantly reduced interaction for the double mutant. On the left are time-dependent BRET ratios, while scatter plots on the right display normalised BRET ratios from four biological replicates (n = 4). Statistical analysis was performed using one-way ANOVA: *P < 0.05, **P < 0.01. Data are presented as mean ± SEM.*

BRET ratios for NIS^{K554A}-Nluc/Rab9-Venus (Figure 6.9 A), NIS^{R555A}-Nluc/Rab9-Venus (Figure 6.9 B), and the double mutants $NIS^{K554A/R555A}$-Nluc/Rab9-Venus (Figure 6.9 C) were all significantly reduced compared to the wild-type NIS-Nluc/Rab9-Venus. Collectively, these findings suggest that mutations within the putative dimerisation interface of NIS impair its proper trafficking from the ER to the trans-Golgi.

6.4 Discussion

Previously, the McCabe group aimed to identify novel residues involved in NIS dimerisation by constructing a homology model based on the crystal structure of the dimeric bacterial protein vSGLT. This modelling effort identified eight key residues (D237, Y242, T243, F244, Q471, A525, K554, and R555) within putative dimerisation interfaces (Thompson et al., 2019).

This chapter provides significant additional insight into the role of specific residues within the putative dimerisation interface of NIS in its dimerisation, function and subcellular localisation. The primary focus was on residues K554 and R555, which have not been studied before.

6.4.1 Two Mutations Within the Dimerisation Interface Potentially Affect NIS Dimerisation

The mutations K554A and R555A within the dimerisation interface appear to potentially impact NIS dimerisation. NanoBiT assay results showed a marked reduction in luminescence for both single and double mutations compared to the wild type.

However, the NanoBiT assay measures luminescence as a proxy for protein-protein interaction but does not provide information on the specific localisation or structural changes in the protein complex. Therefore, it cannot directly confirm whether the observed luminescence changes are solely due to impaired dimerisation or other structural alterations. Future experiments, such as immunofluorescence staining, proximity ligation assays (PLA), and fluorescence resonance energy transfer (FRET), would be needed to validate the NanoBiT results and elucidate the precise mechanisms involved.

6.4.2 Mutating Residues in the Putative Dimerisation Interface Significantly Impairs NIS Function

Radioiodide uptake assays revealed that the K554 and R555 mutations modestly impaired the ability to transport iodide. Specifically, the single mutations K554A and R555A reduced iodide uptake by 18 % and 30 % in HEK293 cells, respectively, and by 24 % and 30 % in HeLa cells, respectively. The double mutation K554A/R555A exhibited an even greater reduction, with a 49% decrease in HEK293 cells and a 34 % decrease in HeLa cells. This indicates that whilst these residues are important for the functional activity of NIS, they are not absolutely imperative.

Moreover, Western blot analysis consistently indicated that the K554A and R555A mutations do not entirely abolish NIS protein expression. Single mutations at either K554 or R555 result in only slightly reduced levels of fully glycosylated NIS, suggesting that the loss of a single residue can be tolerated. However, the combined K554A/R555A mutations had a more pronounced effect, significantly decreasing NIS

protein levels. Interestingly, while the NIS mutants demonstrated enhanced ER localisation in NanoBRET assays, there was no obvious change in the expression of unglycosylated NIS.

6.4.3 Impaired Dimerisation Affects NIS Subcellular Localisation

Most eukaryotic secretory or membrane proteins are delivered to the plasma membrane via the traditional ER-Golgi pathway (Kim et al., 2016). Numerous plasma membrane proteins have been demonstrated to dimerise, facilitating their transport to the plasma membrane (Bocharov et al., 2008; E. Li et al., 2005; Maruyama, 2015; Maurel et al., 2008; Vidi et al., 2008). The NanoBRET assay provided initial insights into how impaired interaction might affect NIS trafficking and localisation in live cells. Mutations in the putative dimerisation interface led to a significant reduction in the BRET ratio with Kras, indicating diminished NIS localisation at the plasma membrane. Conversely, there was an increased interaction with the ER marker Rab1, suggesting that the mutants might be retained in the ER. Moreover, the interaction with the trans-Golgi network marker Rab9 was significantly reduced, further indicating potential disrupted trafficking from the ER to the Golgi.

While these observations suggest that proper dimerisation could be crucial for efficient NIS trafficking through the ER-Golgi pathway to the plasma membrane, more experiments are needed to validate these findings. NanoBRET assays, although useful, need to be complemented with other techniques to confirm the subcellular localisation and interactions of NIS. Future experiments could include direct visualisation techniques such as live-cell imaging, IF microscopy and total internal

reflection fluorescence microscopy (TIRFM), to provide more definitive evidence of NIS dimerisation and its localisation within the cell.

CHAPTER 7 CONCLUDING THOUGHTS AND FUTURE DIRECTIONS

CHAPTER 7 CONCLUDING THOUGHTS AND FUTURE DIRECTIONS

For over eighty years, radioiodide therapy has been a foundational treatment for thyroid cancer, effectively targeting residual cancer cells and distant metastases following surgery (Nguyen et al., 2015). Despite its efficacy, the prognosis for radioiodide-refractory thyroid cancer remains poor (Pitoia et al., 2022). This is primarily due to reduced expression and improper localisation of NIS, which hampers effective radioiodide transport. Additionally, breast cancer is the most commonly diagnosed cancer among women worldwide. The presence of NIS in breast cancers, including triple-negative breast cancers and their metastases, is well-documented. However, its primarily cytoplasmic localisation restricts the efficacy of radioiodine-based therapies (Yao et al., 2015). Consequently, there is a critical need to develop strategies that enhance NIS function and ensure its proper localisation to the plasma membrane, thereby improving therapeutic outcomes for both thyroid and breast cancer.

The experiments of this PhD have comprehensively investigated the mechanisms underlying NIS endocytosis, and have elucidated the impact of various molecular interactions and regulatory pathways on NIS function and localisation. These findings provide a potential foundation for developing novel therapeutic strategies aimed at sensitising cancer cells to radioiodide therapy, potentially leading to improving patient outcomes in oncological treatments involving radioiodine. Based on previous work, three strategies were appraised for their ability to target VCP and enhance iodide uptake by reducing NIS degradation, thereby improving the efficacy of radioiodine therapy.

7.1 Mechanisms of NIS Endocytosis

7.1.1 Investigating the Interaction Between NIS and AP2

Previous studies have identified several motifs crucial for basolateral targeting of NIS and interaction with the AP1 machinery (Darrouzet et al., 2016; Koumarianou et al., 2022). However, the mechanisms governing NIS endocytosis from the plasma membrane remain inadequately understood. Work in this PhD delved into the intricacies of NIS endocytosis, emphasising the pivotal roles of the AP2 adaptor complex and PBF in mediating NIS internalisation through clathrin-mediated endocytosis. Through NanoBiT technology, NIS and the AP2σ2 subunit were shown to physically interact *in vitro*, and this could be reduced by mutating the residues V88 and L103 in AP2σ2. Notably, mutating specific dileucine (562LL563) and diacidic (578EEVAIL583) motifs within NIS also disrupted the binding affinity between NIS and AP2σ2. Meanwhile, mutations in these motifs resulted in significant alterations in NIS surface expression and iodide uptake, underscoring their functional importance. Additionally, the knockdown of AP2 subunits resulted in increased NIS presence at the plasma membrane and enhanced iodide uptake, highlighting the regulatory role of AP2 in NIS endocytosis. Furthermore, this study demonstrated enhanced interactions between NIS and PBF following AP2 subunit knockdown, suggesting potential therapeutic strategies targeting these pathways. Overall, this research provides a more detailed understanding of the molecular mechanisms governing NIS trafficking and function.

7.1.2 Role of Moesin in NIS Endocytosis

Data presented in Chapter 4 elucidated the intricate regulatory network involving AP2, moesin, and PBF in modulating NIS endocytosis. NanoBiT assays demonstrated that knockdown of AP2 subunits increases the luminescence signal between NIS and moesin, suggesting that AP2 might play a crucial role in regulating the interaction between NIS and moesin. Conversely, PBF knockdown led to a decrease in this interaction, indicating that PBF also plays a role in regulating the dynamics between NIS and moesin. Silencing moesin expression enhanced NIS-PBF interaction, indicating potentially competitive dynamics between these proteins. This led to the hypothesis that moesin, particularly through its phosphorylation status, may act as a key regulator in the clathrin-mediated endocytosis pathway, influencing NIS trafficking and degradation.

7.1.3 Future Directions

Future research should focus on examining the hypothesis that the AP2 adaptor complex facilitates the internalisation of NIS via clathrin-mediated endocytosis by maintaining a stable interaction with the σ2 subunit at the plasma membrane. This process is likely initiated by the μ2 subunit of AP2 binding to the YXXΦ motif of PBF, which serves as an endocytic accessory factor (EAF) and triggers endocytosis. Further investigations are needed to determine whether the lack of increased RAI uptake in cancer cells following AP2σ2 ablation, compared to primary thyrocytes, is due to functional redundancy with other EAFs. These studies will be crucial for advancing our understanding of the molecular mechanisms governing NIS trafficking and improving

the efficacy of radioiodine therapy. Moreover, for AP2 subunits, the CSBA assay conducted thus far only involved the knockdown of the AP2α1 subunit, which resulted in increased NIS in both total and cell surface expression. This represents a limitation in this study, as the effects of knockdowns of other AP2 subunits were not assessed. To fully validate the role of each AP2 subunit in NIS trafficking and plasma membrane localisation, further experiments targeting all AP2 subunits are necessary. Meanwhile, visual experiments such as immunofluorescence and confocal microscopy to provide direct evidence of NIS and AP2 colocalisation and trafficking. Additionally, in this study, NanoBiT assays demonstrated that NIS dileucine and diacidic mutants, which exhibited significantly reduced binding to AP2σ2, offer a valuable tool for probing the mechanisms by which AP2 modulates NIS function and iodide uptake.

To further validate the hypothesis that the NIS diacidic motif interacts with AP2σ2, additional experiments such as site-directed mutagenesis and co-immunoprecipitation should be conducted. Overall, immunoprecipitation and GST-pull-down can also be employed to further challenge our NanoBiT assay results, providing additional confirmation of the protein-protein interactions between NIS and the AP2 adaptor complex. Techniques like live-cell imaging, fluorescence resonance energy transfer, or super-resolution microscopy could offer more detailed insights into the spatial dynamics of NIS interaction with the AP2 adaptor complex. These approaches would allow for real-time observation of NIS endocytosis and help validate the hypothesised mechanisms underlying NIS regulation and plasma membrane retention.

The protein PBF has been specifically implicated in the internalisation of NIS within clathrin-coated vesicles (Smith et al., 2009). Clathrin-mediated endocytosis occurs

through clathrin-coated pits, which are formed by the assembly of clathrin triskelia, each composed of three clathrin heavy chains and associated clathrin light chains. This process is facilitated by the AP2 complex (Mettlen et al., 2018). To further elucidate the potential interplay between PBF and AP2 in NIS endocytosis, a simultaneous siRNA knockdown of both genes could be performed, where an additive effect might suggest independent mechanisms of action. Conversely, if PBF and AP2 work in tandem, their cooperative interaction could be assessed using a NanoBiT assay and confocal imaging. Furthermore, the regulatory role of moesin in NIS internalisation should be validated, with a more detailed investigation into the interplay between NIS, AP2, PBF, and moesin necessary to develop a comprehensive model for NIS endocytosis.

7.2 Assessing the Impact of VCP Inhibitors CB-5083 and CB-5339 on Radioiodide Uptake in Breast Cancer

Breast cancer is the most prevalent cancer and the leading cause of cancer-related mortality among women globally (Lima et al., 2021). While the presence of NIS in breast cancer, including triple-negative subtypes, offers potential for radioiodide therapy, its predominantly cytoplasmic localisation poses a significant challenge (Elliyanti et al., 2020). Effective strategies to enhance NIS translocation to the plasma membrane are crucial for realising the therapeutic potential of radioiodine in treating breast cancer. Chapter 5 evaluated the impact of VCP inhibitors CB-5083 and CB-5339 on radioiodide uptake in breast cancer cell lines. Both inhibitors induced a dose-dependent increase in iodide uptake, but these effects were independent of NIS, as they were not inhibited by sodium perchlorate. Western blotting further confirmed low

or undetectable NIS protein levels, highlighting the challenge of low NIS expression in these breast cancer cells.

7.2.1 Future Directions

Given the findings from Chapter 5.1, future research should prioritise alternative strategies to manipulate the subcellular localisation of NIS, particularly by exploring both established and potentially novel binding partners. For instance, PBF has been shown to reduce plasma membrane expression of NIS in thyroid cancer, suggesting a similar mechanism could be at play in breast cancer (Smith et al., 2009). Targeting PBF phosphorylation may offer a promising approach to restoring NIS expression at the plasma membrane. Furthermore, insights from Chapters 3 and 4 underscore the involvement of the AP2 complex and moesin in NIS internalization in thyroid cancer cells. Further experiments can investigate whether these proteins similarly affect NIS expression in breast cancer cells, which could enhance the efficacy of radioiodide therapy in breast cancer.

Moreover, the inherently low NIS expression in breast cancer cells suggests that solely targeting post-translational processes may be insufficient. Future studies should incorporate approaches that include transcriptional activators, post-transcriptional modifications, and combinatorial treatments aimed at simultaneously boosting NIS expression at the plasma membrane and preventing its degradation.

The observed increase in ^{125}I uptake induced by CB-5083 and CB-5339 in a dose-dependent manner, which was not inhibited by sodium perchlorate, suggests that this

uptake is not mediated exclusively by NIS. Further research is needed to investigate the expression and functional roles of alternative iodide transporters, such as pendrin and SMCT, in breast cancer. Understanding these mechanisms in greater depth could lead to the identification of new therapeutic targets, ultimately enhancing the efficacy of radioiodine-based treatments in breast cancer.

7.3 Optimising Clotrimazole Derivatives and NMS-873 Compounds to Enhance NIS Function and Radioiodide Uptake in Cancer Cells

The study of Chapter 5.2 explored the potential of targeting the interaction between NIS and VCP using novel inhibitors to enhance radioiodide uptake in cancer cells. Experiments focused on the development and testing of clotrimazole-derived compounds and NMS-873 derivatives, aiming to improve their bioavailability and efficacy in enhancing NIS function. The clotrimazole derivative GB002 was developed to overcome the poor bioavailability of the parent compound, which would be unlikely to work *in vivo*. However, despite theoretical improvements, GB002 exhibited limited efficacy in enhancing iodide uptake in the tested NIS-expressing cell lines. Further optimisation would be required to realise the full potential of this compound class *in vivo*.

Following this, the development of NMS-873 derivatives (Compounds 22-25) to enhance VCP interaction and bioavailability was investigated. While these compounds demonstrated modest improvements in iodide uptake in the 8505C-NIS cell line, their overall efficacy was limited, as evidenced by the NanoBiT assay results, which showed only moderate disruption of the NIS-VCP interaction. This suggests that while these

compounds can interfere with the VCP-NIS interaction, their impact is not as pronounced as that of previously tested VCP inhibitors like CB-5083 and CB-5339.

7.3.1 Future Directions

7.3.1.1 Optimisation of VCP Inhibitors

The data presented in Chapter 5.2 showed the modest efficacy observed with GB002 and the NMS-873 derivatives, suggesting that further structural refinement to optimise the structure of VCP inhibitors to improve their bioavailability and efficacy is needed. Computational modelling and in silico design, as employed in exploring additional chemical modifications that enhance binding affinity and specificity for VCP, would be required.

7.3.1.2 Combination Therapies

The combination of VCP inhibitors with other therapeutic agents, such as SAHA, has shown some promise. Future studies should explore additional combinational strategies, including the use of transcriptional activators, to simultaneously enhance NIS expression and prevent its degradation. This multi-targeted approach could lead to more robust increases in radioiodide uptake and improve therapeutic outcomes.

7.3.1.3 Investigating Mechanistic Pathways

Mechanistic insights gained from mass spectrometry, which identified novel interacting partners of NIS, previously revealed the pivotal role of VCP in NIS protein processing (Fletcher et al., 2020). Understanding the precise mechanisms by which VCP inhibitors, both competitive and allosteric, affect NIS function is crucial for advancing these compounds toward clinical application. Future studies should delve deeper into the pathways involved in NIS regulation, including the roles of proteasomal degradation and transcriptomic analyses to identify the key players and pathways that are modulated by VCP inhibition.

Additionally, the crucial cofactor of VCP, NPL4, has been shown to be inhibited by disulfiram through its copper-bound diethyldithiocarbamate, $Cu(DDC)_2$ (Skrott et al., 2017). Investigating alternative pathways of VCP inhibition, such as the use of $Cu(DDC)_2$, which has shown dual activity in modulating both NIS transcription and proteasomal degradation *in vitro* and *vivo*, could offer new insights into how VCP inhibitors can be optimised for therapeutic use (unpublished data, McCabe group). The potential for $Cu(DDC)_2$ to be nanoencapsulated for improved *in vivo* stability and bioavailability should also be explored further in preclinical models, with an emphasis on its effects on thyroid and other NIS-expressing cancers.

7.3.1.4 Translating Research to Clinical Applications

The ultimate goal of these studies is to translate the findings into clinically viable therapies for patients with radioiodine-refractory cancers. Future research should

prioritise the development of preclinical models that closely mimic human disease, allowing for a more accurate assessment of the efficacy and safety of these novel VCP inhibitors. This includes expanding the use of xenograft models and genetically engineered mouse models that can provide insights into how these compounds perform in a more complex biological environment.

7.4 Investigating the Role of NIS Dimerisation

Chapter 6 has provided new insights into the potential role of specific residues within the putative dimerisation interface of NIS in its dimerisation, function and subcellular localisation. Through the application of NanoBiT and NanoBRET assays, radioiodide uptake assays and Western blotting, the study identified that mutants at residues K554 and R555 appear to significantly impair NIS interaction, reduce iodide uptake and might alter NIS protein expression and localisation. However, while the data suggest that K554 and R555 are important for NIS dimerisation, function and trafficking, the conclusions drawn are based on indirect measurements. The NanoBiT assay, which indicated a reduction in luminescence due to mutations, does not definitively confirm that dimerisation is disrupted; it only suggests a potential impact. Similarly, the NanoBRET assays indicated altered NIS trafficking and localisation, but these findings require further validation. The results suggest that proper dimerisation does impact NIS function and its correct trafficking to the plasma membrane, but more conclusive evidence is needed. Given these limitations, the current hypothesis—that residues K554 and R555 are crucial for NIS dimerisation and that their mutation disrupts NIS function—requires further validation through additional experiments.

7.4.1 Future Directions

To conclusively validate the findings and further explore the role of NIS dimerisation, several future research directions are needed. This would include co-immunoprecipitation (Co-IP) to assess whether the mutations at K554 and R555 disrupt the physical interaction between NIS monomers. Additionally, proximity ligation assay (PLA) and FRET can offer quantitative insights into the interaction, confirming whether the mutations indeed disrupt dimerisation and to validate NanoBiT results.

Furthermore, validation of NIS localisation and trafficking is essential. Immunofluorescence microscopy could be utilised to validate the NanoBRET data, offering visual confirmation of NIS localisation. This technique will help determine if mutations in K554 and R555 lead to ER retention or altered trafficking of NIS. Live-cell imaging, such as TIRFM or luminescence imaging, could provide real-time insights into NIS trafficking and plasma membrane localisation, further appraising the NanoBRET findings. Further functional analysis is also necessary to understand the broader implications of disrupted NIS dimerisation, such as cross-linking studies and CSBA, to help assess the structural integrity and oligomeric state of NIS, providing additional insights into how mutations impact dimerisation and NIS protein expression. Since the current study focused on specific residues within the putative dimerisation interface, future work should investigate other residues within these and other potential dimerisation interfaces. This could involve mutagenesis screens combined with functional assays to map out the full dimerisation interface and identify other critical residues.

Moreover, future studies should investigate the effect of K554 and R555 mutations in different cellular and tissue contexts, particularly *in vivo* models. It is essential to determine whether RAI-refractory thyroid cancer exhibits impaired NIS dimerisation, and if this impairment contributes to the commonly observed decrease in NIS localisation to the PM in DTC.

7.5 Concluding Remarks

This thesis has provided significant insights into the molecular mechanisms regulating NIS function, particularly focusing on the roles of AP2, PBF, moesin and newly identified endocytosis motifs within the NIS C-terminus. The research has expanded the understanding of NIS dimerisation, trafficking and degradation, offering potential therapeutic targets to enhance NIS-mediated radioiodide uptake in thyroid and breast cancer. The studies conducted here demonstrate that VCP inhibitors, including novel derivatives, can modulate NIS function, albeit not as potently as envisioned. Although the efficacy of these inhibitors *in vivo* remains to be fully explored, the results lay a foundation for future investigations into their therapeutic potential. Additionally, this research has identified critical residues within NIS that are essential for its dimerisation and proper function, with mutations at these sites leading to impaired iodide uptake and altered NIS expression. This investigation represents a step forward in the development of multi-targeted approaches to optimise NIS function and improve therapeutic outcomes for patients with radioiodide-refractory thyroid cancer and breast cancer. By focusing on both the post-translational regulation of NIS and the development of novel VCP inhibitors, this research contributes to a more

comprehensive strategy for enhancing the effectiveness of radioiodide therapy in cancer treatment.

CHAPTER 8 REFERENCES

Acuña-Ruiz, A., Carrasco-López, C., & Santisteban, P. (2023). Genomic and epigenomic profile of thyroid cancer. *Best Pract Res Clin Endocrinol Metab, 37*(1), 101656. doi:10.1016/j.beem.2022.101656

Agrawal, N., Akbani, R., Aksoy, B. A., Ally, A., Arachchi, H., Asa, S. L., . . . Baylin, S. B. (2014). Integrated genomic characterization of papillary thyroid carcinoma. *Cell, 159*(3), 676-690.

Ahn, B. C. (2012). Sodium iodide symporter for nuclear molecular imaging and gene therapy: from bedside to bench and back. *Theranostics, 2*(4), 392-402. doi:10.7150/thno.3722

Ajjan, R. A., Watson, P. F., Findlay, C., Metcalfe, R. A., Crisp, M., Ludgate, M., & Weetman, A. P. (1998). The sodium iodide symporter gene and its regulation by cytokines found in autoimmunity. *J Endocrinol, 158*(3), 351-358. doi:10.1677/joe.0.1580351

Al-Azzawi, A., & Takahashi, T. (2021). Anatomical variations of the thyroid gland: An experimental cadaveric study. *Ann Med Surg (Lond), 70*, 102823. doi:10.1016/j.amsu.2021.102823

Al-Jundi, M., Thakur, S., Gubbi, S., & Klubo-Gwiezdzinska, J. (2020). Novel Targeted Therapies for Metastatic Thyroid Cancer-A Comprehensive Review. *Cancers (Basel), 12*(8). doi:10.3390/cancers12082104

Alhejaily, A. G., Alhuzim, O., & Alwelaie, Y. (2023). Anaplastic thyroid cancer: Pathogenesis, prognostic factors and genetic landscape (Review). *Mol Clin Oncol, 19*(6), 99. doi:10.3892/mco.2023.2695

Alvarez-Nuñez, F., Bussaglia, E., Mauricio, D., Ybarra, J., Vilar, M., Lerma, E., . . . Matias-Guiu, X. (2006). PTEN promoter methylation in sporadic thyroid carcinomas. *Thyroid, 16*(1), 17-23. doi:10.1089/thy.2006.16.17

Alverez, C., Arkin, M. R., Bulfer, S. L., Colombo, R., Kovaliov, M., LaPorte, M. G., . . . Wipf, P. (2015). Structure-Activity Study of Bioisosteric Trifluoromethyl and Pentafluorosulfanyl Indole Inhibitors of the AAA ATPase p97. *ACS Med Chem Lett, 6*(12), 1225-1230. doi:10.1021/acsmedchemlett.5b00364

Anderson, D. J., Le Moigne, R., Djakovic, S., Kumar, B., Rice, J., Wong, S., . . . Rolfe, M. (2015). Targeting the AAA ATPase p97 as an Approach to Treat Cancer through Disruption of Protein Homeostasis. *Cancer Cell, 28*(5), 653-665. doi:10.1016/j.ccell.2015.10.002

Araque, K. A., Gubbi, S., & Klubo-Gwiezdzinska, J. (2020). Updates on the Management of Thyroid Cancer. *Horm Metab Res, 52*(8), 562-577. doi:10.1055/a-1089-7870

Are, C., & Shaha, A. R. (2006). Anaplastic Thyroid Carcinoma: Biology, Pathogenesis, Prognostic Factors, and Treatment Approaches. *Annals of Surgical Oncology, 13*(4), 453-464. doi:10.1245/ASO.2006.05.042

Arighi, E., Borrello, M. G., & Sariola, H. (2005). RET tyrosine kinase signaling in development and cancer. *Cytokine Growth Factor Rev, 16*(4-5), 441-467. doi:10.1016/j.cytogfr.2005.05.010

Arps, D. P., Healy, P., Zhao, L., Kleer, C. G., & Pang, J. C. (2013). Invasive ductal carcinoma with lobular features: a comparison study to invasive ductal and invasive lobular carcinomas of the breast. *Breast Cancer Res Treat, 138*(3), 719-726. doi:10.1007/s10549-013-2493-2

Asioli, S., Erickson, L. A., Righi, A., Jin, L., Volante, M., Jenkins, S., . . . Lloyd, R. V. (2010). Poorly differentiated carcinoma of the thyroid: validation of the Turin proposal and analysis of IMP3 expression. *Mod Pathol, 23*(9), 1269-1278. doi:10.1038/modpathol.2010.117

Aubert, G., & Lansdorp, P. M. (2008). Telomeres and aging. *Physiol Rev, 88*(2), 557-579. doi:10.1152/physrev.00026.2007

Baek, H. S., Ha, J., Ha, S., Bae, J. S., Jung, C. K., & Lim, D. J. (2023). Initial Experiences of Selective RET Inhibitor Selpercatinib in Adults with Metastatic Differentiated Thyroid Carcinoma and Medullary Thyroid Carcinoma: Real-World Case Series in Korea. *Curr Oncol, 30*(3), 3020-3031. doi:10.3390/curroncol30030229

Baloch, Z. W., Asa, S. L., Barletta, J. A., Ghossein, R. A., Juhlin, C. C., Jung, C. K., . . . Mete, O. (2022). Overview of the 2022 WHO Classification of Thyroid Neoplasms. *Endocr Pathol, 33*(1), 27-63. doi:10.1007/s12022-022-09707-3

Bandargal, S., Rajab, M., Forest, V. I., Pusztaszeri, M. P., Hier, M. P., da Silva, S. D., & Payne, R. J. (2023). Characteristics of PTEN Mutation in Thyroid Tumours: A Retrospective Chart Review. *Cancers (Basel), 15*(5). doi:10.3390/cancers15051575

Banerjee, S., Bartesaghi, A., Merk, A., Rao, P., Bulfer, S. L., Yan, Y., . . . Subramaniam, S. (2016). 2.3 Å resolution cryo-EM structure of human p97 and mechanism of allosteric inhibition. *Science, 351*(6275), 871-875. doi:10.1126/science.aad7974

Barroso-González, J., Machado, J. D., García-Expósito, L., & Valenzuela-Fernández, A. (2009). Moesin regulates the trafficking of nascent clathrin-coated vesicles. *J Biol Chem, 284*(4), 2419-2434. doi:10.1074/jbc.M805311200

Beacham, G. M., Partlow, E. A., & Hollopeter, G. (2019). Conformational regulation of AP1 and AP2 clathrin adaptor complexes. *Traffic, 20*(10), 741-751. doi:10.1111/tra.12677

Beňačka, R., Szabóová, D., Guľašová, Z., Hertelyová, Z., & Radoňák, J. (2022). Classic and New Markers in Diagnostics and Classification of Breast Cancer. *Cancers (Basel), 14*(21). doi:10.3390/cancers14215444

Bergström, C. A. S., & Larsson, P. (2018). Computational prediction of drug solubility in water-based systems: Qualitative and quantitative approaches used in the current drug discovery and development setting. *Int J Pharm, 540*(1-2), 185-193. doi:10.1016/j.ijpharm.2018.01.044

Bible, K. C., Kebebew, E., Brierley, J., Brito, J. P., Cabanillas, M. E., Clark, T. J., Jr., . . . Wong-Clark, C. K. (2021). 2021 American Thyroid Association Guidelines for Management of Patients with Anaplastic Thyroid Cancer. *Thyroid, 31*(3), 337-386. doi:10.1089/thy.2020.0944

Bikas, A., Ahmadi, S., Pappa, T., Marqusee, E., Wong, K., Nehs, M. A., . . . Landa, I. (2023). Additional Oncogenic Alterations in RAS-Driven Differentiated Thyroid Cancers Associate with Worse Clinicopathologic Outcomes. *Clin Cancer Res, 29*(14), 2678-2685. doi:10.1158/1078-0432.Ccr-23-0278

Biondi, B., & Cooper, D. S. (2019). Thyroid Hormone Suppression Therapy. *Endocrinol Metab Clin North Am, 48*(1), 227-237. doi:10.1016/j.ecl.2018.10.008

Biondi, B., Filetti, S., & Schlumberger, M. (2005). Thyroid-hormone therapy and thyroid cancer: a reassessment. *Nat Clin Pract Endocrinol Metab, 1*(1), 32-40. doi:10.1038/ncpendmet0020

Bischoff, L. A., Ganly, I., Fugazzola, L., Buczek, E., Faquin, W. C., Haugen, B. R., . . . Randolph, G. W. (2024). Molecular Alterations and Comprehensive Clinical Management of Oncocytic Thyroid Carcinoma: A Review and Multidisciplinary 2023 Update. *JAMA Otolaryngol Head Neck Surg, 150*(3), 265-272. doi:10.1001/jamaoto.2023.4323

Blasco, M. A. (2005). Telomeres and human disease: ageing, cancer and beyond. *Nat Rev Genet, 6*(8), 611-622. doi:10.1038/nrg1656

Bocharov, E. V., Mineev, K. S., Volynsky, P. E., Ermolyuk, Y. S., Tkach, E. N., Sobol, A. G., . . . Arseniev, A. S. (2008). Spatial structure of the dimeric transmembrane domain of the growth factor receptor ErbB2 presumably corresponding to the receptor active state. *J Biol Chem, 283*(11), 6950-6956. doi:10.1074/jbc.M709202200

Boelaert, K., & Franklyn, J. A. (2005). Thyroid hormone in health and disease. *J Endocrinol, 187*(1), 1-15. doi:10.1677/joe.1.06131

Boelaert, K., Smith, V. E., Stratford, A. L., Kogai, T., Tannahill, L. A., Watkinson, J. C., . . . McCabe, C. J. (2007). PTTG and PBF repress the human sodium iodide symporter. *Oncogene, 26*(30), 4344-4356. doi:10.1038/sj.onc.1210221

Boguski, M. S., & McCormick, F. (1993). Proteins regulating Ras and its relatives. *Nature, 366*(6456), 643-654. doi:10.1038/366643a0

Bond, J. A., Wyllie, F. S., Rowson, J., Radulescu, A., & Wynford-Thomas, D. (1994). In vitro reconstruction of tumour initiation in a human epithelium. *Oncogene, 9*(1), 281-290.

Bork, P., Doerks, T., Springer, T. A., & Snel, B. (1999). Domains in plexins: links to integrins and transcription factors. *Trends Biochem Sci, 24*(7), 261-263. doi:10.1016/s0968-0004(99)01416-4

Boucai, L., Zafereo, M., & Cabanillas, M. E. (2024). Thyroid Cancer: A Review. *Jama, 331*(5), 425-435. doi:10.1001/jama.2023.26348

Braverman, L. E., & Ingbar, S. H. (1963). CHANGES IN THYROIDAL FUNCTION DURING ADAPTATION TO LARGE DOSES OF IODIDE. *J Clin Invest, 42*(8), 1216-1231. doi:10.1172/jci104807

Brent, G. A. (2012). Mechanisms of thyroid hormone action. *J Clin Invest, 122*(9), 3035-3043. doi:10.1172/jci60047

Bretscher, A., Edwards, K., & Fehon, R. G. (2002). ERM proteins and merlin: integrators at the cell cortex. *Nat Rev Mol Cell Biol, 3*(8), 586-599. doi:10.1038/nrm882

Brix, K., Lemansky, P., & Herzog, V. (1996). Evidence for extracellularly acting cathepsins mediating thyroid hormone liberation in thyroid epithelial cells. *Endocrinology, 137*(5), 1963-1974. doi:10.1210/endo.137.5.8612537

Brodsky, F. M., Chen, C. Y., Knuehl, C., Towler, M. C., & Wakeham, D. E. (2001). Biological basket weaving: formation and function of clathrin-coated vesicles. *Annu Rev Cell Dev Biol, 17*, 517-568. doi:10.1146/annurev.cellbio.17.1.517

Brose, M. S., Robinson, B. G., Sherman, S. I., Jarzab, B., Lin, C. C., Vaisman, F., . . . Capdevila, J. (2022). Cabozantinib for previously treated radioiodine-refractory differentiated thyroid cancer: Updated results from the phase 3 COSMIC-311 trial. *Cancer, 128*(24), 4203-4212. doi:10.1002/cncr.34493

Brown, L. M., Helmke, S. M., Hunsucker, S. W., Netea-Maier, R. T., Chiang, S. A., Heinz, D. E., . . . Haugen, B. R. (2006). Quantitative and qualitative differences in protein expression between papillary thyroid carcinoma and normal thyroid tissue. *Mol Carcinog, 45*(8), 613-626. doi:10.1002/mc.20193

Cabanillas, M., Drilon, A., Farago, A., Brose, M., McDermott, R., Sohal, D., . . . Chu, E. (2020). 1916P Larotrectinib treatment of advanced TRK fusion thyroid cancer. *Annals of Oncology, 31*, S1086.

Cabanillas, M. E., McFadden, D. G., & Durante, C. (2016). Thyroid cancer. *Lancet, 388*(10061), 2783-2795. doi:10.1016/s0140-6736(16)30172-6

Cabanillas, M. E., McFadden, D. G., & Durante, C. (2016). Thyroid cancer. *The Lancet, 388*(10061), 2783-2795. Retrieved from

https://www.thelancet.com/journals/lancet/article/PIIS0140-6736(16)30172-6/abstract

Calil-Silveira, J., Serrano-Nascimento, C., Laconca, R. C., Schmiedecke, L., Salgueiro, R. B., Kondo, A. K., & Nunes, M. T. (2016). Underlying Mechanisms of Pituitary-Thyroid Axis Function Disruption by Chronic Iodine Excess in Rats. *Thyroid, 26*(10), 1488-1498. doi:10.1089/thy.2015.0338

Canberk, S., Lima, A. R., Correia, M., Batista, R., Soares, P., Máximo, V., & Simões, M. S. (2019). Oncocytic thyroid neoplasms: from histology to molecular biology. *Diagnostic Histopathology, 25*(5), 154-165.

Cancroft, E. T., & Goldsmith, S. J. (1973). 99m Tc-pertechnetate scintigraphy as an aid in the diagnosis of breast masses. *Radiology, 106*(2), 441-444. doi:10.1148/106.2.441

Capdevila, J., Awada, A., Führer-Sakel, D., Leboulleux, S., & Pauwels, P. (2022). Molecular diagnosis and targeted treatment of advanced follicular cell-derived thyroid cancer in the precision medicine era. *Cancer Treat Rev, 106*, 102380. doi:10.1016/j.ctrv.2022.102380

Capdevila, J., Wirth, L. J., Ernst, T., Ponce Aix, S., Lin, C. C., Ramlau, R., . . . Taylor, M. (2020). PD-1 Blockade in Anaplastic Thyroid Carcinoma. *J Clin Oncol, 38*(23), 2620-2627. doi:10.1200/jco.19.02727

Carrasco, N. (1993). Iodide transport in the thyroid gland. *Biochim Biophys Acta, 1154*(1), 65-82. doi:10.1016/0304-4157(93)90017-i

Carvalho, D. P., & Dupuy, C. (2017). Thyroid hormone biosynthesis and release. *Mol Cell Endocrinol, 458*, 6-15. doi:10.1016/j.mce.2017.01.038

Cavalieri, R. R. (1997). Iodine metabolism and thyroid physiology: current concepts. *Thyroid, 7*(2), 177-181. doi:10.1089/thy.1997.7.177

Chaker, L., Bianco, A. C., Jonklaas, J., & Peeters, R. P. (2017). Hypothyroidism. *Lancet, 390*(10101), 1550-1562. doi:10.1016/s0140-6736(17)30703-1

Charafe-Jauffret, E., Monville, F., Bertucci, F., Esterni, B., Ginestier, C., Finetti, P., . . . Jacquemier, J. (2007). Moesin expression is a marker of basal breast carcinomas. *Int J Cancer, 121*(8), 1779-1785. doi:10.1002/ijc.22923

Chen, B., Shi, Y., Xu, Y., & Zhang, J. (2021). The predictive value of coexisting BRAFV600E and TERT promoter mutations on poor outcomes and high tumour aggressiveness in papillary thyroid carcinoma: A systematic review and meta-analysis. *Clinical endocrinology, 94*(5), 731-742.

Chen, C., & Liu, J. (2022). Histone acetylation modifications: A potential targets for the diagnosis and treatment of papillary thyroid cancer. *Front Oncol, 12*, 1053618. doi:10.3389/fonc.2022.1053618

Chen, C. Y., Chen, J., He, L., & Stiles, B. L. (2018). PTEN: Tumor Suppressor and Metabolic Regulator. *Front Endocrinol (Lausanne), 9*, 338. doi:10.3389/fendo.2018.00338

Chen, Y., Xu, Z., Chen, Y., Dai, Y., & Ding, J. (2024). Comparison of the prognosis of medullary breast carcinoma and invasive ductal carcinoma: a SEER-based study. *Transl Cancer Res, 13*(1), 231-248. doi:10.21037/tcr-23-858

Cheng, C., Weiss, L., Leinonen, H., Shmara, A., Yin, H. Z., Ton, T., . . . Kimonis, V. (2022). VCP/p97 inhibitor CB-5083 modulates muscle pathology in a mouse model of VCP inclusion body myopathy. *J Transl Med, 20*(1), 21. doi:10.1186/s12967-021-03186-6

Cheng, S. Y., Leonard, J. L., & Davis, P. J. (2010). Molecular aspects of thyroid hormone actions. *Endocr Rev, 31*(2), 139-170. doi:10.1210/er.2009-0007

Cheng, W., Liu, R., Zhu, G., Wang, H., & Xing, M. (2016). Robust Thyroid Gene Expression and Radioiodine Uptake Induced by Simultaneous Suppression of BRAF V600E and Histone Deacetylase in Thyroid Cancer Cells. *J Clin Endocrinol Metab, 101*(3), 962-971. doi:10.1210/jc.2015-3433

Chiamolera, M. I., & Wondisford, F. E. (2009). Minireview: Thyrotropin-releasing hormone and the thyroid hormone feedback mechanism. *Endocrinology, 150*(3), 1091-1096. doi:10.1210/en.2008-1795

Chien, W., & Pei, L. (2000). A novel binding factor facilitates nuclear translocation and transcriptional activation function of the pituitary tumor-transforming gene product. *J Biol Chem, 275*(25), 19422-19427. doi:10.1074/jbc.M910105199

Chintakuntlawar, A. V., Foote, R. L., Kasperbauer, J. L., & Bible, K. C. (2019). Diagnosis and Management of Anaplastic Thyroid Cancer. *Endocrinol Metab Clin North Am, 48*(1), 269-284. doi:10.1016/j.ecl.2018.10.010

Cho, J. Y., Léveillé, R., Kao, R., Rousset, B., Parlow, A. F., Burak, W. E., Jr., . . . Jhiang, S. M. (2000). Hormonal regulation of radioiodide uptake activity and Na+/I- symporter expression in mammary glands. *J Clin Endocrinol Metab, 85*(8), 2936-2943. doi:10.1210/jcem.85.8.6727

Chou, C. K., Liu, R. T., & Kang, H. Y. (2017). MicroRNA-146b: A Novel Biomarker and Therapeutic Target for Human Papillary Thyroid Cancer. *Int J Mol Sci, 18*(3). doi:10.3390/ijms18030636

Chou, T. F., Bulfer, S. L., Weihl, C. C., Li, K., Lis, L. G., Walters, M. A., . . . Arkin, M. R. (2014). Specific inhibition of p97/VCP ATPase and kinetic analysis demonstrate interaction between D1 and D2 ATPase domains. *J Mol Biol, 426*(15), 2886-2899. doi:10.1016/j.jmb.2014.05.022

Christofer Juhlin, C., Mete, O., & Baloch, Z. W. (2023). The 2022 WHO classification of thyroid tumors: novel concepts in nomenclature and grading. *Endocr Relat Cancer, 30*(2). doi:10.1530/erc-22-0293

Chung, T., Youn, H., Yeom, C. J., Kang, K. W., & Chung, J. K. (2015). Glycosylation of Sodium/Iodide Symporter (NIS) Regulates Its Membrane Translocation and Radioiodine Uptake. *PLoS One, 10*(11), e0142984. doi:10.1371/journal.pone.0142984

Ciregia, F., Giusti, L., Molinaro, A., Niccolai, F., Agretti, P., Rago, T., . . . Lucacchini, A. (2013). Presence in the pre-surgical fine-needle aspiration of potential thyroid biomarkers previously identified in the post-surgical one. *PLoS One, 8*(9), e72911. doi:10.1371/journal.pone.0072911

Citterio, C. E., Targovnik, H. M., & Arvan, P. (2019). The role of thyroglobulin in thyroid hormonogenesis. *Nat Rev Endocrinol, 15*(6), 323-338. doi:10.1038/s41574-019-0184-8

Collins, B. M., McCoy, A. J., Kent, H. M., Evans, P. R., & Owen, D. J. (2002). Molecular architecture and functional model of the endocytic AP2 complex. *Cell, 109*(4), 523-535. doi:10.1016/s0092-8674(02)00735-3

Colombo, C., Pogliaghi, G., Tosi, D., Muzza, M., Bulfamante, G., Persani, L., . . . Cirello, V. (2022). Thyroid cancer harboring PTEN and TP53 mutations: A peculiar molecular and clinical case report. *Front Oncol, 12*, 949098. doi:10.3389/fonc.2022.949098

Cooper, D. S., & Biondi, B. (2012). Subclinical thyroid disease. *Lancet, 379*(9821), 1142-1154. doi:10.1016/s0140-6736(11)60276-6

Cooper, D. S., Doherty, G. M., Haugen, B. R., Kloos, R. T., Lee, S. L., Mandel, S. J., . . . Tuttle, R. M. (2009). Revised American Thyroid Association management guidelines for

patients with thyroid nodules and differentiated thyroid cancer. *Thyroid, 19*(11), 1167-1214. doi:10.1089/thy.2009.0110

Costamagna, E., García, B., & Santisteban, P. (2004). The functional interaction between the paired domain transcription factor Pax8 and Smad3 is involved in transforming growth factor-beta repression of the sodium/iodide symporter gene. *J Biol Chem, 279*(5), 3439-3446. doi:10.1074/jbc.M307138200

Costantini, S., Capone, F., Polo, A., Bagnara, P., & Budillon, A. (2021). Valosin-Containing Protein (VCP)/p97: A Prognostic Biomarker and Therapeutic Target in Cancer. *Int J Mol Sci, 22*(18). doi:10.3390/ijms221810177

Cui, Y., Niu, M., Zhang, X., Zhong, Z., Wang, J., & Pang, D. (2015). High expression of valosin-containing protein predicts poor prognosis in patients with breast carcinoma. *Tumour Biol, 36*(12), 9919-9927. doi:10.1007/s13277-015-3748-9

Dai, G., Levy, O., & Carrasco, N. (1996). Cloning and characterization of the thyroid iodide transporter. *Nature, 379*(6564), 458-460. doi:10.1038/379458a0

Dal Maso, L., Bosetti, C., La Vecchia, C., & Franceschi, S. (2009). Risk factors for thyroid cancer: an epidemiological review focused on nutritional factors. *Cancer Causes Control, 20*(1), 75-86. doi:10.1007/s10552-008-9219-5

Dal Maso, L., Panato, C., Franceschi, S., Serraino, D., Buzzoni, C., Busco, S., . . . Vaccarella, S. (2018). The impact of overdiagnosis on thyroid cancer epidemic in Italy,1998-2012. *Eur J Cancer, 94*, 6-15. doi:10.1016/j.ejca.2018.01.083

Darrouzet, E., Graslin, F., Marcellin, D., Tcheremisinova, I., Marchetti, C., Salleron, L., . . . Pourcher, T. (2016). A systematic evaluation of sorting motifs in the sodium-iodide symporter (NIS). *Biochem J, 473*(7), 919-928. doi:10.1042/bj20151086

Deshaies, R. J. (2014). Proteotoxic crisis, the ubiquitin-proteasome system, and cancer therapy. *BMC Biol, 12*, 94. doi:10.1186/s12915-014-0094-0

Dixon, A. S., Schwinn, M. K., Hall, M. P., Zimmerman, K., Otto, P., Lubben, T. H., . . . Wood, K. V. (2016). NanoLuc Complementation Reporter Optimized for Accurate Measurement of Protein Interactions in Cells. *ACS Chem Biol, 11*(2), 400-408. doi:10.1021/acschembio.5b00753

Dobson, M. E., Diallo-Krou, E., Grachtchouk, V., Yu, J., Colby, L. A., Wilkinson, J. E., . . . Koenig, R. J. (2011). Pioglitazone induces a proadipogenic antitumor response in mice with PAX8-PPARgamma fusion protein thyroid carcinoma. *Endocrinology, 152*(11), 4455-4465. doi:10.1210/en.2011-1178

Dohán, O., De la Vieja, A., Paroder, V., Riedel, C., Artani, M., Reed, M., . . . Carrasco, N. (2003). The sodium/iodide Symporter (NIS): characterization, regulation, and medical significance. *Endocr Rev, 24*(1), 48-77. doi:10.1210/er.2001-0029

Dohán, O., Portulano, C., Basquin, C., Reyna-Neyra, A., Amzel, L. M., & Carrasco, N. (2007). The Na+/I symporter (NIS) mediates electroneutral active transport of the environmental pollutant perchlorate. *Proc Natl Acad Sci U S A, 104*(51), 20250-20255. doi:10.1073/pnas.0707207104

Duan, H., Li, Y., Hu, P., Gao, J., Ying, J., Xu, W., . . . Liang, Z. (2019). Mutational profiling of poorly differentiated and anaplastic thyroid carcinoma by the use of targeted next-generation sequencing. *Histopathology, 75*(6), 890-899. doi:10.1111/his.13942

Dufey, E., Urra, H., & Hetz, C. (2015). ER proteostasis addiction in cancer biology: Novel concepts. *Semin Cancer Biol, 33*, 40-47. doi:10.1016/j.semcancer.2015.04.003

Eggo, M. C., King, W. J., Black, E. G., & Sheppard, M. C. (1996). Functional human thyroid cells and their insulin-like growth factor-binding proteins: regulation by thyrotropin,

cyclic 3',5' adenosine monophosphate, and growth factors. *J Clin Endocrinol Metab, 81*(8), 3056-3062. doi:10.1210/jcem.81.8.8768874

Elisei, R., Schlumberger, M. J., Müller, S. P., Schöffski, P., Brose, M. S., Shah, M. H., . . . Sherman, S. I. (2013). Cabozantinib in progressive medullary thyroid cancer. *J Clin Oncol, 31*(29), 3639-3646. doi:10.1200/jco.2012.48.4659

Elliyanti, A., Rusnita, D., Afriani, N., Susanto, Y. D. B., Susilo, V. Y., Setiyowati, S., & Harahap, W. A. (2020). Analysis Natrium Iodide Symporter Expression in Breast Cancer Subtypes for Radioiodine Therapy Response. *Nucl Med Mol Imaging, 54*(1), 35-42. doi:10.1007/s13139-019-00632-8

Eng, P. H., Cardona, G. R., Fang, S. L., Previti, M., Alex, S., Carrasco, N., . . . Braverman, L. E. (1999). Escape from the acute Wolff-Chaikoff effect is associated with a decrease in thyroid sodium/iodide symporter messenger ribonucleic acid and protein. *Endocrinology, 140*(8), 3404-3410. doi:10.1210/endo.140.8.6893

Eng, P. H., Cardona, G. R., Previti, M. C., Chin, W. W., & Braverman, L. E. (2001). Regulation of the sodium iodide symporter by iodide in FRTL-5 cells. *Eur J Endocrinol, 144*(2), 139-144. doi:10.1530/eje.0.1440139

Enumah, S., Fingeret, A., Parangi, S., Dias-Santagata, D., Sadow, P. M., & Lubitz, C. C. (2020). BRAF(V600E) Mutation is Associated with an Increased Risk of Papillary Thyroid Cancer Recurrence. *World J Surg, 44*(8), 2685-2691. doi:10.1007/s00268-020-05521-2

Eskandari, S., Loo, D. D., Dai, G., Levy, O., Wright, E. M., & Carrasco, N. (1997). Thyroid Na+/I- symporter. Mechanism, stoichiometry, and specificity. *J Biol Chem, 272*(43), 27230-27238. doi:10.1074/jbc.272.43.27230

ESKIN, B. A., PARKER, J. A., BASSETT, J. G., & GEORGE, D. L. (1974). Human breast uptake of radioactive iodine. *Obstetrics & Gynecology, 44*(3), 398-402.

Fayard, E., Tintignac, L. A., Baudry, A., & Hemmings, B. A. (2005). Protein kinase B/Akt at a glance. *J Cell Sci, 118*(Pt 24), 5675-5678. doi:10.1242/jcs.02724

Fehon, R. G., McClatchey, A. I., & Bretscher, A. (2010). Organizing the cell cortex: the role of ERM proteins. *Nat Rev Mol Cell Biol, 11*(4), 276-287. doi:10.1038/nrm2866

Felice, M. D., & Lauro, R. D. (2004). Thyroid development and its disorders: genetics and molecular mechanisms. *Endocr Rev, 25*(5), 722-746. doi:10.1210/er.2003-0028

Feng, F., Yehia, L., Ni, Y., Chang, Y. S., Jhiang, S. M., & Eng, C. (2018). A Nonpump Function of Sodium Iodide Symporter in Thyroid Cancer via Cross-talk with PTEN Signaling. *Cancer Res, 78*(21), 6121-6133. doi:10.1158/0008-5472.Can-18-1954

Ferrari, S. M., Fallahi, P., Politti, U., Materazzi, G., Baldini, E., Ulisse, S., . . . Antonelli, A. (2015). Molecular Targeted Therapies of Aggressive Thyroid Cancer. *Front Endocrinol (Lausanne), 6*, 176. doi:10.3389/fendo.2015.00176

Fiévet, B., Louvard, D., & Arpin, M. (2007). ERM proteins in epithelial cell organization and functions. *Biochim Biophys Acta, 1773*(5), 653-660. doi:10.1016/j.bbamcr.2006.06.013

Fletcher, A., Read, M. L., Thornton, C. E. M., Larner, D. P., Poole, V. L., Brookes, K., . . . McCabe, C. J. (2020). Targeting Novel Sodium Iodide Symporter Interactors ADP-Ribosylation Factor 4 and Valosin-Containing Protein Enhances Radioiodine Uptake. *Cancer Res, 80*(1), 102-115. doi:10.1158/0008-5472.Can-19-1957

Fonseca, T. L., Correa-Medina, M., Campos, M. P., Wittmann, G., Werneck-de-Castro, J. P., Arrojo e Drigo, R., . . . Bianco, A. C. (2013). Coordination of hypothalamic and

pituitary T3 production regulates TSH expression. *J Clin Invest, 123*(4), 1492-1500. doi:10.1172/jci61231

Frattini, M., Ferrario, C., Bressan, P., Balestra, D., De Cecco, L., Mondellini, P., . . . Greco, A. (2004). Alternative mutations of BRAF, RET and NTRK1 are associated with similar but distinct gene expression patterns in papillary thyroid cancer. *Oncogene, 23*(44), 7436-7440. doi:10.1038/sj.onc.1207980

Furuya-Kanamori, L., Bell, K. J. L., Clark, J., Glasziou, P., & Doi, S. A. R. (2016). Prevalence of Differentiated Thyroid Cancer in Autopsy Studies Over Six Decades: A Meta-Analysis. *J Clin Oncol, 34*(30), 3672-3679. doi:10.1200/jco.2016.67.7419

Fuziwara, C. S., Saito, K. C., & Kimura, E. T. (2020). Thyroid Follicular Cell Loss of Differentiation Induced by MicroRNA miR-17-92 Cluster Is Attenuated by CRISPR/Cas9n Gene Silencing in Anaplastic Thyroid Cancer. *Thyroid, 30*(1), 81-94. doi:10.1089/thy.2018.0601

Galrão, A. L., Camargo, R. Y., Friguglietti, C. U., Moraes, L., Cerutti, J. M., Serrano-Nascimento, C., . . . Rubio, I. G. (2014). Hypermethylation of a New Distal Sodium/Iodide Symporter (NIS) enhancer (NDE) is associated with reduced NIS expression in thyroid tumors. *J Clin Endocrinol Metab, 99*(6), E944-952. doi:10.1210/jc.2013-1450

García, B., & Santisteban, P. (2002). PI3K is involved in the IGF-I inhibition of TSH-induced sodium/iodide symporter gene expression. *Mol Endocrinol, 16*(2), 342-352. doi:10.1210/mend.16.2.0774

García-Solís, P., Alfaro, Y., Anguiano, B., Delgado, G., Guzman, R. C., Nandi, S., . . . Aceves, C. (2005). Inhibition of N-methyl-N-nitrosourea-induced mammary carcinogenesis by molecular iodine (I2) but not by iodide (I-) treatment Evidence that I2 prevents cancer promotion. *Mol Cell Endocrinol, 236*(1-2), 49-57. doi:10.1016/j.mce.2005.03.001

Gershengorn, M. C. (1993). Thyrotropin-releasing hormone receptor: cloning and regulation of its expression. *Recent Prog Horm Res, 48*, 341-363. doi:10.1016/b978-0-12-571148-7.50016-6

Giordano, T. J., Haugen, B. R., Sherman, S. I., Shah, M. H., Caoili, E. M., & Koenig, R. J. (2018). Pioglitazone Therapy of PAX8-PPARγ Fusion Protein Thyroid Carcinoma. *J Clin Endocrinol Metab, 103*(4), 1277-1281. doi:10.1210/jc.2017-02533

Gire, V., & Wynford-Thomas, D. (2000). RAS oncogene activation induces proliferation in normal human thyroid epithelial cells without loss of differentiation. *Oncogene, 19*(6), 737-744. doi:10.1038/sj.onc.1203399

Gogna, S., Goldberg, M., Samson, D., Gachabayov, M., Felsenreich, D. M., Azim, A., & Dong, X. D. E. (2020). Medullary Thyroid Cancer in Patients Older than 45-Epidemiologic Trends and Predictors of Survival. *Cancers (Basel), 12*(11). doi:10.3390/cancers12113124

González-Pérez, P., Cirulli, E. T., Drory, V. E., Dabby, R., Nisipeanu, P., Carasso, R. L., . . . Blumen, S. C. (2012). Novel mutation in VCP gene causes atypical amyotrophic lateral sclerosis. *Neurology, 79*(22), 2201-2208. doi:10.1212/WNL.0b013e318275963b

Gouveia, C., Can, N. T., Bostrom, A., Grenert, J. P., van Zante, A., & Orloff, L. A. (2013). Lack of association of BRAF mutation with negative prognostic indicators in papillary thyroid carcinoma: the University of California, San Francisco, experience. *JAMA Otolaryngol Head Neck Surg, 139*(11), 1164-1170. doi:10.1001/jamaoto.2013.4501

Grasberger, H., Ringkananont, U., Lefrancois, P., Abramowicz, M., Vassart, G., & Refetoff, S. (2005). Thyroid transcription factor 1 rescues PAX8/p300 synergism impaired by a

natural PAX8 paired domain mutation with dominant negative activity. *Mol Endocrinol, 19*(7), 1779-1791. doi:10.1210/me.2004-0426

Greider, C. W., & Blackburn, E. H. (2004). Tracking telomerase. *Cell, 116*(2 Suppl), S83-86, 81 p following S86. doi:10.1016/s0092-8674(04)00053-4

Grieco, M., Santoro, M., Berlingieri, M. T., Melillo, R. M., Donghi, R., Bongarzone, I., . . . Vecchio, G. (1990). PTC is a novel rearranged form of the ret proto-oncogene and is frequently detected in vivo in human thyroid papillary carcinomas. *Cell, 60*(4), 557-563. doi:10.1016/0092-8674(90)90659-3

Groot, J. W. d., Links, T. P., Plukker, J. T., Lips, C. J., & Hofstra, R. M. (2006). RET as a diagnostic and therapeutic target in sporadic and hereditary endocrine tumors. *Endocr Rev, 27*(5), 535-560. doi:10.1210/er.2006-0017

Guan, L., Zhao, X., Tang, L., Chen, J., Zhao, J., Guo, M., . . . Xu, L. (2021). Thyroid Transcription Factor-1: Structure, Expression, Function and Its Relationship with Disease. *Biomed Res Int, 2021*, 9957209. doi:10.1155/2021/9957209

Gupta, N., Martin, P. M., Prasad, P. D., & Ganapathy, V. (2006). SLC5A8 (SMCT1)-mediated transport of butyrate forms the basis for the tumor suppressive function of the transporter. *Life Sci, 78*(21), 2419-2425. doi:10.1016/j.lfs.2005.10.028

Gustafson, S., Zbuk, K. M., Scacheri, C., & Eng, C. (2007). Cowden syndrome. *Semin Oncol, 34*(5), 428-434. doi:10.1053/j.seminoncol.2007.07.009

Hamdy, O., Awny, S., & Metwally, I. H. (2020). Medullary thyroid cancer: epidemiological pattern and factors contributing to recurrence and metastasis. *Ann R Coll Surg Engl, 102*(7), 499-503. doi:10.1308/rcsann.2020.0056

Hao, Y., Baker, D., & Ten Dijke, P. (2019). TGF-β-Mediated Epithelial-Mesenchymal Transition and Cancer Metastasis. *Int J Mol Sci, 20*(11). doi:10.3390/ijms20112767

Haugen, B. R., Alexander, E. K., Bible, K. C., Doherty, G. M., Mandel, S. J., Nikiforov, Y. E., . . . Wartofsky, L. (2016). 2015 American Thyroid Association Management Guidelines for Adult Patients with Thyroid Nodules and Differentiated Thyroid Cancer: The American Thyroid Association Guidelines Task Force on Thyroid Nodules and Differentiated Thyroid Cancer. *Thyroid, 26*(1), 1-133. doi:10.1089/thy.2015.0020

Hercbergs, A. (2019). Clinical Implications and Impact of Discovery of the Thyroid Hormone Receptor on Integrin αvβ3-A Review. *Front Endocrinol (Lausanne), 10*, 565. doi:10.3389/fendo.2019.00565

Hermus, M., van der Wilk, B. J., Chang, R. T. H., Collee, G., Noordman, B. J., Coene, P. L. O., . . . Kranenburg, L. W. (2023). Patient preferences for active surveillance vs standard surgery after neoadjuvant chemoradiotherapy in oesophageal cancer treatment: The NOSANO-study. *Int J Cancer, 152*(6), 1183-1190. doi:10.1002/ijc.34327

Hershman, J. M. (1974). Clinical application of thyrotropin-releasing hormone. *New England Journal of Medicine, 290*(16), 886-890.

Hetz, C. (2012). The unfolded protein response: controlling cell fate decisions under ER stress and beyond. *Nat Rev Mol Cell Biol, 13*(2), 89-102. doi:10.1038/nrm3270

Hingorani, M., Spitzweg, C., Vassaux, G., Newbold, K., Melcher, A., Pandha, H., . . . Harrington, K. (2010). The biology of the sodium iodide symporter and its potential for targeted gene delivery. *Curr Cancer Drug Targets, 10*(2), 242-267. doi:10.2174/156800910791054194

Hirabayashi, M., Inoue, K., Tanaka, K., Nakadate, K., Ohsawa, Y., Kamei, Y., . . . Kakizuka, A. (2001). VCP/p97 in abnormal protein aggregates, cytoplasmic vacuoles, and cell

death, phenotypes relevant to neurodegeneration. *Cell Death Differ, 8*(10), 977-984. doi:10.1038/sj.cdd.4400907

Hlozek, J., Pekova, B., Rotnágl, J., Holý, R., & Astl, J. (2022). Genetic Changes in Thyroid Cancers and the Importance of Their Preoperative Detection in Relation to the General Treatment and Determination of the Extent of Surgical Intervention-A Review. *Biomedicines, 10*(7). doi:10.3390/biomedicines10071515

Hofmann, M. C., Kunnimalaiyaan, M., Wang, J. R., Busaidy, N. L., Sherman, S. I., Lai, S. Y., . . . Cabanillas, M. E. (2022). Molecular mechanisms of resistance to kinase inhibitors and redifferentiation in thyroid cancers. *Endocr Relat Cancer, 29*(11), R173-r190. doi:10.1530/erc-22-0129

Hoie, J., Stenwig, A. E., Kullmann, G., & Lindegaard, M. (1988). Distant metastases in papillary thyroid cancer. A review of 91 patients. *Cancer, 61*(1), 1-6. doi:10.1002/1097-0142(19880101)61:1<1::aid-cncr2820610102>3.0.co;2-r

Höning, S., Ricotta, D., Krauss, M., Späte, K., Spolaore, B., Motley, A., . . . Owen, D. J. (2005). Phosphatidylinositol-(4,5)-bisphosphate regulates sorting signal recognition by the clathrin-associated adaptor complex AP2. *Mol Cell, 18*(5), 519-531. doi:10.1016/j.molcel.2005.04.019

Hou, P., Bojdani, E., & Xing, M. (2010). Induction of thyroid gene expression and radioiodine uptake in thyroid cancer cells by targeting major signaling pathways. *J Clin Endocrinol Metab, 95*(2), 820-828. doi:10.1210/jc.2009-1888

Hou, S., Xie, X., Zhao, J., Wu, C., Li, N., Meng, Z., . . . Tan, J. (2020). Downregulation of miR-146b-3p Inhibits Proliferation and Migration and Modulates the Expression and Location of Sodium/Iodide Symporter in Dedifferentiated Thyroid Cancer by Potentially Targeting MUC20. *Front Oncol, 10*, 566365. doi:10.3389/fonc.2020.566365

Hu, S., Liu, D., Tufano, R. P., Carson, K. A., Rosenbaum, E., Cohen, Y., . . . Xing, M. (2006). Association of aberrant methylation of tumor suppressor genes with tumor aggressiveness and BRAF mutation in papillary thyroid cancer. *Int J Cancer, 119*(10), 2322-2329. doi:10.1002/ijc.22110

Huang, L., Wong, T. Y., Lin, R. C., & Furthmayr, H. (1999). Replacement of threonine 558, a critical site of phosphorylation of moesin in vivo, with aspartate activates F-actin binding of moesin: regulation by conformational change. *Journal of Biological Chemistry, 274*(18), 12803-12810.

Huc-Brandt, S., Marcellin, D., Graslin, F., Averseng, O., Bellanger, L., Hivin, P., . . . Darrouzet, E. (2011). Characterisation of the purified human sodium/iodide symporter reveals that the protein is mainly present in a dimeric form and permits the detailed study of a native C-terminal fragment. *Biochim Biophys Acta, 1808*(1), 65-77. doi:10.1016/j.bbamem.2010.08.013

Hulbert, A. J. (2000). Thyroid hormones and their effects: a new perspective. *Biol Rev Camb Philos Soc, 75*(4), 519-631. doi:10.1017/s146479310000556x

Ibrahimpasic, T., Ghossein, R., Shah, J. P., & Ganly, I. (2019). Poorly Differentiated Carcinoma of the Thyroid Gland: Current Status and Future Prospects. *Thyroid, 29*(3), 311-321. doi:10.1089/thy.2018.0509

Iosco, C., Cosentino, C., Sirna, L., Romano, R., Cursano, S., Mongia, A., . . . Rhoden, K. J. (2014). Anoctamin 1 is apically expressed on thyroid follicular cells and contributes to ATP- and calcium-activated iodide efflux. *Cell Physiol Biochem, 34*(3), 966-980. doi:10.1159/000366313

Ishizaka, Y., Itoh, F., Tahira, T., Ikeda, I., Sugimura, T., Tucker, J., . . . Nagao, M. (1989). Human ret proto-oncogene mapped to chromosome 10q11.2. *Oncogene, 4*(12), 1519-1521.

Ito, Y., Miyauchi, A., Kihara, M., Fukushima, M., Higashiyama, T., & Miya, A. (2018). Overall Survival of Papillary Thyroid Carcinoma Patients: A Single-Institution Long-Term Follow-Up of 5897 Patients. *World J Surg, 42*(3), 615-622. doi:10.1007/s00268-018-4479-z

Ito, Y., Miyauchi, A., & Oda, H. (2018). Low-risk papillary microcarcinoma of the thyroid: A review of active surveillance trials. *Eur J Surg Oncol, 44*(3), 307-315. doi:10.1016/j.ejso.2017.03.004

Ito, Y., Yoshida, H., Maruo, R., Morita, S., Takano, T., Hirokawa, M., . . . Miyauchi, A. (2009). BRAF mutation in papillary thyroid carcinoma in a Japanese population: its lack of correlation with high-risk clinicopathological features and disease-free survival of patients. *Endocr J, 56*(1), 89-97. doi:10.1507/endocrj.k08e-208

Jackson, L. P., Kelly, B. T., McCoy, A. J., Gaffry, T., James, L. C., Collins, B. M., . . . Owen, D. J. (2010). A large-scale conformational change couples membrane recruitment to cargo binding in the AP2 clathrin adaptor complex. *Cell, 141*(7), 1220-1229. doi:10.1016/j.cell.2010.05.006

Jannin, A., Escande, A., Al Ghuzlan, A., Blanchard, P., Hartl, D., Chevalier, B., . . . Hadoux, J. (2022). Anaplastic Thyroid Carcinoma: An Update. *Cancers (Basel), 14*(4). doi:10.3390/cancers14041061

Jansen, H. I., Boelen, A., Heijboer, A. C., Bruinstroop, E., & Fliers, E. (2023). Hypothyroidism: The difficulty in attributing symptoms to their underlying cause. *Front Endocrinol (Lausanne), 14*, 1130661. doi:10.3389/fendo.2023.1130661

Jeon, M. J., Chun, S. M., Kim, D., Kwon, H., Jang, E. K., Kim, T. Y., . . . Kim, W. G. (2016). Genomic Alterations of Anaplastic Thyroid Carcinoma Detected by Targeted Massive Parallel Sequencing in a BRAF(V600E) Mutation-Prevalent Area. *Thyroid, 26*(5), 683-690. doi:10.1089/thy.2015.0506

Jin, S., Borkhuu, O., Bao, W., & Yang, Y. T. (2016). Signaling Pathways in Thyroid Cancer and Their Therapeutic Implications. *J Clin Med Res, 8*(4), 284-296. doi:10.14740/jocmr2480w

Johnson, J. L., & Felicetta, J. V. (1992). Hyperthyroidism: a comprehensive review. *J Am Acad Nurse Pract, 4*(1), 8-14. doi:10.1111/j.1745-7599.1992.tb01105.x

Kadlecova, Z., Spielman, S. J., Loerke, D., Mohanakrishnan, A., Reed, D. K., & Schmid, S. L. (2017). Regulation of clathrin-mediated endocytosis by hierarchical allosteric activation of AP2. *J Cell Biol, 216*(1), 167-179. doi:10.1083/jcb.201608071

Kambe, F., Nomura, Y., Okamoto, T., & Seo, H. (1996). Redox regulation of thyroid-transcription factors, Pax-8 and TTF-1, is involved in their increased DNA-binding activities by thyrotropin in rat thyroid FRTL-5 cells. *Mol Endocrinol, 10*(7), 801-812. doi:10.1210/mend.10.7.8813721

Kaminsky, S. M., Levy, O., Salvador, C., Dai, G., & Carrasco, N. (1994). Na(+)-I- symport activity is present in membrane vesicles from thyrotropin-deprived non-I(-)-transporting cultured thyroid cells. *Proc Natl Acad Sci U S A, 91*(9), 3789-3793. doi:10.1073/pnas.91.9.3789

Karger, S., Berger, K., Eszlinger, M., Tannapfel, A., Dralle, H., Paschke, R., & Führer, D. (2005). Evaluation of peroxisome proliferator-activated receptor-gamma expression in benign and malignant thyroid pathologies. *Thyroid, 15*(9), 997-1003. doi:10.1089/thy.2005.15.997

Katoh, H., Yamashita, K., Enomoto, T., & Watanabe, M. (2015). Classification and general considerations of thyroid cancer. *Ann Clin Pathol, 3*(1), 1045.

Kelly, B. T., Graham, S. C., Liska, N., Dannhauser, P. N., Höning, S., Ungewickell, E. J., & Owen, D. J. (2014). Clathrin adaptors. AP2 controls clathrin polymerization with a membrane-activated switch. *Science, 345*(6195), 459-463. doi:10.1126/science.1254836

Kelly, B. T., McCoy, A. J., Späte, K., Miller, S. E., Evans, P. R., Höning, S., & Owen, D. J. (2008). A structural explanation for the binding of endocytic dileucine motifs by the AP2 complex. *Nature, 456*(7224), 976-979. doi:10.1038/nature07422

Khan, M. S., Qadri, Q., Makhdoomi, M. J., Wani, M. A., Malik, A. A., Niyaz, M., . . . Mudassar, S. (2020). RET/PTC Gene Rearrangements in Thyroid Carcinogenesis: Assessment and Clinico-Pathological Correlations. *Pathol Oncol Res, 26*(1), 507-513. doi:10.1007/s12253-018-0540-3

Kilbane, M. T., Ajjan, R. A., Weetman, A. P., Dwyer, R., McDermott, E. W., O'Higgins, N. J., & Smyth, P. P. (2000). Tissue iodine content and serum-mediated 125I uptake-blocking activity in breast cancer. *J Clin Endocrinol Metab, 85*(3), 1245-1250. doi:10.1210/jcem.85.3.6442

Kilgas, S., & Ramadan, K. (2023). Inhibitors of the ATPase p97/VCP: From basic research to clinical applications. *Cell Chem Biol, 30*(1), 3-21. doi:10.1016/j.chembiol.2022.12.007

Kim, J., Noh, S. H., Piao, H., Kim, D. H., Kim, K., Cha, J. S., . . . Lee, M. G. (2016). Monomerization and ER Relocalization of GRASP Is a Requisite for Unconventional Secretion of CFTR. *Traffic, 17*(7), 733-753. doi:10.1111/tra.12403

Kim, M., & Kim, B. H. (2021). Current Guidelines for Management of Medullary Thyroid Carcinoma. *Endocrinol Metab (Seoul), 36*(3), 514-524. doi:10.3803/EnM.2021.1082

Kim, T. H., Park, Y. J., Lim, J. A., Ahn, H. Y., Lee, E. K., Lee, Y. J., . . . Park, D. J. (2012). The association of the BRAF(V600E) mutation with prognostic factors and poor clinical outcome in papillary thyroid cancer: a meta-analysis. *Cancer, 118*(7), 1764-1773. doi:10.1002/cncr.26500

Kimura, E. T., Nikiforova, M. N., Zhu, Z., Knauf, J. A., Nikiforov, Y. E., & Fagin, J. A. (2003). High prevalence of BRAF mutations in thyroid cancer: genetic evidence for constitutive activation of the RET/PTC-RAS-BRAF signaling pathway in papillary thyroid carcinoma. *Cancer Res, 63*(7), 1454-1457.

Knostman, K. A., McCubrey, J. A., Morrison, C. D., Zhang, Z., Capen, C. C., & Jhiang, S. M. (2007). PI3K activation is associated with intracellular sodium/iodide symporter protein expression in breast cancer. *BMC Cancer, 7*, 137. doi:10.1186/1471-2407-7-137

Knowles, P. P., Murray-Rust, J., Kjaer, S., Scott, R. P., Hanrahan, S., Santoro, M., . . . McDonald, N. Q. (2006). Structure and chemical inhibition of the RET tyrosine kinase domain. *J Biol Chem, 281*(44), 33577-33587. doi:10.1074/jbc.M605604200

Kobayashi, H., Sagara, J., Kurita, H., Morifuji, M., Ohishi, M., Kurashina, K., & Taniguchi, S. (2004). Clinical significance of cellular distribution of moesin in patients with oral squamous cell carcinoma. *Clin Cancer Res, 10*(2), 572-580. doi:10.1158/1078-0432.ccr-1323-03

Kogai, T., & Brent, G. A. (2012). The sodium iodide symporter (NIS): regulation and approaches to targeting for cancer therapeutics. *Pharmacol Ther, 135*(3), 355-370. doi:10.1016/j.pharmthera.2012.06.007

Kogai, T., Sajid-Crockett, S., Newmarch, L. S., Liu, Y. Y., & Brent, G. A. (2008). Phosphoinositide-3-kinase inhibition induces sodium/iodide symporter expression in rat thyroid cells and human papillary thyroid cancer cells. *J Endocrinol, 199*(2), 243-252. doi:10.1677/joe-08-0333

Kogai, T., Taki, K., & Brent, G. A. (2006). Enhancement of sodium/iodide symporter expression in thyroid and breast cancer. *Endocr Relat Cancer, 13*(3), 797-826. doi:10.1677/erc.1.01143

Koller, K. J., Wolff, R. S., Warden, M. K., & Zoeller, R. T. (1987). Thyroid hormones regulate levels of thyrotropin-releasing-hormone mRNA in the paraventricular nucleus. *Proc Natl Acad Sci U S A, 84*(20), 7329-7333. doi:10.1073/pnas.84.20.7329

Kondo, T., Nakazawa, T., Ma, D., Niu, D., Mochizuki, K., Kawasaki, T., . . . Katoh, R. (2009). Epigenetic silencing of TTF-1/NKX2-1 through DNA hypermethylation and histone H3 modulation in thyroid carcinomas. *Lab Invest, 89*(7), 791-799. doi:10.1038/labinvest.2009.50

Koumarianou, P., Fernández-Méndez, C., Fajardo-Delgado, D., Mielu, L. M., Santisteban, P., & De la Vieja, A. (2022). Basolateral Sorting of the Sodium/Iodide Symporter Is Mediated by Adaptor Protein 1 Clathrin Adaptor Complexes. *Thyroid, 32*(10), 1259-1270. doi:10.1089/thy.2022.0163

Kovtun, O., Dickson, V. K., Kelly, B. T., Owen, D. J., & Briggs, J. A. G. (2020). Architecture of the AP2/clathrin coat on the membranes of clathrin-coated vesicles. *Sci Adv, 6*(30), eaba8381. doi:10.1126/sciadv.aba8381

Krishna, M., & Narang, H. (2008). The complexity of mitogen-activated protein kinases (MAPKs) made simple. *Cell Mol Life Sci, 65*(22), 3525-3544. doi:10.1007/s00018-008-8170-7

Kure, S., & Ohashi, R. (2020). Thyroid Hürthle Cell Carcinoma: Clinical, Pathological, and Molecular Features. *Cancers (Basel), 13*(1). doi:10.3390/cancers13010026

Laha, D., Nilubol, N., & Boufraqech, M. (2020). New Therapies for Advanced Thyroid Cancer. *Front Endocrinol (Lausanne), 11*, 82. doi:10.3389/fendo.2020.00082

Lakshmanan, A., Wojcicka, A., Kotlarek, M., Zhang, X., Jazdzewski, K., & Jhiang, S. M. (2015). microRNA-339-5p modulates Na+/I- symporter-mediated radioiodide uptake. *Endocr Relat Cancer, 22*(1), 11-21. doi:10.1530/erc-14-0439

Lan, T. H., Liu, Q., Li, C., Wu, G., & Lambert, N. A. (2012). Sensitive and high resolution localization and tracking of membrane proteins in live cells with BRET. *Traffic, 13*(11), 1450-1456. doi:10.1111/j.1600-0854.2012.01401.x

Landa, I., Ibrahimpasic, T., Boucai, L., Sinha, R., Knauf, J. A., Shah, R. H., . . . Xu, B. (2016). Genomic and transcriptomic hallmarks of poorly differentiated and anaplastic thyroid cancers. *The Journal of clinical investigation, 126*(3), 1052-1066.

Landa, I., Pozdeyev, N., Korch, C., Marlow, L. A., Smallridge, R. C., Copland, J. A., . . . Schweppe, R. E. (2019). Comprehensive Genetic Characterization of Human Thyroid Cancer Cell Lines: A Validated Panel for Preclinical Studies. *Clin Cancer Res, 25*(10), 3141-3151. doi:10.1158/1078-0432.Ccr-18-2953

Lankes, W. T., & Furthmayr, H. (1991). Moesin: a member of the protein 4.1-talin-ezrin family of proteins. *Proc Natl Acad Sci U S A, 88*(19), 8297-8301. doi:10.1073/pnas.88.19.8297

Larouche, V., Akirov, A., Thomas, C. M., Krzyzanowska, M. K., & Ezzat, S. (2019). A primer on the genetics of medullary thyroid cancer. *Curr Oncol, 26*(6), 389-394. doi:10.3747/co.26.5553

Le Moigne, R., Aftab, B. T., Djakovic, S., Dhimolea, E., Valle, E., Murnane, M., . . . Rolfe, M. (2017). The p97 Inhibitor CB-5083 Is a Unique Disrupter of Protein Homeostasis in Models of Multiple Myeloma. *Mol Cancer Ther, 16*(11), 2375-2386. doi:10.1158/1535-7163.Mct-17-0233

Leandro-García, L. J., & Landa, I. (2023). Mechanistic Insights of Thyroid Cancer Progression. *Endocrinology, 164*(9). doi:10.1210/endocr/bqad118

Leboulleux, S., Do Cao, C., Zerdoud, S., Attard, M., Bournaud, C., Lacroix, L., . . . Terroir-Cassou-Mounat, M. (2023). A phase II redifferentiation trial with dabrafenib-trametinib and 131I in metastatic radioactive iodine refractory BRAF p. V600E-mutated differentiated thyroid cancer. *Clinical Cancer Research, 29*(13), 2401-2409.

Lechan, R. M., Qi, Y., Jackson, I. M., & Mahdavi, V. (1994). Identification of thyroid hormone receptor isoforms in thyrotropin-releasing hormone neurons of the hypothalamic paraventricular nucleus. *Endocrinology, 135*(1), 92-100. doi:10.1210/endo.135.1.7516871

Lee, S. Y., & Pearce, E. N. (2023). Hyperthyroidism: A Review. *Jama, 330*(15), 1472-1483. doi:10.1001/jama.2023.19052

Leestemaker, Y., & Ovaa, H. (2017). Tools to investigate the ubiquitin proteasome system. *Drug Discov Today Technol, 26*, 25-31. doi:10.1016/j.ddtec.2017.11.006

Leinonen, H., Cheng, C., Pitkänen, M., Sander, C. L., Zhang, J., Saeid, S., . . . Palczewski, K. (2021). A p97/Valosin-Containing Protein Inhibitor Drug CB-5083 Has a Potent but Reversible Off-Target Effect on Phosphodiesterase-6. *J Pharmacol Exp Ther, 378*(1), 31-41. doi:10.1124/jpet.120.000486

Leo, S. D., Trevisan, M., & Fugazzola, L. (2020). Recent advances in the management of anaplastic thyroid cancer. *Thyroid Res, 13*(1), 17. doi:10.1186/s13044-020-00091-w

Leoni, S. G., Kimura, E. T., Santisteban, P., & De la Vieja, A. (2011). Regulation of thyroid oxidative state by thioredoxin reductase has a crucial role in thyroid responses to iodide excess. *Mol Endocrinol, 25*(11), 1924-1935. doi:10.1210/me.2011-0038

Levy, A. De la Vieja, C. S. Ginter, C. Riedel, G. D., & Carrasco, N. (1998). N-linked glycosylation of the thyroid Na+/I- symporter (NIS). Implications for its secondary structure model. *J Biol Chem, 273*(35), 22657-22663. doi:10.1074/jbc.273.35.22657

Levy, Christopher S. Ginter, Antonio De la Vieja, Daniel Levy, & Carrasco, N. (1998). Identification of a structural requirement for thyroid Na+/I- symporter (NIS) function from analysis of a mutation that causes human congenital hypothyroidism. *FEBS Lett, 429*(1), 36-40. doi:10.1016/s0014-5793(98)00522-5

Li, Huang, X., Wei, J., Huang, H., Liu, Z., Hu, J., . . . Huang, Q. (2022). Role of moesin and its phosphorylation in VE-cadherin expression and distribution in endothelial adherens junctions. *Cell Signal, 100*, 110466. doi:10.1016/j.cellsig.2022.110466

Li, E., You, M., & Hristova, K. (2005). Sodium dodecyl sulfate-polyacrylamide gel electrophoresis and forster resonance energy transfer suggest weak interactions between fibroblast growth factor receptor 3 (FGFR3) transmembrane domains in the absence of extracellular domains and ligands. *Biochemistry, 44*(1), 352-360. doi:10.1021/bi048480k

Li, H., Waites, C. L., Staal, R. G., Dobryy, Y., Park, J., Sulzer, D. L., & Edwards, R. H. (2005). Sorting of vesicular monoamine transporter 2 to the regulated secretory pathway confers the somatodendritic exocytosis of monoamines. *Neuron, 48*(4), 619-633. doi:10.1016/j.neuron.2005.09.033

Li, J., & Zhang, Q. (2022). Intrathyroidal feedforward and feedback network regulating thyroid hormone synthesis and secretion. *Front Endocrinol (Lausanne), 13*, 992883. doi:10.3389/fendo.2022.992883

Li, J., & Zhang, Q. (2022). Intrathyroidal feedforward and feedback network regulating thyroid hormone synthesis and secretion. *13*, 992883.

Li, L., Lv, B., Chen, B., Guan, M., Sun, Y., Li, H., . . . Zeng, Q. (2015). Inhibition of miR-146b expression increases radioiodine-sensitivity in poorly differential thyroid carcinoma via positively regulating NIS expression. *Biochem Biophys Res Commun, 462*(4), 314-321. doi:10.1016/j.bbrc.2015.04.134

Li, M., Brito, J. P., & Vaccarella, S. (2020). Long-Term Declines of Thyroid Cancer Mortality: An International Age-Period-Cohort Analysis. *Thyroid, 30*(6), 838-846. doi:10.1089/thy.2019.0684

Li, M., Dal Maso, L., & Vaccarella, S. (2020). Global trends in thyroid cancer incidence and the impact of overdiagnosis. *Lancet Diabetes Endocrinol, 8*(6), 468-470. doi:10.1016/s2213-8587(20)30115-7

Li, M., Zheng, R., Dal Maso, L., Zhang, S., Wei, W., & Vaccarella, S. (2021). Mapping overdiagnosis of thyroid cancer in China. *Lancet Diabetes Endocrinol, 9*(6), 330-332. doi:10.1016/s2213-8587(21)00083-8

Li, S., Wang, F., Zhang, G., & Chou, T. F. (2022). NMS-873 Leads to Dysfunctional Glycometabolism in A p97-Independent Manner in HCT116 Colon Cancer Cells. *Pharmaceutics, 14*(4). doi:10.3390/pharmaceutics14040764

Lima, S. M., Kehm, R. D., & Terry, M. B. (2021). Global breast cancer incidence and mortality trends by region, age-groups, and fertility patterns. *EClinicalMedicine, 38*, 100985. doi:10.1016/j.eclinm.2021.100985

Limaiem, F., Rehman, A., Anastasopoulou, C., & Mazzoni, T. (2024). Papillary Thyroid Carcinoma. In *StatPearls*. Treasure Island (FL): StatPearls Publishing

Copyright © 2024, StatPearls Publishing LLC.

Lin, H. Y., Cody, V., Davis, F. B., Hercbergs, A. A., Luidens, M. K., Mousa, S. A., & Davis, P. J. (2011). Identification and functions of the plasma membrane receptor for thyroid hormone analogues. *Discov Med, 11*(59), 337-347.

Lin, J. D., & Chao, T. C. (2006). Follicular thyroid carcinoma: From diagnosis to treatment. *Endocr J, 53*(4), 441-448. doi:10.1507/endocrj.kr-77

Lindholm, J., & Laurberg, P. (2010). Hyperthyroidism, exophthalmos, and goiter: historical notes on the orbitopathy. *Thyroid, 20*(3), 291-300. doi:10.1089/thy.2009.0340

Liu, R., & Xing, M. (2016). TERT promoter mutations in thyroid cancer. *Endocr Relat Cancer, 23*(3), R143-155. doi:10.1530/erc-15-0533

Liu, S., Ye, X., Liu, W., Liu, L., Li, D., Lin, Q., & Wang, T. (2022). Cryo-EM structure of dodecamer human p97 in complex with NMS-873 reveals S(765)-G(779) peptide plays critical role for D2 ring oligomerization. *Biochem Biophys Res Commun, 601*, 146-152. doi:10.1016/j.bbrc.2022.02.056

LiVolsi, V. A. (2011). Papillary thyroid carcinoma: an update. *Mod Pathol, 24 Suppl 2*, S1-9. doi:10.1038/modpathol.2010.129

Lu, L., Wang, J. R., Henderson, Y. C., Bai, S., Yang, J., Hu, M., . . . Gao, R. (2023). Anaplastic transformation in thyroid cancer revealed by single-cell transcriptomics. *J Clin Invest, 133*(11). doi:10.1172/jci169653

Ma, R., Morshed, S. A., Latif, R., & Davies, T. F. (2017). TAZ Induction Directs Differentiation of Thyroid Follicular Cells from Human Embryonic Stem Cells. *Thyroid, 27*(2), 292-299. doi:10.1089/thy.2016.0264

Mady, L. J., Grimes, M. C., Khan, N. I., Rao, R. H., Chiosea, S. I., Yip, L., . . . Duvvuri, U. (2020). Molecular Profile of Locally Aggressive Well Differentiated Thyroid Cancers. *Sci Rep, 10*(1), 8031. doi:10.1038/s41598-020-64635-8

Maehama, T., & Dixon, J. E. (1998). The tumor suppressor, PTEN/MMAC1, dephosphorylates the lipid second messenger, phosphatidylinositol 3,4,5-trisphosphate. *J Biol Chem, 273*(22), 13375-13378. doi:10.1074/jbc.273.22.13375

Maghsoomi, Z., Emami, Z., Malboosbaf, R., Malek, M., & Khamseh, M. E. (2021). Efficacy and safety of peptide receptor radionuclide therapy in advanced radioiodine-refractory differentiated thyroid cancer and metastatic medullary thyroid cancer: a systematic review. *BMC Cancer, 21*(1), 579. doi:10.1186/s12885-021-08257-x

Magliano, Lauro, R. D., & Zannini, M. (2000). Pax8 has a key role in thyroid cell differentiation. *Proc Natl Acad Sci U S A, 97*(24), 13144-13149. doi:10.1073/pnas.240336397

Maia, A. L., Kim, B. W., Huang, S. A., Harney, J. W., & Larsen, P. R. (2005). Type 2 iodothyronine deiodinase is the major source of plasma T3 in euthyroid humans. *J Clin Invest, 115*(9), 2524-2533. doi:10.1172/JCI25083

Manasanch, E. E., & Orlowski, R. Z. (2017). Proteasome inhibitors in cancer therapy. *Nat Rev Clin Oncol, 14*(7), 417-433. doi:10.1038/nrclinonc.2016.206

Maniakas, A., Dadu, R., Busaidy, N. L., Wang, J. R., Ferrarotto, R., Lu, C., . . . Zafereo, M. (2020). Evaluation of Overall Survival in Patients With Anaplastic Thyroid Carcinoma, 2000-2019. *JAMA Oncol, 6*(9), 1397-1404. doi:10.1001/jamaoncol.2020.3362

Mansfield, A. S., Subbiah, V., Schuler, M. H., Zhu, V. W., Hadoux, J., Brose, M. S., . . . Adkins, D. (2022). Pralsetinib in patients (pts) with advanced or metastatic RET-altered thyroid cancer (TC): Updated data from the ARROW trial. In: American Society of Clinical Oncology.

Mao, X. C., Yu, W. Q., Shang, J. B., & Wang, K. J. (2017). Clinical characteristics and treatment of thyroid cancer in children and adolescents: a retrospective analysis of 83 patients. *J Zhejiang Univ Sci B, 18*(5), 430-436. doi:10.1631/jzus.B1600308

Marcus, L., Donoghue, M., Aungst, S., Myers, C. E., Helms, W. S., Shen, G., . . . Pazdur, R. (2021). FDA Approval Summary: Entrectinib for the Treatment of NTRK gene Fusion Solid Tumors. *Clin Cancer Res, 27*(4), 928-932. doi:10.1158/1078-0432.Ccr-20-2771

Marotta, V., Bifulco, M., & Vitale, M. (2021). Significance of RAS Mutations in Thyroid Benign Nodules and Non-Medullary Thyroid Cancer. *Cancers (Basel), 13*(15). doi:10.3390/cancers13153785

Marques, A. R., Espadinha, C., Catarino, A. L., Moniz, S., Pereira, T., Sobrinho, L. G., & Leite, V. (2002). Expression of PAX8-PPAR gamma 1 rearrangements in both follicular thyroid carcinomas and adenomas. *J Clin Endocrinol Metab, 87*(8), 3947-3952. doi:10.1210/jcem.87.8.8756

Marrazzo, E., Frusone, F., Milana, F., Sagona, A., Gatzemeier, W., Barbieri, E., . . . Tinterri, C. (2020). Mucinous breast cancer: A narrative review of the literature and a retrospective tertiary single-centre analysis. *Breast, 49*, 87-92. doi:10.1016/j.breast.2019.11.002

Martín, M., Modenutti, C. P., Peyret, V., Geysels, R. C., Darrouzet, E., Pourcher, T., . . . Nicola, J. P. (2019). A Carboxy-Terminal Monoleucine-Based Motif Participates in the

Basolateral Targeting of the Na+/I- Symporter. *Endocrinology, 160*(1), 156-168. doi:10.1210/en.2018-00603

Martín, M., Salleron, L., Peyret, V., Geysels, R. C., Darrouzet, E., Lindenthal, S., . . . Nicola, J. P. (2021). The PDZ protein SCRIB regulates sodium/iodide symporter (NIS) expression at the basolateral plasma membrane. *Faseb j, 35*(8), e21681. doi:10.1096/fj.202100303R

Martini, M., De Santis, M. C., Braccini, L., Gulluni, F., & Hirsch, E. (2014). PI3K/AKT signaling pathway and cancer: an updated review. *Ann Med, 46*(6), 372-383. doi:10.3109/07853890.2014.912836

Maruyama, I. N. (2015). Activation of transmembrane cell-surface receptors via a common mechanism? The "rotation model". *Bioessays, 37*(9), 959-967. doi:10.1002/bies.201500041

Matsui, T., Maeda, M., Doi, Y., Yonemura, S., Amano, M., Kaibuchi, K., . . . Tsukita, S. (1998). Rho-kinase phosphorylates COOH-terminal threonines of ezrin/radixin/moesin (ERM) proteins and regulates their head-to-tail association. *J Cell Biol, 140*(3), 647-657. doi:10.1083/jcb.140.3.647

Mauchamp, J., Mirrione, A., Alquier, C., & André, F. (1998). Follicle-like structure and polarized monolayer: role of the extracellular matrix on thyroid cell organization in primary culture. *Biol Cell, 90*(5), 369-380.

Maurel, D., Comps-Agrar, L., Brock, C., Rives, M. L., Bourrier, E., Ayoub, M. A., . . . Pin, J. P. (2008). Cell-surface protein-protein interaction analysis with time-resolved FRET and snap-tag technologies: application to GPCR oligomerization. *Nat Methods, 5*(6), 561-567. doi:10.1038/nmeth.1213

Mazzaferri, E. L., & Kloos, R. T. (2001). Clinical review 128: Current approaches to primary therapy for papillary and follicular thyroid cancer. *J Clin Endocrinol Metab, 86*(4), 1447-1463. doi:10.1210/jcem.86.4.7407

McCabe, C. J., Boelaert, K., Tannahill, L. A., Heaney, A. P., Stratford, A. L., Khaira, J. S., . . . Gittoes, N. J. (2002). Vascular endothelial growth factor, its receptor KDR/Flk-1, and pituitary tumor transforming gene in pituitary tumors. *J Clin Endocrinol Metab, 87*(9), 4238-4244. doi:10.1210/jc.2002-020309

McHenry, C. R., & Phitayakorn, R. (2011). Follicular adenoma and carcinoma of the thyroid gland. *Oncologist, 16*(5), 585-593. doi:10.1634/theoncologist.2010-0405

McKelvey, B. A., Umbricht, C. B., & Zeiger, M. A. (2020). Telomerase Reverse Transcriptase (TERT) Regulation in Thyroid Cancer: A Review. *Front Endocrinol (Lausanne), 11*, 485. doi:10.3389/fendo.2020.00485

McLaughlin, M. B., Awosika, A. O., & Jialal, I. (2023). Calcitonin. In *StatPearls*. Treasure Island (FL): StatPearls Publishing

Copyright © 2023, StatPearls Publishing LLC.

Mettlen, M., Chen, P. H., Srinivasan, S., Danuser, G., & Schmid, S. L. (2018). Regulation of Clathrin-Mediated Endocytosis. *Annu Rev Biochem, 87*, 871-896. doi:10.1146/annurev-biochem-062917-012644

Michie, K. A., Bermeister, A., Robertson, N. O., Goodchild, S. C., & Curmi, P. M. G. (2019). Two Sides of the Coin: Ezrin/Radixin/Moesin and Merlin Control Membrane Structure and Contact Inhibition. *Int J Mol Sci, 20*(8). doi:10.3390/ijms20081996

Miller, K. A., Yeager, N., Baker, K., Liao, X. H., Refetoff, S., & Di Cristofano, A. (2009). Oncogenic Kras requires simultaneous PI3K signaling to induce ERK activation and

transform thyroid epithelial cells in vivo. *Cancer Res, 69*(8), 3689-3694. doi:10.1158/0008-5472.Can-09-0024

Miyauchi, A., & Ito, Y. (2019). Conservative Surveillance Management of Low-Risk Papillary Thyroid Microcarcinoma. *Endocrinol Metab Clin North Am, 48*(1), 215-226. doi:10.1016/j.ecl.2018.10.007

Miyazaki, Y., Shimizu, J., Kubo, Y., Tabata, N., & Aso, T. (2022). Quantitative classification of invasive and noninvasive breast cancer using dynamic magnetic resonance imaging of the mammary gland. *J Clin Imaging Sci, 12*, 45. doi:10.25259/jcis_56_2022

Morris, L. G., Sikora, A. G., Tosteson, T. D., & Davies, L. (2013). The increasing incidence of thyroid cancer: the influence of access to care. *Thyroid, 23*(7), 885-891. doi:10.1089/thy.2013.0045

Moyzis, R. K., Buckingham, J. M., Cram, L. S., Dani, M., Deaven, L. L., Jones, M. D., . . . Wu, J. R. (1988). A highly conserved repetitive DNA sequence, (TTAGGG)n, present at the telomeres of human chromosomes. *Proc Natl Acad Sci U S A, 85*(18), 6622-6626. doi:10.1073/pnas.85.18.6622

Mulrine, H. M., Skeaff, S. A., Ferguson, E. L., Gray, A. R., & Valeix, P. (2010). Breast-milk iodine concentration declines over the first 6 mo postpartum in iodine-deficient women. *Am J Clin Nutr, 92*(4), 849-856. doi:10.3945/ajcn.2010.29630

Neve, R. M., Chin, K., Fridlyand, J., Yeh, J., Baehner, F. L., Fevr, T., . . . Gray, J. W. (2006). A collection of breast cancer cell lines for the study of functionally distinct cancer subtypes. *Cancer Cell, 10*(6), 515-527. doi:10.1016/j.ccr.2006.10.008

Nguyen, Q. T., Lee, E. J., Huang, M. G., Park, Y. I., Khullar, A., & Plodkowski, R. A. (2015). Diagnosis and treatment of patients with thyroid cancer. *Am Health Drug Benefits, 8*(1), 30-40. Retrieved from https://www.ncbi.nlm.nih.gov/pmc/articles/PMC4415174/pdf/ahdb-08-030.pdf

Niafar, M., Pourafkari, L., Aminmozaffari, S., & Nader, N. D. (2016). Association of Vitamin D Deficiency and Thyroid Function in Postmenopausal Women. *Adv Pharm Bull, 6*(4), 639-644. doi:10.15171/apb.2016.078

Nicola, J. P., Carrasco, N., & Amzel, L. M. (2014). Physiological sodium concentrations enhance the iodide affinity of the Na+/I- symporter. *Nat Commun, 5*, 3948. doi:10.1038/ncomms4948

Nicola, J. P., Nazar, M., Mascanfroni, I. D., Pellizas, C. G., & Masini-Repiso, A. M. (2010). NF-kappaB p65 subunit mediates lipopolysaccharide-induced Na(+)/I(-) symporter gene expression by involving functional interaction with the paired domain transcription factor Pax8. *Mol Endocrinol, 24*(9), 1846-1862. doi:10.1210/me.2010-0102

Nicola, J. P., Vélez, M. L., Lucero, A. M., Fozzatti, L., Pellizas, C. G., & Masini-Repiso, A. M. (2009). Functional toll-like receptor 4 conferring lipopolysaccharide responsiveness is expressed in thyroid cells. *Endocrinology, 150*(1), 500-508. doi:10.1210/en.2008-0345

Nikiforov, Y. E. (2002). RET/PTC rearrangement in thyroid tumors. *Endocrine pathology, 13*, 3-16.

Nikiforov, Y. E., Ohori, N. P., Hodak, S. P., Carty, S. E., LeBeau, S. O., Ferris, R. L., . . . Nikiforova, M. N. (2011). Impact of mutational testing on the diagnosis and management of patients with cytologically indeterminate thyroid nodules: a prospective analysis of 1056 FNA samples. *J Clin Endocrinol Metab, 96*(11), 3390-3397. doi:10.1210/jc.2011-1469

Nikiforov, Y. E., Yip, L., & Nikiforova, M. N. (2013). New strategies in diagnosing cancer in thyroid nodules: impact of molecular markers. *Clin Cancer Res, 19*(9), 2283-2288. doi:10.1158/1078-0432.Ccr-12-1253

Nilsson, M., & Fagman, H. (2017). Development of the thyroid gland. *Development, 144*(12), 2123-2140. doi:10.1242/dev.145615

Niwa, H., Ewens, C. A., Tsang, C., Yeung, H. O., Zhang, X., & Freemont, P. S. (2012). The role of the N-domain in the ATPase activity of the mammalian AAA ATPase p97/VCP. *J Biol Chem, 287*(11), 8561-8570. doi:10.1074/jbc.M111.302778

Nomachi, A., Yoshinaga, M., Liu, J., Kanchanawong, P., Tohyama, K., Thumkeo, D., . . . Hirata, T. (2013). Moesin controls clathrin-mediated S1PR1 internalization in T cells. *PLoS One, 8*(12), e82590. doi:10.1371/journal.pone.0082590

Oh, J. M., & Ahn, B. C. (2021). Molecular mechanisms of radioactive iodine refractoriness in differentiated thyroid cancer: Impaired sodium iodide symporter (NIS) expression owing to altered signaling pathway activity and intracellular localization of NIS. *Theranostics, 11*(13), 6251-6277. doi:10.7150/thno.57689

Ohno, H., Fournier, M. C., Poy, G., & Bonifacino, J. S. (1996). Structural determinants of interaction of tyrosine-based sorting signals with the adaptor medium chains. *J Biol Chem, 271*(46), 29009-29015. doi:10.1074/jbc.271.46.29009

Ohno, M., Zannini, M., Levy, O., Carrasco, N., & di Lauro, R. (1999). The paired-domain transcription factor Pax8 binds to the upstream enhancer of the rat sodium/iodide symporter gene and participates in both thyroid-specific and cyclic-AMP-dependent transcription. *Mol Cell Biol, 19*(3), 2051-2060. doi:10.1128/mcb.19.3.2051

Olson, E., Wintheiser, G., Wolfe, K. M., Droessler, J., & Silberstein, P. T. (2019). Epidemiology of Thyroid Cancer: A Review of the National Cancer Database, 2000-2013. *Cureus, 11*(2), e4127. doi:10.7759/cureus.4127

Pacini, F., Castagna, M. G., Cipri, C., & Schlumberger, M. (2010). Medullary thyroid carcinoma. *Clin Oncol (R Coll Radiol), 22*(6), 475-485. doi:10.1016/j.clon.2010.05.002

Pacini, F., Fuhrer, D., Elisei, R., Handkiewicz-Junak, D., Leboulleux, S., Luster, M., . . . Smit, J. W. (2022). 2022 ETA Consensus Statement: What are the indications for post-surgical radioiodine therapy in differentiated thyroid cancer? *Eur Thyroid J, 11*(1). doi:10.1530/etj-21-0046

Parameswaran, R., Shulin Hu, J., Min En, N., Tan, W. B., & Yuan, N. K. (2017). Patterns of metastasis in follicular thyroid carcinoma and the difference between early and delayed presentation. *Ann R Coll Surg Engl, 99*(2), 151-154. doi:10.1308/rcsann.2016.0300

Park, J., Kim, D., Lee, J. O., Park, H. C., Ryu, B. Y., Kim, J. H., . . . Chung, Y. J. (2022). Dissection of molecular and histological subtypes of papillary thyroid cancer using alternative splicing profiles. *Exp Mol Med, 54*(3), 263-272. doi:10.1038/s12276-022-00740-0

Paroder-Belenitsky, M., Maestas, M. J., Dohán, O., Nicola, J. P., Reyna-Neyra, A., Follenzi, A., . . . Carrasco, N. (2011). Mechanism of anion selectivity and stoichiometry of the Na+/I- symporter (NIS). *Proc Natl Acad Sci U S A, 108*(44), 17933-17938. doi:10.1073/pnas.1108278108

Paschke, R., Cantara, S., Crescenzi, A., Jarzab, B., Musholt, T. J., & Sobrinho Simoes, M. (2017). European Thyroid Association Guidelines regarding Thyroid Nodule Molecular Fine-Needle Aspiration Cytology Diagnostics. *Eur Thyroid J, 6*(3), 115-129. doi:10.1159/000468519

Patel, J., Landers, K., Li, H., Mortimer, R. H., & Richard, K. (2011). Thyroid hormones and fetal neurological development. *J Endocrinol, 209*(1), 1-8. doi:10.1530/joe-10-0444

Pearson, M. A., Reczek, D., Bretscher, A., & Karplus, P. A. (2000). Structure of the ERM protein moesin reveals the FERM domain fold masked by an extended actin binding tail domain. *Cell, 101*(3), 259-270. doi:10.1016/s0092-8674(00)80836-3

Peeters, R. P. (2017). Subclinical Hypothyroidism. *N Engl J Med, 376*(26), 2556-2565. doi:10.1056/NEJMcp1611144

Pekary, A. E., & Hershman, J. M. (1998). Tumor necrosis factor, ceramide, transforming growth factor-beta1, and aging reduce Na+/I- symporter messenger ribonucleic acid levels in FRTL-5 cells. *Endocrinology, 139*(2), 703-712. doi:10.1210/endo.139.2.5760

Pellegriti, G., Frasca, F., Regalbuto, C., Squatrito, S., & Vigneri, R. (2013). Worldwide increasing incidence of thyroid cancer: update on epidemiology and risk factors. *J Cancer Epidemiol, 2013*, 965212. doi:10.1155/2013/965212

Perez, C. M., Liang, X., Gupta, D., Conceição, M., Mäger, I., Andaloussi, S. E., . . . Roberts, T. C. (2023). An extracellular vesicle delivery platform based on the PTTG1IP protein. *bioRxiv*, 2023.2008. 2018.553853.

Persani, L. (1998). Hypothalamic thyrotropin-releasing hormone and thyrotropin biological activity. *Thyroid, 8*(10), 941-946. doi:10.1089/thy.1998.8.941

Pettersen, E. F., Goddard, T. D., Huang, C. C., Couch, G. S., Greenblatt, D. M., Meng, E. C., & Ferrin, T. E. (2004). UCSF Chimera--a visualization system for exploratory research and analysis. *J Comput Chem, 25*(13), 1605-1612. doi:10.1002/jcc.20084

Pfleger, K. D., & Eidne, K. A. (2006). Illuminating insights into protein-protein interactions using bioluminescence resonance energy transfer (BRET). *Nat Methods, 3*(3), 165-174. doi:10.1038/nmeth841

Pirahanchi, Y., Toro, F., & Jialal, I. (2024). Physiology, Thyroid Stimulating Hormone. In *StatPearls*. Treasure Island (FL): StatPearls Publishing

Copyright © 2024, StatPearls Publishing LLC.

Pitoia, F., Jerkovich, F., Trimboli, P., & Smulever, A. (2022). New approaches for patients with advanced radioiodine-refractory thyroid cancer. *World Journal of Clinical Oncology, 13*(1), 9.

Pizzato, M., Li, M., Vignat, J., Laversanne, M., Singh, D., La Vecchia, C., & Vaccarella, S. (2022). The epidemiological landscape of thyroid cancer worldwide: GLOBOCAN estimates for incidence and mortality rates in 2020. *Lancet Diabetes Endocrinol, 10*(4), 264-272. doi:10.1016/s2213-8587(22)00035-3

Placzkowski, K. A., Reddi, H. V., Grebe, S. K., Eberhardt, N. L., & McIver, B. (2008). The Role of the PAX8/PPARgamma Fusion Oncogene in Thyroid Cancer. *PPAR Res, 2008*, 672829. doi:10.1155/2008/672829

Plantinga, T. S., Heinhuis, B., Gerrits, D., Netea, M. G., Joosten, L. A., Hermus, A. R., . . . Netea-Maier, R. T. (2014). mTOR Inhibition promotes TTF1-dependent redifferentiation and restores iodine uptake in thyroid carcinoma cell lines. *J Clin Endocrinol Metab, 99*(7), E1368-1375. doi:10.1210/jc.2014-1171

Plantinga, T. S., Tesselaar, M. H., Morreau, H., Corssmit, E. P., Willemsen, B. K., Kusters, B., . . . Netea-Maier, R. T. (2016). Autophagy activity is associated with membranous sodium iodide symporter expression and clinical response to radioiodine therapy in non-medullary thyroid cancer. *Autophagy, 12*(7), 1195-1205. doi:10.1080/15548627.2016.1174802

Podolski, A., Castellucci, E., & Halmos, B. (2019). Precision medicine: BRAF mutations in thyroid cancer. *Precision Cancer Medicine, 2*.

Pozdeyev, N., Gay, L. M., Sokol, E. S., Hartmaier, R., Deaver, K. E., Davis, S., . . . Bowles, D. W. (2018). Genetic Analysis of 779 Advanced Differentiated and Anaplastic Thyroid Cancers. *Clin Cancer Res, 24*(13), 3059-3068. doi:10.1158/1078-0432.Ccr-18-0373

Praefcke, G. J., Ford, M. G., Schmid, E. M., Olesen, L. E., Gallop, J. L., Peak-Chew, S. Y., . . . McMahon, H. T. (2004). Evolving nature of the AP2 alpha-appendage hub during clathrin-coated vesicle endocytosis. *Embo j, 23*(22), 4371-4383. doi:10.1038/sj.emboj.7600445

Prete, A., Matrone, A., Gambale, C., Torregrossa, L., Minaldi, E., Romei, C., . . . Elisei, R. (2021). Poorly Differentiated and Anaplastic Thyroid Cancer: Insights into Genomics, Microenvironment and New Drugs. *Cancers (Basel), 13*(13). doi:10.3390/cancers13133200

Priya, S. R., Dravid, C. S., Digumarti, R., & Dandekar, M. (2017). Targeted Therapy for Medullary Thyroid Cancer: A Review. *Front Oncol, 7*, 238. doi:10.3389/fonc.2017.00238

Pryma, D. A., & Mandel, S. J. (2014). Radioiodine therapy for thyroid cancer in the era of risk stratification and alternative targeted therapies. *J Nucl Med, 55*(9), 1485-1491. doi:10.2967/jnumed.113.131508

Pstrąg, N., Ziemnicka, K., Bluyssen, H., & Wesoły, J. (2018). Thyroid cancers of follicular origin in a genomic light: in-depth overview of common and unique molecular marker candidates. *Molecular cancer, 17*, 1-17.

Pylayeva-Gupta, Y., Grabocka, E., & Bar-Sagi, D. (2011). RAS oncogenes: weaving a tumorigenic web. *Nat Rev Cancer, 11*(11), 761-774. doi:10.1038/nrc3106

Qin, H., & Patel, M. R. (2022). The Challenge and Opportunity of NTRK Inhibitors in Non-Small Cell Lung Cancer. *Int J Mol Sci, 23*(6). doi:10.3390/ijms23062916

Rahbari, R., Zhang, L., & Kebebew, E. (2010). Thyroid cancer gender disparity. *Future Oncol, 6*(11), 1771-1779. doi:10.2217/fon.10.127

Raman, P., & Koenig, R. J. (2014). Pax-8–PPAR-γ fusion protein in thyroid carcinoma. *Nature Reviews Endocrinology, 10*(10), 616-623.

Rao, R. V., Poksay, K. S., Castro-Obregon, S., Schilling, B., Row, R. H., del Rio, G., . . . Bredesen, D. E. (2004). Molecular components of a cell death pathway activated by endoplasmic reticulum stress. *J Biol Chem, 279*(1), 177-187. doi:10.1074/jbc.M304490200

Rasheed, & Xu, B. (2019). Molecular Alterations in Thyroid Carcinoma. *Surg Pathol Clin, 12*(4), 921-930. doi:10.1016/j.path.2019.08.002

Rasmussen, A. K., Kayser, L., Feldt-Rasmussen, U., & Bendtzen, K. (1994). Influence of tumour necrosis factor-alpha, tumour necrosis factor-beta and interferon-gamma, separately and added together with interleukin-1 beta, on the function of cultured human thyroid cells. *J Endocrinol, 143*(2), 359-365. doi:10.1677/joe.0.1430359

Rathod, M., Chatterjee, S., Dutta, S., Kalraiya, R., Bhattacharyya, D., & De, A. (2019). Mannose glycosylation is an integral step for NIS localization and function in human breast cancer cells. *J Cell Sci, 132*(20). doi:10.1242/jcs.232058

Raue, F., & Frank-Raue, K. (2015). Epidemiology and clinical presentation of medullary thyroid carcinoma. *Medullary Thyroid Carcinoma: Biology–Management–Treatment*, 61-90.

Read, M. L., Brookes, K., Thornton, C. E. M., Fletcher, A., Nieto, H. R., Alshahrani, M., . . . McCabe, C. J. (2022). Targeting non-canonical pathways as a strategy to modulate the sodium iodide symporter. *Cell Chem Biol, 29*(3), 502-516.e507. doi:10.1016/j.chembiol.2021.07.016

Read, M. L., Brookes, K., Zha, L., Manivannan, S., Kim, J., Kocbiyik, M., . . . McCabe, C. J. (2024). Combined Vorinostat and Chloroquine Inhibit Sodium-Iodide Symporter Endocytosis and Enhance Radionuclide Uptake In Vivo. *Clin Cancer Res, 30*(7), 1352-1366. doi:10.1158/1078-0432.Ccr-23-2043

Read, M. L., Fong, J. C., Modasia, B., Fletcher, A., Imruetaicharoenchoke, W., Thompson, R. J., . . . McCabe, C. J. (2017). Elevated PTTG and PBF predicts poor patient outcome and modulates DNA damage response genes in thyroid cancer. *Oncogene, 36*(37), 5296-5308. doi:10.1038/onc.2017.154

Read, M. L., Lewy, G. D., Fong, J. C., Sharma, N., Seed, R. I., Smith, V. E., . . . McCabe, C. J. (2011). Proto-oncogene PBF/PTTG1IP regulates thyroid cell growth and represses radioiodide treatment. *Cancer Res, 71*(19), 6153-6164. doi:10.1158/0008-5472.Can-11-0720

Read, M. L., Modasia, B., Fletcher, A., Thompson, R. J., Brookes, K., Rae, P. C., . . . McCabe, C. J. (2018). PTTG and PBF Functionally Interact with p53 and Predict Overall Survival in Head and Neck Cancer. *Cancer Res, 78*(20), 5863-5876. doi:10.1158/0008-5472.Can-18-0855

Renier, C., Vogel, H., Offor, O., Yao, C., & Wapnir, I. (2010). Breast cancer brain metastases express the sodium iodide symporter. *J Neurooncol, 96*(3), 331-336. doi:10.1007/s11060-009-9971-8

Renier, C., Yao, C., Goris, M., Ghosh, M., Katznelson, L., Nowles, K., . . . Wapnir, I. (2009). Endogenous NIS expression in triple-negative breast cancers. *Ann Surg Oncol, 16*(4), 962-968. doi:10.1245/s10434-008-0280-9

Ricci, C., Salvemini, A., Dalmiglio, C., Castagna, M. G., & Cantara, S. (2023). From Circulating Tumor Cells to Mirna: New Challenges in the Diagnosis and Prognosis of Medullary Thyroid Cancer. *Cancers (Basel), 15*(15). doi:10.3390/cancers15154009

Riedel, C., Levy, O., & Carrasco, N. (2001). Post-transcriptional regulation of the sodium/iodide symporter by thyrotropin. *J Biol Chem, 276*(24), 21458-21463. doi:10.1074/jbc.M100561200

Riesco-Eizaguirre, G., Rodríguez, I., De la Vieja, A., Costamagna, E., Carrasco, N., Nistal, M., & Santisteban, P. (2009). The BRAFV600E oncogene induces transforming growth factor beta secretion leading to sodium iodide symporter repression and increased malignancy in thyroid cancer. *Cancer Res, 69*(21), 8317-8325. doi:10.1158/0008-5472.Can-09-1248

Riesco-Eizaguirre, G., Santisteban, P., & De la Vieja, A. (2021). The complex regulation of NIS expression and activity in thyroid and extrathyroidal tissues. *Endocr Relat Cancer, 28*(10), T141-t165. doi:10.1530/erc-21-0217

Riesco-Eizaguirre, G., Wert-Lamas, L., Perales-Patón, J., Sastre-Perona, A., Fernández, L. P., & Santisteban, P. (2015). The miR-146b-3p/PAX8/NIS Regulatory Circuit Modulates the Differentiation Phenotype and Function of Thyroid Cells during Carcinogenesis. *Cancer Res, 75*(19), 4119-4130. doi:10.1158/0008-5472.Can-14-3547

Rillema, J. A., & Hill, M. A. (2003). Pendrin transporter carries out iodide uptake into MCF-7 human mammary cancer cells. *Exp Biol Med (Maywood), 228*(9), 1078-1082. doi:10.1177/153537020322800915

Rillema, J. A., & Yu, T. X. (1996). Prolactin stimulation of iodide uptake into mouse mammary gland explants. *Am J Physiol, 271*(5 Pt 1), E879-882. doi:10.1152/ajpendo.1996.271.5.E879

Rillema, J. A., Yu, T. X., & Jhiang, S. M. (2000). Effect of prolactin on sodium iodide symporter expression in mouse mammary gland explants. *Am J Physiol Endocrinol Metab, 279*(4), E769-772. doi:10.1152/ajpendo.2000.279.4.E769

Rodriguez, A. M., Perron, B., Lacroix, L., Caillou, B., Leblanc, G., Schlumberger, M., . . . Pourcher, T. (2002). Identification and characterization of a putative human iodide transporter located at the apical membrane of thyrocytes. *J Clin Endocrinol Metab, 87*(7), 3500-3503. doi:10.1210/jcem.87.7.8797

Rohner, F., Zimmermann, M., Jooste, P., Pandav, C., Caldwell, K., Raghavan, R., & Raiten, D. J. (2014). Biomarkers of nutrition for development--iodine review. *J Nutr, 144*(8), 1322s-1342s. doi:10.3945/jn.113.181974

Ronga, G., Bruno, R., Puxeddu, E., Calcinaro, F., Montesano, T., Travascio, L., . . . Russo, D. (2007). Radioiodine uptake in non-lactating mammary glands: evidence for a causative role of hyperprolactinemia. *Thyroid, 17*(4), 363-366. doi:10.1089/thy.2006.0282

Rosai, J., Albores Saavedra, J., & Asioli, S. (2017). WHO classification of tumours of endocrine organs. *IARC: Lyon*.

Rosen, R. D., & Sapra, A. (2024). Embryology, Thyroid. In *StatPearls*. Treasure Island (FL): StatPearls Publishing

Copyright © 2024, StatPearls Publishing LLC.

Roux, B., Vaganay, C., Vargas, J. D., Alexe, G., Benaksas, C., Pardieu, B., . . . Benajiba, L. (2021). Targeting acute myeloid leukemia dependency on VCP-mediated DNA repair through a selective second-generation small-molecule inhibitor. *Sci Transl Med, 13*(587). doi:10.1126/scitranslmed.abg1168

Russo, D., Durante, C., Bulotta, S., Puppin, C., Puxeddu, E., Filetti, S., & Damante, G. (2013). Targeting histone deacetylase in thyroid cancer. *Expert Opin Ther Targets, 17*(2), 179-193. doi:10.1517/14728222.2013.740013

Saadeh, P. B., Mehrara, B. J., Steinbrech, D. S., Spector, J. A., Greenwald, J. A., Chin, G. S., . . . Longaker, M. T. (2000). Mechanisms of fibroblast growth factor-2 modulation of vascular endothelial growth factor expression by osteoblastic cells. *Endocrinology, 141*(6), 2075-2083. doi:10.1210/endo.141.6.7502

Sakaguchi, K., Okiyama, Y., & Tanaka, S. (2021). In silico modeling of PAX8-PPARγ fusion protein in thyroid carcinoma: influence of structural perturbation by fusion on ligand-binding affinity. *J Comput Aided Mol Des, 35*(5), 629-642. doi:10.1007/s10822-021-00381-x

Salama, A. K. S., Li, S., Macrae, E. R., Park, J. I., Mitchell, E. P., Zwiebel, J. A., . . . Flaherty, K. T. (2020). Dabrafenib and Trametinib in Patients With Tumors With BRAF(V600E) Mutations: Results of the NCI-MATCH Trial Subprotocol H. *J Clin Oncol, 38*(33), 3895-3904. doi:10.1200/jco.20.00762

Salehian, B., & Samoa, R. (2013). RET gene abnormalities and thyroid disease: who should be screened and when. *J Clin Res Pediatr Endocrinol, 5 Suppl 1*(Suppl 1), 70-78. doi:10.4274/Jcrpe.870

Salvatore, D., Santoro, M., & Schlumberger, M. (2021). The importance of the RET gene in thyroid cancer and therapeutic implications. *Nat Rev Endocrinol, 17*(5), 296-306. doi:10.1038/s41574-021-00470-9

Santoro, M., Rosati, R., Grieco, M., Berlingieri, M. T., D'Amato, G. L., de Franciscis, V., & Fusco, A. (1990). The ret proto-oncogene is consistently expressed in human pheochromocytomas and thyroid medullary carcinomas. *Oncogene, 5*(10), 1595-1598.

Sapin, R., & Schlienger, J. L. (2003). [Thyroxine (T4) and tri-iodothyronine (T3) determinations: techniques and value in the assessment of thyroid function]. *Ann Biol Clin (Paris), 61*(4), 411-420.

Schubert, L., Mariko, M. L., Clerc, J., Huillard, O., & Groussin, L. (2023). MAPK Pathway Inhibitors in Thyroid Cancer: Preclinical and Clinical Data. *Cancers (Basel), 15*(3). doi:10.3390/cancers15030710

Scott, D. A., Wang, R., Kreman, T. M., Sheffield, V. C., & Karniski, L. P. (1999). The Pendred syndrome gene encodes a chloride-iodide transport protein. *Nat Genet, 21*(4), 440-443. doi:10.1038/7783

Segerson, T. P., Kauer, J., Wolfe, H. C., Mobtaker, H., Wu, P., Jackson, I. M., & Lechan, R. M. (1987). Thyroid hormone regulates TRH biosynthesis in the paraventricular nucleus of the rat hypothalamus. *Science, 238*(4823), 78-80. doi:10.1126/science.3116669

Segura-Cabrera, A., Tripathi, R., Zhang, X., Gui, L., Chou, T. F., & Komurov, K. (2017). A structure- and chemical genomics-based approach for repositioning of drugs against VCP/p97 ATPase. *Sci Rep, 7*, 44912. doi:10.1038/srep44912

Seidlin, S. M., Marinelli, L. D., & Oshry, E. (1946). Radioactive iodine therapy; effect on functioning metastases of adenocarcinoma of the thyroid. *J Am Med Assoc, 132*(14), 838-847. doi:10.1001/jama.1946.02870490016004

Serrano-Nascimento, C., & Nunes, M. T. (2022). Perchlorate, nitrate, and thiocyanate: Environmental relevant NIS-inhibitors pollutants and their impact on thyroid function and human health. *Front Endocrinol (Lausanne), 13*, 995503. doi:10.3389/fendo.2022.995503

Sharma, G. N., Dave, R., Sanadya, J., Sharma, P., & Sharma, K. K. (2010). Various types and management of breast cancer: an overview. *J Adv Pharm Technol Res, 1*(2), 109-126.

Shen, H., Zhu, R., Liu, Y., Hong, Y., Ge, J., Xuan, J., . . . Li, Q. (2024). Radioiodine-refractory differentiated thyroid cancer: Molecular mechanisms and therapeutic strategies for radioiodine resistance. *Drug Resist Updat, 72*, 101013. doi:10.1016/j.drup.2023.101013

Shi, X., Liu, R., Qu, S., Zhu, G., Bishop, J., Liu, X., . . . Xing, M. (2015). Association of TERT promoter mutation 1,295,228 C>T with BRAF V600E mutation, older patient age, and distant metastasis in anaplastic thyroid cancer. *J Clin Endocrinol Metab, 100*(4), E632-637. doi:10.1210/jc.2014-3606

Sippel, R. S., Kunnimalaiyaan, M., & Chen, H. (2008). Current management of medullary thyroid cancer. *Oncologist, 13*(5), 539-547. doi:10.1634/theoncologist.2007-0239

Skrott, Z., Mistrik, M., Andersen, K. K., Friis, S., Majera, D., Gursky, J., . . . Bartek, J. (2017). Alcohol-abuse drug disulfiram targets cancer via p97 segregase adaptor NPL4. *Nature, 552*(7684), 194-199. doi:10.1038/nature25016

Smanik, P. A., Liu, Q., Furminger, T. L., Ryu, K., Xing, S., Mazzaferri, E. L., & Jhiang, S. M. (1996). Cloning of the human sodium lodide symporter. *Biochem Biophys Res Commun, 226*(2), 339-345. doi:10.1006/bbrc.1996.1358

Smanik, P. A., Ryu, K. Y., Theil, K. S., Mazzaferri, E. L., & Jhiang, S. M. (1997). Expression, exon-intron organization, and chromosome mapping of the human sodium iodide symporter. *Endocrinology, 138*(8), 3555-3558. doi:10.1210/endo.138.8.5262

Smith, V. E., Franklyn, J. A., & McCabe, C. J. (2011). Expression and function of the novel proto-oncogene PBF in thyroid cancer: a new target for augmenting radioiodine uptake. *J Endocrinol, 210*(2), 157-163. doi:10.1530/joe-11-0064

Smith, V. E., Read, M. L., Turnell, A. S., Watkins, R. J., Watkinson, J. C., Lewy, G. D., . . . McCabe, C. J. (2009). A novel mechanism of sodium iodide symporter repression in differentiated thyroid cancer. *J Cell Sci, 122*(Pt 18), 3393-3402. doi:10.1242/jcs.045427

Smith, V. E., Sharma, N., Watkins, R. J., Read, M. L., Ryan, G. A., Kwan, P. P., . . . McCabe, C. J. (2013). Manipulation of PBF/PTTG1IP phosphorylation status; a potential new therapeutic strategy for improving radioiodine uptake in thyroid and other tumors. *J Clin Endocrinol Metab, 98*(7), 2876-2886. doi:10.1210/jc.2012-3640

Smolarz, B., Nowak, A. Z., & Romanowicz, H. (2022). Breast Cancer-Epidemiology, Classification, Pathogenesis and Treatment (Review of Literature). *Cancers (Basel), 14*(10). doi:10.3390/cancers14102569

Soares, P., Trovisco, V., Rocha, A. S., Lima, J., Castro, P., Preto, A., . . . Sobrinho-Simões, M. (2003). BRAF mutations and RET/PTC rearrangements are alternative events in the etiopathogenesis of PTC. *Oncogene, 22*(29), 4578-4580. doi:10.1038/sj.onc.1206706

Socolow, E. L., Dunlap, D., Sobel, R. A., & Ingbar, S. H. (1968). A correlative study of the effect of iodide administration in the rat on thyroidal iodide transport and organic iodine content. *Endocrinology, 83*(4), 737-743. doi:10.1210/endo-83-4-737

Song, H., Zhang, J., Ning, L., Zhang, H., Chen, D., Jiao, X., & Zhang, K. (2018). The MEK1/2 Inhibitor AZD6244 Sensitizes BRAF-Mutant Thyroid Cancer to Vemurafenib. *Med Sci Monit, 24*, 3002-3010. doi:10.12659/msm.910084

Song, J., Qiu, W., Deng, X., Qiu, Z., Fan, Y., & Yang, Z. (2018). A somatic mutation of RasGRP3 decreases Na(+)/I(-) symporter expression in metastases of radioactive iodine-refractory thyroid cancer by stimulating the Akt signaling pathway. *Am J Cancer Res, 8*(9), 1847-1855.

Spitzweg, C., Harrington, K. J., Pinke, L. A., Vile, R. G., & Morris, J. C. (2001). Clinical review 132: The sodium iodide symporter and its potential role in cancer therapy. *J Clin Endocrinol Metab, 86*(7), 3327-3335. doi:10.1210/jcem.86.7.7641

Spitzweg, C., Joba, W., Morris, J. C., & Heufelder, A. E. (1999). Regulation of sodium iodide symporter gene expression in FRTL-5 rat thyroid cells. *Thyroid, 9*(8), 821-830. doi:10.1089/thy.1999.9.821

Stevens, A., Meier, J., Bhat, A., Knight, S. J., Vanness, D. J., & Balentine, C. (2023). Reassessing surgical guidelines for papillary thyroid cancer impact on survival: Expanding indications for lobectomy. *Surgery, 174*(3), 542-548. doi:10.1016/j.surg.2023.05.033

Stratford, A. L., Boelaert, K., Tannahill, L. A., Kim, D. S., Warfield, A., Eggo, M. C., . . . McCabe, C. J. (2005). Pituitary tumor transforming gene binding factor: a novel transforming gene in thyroid tumorigenesis. *J Clin Endocrinol Metab, 90*(7), 4341-4349. doi:10.1210/jc.2005-0523

Su, D. H., Chang, T. C., & Chang, S. H. (2019). Prognostic factors on outcomes of follicular thyroid cancer. *J Formos Med Assoc, 118*(7), 1144-1153. doi:10.1016/j.jfma.2018.11.010

Subbiah, V., Bang, Y.-J., Lassen, U. N., Wainberg, Z. A., Soria, J.-C., Wen, P. Y., . . . De Braud, F. G. (2016). ROAR: a phase 2, open-label study in patients (pts) with BRAF V600E–mutated rare cancers to investigate the efficacy and safety of dabrafenib (D) and trametinib (T) combination therapy. In: American Society of Clinical Oncology.

Subbiah, V., Kreitman, R. J., Wainberg, Z. A., Cho, J. Y., Schellens, J. H. M., Soria, J. C., . . . Keam, B. (2018). Dabrafenib and Trametinib Treatment in Patients With Locally Advanced or Metastatic BRAF V600-Mutant Anaplastic Thyroid Cancer. *J Clin Oncol, 36*(1), 7-13. doi:10.1200/jco.2017.73.6785

Subbiah, V., Kreitman, R. J., Wainberg, Z. A., Cho, J. Y., Schellens, J. H. M., Soria, J. C., . . . Keam, B. (2022). Dabrafenib plus trametinib in patients with BRAF V600E-mutant anaplastic thyroid cancer: updated analysis from the phase II ROAR basket study. *Ann Oncol, 33*(4), 406-415. doi:10.1016/j.annonc.2021.12.014

Sugino, K., Kameyama, K., Ito, K., Nagahama, M., Kitagawa, W., Shibuya, H., . . . Ito, K. (2012). Outcomes and prognostic factors of 251 patients with minimally invasive follicular thyroid carcinoma. *Thyroid, 22*(8), 798-804. doi:10.1089/thy.2012.0051

Sugitani, I., Ito, Y., Takeuchi, D., Nakayama, H., Masaki, C., Shindo, H., . . . Miyauchi, A. (2021). Indications and Strategy for Active Surveillance of Adult Low-Risk Papillary Thyroid Microcarcinoma: Consensus Statements from the Japan Association of Endocrine Surgery Task Force on Management for Papillary Thyroid Microcarcinoma. *Thyroid, 31*(2), 183-192. doi:10.1089/thy.2020.0330

Sun, X., & Qiu, H. (2020). Valosin-Containing Protein, a Calcium-Associated ATPase Protein, in Endoplasmic Reticulum and Mitochondrial Function and Its Implications for Diseases. *Int J Mol Sci, 21*(11). doi:10.3390/ijms21113842

Sun, Y. S., Zhao, Z., Yang, Z. N., Xu, F., Lu, H. J., Zhu, Z. Y., . . . Zhu, H. P. (2017). Risk Factors and Preventions of Breast Cancer. *Int J Biol Sci, 13*(11), 1387-1397. doi:10.7150/ijbs.21635

Syed, A., Vanka, S. A., Escudero, I., Ismail, R., & Krayem, H. (2022). Oncocytic Cell Carcinoma of the Thyroid: A Case Report and an Overview of the Diagnosis, Treatment Modalities, and Prognosis. *Cureus, 14*(10), e30298. doi:10.7759/cureus.30298

Szanto, I., Pusztaszeri, M., & Mavromati, M. (2019). H(2)O(2) Metabolism in Normal Thyroid Cells and in Thyroid Tumorigenesis: Focus on NADPH Oxidases. *Antioxidants (Basel), 8*(5). doi:10.3390/antiox8050126

Szinnai, G., Lacroix, L., Carré, A., Guimiot, F., Talbot, M., Martinovic, J., . . . Polak, M. (2007). Sodium/iodide symporter (NIS) gene expression is the limiting step for the onset of thyroid function in the human fetus. *J Clin Endocrinol Metab, 92*(1), 70-76. doi:10.1210/jc.2006-1450

Takahashi, M., Ritz, J., & Cooper, G. M. (1985). Activation of a novel human transforming gene, ret, by DNA rearrangement. *Cell, 42*(2), 581-588. doi:10.1016/0092-8674(85)90115-1

Takaya, K., Yoshimasa, T., Arai, H., Tamura, N., Miyamoto, Y., Itoh, H., & Nakao, K. (1996). Expression of the RET proto-oncogene in normal human tissues, pheochromocytomas, and other tumors of neural crest origin. *J Mol Med (Berl), 74*(10), 617-621. doi:10.1007/s001090050065

Taki, K., Kogai, T., Kanamoto, Y., Hershman, J. M., & Brent, G. A. (2002). A thyroid-specific far-upstream enhancer in the human sodium/iodide symporter gene requires Pax-8 binding and cyclic adenosine 3',5'-monophosphate response element-like sequence binding proteins for full activity and is differentially regulated in normal and thyroid cancer cells. *Mol Endocrinol, 16*(10), 2266-2282. doi:10.1210/me.2002-0109

Tanaka, T. N., Alloju, S. K., Oh, D. K., & Cohen, E. E. (2015). Thyroid cancer: molecular pathogenesis, tyrosine kinase inhibitors, and other new therapies. *Am J Hematol Oncol, 11*(4), 5-9.

Tang, W. K., & Xia, D. (2016). Role of the D1-D2 Linker of Human VCP/p97 in the Asymmetry and ATPase Activity of the D1-domain. *Sci Rep, 6*, 20037. doi:10.1038/srep20037

Tao, X. F., Liu, C., Bai, Y., & Chen, X. (2011). [Study of the correlation of papillary thyroid carcinoma's invasion with Ezrin, Moesin and E-Cadherin]. *Zhonghua Er Bi Yan Hou Tou Jing Wai Ke Za Zhi, 46*(9), 761-763.

Tavares, C., Eloy, C., Melo, M., Gaspar da Rocha, A., Pestana, A., Batista, R., . . . Soares, P. (2018). mTOR Pathway in Papillary Thyroid Carcinoma: Different Contributions of mTORC1 and mTORC2 Complexes for Tumor Behavior and SLC5A5 mRNA Expression. *Int J Mol Sci, 19*(5). doi:10.3390/ijms19051448

Taylor, P. N., Albrecht, D., Scholz, A., Gutierrez-Buey, G., Lazarus, J. H., Dayan, C. M., & Okosieme, O. E. (2018). Global epidemiology of hyperthyroidism and hypothyroidism. *Nat Rev Endocrinol, 14*(5), 301-316. doi:10.1038/nrendo.2018.18

Tazebay, U. H., Wapnir, I. L., Levy, O., Dohan, O., Zuckier, L. S., Zhao, Q. H., . . . Carrasco, N. (2000). The mammary gland iodide transporter is expressed during lactation and in breast cancer. *Nat Med, 6*(8), 871-878. doi:10.1038/78630

Thangaraju, M., Gopal, E., Martin, P. M., Ananth, S., Smith, S. B., Prasad, P. D., . . . Ganapathy, V. (2006). SLC5A8 triggers tumor cell apoptosis through pyruvate-dependent inhibition of histone deacetylases. *Cancer Res, 66*(24), 11560-11564. doi:10.1158/0008-5472.Can-06-1950

Thompson, R. J., Fletcher, A., Brookes, K., Nieto, H., Alshahrani, M. M., Mueller, J. W., . . . McCabe, C. J. (2019). Dimerization of the Sodium/Iodide Symporter. *Thyroid, 29*(10), 1485-1498. doi:10.1089/thy.2019.0034

Tiulpakov, A., White, C. W., Abhayawardana, R. S., See, H. B., Chan, A. S., Seeber, R. M., . . . Pfleger, K. D. (2016). Mutations of Vasopressin Receptor 2 Including Novel L312S Have Differential Effects on Trafficking. *Mol Endocrinol, 30*(8), 889-904. doi:10.1210/me.2016-1002

Tobys, D., Kowalski, L. M., Cziudaj, E., Müller, S., Zentis, P., Pach, E., . . . Höning, S. (2021). Inhibition of clathrin-mediated endocytosis by knockdown of AP-2 leads to alterations in the plasma membrane proteome. *Traffic, 22*(1-2), 6-22. doi:10.1111/tra.12770

Traub, L. M., Downs, M. A., Westrich, J. L., & Fremont, D. H. (1999). Crystal structure of the alpha appendage of AP-2 reveals a recruitment platform for clathrin-coat assembly. *Proc Natl Acad Sci U S A, 96*(16), 8907-8912. doi:10.1073/pnas.96.16.8907

Tuttle, R. M., Fagin, J. A., Minkowitz, G., Wong, R. J., Roman, B., Patel, S., . . . Morris, L. G. T. (2017). Natural History and Tumor Volume Kinetics of Papillary Thyroid Cancers During Active Surveillance. *JAMA Otolaryngol Head Neck Surg, 143*(10), 1015-1020. doi:10.1001/jamaoto.2017.1442

Tuttle, R. M., & Sherman, E. J. (2016). Anaplastic thyroid cancer. *U: UptoDate, Cooper DS, Ross DS.[Internet] Waltham MA: UpToDate*.

Upadhyay, G., Singh, R., Agarwal, G., Mishra, S. K., Pal, L., Pradhan, P. K., . . . Godbole, M. M. (2003). Functional expression of sodium iodide symporter (NIS) in human breast cancer tissue. *Breast Cancer Res Treat, 77*(2), 157-165. doi:10.1023/a:1021321409159

Uyttersprot, N., Pelgrims, N., Carrasco, N., Gervy, C., Maenhaut, C., Dumont, J. E., & Miot, F. (1997). Moderate doses of iodide in vivo inhibit cell proliferation and the expression of thyroperoxidase and Na+/I- symporter mRNAs in dog thyroid. *Mol Cell Endocrinol, 131*(2), 195-203. doi:10.1016/s0303-7207(97)00108-1

Vaccarella, S., Franceschi, S., Bray, F., Wild, C. P., Plummer, M., & Dal Maso, L. (2016). Worldwide Thyroid-Cancer Epidemic? The Increasing Impact of Overdiagnosis. *N Engl J Med, 375*(7), 614-617. doi:10.1056/NEJMp1604412

van den Hove, M. F., Croizet-Berger, K., Jouret, F., Guggino, S. E., Guggino, W. B., Devuyst, O., & Courtoy, P. J. (2006). The loss of the chloride channel, ClC-5, delays apical iodide efflux and induces a euthyroid goiter in the mouse thyroid gland. *Endocrinology, 147*(3), 1287-1296. doi:10.1210/en.2005-1149

Vassart, G., & Dumont, J. E. (1992). The thyrotropin receptor and the regulation of thyrocyte function and growth. *Endocrine Reviews, 13*(3), 596-611.

Velasco, I., Bath, S. C., & Rayman, M. P. (2018). Iodine as Essential Nutrient during the First 1000 Days of Life. *Nutrients, 10*(3). doi:10.3390/nu10030290

Venkataraman, G. M., Yatin, M., Marcinek, R., & Ain, K. B. (1999). Restoration of iodide uptake in dedifferentiated thyroid carcinoma: relationship to human Na+/I-symporter gene methylation status. *J Clin Endocrinol Metab, 84*(7), 2449-2457. doi:10.1210/jcem.84.7.5815

Vidi, P. A., Chen, J., Irudayaraj, J. M., & Watts, V. J. (2008). Adenosine A(2A) receptors assemble into higher-order oligomers at the plasma membrane. *FEBS Lett, 582*(29), 3985-3990. doi:10.1016/j.febslet.2008.09.062

Vieja, A. D. l., Ginter, C., & Carrasco, N. (2000). *Topology of the sodium/iodide symporter.* Paper presented at the Program of the 12th International Thyroid Congress, Kyoto, Japan.

Vinagre, J., Almeida, A., Pópulo, H., Batista, R., Lyra, J., Pinto, V., . . . Soares, P. (2013). Frequency of TERT promoter mutations in human cancers. *Nat Commun, 4*, 2185. doi:10.1038/ncomms3185

Visser, T. J. (2007). Thyroid hormone transporters. *Horm Res, 68 Suppl 5*, 28-30. doi:10.1159/000110469

Vo, T., Xing, Y., Meric-Bernstam, F., Mirza, N., Vlastos, G., Symmans, W. F., . . . Hunt, K. K. (2007). Long-term outcomes in patients with mucinous, medullary, tubular, and invasive ductal carcinomas after lumpectomy. *Am J Surg, 194*(4), 527-531. doi:10.1016/j.amjsurg.2007.06.012

Volante, M., Rapa, I., & Papotti, M. (2008). Poorly differentiated thyroid carcinoma: diagnostic features and controversial issues. *Endocr Pathol, 19*(3), 150-155. doi:10.1007/s12022-008-9040-4

Wächter, S., Damanakis, A. I., Elxnat, M., Roth, S., Wunderlich, A., Verburg, F. A., . . . Di Fazio, P. (2018). Epigenetic Modifications in Thyroid Cancer Cells Restore NIS and Radio-Iodine Uptake and Promote Cell Death. *J Clin Med, 7*(4). doi:10.3390/jcm7040061

Waks, A. G., & Winer, E. P. (2019). Breast Cancer Treatment: A Review. *Jama, 321*(3), 288-300. doi:10.1001/jama.2018.19323

Walter, P., & Ron, D. (2011). The unfolded protein response: from stress pathway to homeostatic regulation. *Science, 334*(6059), 1081-1086. doi:10.1126/science.1209038

Wang, F., Li, S., Gan, T., Stott, G. M., Flint, A., & Chou, T. F. (2020). Allosteric p97 Inhibitors Can Overcome Resistance to ATP-Competitive p97 Inhibitors for Potential Anticancer Therapy. *ChemMedChem, 15*(8), 685-694. doi:10.1002/cmdc.201900722

Wang, J. R., Montierth, M., Xu, L., Goswami, M., Zhao, X., Cote, G., . . . Cabanillas, M. E. (2022). Impact of Somatic Mutations on Survival Outcomes in Patients With

Anaplastic Thyroid Carcinoma. *JCO Precis Oncol, 6*, e2100504. doi:10.1200/po.21.00504

Wang, L. H., Wehland, M., Wise, P. M., Infanger, M., Grimm, D., & Kreissl, M. C. (2023). Cabozantinib, Vandetanib, Pralsetinib and Selpercatinib as Treatment for Progressed Medullary Thyroid Cancer with a Main Focus on Hypertension as Adverse Effect. *Int J Mol Sci, 24*(3). doi:10.3390/ijms24032312

Wapnir, I. L., Goris, M., Yudd, A., Dohan, O., Adelman, D., Nowels, K., & Carrasco, N. (2004). The Na+/I- symporter mediates iodide uptake in breast cancer metastases and can be selectively down-regulated in the thyroid. *Clin Cancer Res, 10*(13), 4294-4302. doi:10.1158/1078-0432.Ccr-04-0074

Wapnir, I. L., van de Rijn, M., Nowels, K., Amenta, P. S., Walton, K., Montgomery, K., . . . Carrasco, N. (2003). Immunohistochemical profile of the sodium/iodide symporter in thyroid, breast, and other carcinomas using high density tissue microarrays and conventional sections. *J Clin Endocrinol Metab, 88*(4), 1880-1888. doi:10.1210/jc.2002-021544

Watkins, R. J., Imruetaicharoenchoke, W., Read, M. L., Sharma, N., Poole, V. L., Gentilin, E., . . . McCabe, C. J. (2016). Pro-invasive Effect of Proto-oncogene PBF Is Modulated by an Interaction with Cortactin. *J Clin Endocrinol Metab, 101*(12), 4551-4563. doi:10.1210/jc.2016-1932

Wejaphikul, K., Groeneweg, S., Hilhorst-Hofstee, Y., Chatterjee, V. K., Peeters, R. P., Meima, M. E., & Visser, W. E. (2019). Insight Into Molecular Determinants of T3 vs T4 Recognition From Mutations in Thyroid Hormone Receptor α and β. *J Clin Endocrinol Metab, 104*(8), 3491-3500. doi:10.1210/jc.2018-02794

Wells, S. A., Jr., Asa, S. L., Dralle, H., Elisei, R., Evans, D. B., Gagel, R. F., . . . Waguespack, S. G. (2015). Revised American Thyroid Association guidelines for the management of medullary thyroid carcinoma. *Thyroid, 25*(6), 567-610. doi:10.1089/thy.2014.0335

Wells, S. A., Jr., Robinson, B. G., Gagel, R. F., Dralle, H., Fagin, J. A., Santoro, M., . . . Schlumberger, M. J. (2012). Vandetanib in patients with locally advanced or metastatic medullary thyroid cancer: a randomized, double-blind phase III trial. *J Clin Oncol, 30*(2), 134-141. doi:10.1200/jco.2011.35.5040

Wirth, L. J., Sherman, E., Robinson, B., Solomon, B., Kang, H., Lorch, J., . . . Cabanillas, M. E. (2020). Efficacy of Selpercatinib in RET-Altered Thyroid Cancers. *N Engl J Med, 383*(9), 825-835. doi:10.1056/NEJMoa2005651

Wolff, J. (1964). TRANSPORT OF IODIDE AND OTHER ANIONS IN THE THYROID GLAND. *Physiol Rev, 44*, 45-90. doi:10.1152/physrev.1964.44.1.45

Wolff, J., & Chaikoff, I. L. (1948). Plasma inorganic iodide as a homeostatic regulator of thyroid function. *J Biol Chem, 174*(2), 555-564.

Wolff, J., Chaikoff, I. L., & et al. (1949). The temporary nature of the inhibitory action of excess iodine on organic iodine synthesis in the normal thyroid. *Endocrinology, 45*(5), 504-513, illust. doi:10.1210/endo-45-5-504

Wondisford, F. E., Farr, E. A., Radovick, S., Steinfelder, H. J., Moates, J. M., McClaskey, J. H., & Weintraub, B. D. (1989). Thyroid hormone inhibition of human thyrotropin beta-subunit gene expression is mediated by a cis-acting element located in the first exon. *J Biol Chem, 264*(25), 14601-14604.

Xia, D., Tang, W. K., & Ye, Y. (2016). Structure and function of the AAA+ ATPase p97/Cdc48p. *Gene, 583*(1), 64-77. doi:10.1016/j.gene.2016.02.042

Xing, M. (2005). BRAF mutation in thyroid cancer. *Endocr Relat Cancer, 12*(2), 245-262. doi:10.1677/erc.1.0978

Xing, M. (2007). Gene methylation in thyroid tumorigenesis. *Endocrinology, 148*(3), 948-953. doi:10.1210/en.2006-0927

Xing, M. (2010). Genetic alterations in the phosphatidylinositol-3 kinase/Akt pathway in thyroid cancer. *Thyroid, 20*(7), 697-706. doi:10.1089/thy.2010.1646

Xing, M. (2013). Molecular pathogenesis and mechanisms of thyroid cancer. *Nat Rev Cancer, 13*(3), 184-199. doi:10.1038/nrc3431

Xing, M. (2016). Clinical utility of RAS mutations in thyroid cancer: a blurred picture now emerging clearer. *BMC Med, 14*, 12. doi:10.1186/s12916-016-0559-9

Xing, M., Usadel, H., Cohen, Y., Tokumaru, Y., Guo, Z., Westra, W. B., . . . Sidransky, D. (2003). Methylation of the thyroid-stimulating hormone receptor gene in epithelial thyroid tumors: a marker of malignancy and a cause of gene silencing. *Cancer Res, 63*(9), 2316-2321.

Yamashita, T. S., Baky, F. J., McKenzie, T. J., Thompson, G. B., Farley, D. R., Lyden, M. L., & Dy, B. M. (2020). Occurrence and Natural History of Thyroid Cancer in Patients with Cowden Syndrome. *Eur Thyroid J, 9*(5), 243-246. doi:10.1159/000506422

Yamazaki, H., Sugino, K., Katoh, R., Matsuzu, K., Kitagawa, W., Nagahama, M., . . . Ito, K. (2024). Role of the Degree of Vascular Invasion in Predicting Prognosis of Follicular Thyroid Carcinoma. *J Clin Endocrinol Metab, 109*(5), 1291-1300. doi:10.1210/clinem/dgad689

Yao, C., Pan, Y., Li, Y., Xu, X., Lin, Y., Wang, W., & Wang, S. (2015). Effect of sodium/iodide symporter (NIS)-mediated radioiodine therapy on estrogen receptor-negative breast cancer. *Oncol Rep, 34*(1), 59-66. doi:10.3892/or.2015.3946

Yaspo, M. L., Aaltonen, J., Horelli-Kuitunen, N., Peltonen, L., & Lehrach, H. (1998). Cloning of a novel human putative type Ia integral membrane protein mapping to 21q22.3. *Genomics, 49*(1), 133-136. doi:10.1006/geno.1998.5217

Yue, C. H., Oner, M., Chiu, C. Y., Chen, M. C., Teng, C. L., Wang, H. Y., . . . Lin, H. (2021). RET Regulates Human Medullary Thyroid Cancer Cell Proliferation through CDK5 and STAT3 Activation. *Biomolecules, 11*(6). doi:10.3390/biom11060860

Yue, J., & López, J. M. (2020). Understanding MAPK Signaling Pathways in Apoptosis. *Int J Mol Sci, 21*(7). doi:10.3390/ijms21072346

Yutan, E., & Clark, O. H. (2001). Hürthle cell carcinoma. *Curr Treat Options Oncol, 2*(4), 331-335. doi:10.1007/s11864-001-0026-4

Zaballos, M. A., & Santisteban, P. (2017). Key signaling pathways in thyroid cancer. *J Endocrinol, 235*(2), R43-r61. doi:10.1530/joe-17-0266

Zeng, P. Y. F., Prokopec, S. D., Lai, S. Y., Pinto, N., Chan-Seng-Yue, M. A., Clifton-Bligh, R., . . . Nichols, A. C. (2024). The genomic and evolutionary landscapes of anaplastic thyroid carcinoma. *Cell Rep, 43*(3), 113826. doi:10.1016/j.celrep.2024.113826

Zhang, J., & Lazar, M. A. (2000). The mechanism of action of thyroid hormones. *Annu Rev Physiol, 62*, 439-466. doi:10.1146/annurev.physiol.62.1.439

Zhang, Y., Yu, J., Grachtchouk, V., Qin, T., Lumeng, C. N., Sartor, M. A., & Koenig, R. J. (2017). Genomic binding of PAX8-PPARG fusion protein regulates cancer-related pathways and alters the immune landscape of thyroid cancer. *Oncotarget, 8*(4), 5761-5773. doi:10.18632/oncotarget.14050

Zhang, Z., Liu, D., Murugan, A. K., Liu, Z., & Xing, M. (2014). Histone deacetylation of NIS promoter underlies BRAF V600E-promoted NIS silencing in thyroid cancer. *Endocr Relat Cancer, 21*(2), 161-173. doi:10.1530/erc-13-0399

Zhao, J. Y., Wang, H. J., Wang, H. P., Yao, J. M., Wu, X. Y., Shang, H. X., . . . Liao, L. (2015). Methylation of sodium iodide symporter promoter correlated with aggressiveness and metastasis in papillary thyroid carcinoma: a meta-analysis. *Int J Clin Exp Med, 8*(7), 10731-10738. Retrieved from https://www.ncbi.nlm.nih.gov/pmc/articles/PMC4565248/pdf/ijcem0008-10731.pdf

Zhong, X., Shen, Y., Ballar, P., Apostolou, A., Agami, R., & Fang, S. (2004). AAA ATPase p97/valosin-containing protein interacts with gp78, a ubiquitin ligase for endoplasmic reticulum-associated degradation. *J Biol Chem, 279*(44), 45676-45684. doi:10.1074/jbc.M409034200

Zhou, H. J., Wang, J., Yao, B., Wong, S., Djakovic, S., Kumar, B., . . . Wustrow, D. (2015). Discovery of a First-in-Class, Potent, Selective, and Orally Bioavailable Inhibitor of the p97 AAA ATPase (CB-5083). *J Med Chem, 58*(24), 9480-9497. doi:10.1021/acs.jmedchem.5b01346

Zhu, X., Morales, F. C., Agarwal, N. K., Dogruluk, T., Gagea, M., & Georgescu, M. M. (2013). Moesin is a glioma progression marker that induces proliferation and Wnt/β-catenin pathway activation via interaction with CD44. *Cancer Res, 73*(3), 1142-1155. doi:10.1158/0008-5472.Can-12-1040

Zidan, J., Kassem, S., & Kuten, A. (2000). Follicular carcinoma of the thyroid gland: prognostic factors, treatment, and survival. *Am J Clin Oncol, 23*(1), 1-5. doi:10.1097/00000421-200002000-00001

Zimmermann, M. B., & Boelaert, K. (2015). Iodine deficiency and thyroid disorders. *Lancet Diabetes Endocrinol, 3*(4), 286-295. doi:10.1016/s2213-8587(14)70225-6

Zou, H., McGarry, T. J., Bernal, T., & Kirschner, M. W. (1999). Identification of a vertebrate sister-chromatid separation inhibitor involved in transformation and tumorigenesis. *Science, 285*(5426), 418-422. doi:10.1126/science.285.5426.418